Influence of Climate Change on the Changing Arctic and Sub-Arctic Conditions

NATO Science for Peace and Security Series

This Series presents the results of scientific meetings supported under the NATO Programme: Science for Peace and Security (SPS).

The NATO SPS Programme supports meetings in the following Key Priority areas: (1) Defence Against Terrorism; (2) Countering other Threats to Security and (3) NATO, Partner and Mediterranean Dialogue Country Priorities. The types of meeting supported are generally "Advanced Study Institutes" and "Advanced Research Workshops". The NATO SPS Series collects together the results of these meetings. The meetings are co-organized by scientists from NATO countries and scientists from NATO's "Partner" or "Mediterranean Dialogue" countries. The observations and recommendations made at the meetings, as well as the contents of the volumes in the Series, reflect those of participants and contributors only; they should not necessarily be regarded as reflecting NATO views or policy.

Advanced Study Institutes (ASI) are high-level tutorial courses intended to convey the latest developments in a subject to an advanced-level audience

Advanced Research Workshops (ARW) are expert meetings where an intense but informal exchange of views at the frontiers of a subject aims at identifying directions for future action

Following a transformation of the programme in 2006 the Series has been re-named and re-organised. Recent volumes on topics not related to security, which result from meetings supported under the programme earlier, may be found in the NATO Science Series.

The Series is published by IOS Press, Amsterdam, and Springer, Dordrecht, in conjunction with the NATO Public Diplomacy Division.

Sub-Series

A.	Chemistry and Biology	Springer
B.	Physics and Biophysics	Springer
C.	Environmental Security	Springer
D.	Information and Communication Security	IOS Press
E.	Human and Societal Dynamics	IOS Press

http://www.nato.int/science
http://www.springer.com
http://www.iospress.nl

Series C: Environmental Security

Influence of Climate Change on the Changing Arctic and Sub-Arctic Conditions

edited by

Jacques C.J. Nihoul
University of Liège, Belgium

and

Andrey G. Kostianoy
P.P. Shirshov Institute of Oceanology
Russian Academy of Sciences
Moscow, Russia

Published in cooperation with NATO Public Diplomacy Division

Proceedings of the NATO Advanced Research Workshop on
Influence of Climate Change on the Changing Arctic
and Sub-Arctic Conditions
Liège, Belgium
8–10 May 2008

Library of Congress Control Number: 2008942053

ISBN 978-1-4020-9459-0 (PB)
ISBN 978-1-4020-9458-3 (HB)
ISBN 978-1-4020-9460-6 (e-book)

Published by Springer,
P.O. Box 17, 3300 AA Dordrecht, The Netherlands.

www.springer.com

Printed on acid-free paper

Contents

Contributors

Nathalie Fagel
Département de Géologie
U.R. Argiles et Paléoclimats
University of Liège
Liège, Belgium
Nathalie.Fagel@ulg.ac.be

Louis Fortier
Quebec-Ocean
Département de biologie
Université Laval
Quebec, Canada
Louis.Fortier@bio.ulaval.ca

Jonathan Gagnon
Département de Biologie et
Québec-Océan
Pavillon Alexandre-Vachon
Université Laval
Québec, Canada

Viacheslav V. Gordeev
P.P. Shirshov Institute of
Oceanology
Russian Academy of Sciences
Moscow, Russia
gordeev@ocean.ru

Jim Hamilton
Coastal Ocean Science
Bedford Institute of Oceanography
Fisheries and Ocean Canada
Dartmouth, Canada
hamiltonj@mar.dfo-mpo.gc.ca

Motoyoshi Ikeda
Graduate School of
Environmental Science
Hokkaido University
Sapporo, Japan
mikeda@ees.hokudai.ac.jp

Martin O. Jeffries
National Science Foundation
Office of Polar Programs
Arlington, USA
mjeffrie@nsf.gov

Andrey G. Kostianoy
P.P. Shirshov Institute of
Oceanology
Russian Academy of Sciences
Moscow, Russia
kostianoy@online.ru

Marina D. Kravchishina
P.P. Shirshov Institute of
Oceanology
Russian Academy of Sciences
Moscow, Russia
kravchishina@ocean.ru

Louis Legendre
UPMC Université Paris 06, UMR
7093, Laboratoire d'Océanographie
de Villefranche
Villefranche-sur-Mer, France
legendre@obs-vlfr.fr

Igor A. Melnikov
P.P. Shirshov Institute of
Oceanology
Russian Academy of Sciences
Moscow, Russia
migor@online.ru

Leonid M. Mitnik
V.I. Il-ichev Pacific
Oceanological Institute
Far Eastern Branch,
Russian Academy of Sciences
Vladivostok, Russia
mitnik@poi.dvo.ru

Jacques C.J. Nihoul
Modelenvironment
University of Liège
Liège, Belgium
J.Nihoul@ulg.ac.be

James E. Overland
Pacific Marine Environmental
Laboratory, NOAA
Seattle, USA
James.E.Overland@noaa.gov

Clarence Pautzke
North Pacific Research Board
Anchorage, Alaska, USA
cpautzke@nprb.org

Ingrid Peterson
Coastal Ocean Science
Bedford Institute of Oceanography
Fisheries and Ocean Canada
Dartmouth, Canada
PetersonI@mar.dfo-mpo.gc.ca

Oleg M. Pokrovsky
Main Geophysical Observatory
St. Petersburg, Russia
pokrov@main.mgo.rssi.ru

Roger Pettipas
Coastal Ocean Science
Bedford Institute of Oceanography
Fisheries and Ocean Canada
Dartmouth, Canada
pettipasr@mar.dfo-mpo.gc.ca

Simon Prinsenberg
Ocean Sciences Division
Bedford Institute of Oceanography
Fisheries and Ocean Canada
Dartmouth, Canada
prinsenbergs@mar.dfo-mpo.gc.ca

Richard B. Rivkin
Ocean Sciences Centre
Memorial University of
Newfoundland,
St. John's, Newfoundland, Canada
rrivkin@mun.ca

Evgeny A. Romankevich
P.P. Shirshov Institute of
Oceanology
Russian Academy of Sciences
Moscow, Russia
romankevich@mail.ru

Jean-Éric Tremblay
Département de Biologie et
Québec-Océan
Pavillon Alexandre-Vachon
Université Laval
Québec, Canada
Jean-Eric.Tremblay@bio.ulaval.ca

Alexander A. Vetrov
P.P. Shirshov Institute of
Oceanology
Russian Academy of Sciences
Moscow, Russia
vetrov@ocean.ru

Francis Wiese
North Pacific Research Board
Anchorage, Alaska, USA
francis.wiese@nprb.org

William J. Wiseman, Jr.
National Science Foundation
Office of Polar Programs
Arlington, USA
wwiseman@nsf.gov

Igor S. Zonn
Engineering Scientific Production
Center for Water Economy
Reclamation and Ecology
Moscow, Russia
igorzonn@mtu-net.ru

Overture

Jacques C.J. Nihoul[1] and Louis Fortier[2]

1 Modelenvironment, Sart Tilman, 4000 Liège, Belgium, J.Nihoul@ulg.ac.be
2 Quebec-Ocean, Département de biologie, Pavillon Alexandre-Vachon, local 2079-A, Université Laval, Quebec G1K 7P4, Canada, Louis.Fortier@bio.ulaval.ca

Oceanography and surveillance of the rapidly changing Arctic and Sub-Arctic

Recent investigations suggest that current atmospheric models underestimate future global warming. The Intergovernmental Panel on Climate Change estimates that the global average temperature could increase as much as 5.8°C by the end of the 21st century. But these estimates don't factor in some feedback mechanisms that may be triggered by rising temperatures. For instance, accelerated decomposition in soils and changes in ocean chemistry may add considerably to greenhouse gases and further intensify warming (http://sciencenow.sciencemag.org/cgi/content/full/2006/526/1?rss=1).

The current warming trends in the Arctic may shove the Arctic system into a seasonally ice-free state not seen for more than 1 million years. The melting is accelerating, and researchers were unable to identify natural processes that might slow the deicing of the Arctic. Such substantial additional melting of Arctic and Antarctic glaciers and ice sheets would raise the sea level worldwide, flooding the coastal areas where many of the world's population lives. Studies, led by scientists at the National Center for Atmospheric Research (NCAR) and the University of Arizona, show that greenhouse gas increases over the next century could warm the Arctic by 3–5°C in summertime. Thus, Arctic summers by 2100 may be as warm as they were nearly 130,000 years ago, when sea levels eventually rose up to 6 m higher than today (http://www.ucar.edu/news/releases/2006/melting.shtml).

Greenland's glaciers are melting into the sea twice as fast as previously believed, says a new report published in *Science* (17 February 2006). The scientists do not understand the mechanism causing glaciers to flow and melt more rapidly. In 1996, the amount of water produced by melting ice in Greenland was about 90 times the amount consumed by Los Angeles in a year. Last year, the melted ice amounted to 225 times the volume of water that Los Angeles uses annually. The study also highlights how seemingly small changes in temperature can have massive effects.

The Barents Sea, Iceland and Greenland waters, the Newfoundland/Labrador Shelf, the Bering Sea, the Oyashio Shelf, and the Sea of Okhotsk are among the regions that support the most important fisheries of the Northern Hemisphere.

J.C.J. Nihoul and A.G. Kostianoy (eds.), *Influence of Climate Change on the Changing Arctic and Sub-Arctic Conditions*,

They are located at the southern extreme of seasonal sea ice cover, and thus are likely to be exceptionally sensitive to variations in climate that impact the extend and duration of sea ice cover. Sea ice is a forcing mechanism that affects the timing, amount and fate of primary production and the survival of larval fish.

Sea ice influences the temperature and salinity of the water column, its hydrographic structure, the availability of light for photosynthesis, and the spatial distribution of fish and their predators. Changes in the dynamics of sea ice will have profound influences on the ability of a region to support fish, and fisheries. Reduced ice coverage potentially will mean a larger area exposed to winter mixing and cooling. There will be reduced brine rejection during sea-ice formation and reduced sea-ice melt, thereby decreasing the seasonality in salinity. The reduction, or even absence, of sea-ice melt will lead to weaker stratification and hence the potential for increased vertical mixing.

Changes in salinity could also modify density-driven currents. Small changes in air or sea temperatures or wind patterns can create large changes in the timing, extent, and duration of ice cover. Recent studies in the Bering Sea suggest that spring sea ice melt-back in the northern region now occurs 2–3 weeks earlier than in the past. Changes to the spring melt-back have direct effects on the timing and fate of primary production, and the amount of melting sea ice affects bottom temperatures and benthic ecosystems. Sea ice is a critical habitat for several species of seals and walrus, and the persistence and location of sea ice affects the migratory routes of cetaceans. Thus, sea ice cover is one of the most important climate-related variables and it directly impacts the ecology of all of the Sub-Arctic Seas. Climate change, and in particular global warming, will have an immense impact on these regions, and this may first be apparent in the sea-ice record, considered a sensitive indicator of a warming climate.

There is considerable concern that the combined effects of climate change and fisheries removals may shift marine ecosystems into alternative states which may have a lower yield of species valuable to people. Climate change can affect both the base of a marine food web and its productivity, and the distribution and abundance of upper trophic-level consumers. In the North Atlantic and North Pacific Oceans, decadal-scale climate changes have impacted stocks of phytoplankton, zooplankton and fish. In the North Atlantic, climate plays a significant role in the population dynamics of the economically important cod.

In recent years, major changes in phytoplankton and zooplankton stocks and the abundance and productivity of commercially important groundfish, marine mammals and seabirds have been correlated with temporal shifts in physical forcing. In particular, seemingly small shifts in the long-term mean values of atmospheric variables, at least when compared to their interannual variability, may result in major changes in the productivity of standing stocks of fish populations.

The flows through Sub-Arctic Seas on their way to or from the Arctic are predicted to change under future climate scenarios. To determine how any change will impact the Sub-Arctic and beyond, we need to understand the physical processes associated with these currents. This would include transport, mixing and

modification of hydrographic properties as well as the transport of planktonic organisms.

Any long-term warming of the climate will almost certainly be accompanied by a change in the number, intensity and tracks of storms. Fewer and weaker winter storms could reduce vertical mixing, thereby producing a ultimately lower nutrient concentrations at the end of winter, prior to the spring bloom. Lower concentrations of nutrients could reduce primary production, and that in turn could impact upon the rest of the food web, such as survival of first feeding fish larvae. On the other hand, if such winds were accompanied by reduced ice coverage, there could be more vertical mixing during the winter and hence higher nutrient concentrations. A change in the number a/or strength of summer storms might also impact post spring bloom primary production. More storms could lead to greater cloud cover, in turn modifying insolation, and thus decreasing sea surface temperature and primary production.

There is the potential for climate change to cause shifts in the distribution and abundance of predators that in turn control the abundance of lower trophic level organisms such as small fish or zooplankton. Alternatively, changes in the primary or secondary production may affect the abundance of higher trophic level organisms that can be supported. Fisheries affect control by removing vast quantities of target species, as well as lesser amounts of non-target species. These removals alter the structure and function of marine ecosystems, and provide ecological space for the increase of non-target species. Thus, the relative importance of natural variability and human factors change is an issue of great scientific and management relevance.

Comparison of the forcing mechanisms among the Arctic and Sub-Arctic Seas would be useful for learning more about these ecosystems, and the responses of their biological components, including commercially exploited fish stocks, to variation in physical forcing mechanisms (Hunt, G.L., Drinkwater KF 2005 Globec Report no 20).

The Arctic is undergoing nothing less than a great rush for virgin territory and natural resources worth hundreds of billions of dollars. Even before the polar ice began shrinking more each summer, countries were pushing into the frigid Barents Sea, lured by undersea oil and gas fields and emboldened by advances in technology. But now, as thinning ice stands to simplify construction of drilling rigs, exploration is likely to move even farther north. The polar thaw is also starting to unlock other treasures: lucrative shipping routes, perhaps even the storied Northwest Passage; new cruise ship destinations; and important commercial fisheries. Recent studies have also projected that in a few decades there could be lucrative fishing grounds in waters that were largely untouched throughout human history.

Until recently, northern Bering Sea ecosystems were characterized by extensive seasonal sea ice cover, high water column and sediment carbon production, and tight pelagic-benthic coupling of organic production. New research published in *Science* (March 2006) shows that these ecosystems are shifting away from these

characteristics. The colonization of new rivers by pink salmon is just one of many changes in fish and crab stocks that appear linked to retreating sea ice and warming waters in the Chukchi Sea and, farther south, the Bering Sea. The changes are important because the Bering is rich with pollock, salmon, halibut and crab, already yielding nearly half of America's seafood catch and a third of Russia's. In a 2002 report for the United States Navy on climate change and the Arctic Ocean, the Arctic Research Commission concluded that species were moving north through the Bering Strait. Climate warming is likely to bring extensive fishing activity to the Arctic, particularly in the Barents Sea and Beaufort-Chuckchi region where commercial operations have been minimal in the past.

But problems could emerge, as well, as stocks shift from the waters of one country to those of another. Snow crabs, for example, appear to be moving away from Alaska, north and west toward Russia, as the sea ice retreats. The valuable fishery could eventually move entirely out of American waters, some federal fisheries scientists said.

The study, using the NCAR-based Community Climate System Model (CCSM), is the first to examine the state of permafrost in a global model that includes interactions among the atmosphere, ocean, land, and sea ice as well as a soil model that depicts freezing and thawing. Results show that global warming may decimate the top 3 m or more of perennially frozen soil across the Northern Hemisphere, altering ecosystems as well as damaging buildings and roads across Canada, Alaska, and Russia. New simulations from the National Center for Atmospheric Research (NCAR) show that over half of the area covered by this topmost layer of permafrost could thaw by 2050 and as much as 90% by 2100. Scientists expect the thawing to increase runoff to the Arctic Ocean and release vast amounts of carbon into the atmosphere (http://www.ucar.edu/news/releases/2005/permafrost.shtml).

The existence of hydrate of methane is known under the oceans – They exist also under the permafrost. They constitute a substantial source of energy which will be exploited in the near future. If an important quantity of methane was subsequently released in the atmosphere, the warming would be dramatic (comparable to the Palaeocene catastrophe 55 million years ago).

One of the additional stresses on the arctic regions results from the increase in ultraviolet radiation reaching the earth's surface as a result of the decrease of atmospheric ozone triggered by climatic changes – ultraviolet radiations are likely to remain at a high level, in particular during spring when ecosystems are the most vulnerable.

A problem of sovereignty and security

With only fragments of the Arctic ever surveyed, by icebreakers or nuclear submarines, various countries are mounting new mapping expeditions to claim the most territory they can.

Claims of expanded territory are being pursued the world over, but the Arctic Ocean is where experts foresee the most conflict. Only there do the boundaries of five nations – Russia, Canada, Denmark, Norway and the United States – converge, the way sections of an orange meet at the stem. (The three other Arctic nations, Iceland, Sweden and Finland, do not have coasts on the ocean.)

In 2001, when Russia laid claim to nearly half the Arctic Ocean, the claim was rejected. And now Russia hopes the recent voyage of its research ship Akademik Fyodorov to the North Pole will yield mapping data in its favour.

In June, Denmark and Canada announced that they would conduct a joint surveying project of uncharted parts of the Arctic Ocean near their coasts.

Denmark is particularly interested in proving that a 1,600 km undersea mountain range, the Lomonosov Ridge, is linked geologically to Greenland, which is a semiautonomous Danish territory. If it finds such a link, Denmark could make a case that the North Pole belongs to the Danes.

Canada could also claim a huge area and then face challenges from the other Arctic nations. The United States could petition for a swath of Arctic seabed larger than California.

Two other arctic conflicts concern Canada – in the east, the island of Hans, situated between the Groënland and the island of Ellesmere is a bone of contention with Denmark. The stake is strategic for the control of sea-borne trade and the exploitation of petrol and gas resources. In the north-west arctic which could contain up to a quarter of the world petrol and gas reserves, there are large expectations and competition but, in the Beaufort Sea, a long time dispute persists on the border between the United States and Canada… in a region of important submarine oil and gas – fields. The same problem exists in the extreme Arctic rich in petrol and gas and junction-point of the continental shelves of the United State, Canada and Russia – There, each country can assert its rights on the soil and subsoil adjacent to its continental shelf in pursuance of the United Nations convention on the law of the sea.

The thawing of the Arctic Ocean would help create the so-called Arctic Bridge, a shipping route with Arctic countries' ports as the logical terminals.

The advantage of maritime short-cuts across the top of the world can be startling. For example, shipments from Murmansk to midcontinental North America by the well-worn route through the St. Lawrence Seaway and Great Lakes to Thunder Bay, in western Ontario, typically take 17 days. The voyage from Murmansk to Churchill is only 8 days under good conditions, and from Churchill, rail links run through Manitoba, the American Midwest and points south all the way to Monterrey, Mexico.

Murmansk was also once the anchor of the Soviet Union's Northern Sea Route, which stretched nearly 5,600 km to the rich nickel mines at Norilsk and on the newly established Arctic colonies at Dikson, Khatanga, Tiksi and Pevek before reaching the Bering Sea. The same way an Arctic Bridge could drastically cut the distance to Canada, a revived Northern Sea Route could shorten the journey for goods and raw materials from Northeast Asia to Europe by 40%.

There is, of course, a third Arctic shipping route: the Northwest Passage. It would be the last of the three main routes to succumb to the thaw.

But some Canadian officials, eyeing what will happen in 20 years, say it is all the more justification for investing in the rebirth of Churchill.

All countries intend to defend their sovereignty in a region which more and more arouses cupidity. Important litigations can be foreseen: for the sea control (with annual duration of opening of navigable routes) for the exploitation of natural resources (petrol and gas) as well as in matter of security with the opening of a new point of regular entry in North America.

Climate and geophysical changes will liberate vast areas of ocean whose oceanography has not yet been sampled, surveyed documented, modelled and whose hydrodynamics, biogeochemistry and biology is still largely unknown. In relation to the International Polar Year in 2007–2008, European Commission highlights the following research priorities in polar regions: (i) world climate change; (ii) the Arctic Ice Cover Simulation Experiment (AICSEX) project, which has focused on the Arctic ice cap, its evolution and modelling; (iii) measurement of marine currents, temperature and salinity, carbon uptake, atmospheric circulation and pollution, as new data will be available from new ice free regions. Investigations in the Arctic polar regions have a direct impact on the European Union and its citizens.

Global warming effects on the Arctic and Sub-Arctic Seas

Jacques C.J. Nihoul

Modelenvironment, University of Liège, Sart Tilman, B-4000 Liege, Belgium, J.Nihoul@ulg.ac.be

Abstract

After a rather hydrostatic approach to global warming (mean earth temperature increasing, ice melting, sea level raising) one came to realize that the effects of global warming were more of a hydrodynamic nature and that the ocean dynamics and its modifications in response to global warming constituted an essential factor. Taking into account the effect of global warming on ocean temperature distribution and currents contributed to a large extent to clarify the problem. The next step was obviously to include the effect of global warming on the atmospheric circulation. We would like to illustrate this point by briefly discussing the so-called North Atlantic Oscillation (NAO).

The North Atlantic Oscillation (NAO)

The NAO dictates much of the Climate variability from the eastern seaboard of North America to Siberia and from the Arctic to the subtropical Atlantic, especially during the boreal winter (Hurrett et al. 2003).

NAO refers to a redistribution of atmospheric mass between the Arctic and subtropical Atlantic. The NAO is traditionally described by two weather maps showing the distribution of sea level pressure (SLP) over the North Atlantic in two typical "educational" situations: NAO^+ and NAO^- when the pressure difference between Lisbon and Reykjavik is respectively positive and negative (Figs. 1, 2).

The NAO is understood to swing from one phase to another to produce large changes in the mean wind speed and direction over the Atlantic, the heat and moisture transport between the Atlantic and the neighbouring continents and the intensity and number of storms, their paths, and the associated weather. Such variations have a significant impact on the wind and buoyancy-driven ocean circulation as well as on the site and intensity of water mass transformation (Fig. 3).

J.C.J. Nihoul and A.G. Kostianoy (eds.), *Influence of Climate Change on the Changing Arctic and Sub-Arctic Conditions*,

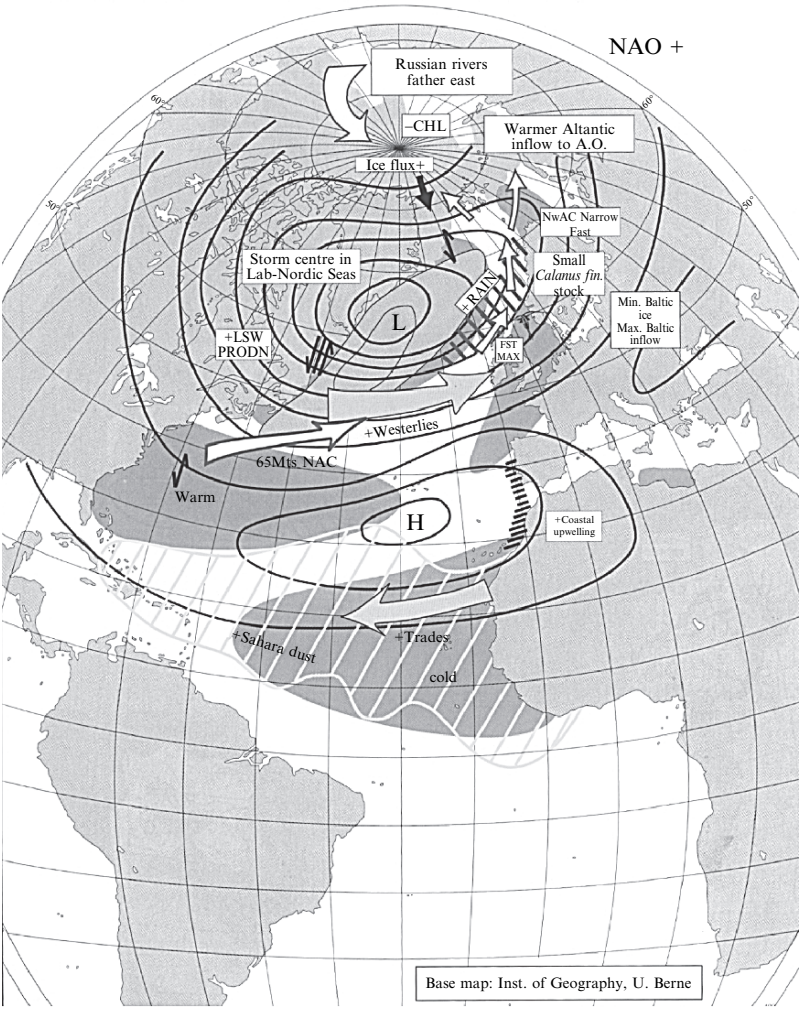

Fig. 1. A schematic of the Atlantic–Arctic sector under NAO positive conditions (Stenseth et al. 2004).

In NAO+ winter situations, enhanced westerly flow across the North Atlantic moves warm and moist maritime air over Europe, northerlies over Greenland and northeastern Canada carry cold air southwards, decreasing SST and land temperatures over the North-West Atlantic, the Labrador Sea ice extends further south

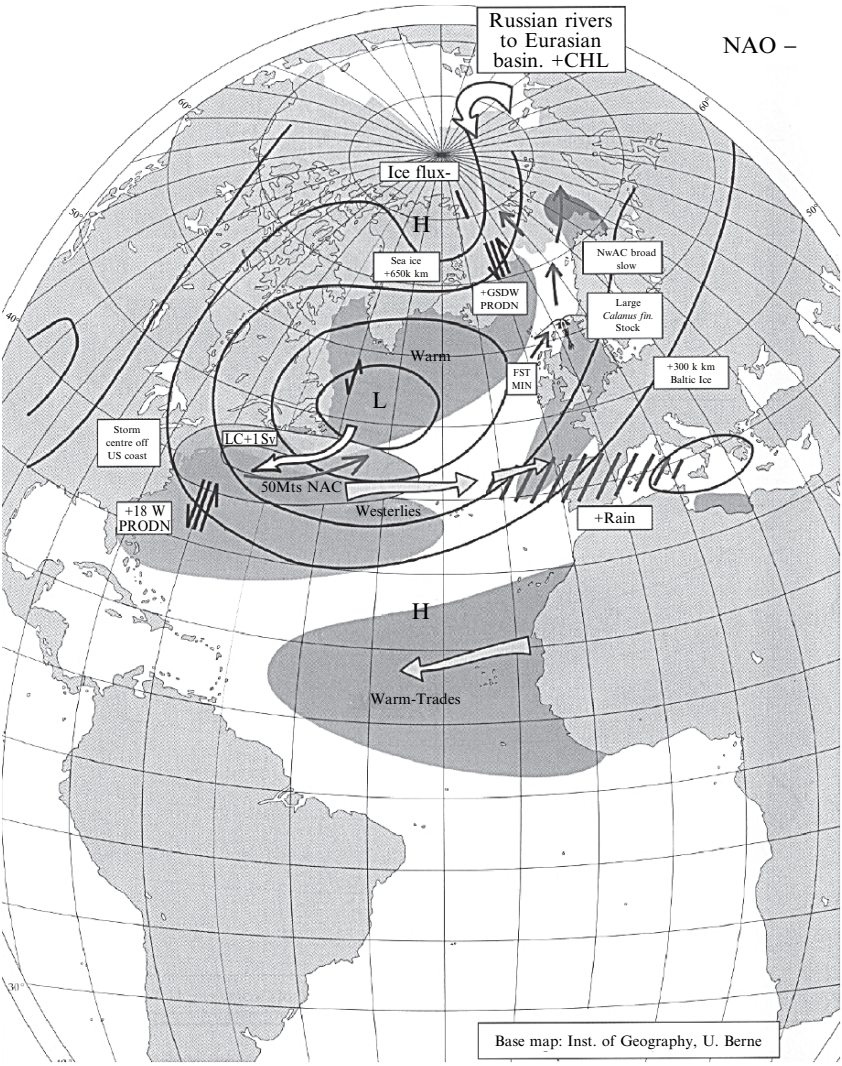

Fig. 2. A schematic of the Atlantic–Arctic sector under NAO negative conditions (Stenseth et al. 2004).

while the Greenland Sea ice boundary is found to the North of its climatological mean extent. NAO^+ winters, associated with chill, dry, northwesterlies across the Labrador Sea are characterized by deep-reaching convective renewal of LSW and widespread distribution of chilled SST across the Northwest Atlantic.

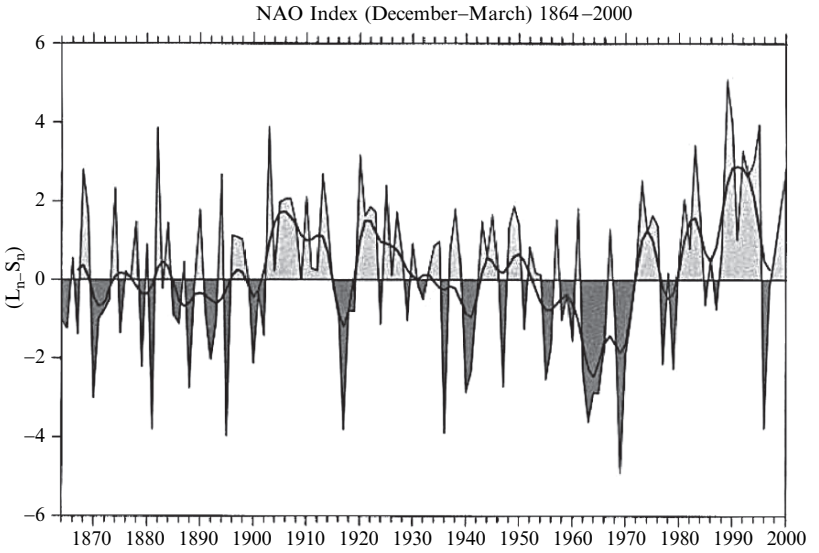

Fig. 3. Winter (December–March) index of the NAO based on the difference of normalized SLP between Lisbon, Portugal, and Stykkisholmur/Reykjavik, Iceland form 1864 through 2000. The heavy solid line represents the index smoothed to remove fluctuations with periods less than 4 years (Stenseth et al. 2004).

The NAO strange attractors

However, examining records of the fluctuations of the NAO index over more than a century, one realizes that the jumps from one value of the index to the next value of the same or different sign occur rather at random, strongly suggesting that the case study situations, although exemplary, do not actually describe two definite states of the atmosphere but two strange attractors: the system attracted by NAO^+ oscillates in its vicinity until it finds a way out and goes to NAO^-, oscillates in its vicinity until it finds a way out and goes back to the vicinity of NAO^{+-} (Fig. 4).

The records show also a definite trend towards the positive NAO phase in recent decades and the increased attractiveness of the positive phase has often been attributed to a global warming effect.

One should however be attentive to the fact that, in addition to possible jumps between NAO^+ and NAO^- (with a possible predominance of NAO^+ attributed to global warming) small deviations from the "educational" weather maps may occur as the system wanders in the vicinity of one or the other strange attractor.

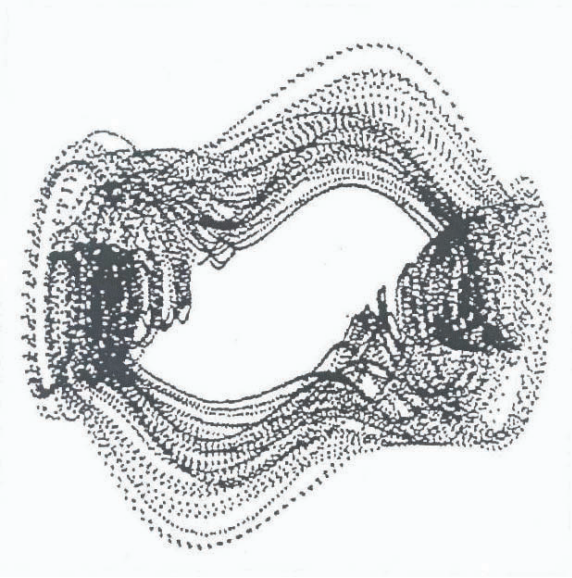

Fig. 4. An educational image of trajectones jumping from one strange attractor to the other.

For instance, NAO^+ conditions of the most recent winters have shown a shut-down of Labrador Sea Convection. In just two and three winters, the long-sustained cooling and freshening of LSW has been largely reversed. A comparison of Atlantic SLP anomaly pattern between the 1995–1999 period with that for 1999–2000 shows a slight east and northeast displacement, in the more recent period, responsible for important differences to the marine climate of the West Greenland Banks and to the convective center of the Labrador Sea.

The NAO is reminiscent of the pioneer work of Lorenz (1990) who, with the help of a severely truncated and simplified model of atmospheric dynamics, essentially, a layer of fluid heated from below, showed that for small values of the Rayleigh number (a non-dimensional measure of the temperature difference between the lower layer and the upper layer), heat was transported by conduction; for higher values of the Rayleigh number, convective cells appeared to transport heat, for still higher values of the Rayleigh number, two strange attractors appear and the system may jump from one to the other as described above.

Further increase of the Rayleigh number, however sees the strange attractors disappear and a limit cycle appear.

Could it be the same bifurcation as the one which we observed in the NAO Index in the last decades 1970–2000 and that many authors attributed to global warming?

Even if this is stretching the comparison a little far, one should remark that, in Lorenz's model, a further increase of the Rayleigh number makes away with the limit cycle and the strange attractors reappear.

Further increase of the Rayleigh number generates an intermittent succession of periodic regimes and bursts of disorder (Nihoul 2007).

In fact, although models like the Lorentz model and the NAO Index representation are helpful to guide one's intuition of possible bifurcations of the atmospheric dynamics they are far too rudimentary to describe the dynamics of the system where the number of spatial modes generated by nonlinear interactions can be the determinant factor (Nihoul 2007).

One should thus be extremely careful in interpreting the NAO Index and presumably also in looking in its variations for global warming indications.

References

Hurrell JW, Kushnir Y, Ottersen G, Visbeck M (2003) The North Atlantic Oscillation. Climatic significance and environmental impact. Geophysical Monograph Series, 134. American Geophysical Union, Washington, DC, 279 pp

Lorenz EN (1990) Can chaos and intransitivity lead to internannual variability. Tellus, 42 A, 378–389

Nihoul JCJ (2007) Chaos, diversity, turbulence and sustainable development. International Journal of Computing Science and Mathematics, 1, 1, 107–114

Stenseth NCh, Ottersen G, Hirnel JW, Belgrano A (2004) Marine Ecosystems and Climate Variation, Oxford University Press, Oxford, 252 pp

The case for global warming in the Arctic

James E. Overland

NOAA/Pacific Marine Environmental Laboratory, Seattle, WA 98115, USA,
James.E.Overland@noaa.gov

Abstract

Attribution of the causes for the recent large changes in the Arctic, including sea ice, temperatures, and biological impacts, is formidable task because it is difficult to separate the signal due to anthropogenic greenhouse gases from the background of large natural climate variability. However, initial observational and modeling evidence of an anthropogenic influence in the Arctic has emerged over the last decade. I address this issue through application of methodological, evidentiary, and performance scientific standards which consist of three parts: is change occurring, which is the most consistent among a range of possible causes, and are these causes predictive? At the end of the 20th and beginning of the 21st century Arctic-wide warming is distinctive from the regional patterns of temperature anomalies that were seen earlier in the 20th century. IPCC model simulation results for the 1930s warm and 1960s cold temperature anomalies are consistent with natural climate variability, but all models show the influence of external forcing from greenhouse gases on warm temperature anomalies in the 1990s, and projections for the future. The recent sea ice reduction of summer 2007 Arctic by 40% compared to its 1980s extent is particularly scary and suggests that other surprises may be in store for the Arctic climate system. Sea ice loss appears to be on a fast track relative to consensus projections by IPCC models. This dramatic sea ice reduction was likely caused by a *combination* of greenhouse gas increases, fortuitous timing in the natural variability of the atmospheric general circulation, and positive feedbacks associated with a reduction in sea ice.

Introduction

In these days of discussion of the future extinction of polar bears and the use of Arctic ice-free shipping routes, it might seem strange to look at the case for a global warming influence in the Arctic in more detail. While it is predicted by models that the Arctic will warm faster than more southerly latitudes, and multiple indicators of climate change show large shifts over the last two decades, the attribution of change due to greenhouse gas increases is still difficult because of

J.C.J. Nihoul and A.G. Kostianoy (eds.), *Influence of Climate Change on the Changing Arctic and Sub-Arctic Conditions*,

the relative influence of the large range of climate extremes from natural (intrinsic) variability. Such decadal variability is often observed as changes in wind patterns (Maslanik et al. 2007). As little as 8 years ago Serreze et al. (2000, 2007) commented that "Taken together, these results paint a reasonably coherent picture of [Arctic] change, but their interpretation as signals of enhanced greenhouse warming is open to debate." Since then evidence of an anthropogenic influence in the Arctic is emerging as discussed in this paper, along with an improved understanding of the structure of intrinsic variability and internal feedbacks within the Arctic. Such feedbacks include cloud cover and shifts in the relative area coverage of ice and ocean.

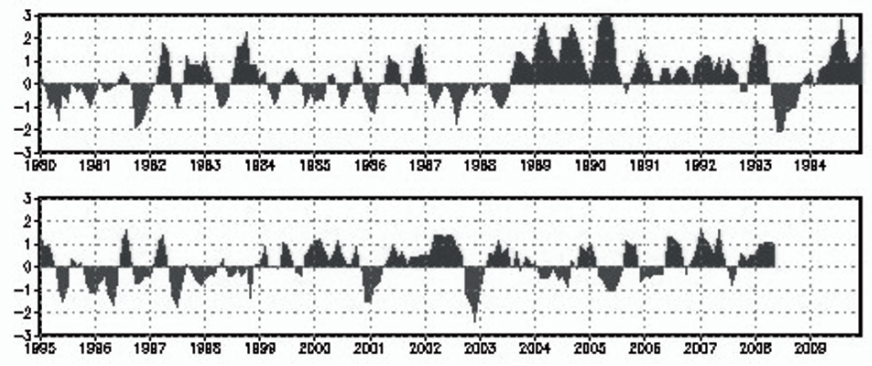

Fig. 1. Three-month running mean of the Arctic Oscillation index. (From the CPC web site.)

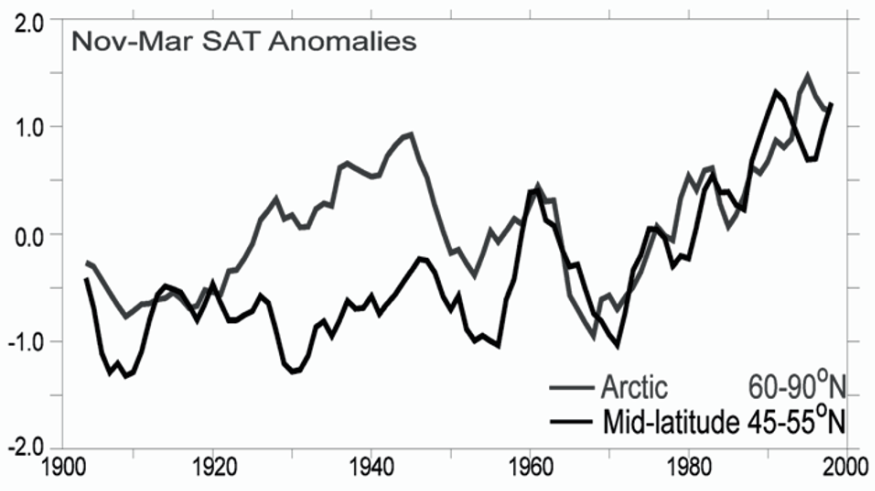

Fig. 2. Arctic-wide and mid-latitude surface air temperature anomalies for the 20th century. A 5-year running mean is applied.

In the mid to late 1990s the climate pattern known as the Arctic Oscillation (AO) had a persistent run of positive values from 1989 to 1995, which advects warmer air into the Eurasian Arctic compared to years when it is in its negative phase (Fig. 1). There was considerable opinion that this persistence was an indication of anthropogenic climate change (Palmer 1999; Feldstein 2002), but after 1996 this argument was rejected as the phase of the AO became more random from year to year while Arctic indicators showed continued warm conditions (Overland and Wang 2005). A second example of natural variability is the 1930s warm period in certain parts of the Arctic, which appears not unlike the period of the 1990s when Arctic-wide averages are compared (Fig. 2).

As will be discussed in section "Arctic change", the cumulative impacts of the AO and other climate patterns acting in concert with external forcings such as greenhouse gases and internal feedbacks are important to explain historical temperature changes in the Arctic and the recent rapid loss of sea ice in summer. Further, while Fig. 2 looks like a climate oscillation, the true story is that the causes of the temperature maxima are different in the 1930s and 1990s. Before taking up current evidence about the Arctic, we digress and address the general issue of application of the scientific method in understanding climate change.

How do we know we are not wrong?

There are numerous examples of scientific ideas being challenged and overturned. These include a geocentric universe, fixity of species, the absolute nature of time and space, and the lack of mobility of continents. But over the history of science there are accepted scientific standard for evaluating claims that over time have resolved such issues. Four main scientific methods are:

- Methodological standards: Induction (generalization from observations), Deduction, and Falsification (be disprovable)
- Evidence standards: Reliability (replication, independent corroboration, and peer review), Consistency of multiple lines of evidence
- Performance standards: Predictive, Consistent over time, Useful and
- Community standards: Provides the best explanation among competing hypotheses, Rejection of speculative hypotheses

Two applications of these standards are the rejection of the coming of the ice age in the 1970s and continental drift. In the first case there was no major consensus in the scientific community and in the second case the strongest skeptics only focused on one type of data, geodetic evidence.

For global warming the case is laid out in the IPCC 4th Assessment Report: "The warming of the climate system is unequivocal" and "most of the observed increase in global average temperature since the mid-20th century is very likely due to the observed increase in anthropogenic greenhouse gas concentrations

(IPCC 2007)". The development of the Report consists of three parts: change is occurring, these changes are then related to most plausible causes, and finally projections are made. There is a deductive relation between the quantitative increases in carbon dioxide and increases in temperature. Rise in CO_2 is coincident with massive increases in fossil fuel burning since the industrial revolution. But can we apply these standards to change in a specific region such as the Arctic?

Arctic change

Data

First, there is a consilience of indicators of climate change in the Arctic, including increased temperatures, diminished sea ice, degraded permafrost, enlarged melt area on Greenland, increased water vapor, decreased snow extent, increasing number of forest fires, increased river discharge, and resulting ecosystem impacts. Certainly one of the most dramatic indicators is the reduction of summer sea ice extent, 40% below the average extent of the 1980s and over 20% below the previous record minimum of 2005. This 1-year drop in sea ice extent is three standard deviations beyond that of the year-to-year variability in the historical sea ice record beginning in 1979.

Global climate models generally project that the temperature increase in the Arctic will be larger than at more southerly latitudes and that the increase due to anthropogenic forcing will have an Arctic-wide character (Chapman and Walsh 2007). Figure 3A shows the annual temperature anomalies in 2001–2007 for the globe and Fig. 3B shows the climate projections for 2020–2029; both signal a rather uniform polar amplification. If one looks more regionally, temperature anomalies for spring 2000–2005 had a minimum increase of +1°C throughout the Arctic, with a hot spot near eastern Siberia of over +3°C, relative to the 1958–1998 mean (Fig. 4A). Since that time the background temperatures have remained positive but the location of the hot spot has shifted to the Atlantic side of the Arctic as the regional wind pattern has changed. Autumn temperature anomalies for 2005–2007 over much of the central Arctic basin were greater than +6°C in response to thin or no sea ice at the end of summer (Fig. 4B Left); this is also a prediction of climate models. For comparison we show the winter surface temperature anomalies for the AO positive years of 1989–1995 (Fig. 4B Right). Here the increased temperatures are not Arctic-wide and can be explained by the natural variability of the wind pattern associated with the AO with the warm anomalies over Eurasia.

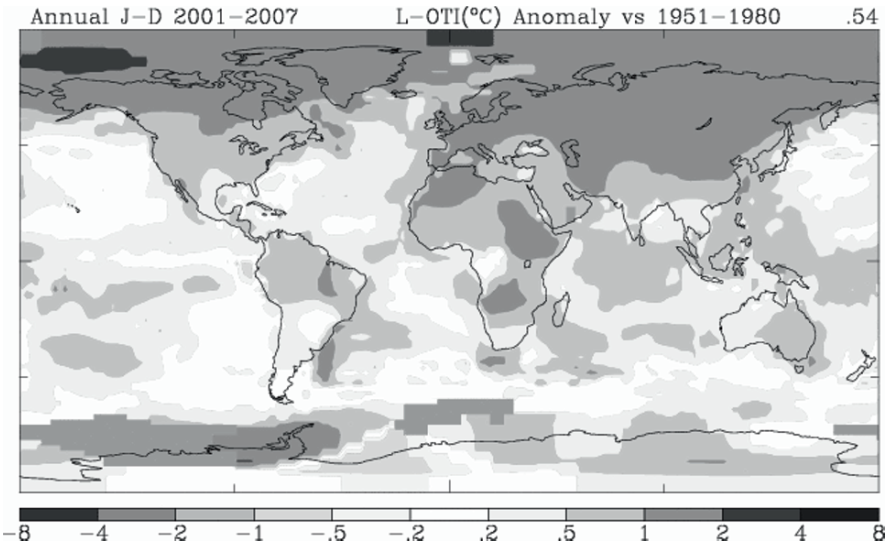

Fig. 3A. Global-annual temperature anomalies for 2001–2007 relative to a 1951–1980 baseline. (From the GISS web site.)

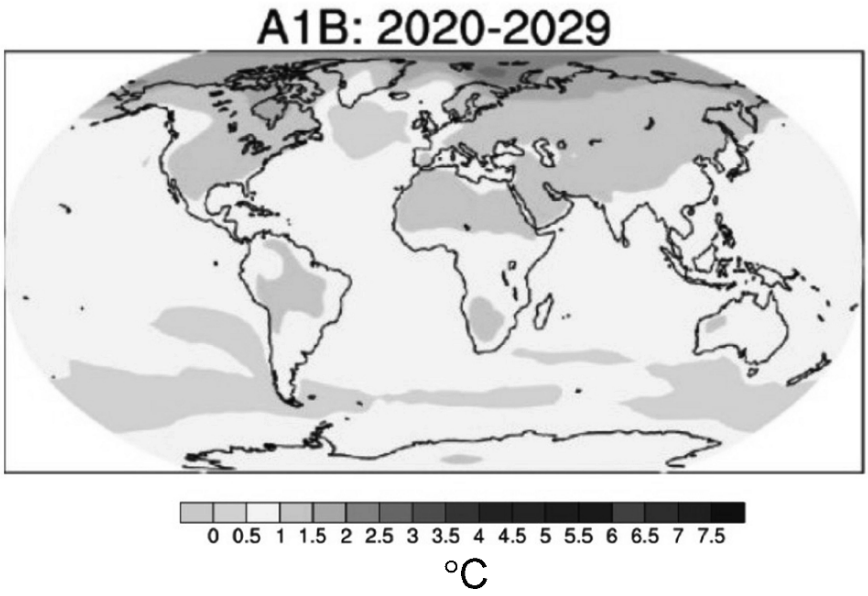

Fig. 3B. IPCC model forecast temperatures for 2020–2029 using a midrange emission scenario (A1B). (From the IPCC Report.)

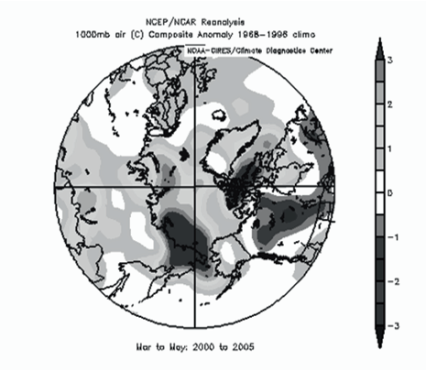

Fig. 4A. 2000–2005 Spring (Mar–May) near surface air temperature anomalies.

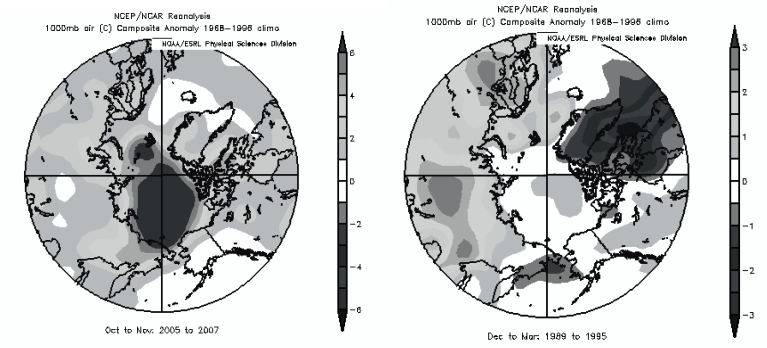

Fig. 4B. *Left* – 2005–2007 Fall (Oct–Nov) air temperature anomalies. *Right* – 1989–1995 winter (Dec–Mar) air temperature anomalies when the AO was strongly positive. (From the CDC web site.)

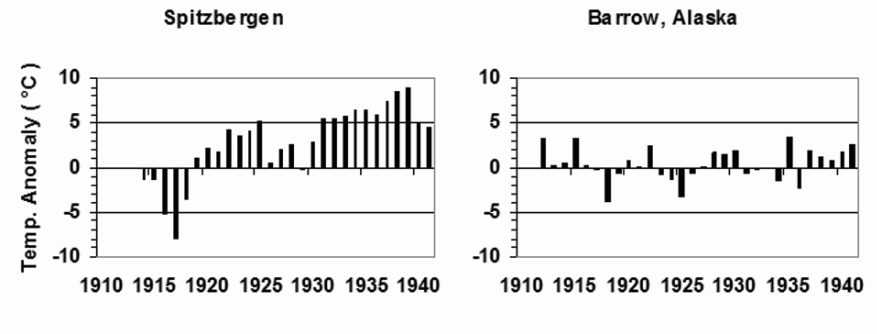

Fig. 5. Spitzbergen and Barrow, AK winter (Nov–Mar) temperature anomalies based on a 1912–1926 base period.

Likewise, if we look at the temperatures of the 1930s, the Spitzbergen station had temperatures greater than 5°C above its mean before 1930 (Fig. 5). With reference to the 20th century Arctic temperature record (Fig. 2), most of the "Arctic-wide average" 1°C anomaly in the 1930s was contributed by this one station. In fact, Barrow, Alaska showed no positive temperature anomaly throughout the 1930s. If we look year by year in the 20th century and back to the first IPY in 1883 (Wood and Overland 2006), we see only regional positive temperature anomalies, rather than background Arctic-wide anomalies as in the last decade. We take the recent Arctic-wide temperature increases as evidence of a global warming signal in the Arctic.

Models

Reproducing decadal and longer variability in coupled General Circulation Models (GCMs) is a critical test for understanding processes in the Arctic climate system and increasing the confidence in the Intergovernmental Panel on Climate Change (IPCC) model projections. Twentieth century simulations, control runs without external forcing, and 21st century projections are available for 20 coupled GCMs for the IPCC 4th Assessment (Wang et al. 2007). Warm anomalies in the Arctic during the last decade are reproduced by all models. In contrast, only eight models have variance comparable with the variance in the 20th century observations. Since we are interested in when an anthropogenic signal may exceed natural variability, we concentrate on those models which pass an observational selection constraint based on having sufficient variance.

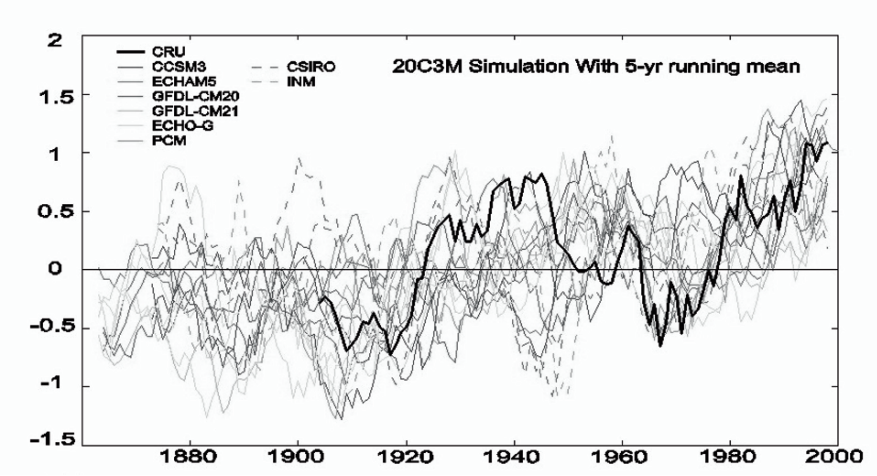

Fig. 6. Observed arctic temperatures (heavy black line-similar to Fig. 2) and IPCC model simulations of arctic temperatures for the 20th century. (From Wang et al. 2007.)

Figure 6 shows the observed Arctic temperatures for the 20th century (heavy line) and simulations for different ensemble members from separate models. Ensembles for a given model are different simulations which start with slightly different initial conditions. The range of simulations, which show different timing of maximum and minimum temperature events, shows the influence of the chaotic nature of the climate system. The random timing of mid-century warm anomalies over the different ensemble members suggests that the observed mid-century warm periods are consistent with intrinsic climate variability. The positive departure of all ensemble members at the end of the century supports the conclusion of an external anthropogenic forcing, and thus a global warming signal for the Arctic.

2007 sea ice loss – the fast track of Arctic change

The loss of 40% of sea ice extent on the Pacific side of the Arctic in 2007 relative to climatology resulted from an unusually persistent high surface pressure/ southerly wind pattern from June through August that transported heat and altered cloud distributions. The winds also advected sea ice across the central Arctic toward the Atlantic sector (Gascard et al. 2008). A similar pressure pattern also occurred in 1987 and 1977 with no remarkable effect on sea ice extent. The 2007 event, however, followed the steady preconditioning of the ice pack by two decades of thinning and area reduction (Rigor and Wallace 2004; Nghiem et al. 2007; Overland et al. 2008).

Although it is difficult to attribute a single event to anthropogenic climate change, there are several lines of evidence that support this conclusion. The 2007 ice loss greatly exceeded that in any other year in the observational record. Control runs of global climate models (with no anthropogenic forcing) do not exhibit similar sea ice loss, but large year-on-year decreases are simulated in some model ensemble members with anthropogenic forcing (Holland et al. 2006). While we would not claim that the chain of events in the National Center for Atmospheric Research (NCAR) model in Fig. 7 is identical to those leading up to the 2007 sea ice minimum, several features are similar. The large drop in the model projection of sea ice extent near 2013 in one ensemble member (black line), along with the range of ensemble members (other colors), implicate long-term anthropogenic forcing combined with large intrinsic atmospheric variability and sea-ice related feedbacks. The modeled minimum sea ice cover rebounds in subsequent years from its low value of 4 million square kilometers – comparable to the observed 2007 minimum extent – but it never recovers to 1980–1990 values.

Based on observations and similarity to model projections, the dramatic Arctic sea ice reduction in 2007 was likely caused by a *combination* of increased temperatures in response to greenhouse gas increases, fortuitous timing in the natural variability of the atmospheric general circulation, and positive feedbacks associated with a reduction in sea ice. Sea ice models without anthropogenic

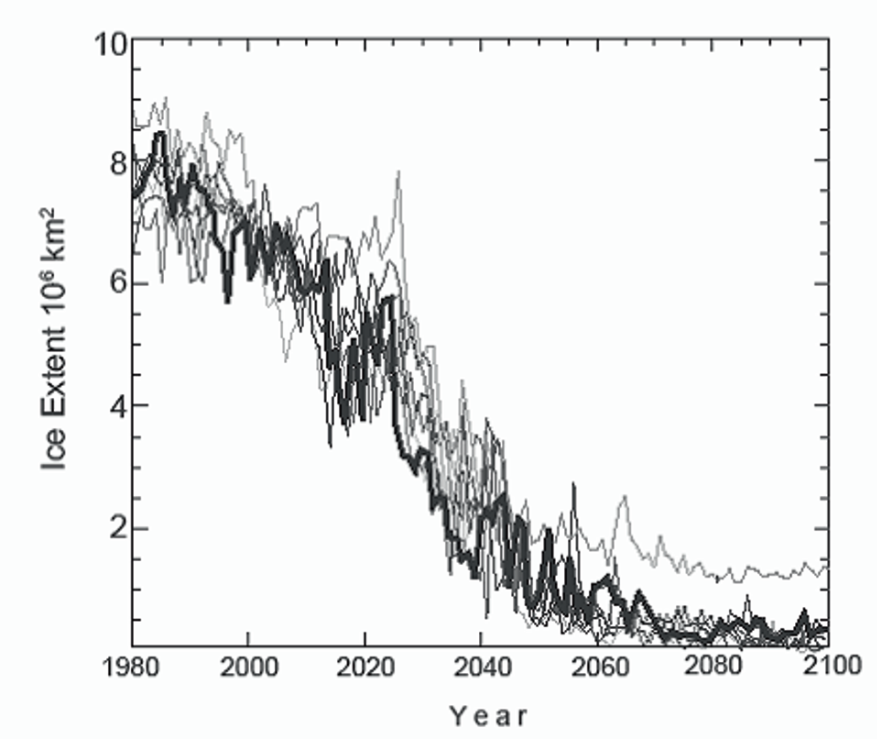

Fig. 7. Different Arctic Sea ice area projections from the NCAR CCSM3 model. (Modified from Holland et al. 2006.)

forcing (control runs) do not generate such sea ice minimums, nor does simple extrapolation of temperatures from greenhouse gas warming initiate the observed open water areas. Thus it is not a question of whether global warming or natural variability is the primary cause of the 2007 sea ice event; both were required.

IPCC projections of sea ice loss from the better subset of models show sea ice minimums beyond 2050 (Stroeve et al. 2007; Overland et al. 2008). But these are projections which average over multiple ensembles to give an expected value. It appears that the real world is on a faster trajectory of sea ice loss than the expected value projected by IPCC models. C. Bitz (2008, personal communication) notes that this fast behavior, while it exists in models, occurs in less than 5% of the simulated future years in the NCAR model. Thus, it is important to understand that while summary IPCC projections were based on averages of many model runs, reality is but a single realization. This does not mean that all the IPCC model forecasts are wrong; it just means that there is a difference in the average of the projections over all ensembles and our single realization. Thus the sea ice event of 2007 points to the simultaneous impact of natural variability and global warming in the Arctic, to give us a much earlier timing for sea ice loss than anticipated. The

new fast track is consistent with an ice-free summer Arctic before 2030, as suggested by Stroeve et al. (2008).

Conclusion

Applying the scientific standards of section "How do we know we are not wrong?", we are beginning to see a global warming signal emerging from the background of large natural variability in the Arctic. There are large changes occurring in the Arctic across physical and biological systems. While some of the extreme magnitudes of these signals going back to the early 20th century can be explained by natural variations in climate patterns such as the AO, the impact of these patterns is regional. Today we see an indication of Arctic-wide trends, with a continued superposition of the influence from these regional patterns.

Results from models independently support this conclusion and point to the ultimate causality of recent Arctic climate change as having an anthropogenic component. The multiple model results in Fig. 6 show that natural variability is large over most of the 20th century. All simulations show this large decadal variability, but the multiple ensembles point to a random phasing between ensemble members, an indication of chaotic-like behavior from natural variability. The only exception is at the end of the series in the 1990s when all the ensembles show positive temperatures due to the influence of external forcing from greenhouse gases. While other causes such as solar cycles and influences from volcanoes are included in the model simulations, the most consistent explanation of the large differences between ensemble members during most of the 20th century, and their convergence at the end of the century, is large natural (intrinsic) variability of the climate system and anthropogenic forcing.

The recent behavior of Arctic sea ice is particularly scary and suggests that other surprises may be in store for the Arctic climate system. As can be inferred from observational analysis and climate models, the dramatic Arctic sea ice reduction in 2007 was likely caused by a combination of increased temperatures in response to greenhouse gas increases, fortuitous timing in the natural variability of the atmospheric general circulation, and positive feedbacks associated with a reduction in sea ice. Natural variability alone or simply extrapolating a greenhouse warming trend is not sufficient individually to induce the additional melting of sea ice in 2007.

While changes in the Arctic meet minimum methodological, evidentiary, and performance standards for anthropogenic forcing, understanding of Arctic climate processes is still incomplete. Application of community standards does provide the best explanation among competing hypotheses: that change to a new climate state in the Arctic with regard to temperature, sea ice, and their direct impacts, is due to a combination of internal chaotic variability within the climate system, external forcing from global warming, and Arctic feedback processes.

Acknowledgments

Much of the material for section "How do we know we are not wrong?" was taken from a presentation by N. Oreskes at the American Meteorological Society:
http://www.ametsoc.org/atmospolicy/presentations/oreskes%20presentation%20for%20web.pdf
I appreciate the support from the Arctic Program of the NOAA Climate Office. This is contribution 3223 from NOAA's Pacific Marine Environmental Laboratory.

References

Chapman WL, Walsh JE (2007) Simulations of arctic temperature and pressure by global coupled models. J Climate, 20, 609–632

Feldstein SB (2002) The recent trend and variance increases of the annular mode. J Climate, 15, 88–94

Gascard J-C et al. (2008) Exploring arctic transpolar drift during dramatic sea ice retreat. Eos Trans AGU, 89(3), 21

Holland MM, Bitz CM, Tremblay B (2006) Future abrupt reductions in the summer Arctic Sea ice. Geophys Res Lett, 33, L23503, doi: 10.1029/2006GL028024

IPCC 2007, Climate change (2007) Synthesis Report, Summary for Policymakers, 22 pp

Maslanik J, Drobot S, Fowler C, Emery W, Barry R (2007) On the arctic climate paradox and the continuing role of atmospheric circulation in affecting sea ice conditions. Geophys Res Lett, 34, L03711, doi: 10.1029/2006GL028269

Nghiem SV, Rigor IG, Perovich DK, Clemente-Colón P, Weatherly JW, Neumann G (2007) Rapid reduction of Arctic perennial sea ice. Geophys Res Lett, 34, L19504, doi: 10.1029/2007GL031138

Overland JE, Wang M (2005) The arctic climate paradox: the recent decrease of the arctic oscillation. Geophys Res Lett, 32, doi: 10.1029/2004GL021752

Overland JE, Wang M, Salo S (2008) The recent arctic warm period. Tellus (in preparation)

Palmer TN (1999) A nonlinear dynamical perspective on climate prediction. J Climate, 12, 575–591

Rigor IG, Wallace JM (2004) Variations in the age of Arctic Sea-ice and summer sea-ice extent. Geophys Res Lett, 31, L09401, doi: 10.1029/2004GL019492

Serreze MC, Walsh JE, Chapin FS III, Osterkamp T, Dyurgerov M, Romanovsky V, Oechel, J Morison WC, Zhang T, Barry RG (2000) Observational evidence of recent change in the northern high-latitude environment. Climatic Change, 46, 159–207

Serreze MC, Holland MM, Stroeve S (2007) Perspectives on the arctic's shrinking sea-ice cover. Science, 315, 1533–1536

Stroeve J, Holland MM, Meier W, Scambos T, Serreze M (2007) Arctic Sea ice decline, Faster than forecast. Geophys Res Lett, 24, L09501, doi: 10.1029/2007GL029703

Stroeve J, Serreze M, Drobot S, Gearheard S, Holland M, Maslanik J, Meier W, Scambos T (2008) Arctic Sea ice extent plummets in 2007. Eos Trans AGU, 89(2), 13

Wang M, Overland JE, Kattsov V, Walsh JE, Zhang X, Pavlova T (2007) Intrinsic versus forced variation in coupled climate model simulations over the arctic during the 20th century. J Climate, 20, 1093–1107

Wood KR, Overland JE (2006) Climate lessons from the first international polar year. Bull Am Meteorol Soc, 87, 1685–1697

A coherency between the North Atlantic temperature nonlinear trend, the eastern Arctic ice extent drift and change in the atmospheric circulation regimes over the northern Eurasia

Oleg M. Pokrovsky

Main Geophysical Observatory, St. Petersburg, 194021, Russia, pokrov@main.mgo.rssi.ru

Abstract

Atlantic Multidecadal Oscillation (AMO) monthly time series were investigated for last 150 years by implementation of a comprehensive smoothing technique controlled by cross-validation procedure, which provided more statistically significant trend evaluation than moving average or linear trend techniques. It was found that there is a winter sea surface temperature (SST) oscillation of around the 64–69 year scale behind a known SST fluctuation of decadal scale for winter months. The AMO trend demonstrates waters warming in the first part of 20th century, cooling period in 50th and 60th, and warming in 80th–90th years. This result confirms the global ocean conveyer theory of Broker. Weak AMO linear trend respond to the greenhouse warming effect related to carbon dioxide concentration increasing. It demonstrates a slow warming behind a more strong (in amplitude) oscillation responded to still not well understood world ocean properties. This result was confirmed by independent research based on wavelet analysis of the same time series. The ice extent (IE) smoothed curve in Barents and Kara Seas shows a coherent behavior: two minimums (in 20th–30th and in 80th–90th) and one maximum in the middle of 20th century. Coherency of the AMO/NAO/IE trends, on one hand, and SLP/SAT trends, on other hand, proved a close relationship existed in various modules of the climate system (atmosphere–ocean–glacial cover) in the Northern Hemisphere.

Introduction

The aim of this paper is to reveal existed linkages between interrelated processes occurred in the ocean and atmosphere of the Atlantic–Arctic climate system. Warming of surface Atlantic waters during last 3 decades led to substantial increasing of SST (sea surface temperature) in shelf Eastern Arctic Seas (Barents, Kara and Laptev) documented by satellite data. That in turn caused a rapid reduction

J.C.J. Nihoul and A.G. Kostianoy (eds.), *Influence of Climate Change on the Changing Arctic and Sub-Arctic Conditions*,

of ice extent in Kara and Laptev Seas in late summer and early autumn. This phenomenon was confirmed by analysis of microwave satellite measurements started in 1978 (Belchansky et al. 2005). Ice melting led to abrupt changes in heat and radiation budgets at the boundary air-sea surface due to albedo rapid decreasing. That in turn accelerates various feedbacks including energy exchange processes. Heat fluxes from sea surface to atmosphere over free of ice areas of Kara and Laptev Seas appeared in autumn during last 3 years probably caused a large-scale depression in atmospheric pressure field over Northern Asia and changes in atmospheric circulation regimes.

North Atlantic and Arctic SST trends

Positive trend of SST in many areas of North Atlantic and its modulation In Arctic Ocean for last 60 years was discussed in (Pokrovsky and Timokhov 2005). This paper demonstrated a positive trend of the monthly SST averaged over the whole North Atlantic basin. It is necessary to note that there is the *Atlantic Multi-Decadal Oscillation (AMO)* of the North Atlantic SST (Enfield et al. 2001). Smoothing technique (Pokrovsky et al. 2004) based on a cross-validation criterion allows us to filter out high frequency oscillation. When applied to the climate series it permits to reveal a natural oscillation of the spatially averaged SST in the North Atlantic for winter months (Fig. 1). The AMO variability is pronounced: its range (0.49°C) is larger than either the range of interannual to decadal variability (0.46°C) or the integrated trend over the period 1870–1999 (0.38°C). The index shows persistent warm (pre-1900, 1930s–1950s) and cool (1900s–1920s, 1960s–1980s) phases typically lasting a few decades, as well as the onset of a warm phase in the 1990s. Here “alpha” is a parameter providing a specific smoothing rate (Tikhonov 1963). Above oscillation has a time scale of 64 year. Meanwhile, a linear trend demonstrates the CO_2 greenhouse effect. Therefore, superposition of the greenhouse effect and a positive phase of Atlantic SST provide rapid water warming during last 3 decades. Is the AMO a natural phenomenon, or is it related to global warming? Instruments have observed AMO cycles only for the last 150 years, not long enough to conclusively answer this question. However, studies of paleoclimate proxies, such as tree rings and ice cores, have shown that oscillations similar to those observed instrumentally have been occurring for at least the last millennium (Gray et al. 2004). This is clearly longer than modern man has been affecting climate, so the AMO is probably a natural climate oscillation. In the 20th century, the climate swings of the AMO have alternately camouflaged and exaggerated the greenhouse warming, and made attribution of global warming more difficult to ascertain. Thus, the AMO is a hypothetical mode of natural variability occurring in the North Atlantic Ocean and which has its principle expression in the SST field. Knight et al. (2005) informed that the Hadley Centre model produces a rather realistic AMO with a period of 70–120 years. And

the model AMO persists throughout the 1,400-year run, they note, suggesting that the real-world AMO goes back much further than the past century of observations does. Thus, the AMO is a genuine quasi-periodic cycle of internal climate variability persisting for many centuries, and is related to variability in the oceanic thermohaline circulation (THC). Judging by the 1,400-year simulation's AMO, Knight and colleagues predict that the conveyor will begin to slow within a decade or so. Subsequent slowing would offset – although only temporarily – a "fairly small fraction" of the greenhouse warming expected in the Northern Hemisphere in the next 30 years. Likewise, Sutton and Hodson (2005) predict more drought-prone summers in the central United States in the next few decades. The aim of this paper is to investigate a linkage between the AMO and the Arctic ice extent during last century. Unfortunately, models are not reliable enough to reproduce ice concentration in Arctic Ocean with appropriate accuracy. Therefore, our approach is to implement sophisticated methods for climate time series analysis. These are: (1) a new smoothing algorithm based on Wahba's cross-validation, Cleveland's local polynomial approximation and Tikhonov's regularization; (2) Morlet's wavelet analysis (Cleveland 1979; Goupillaud et al. 1984; Tikhonov 1963; Wahba 1985).

Modulation of the ice extent in Kara Sea

Natural variability, such as that associated with the AMO and NAO, and other circulation patterns, has and will continue to have strong impacts on the Arctic sea-ice cover. Links between altered ocean heat transport and observed ice loss remain to be resolved, as does the attribution of these transport changes, but pulses such as those currently poised to enter the Arctic Ocean from the Atlantic could provide a trigger for a rapid transition. We are not yet capable of predicting exactly when the AMO will switch, in any deterministic sense. Computer models, such as those that predict El Niño, are far from being able to do this. What it is possible to do at present is to calculate the probability that a change in the AMO will occur within a given future time frame. Probabilistic projections of this kind may prove to be very useful for long-term planning in climate sensitive applications. In this respect the wavelet tools might be useful to trace the short-term climate fluctuations of various scales. We used reconstructed time series of ice extent in Russian shelf seas for last century (Polyakov and Johnson 2000; Polyakov et al. 2003). Smoothed curve (Fig. 2) demonstrated 60 years natural oscillation scale, which is similar with similar Atlantic SST (Fig. 1). One can found mutual consistency of both curves. Positive SST anomalies correspond to negative deviations in the ice extent, but with some delay in first half of last century. Figure 1 demonstrated 20 years staying in positive phase during 1940–1960. Corresponding transition in the ice extent to a positive phase started after 18 years staying in negative phase (Fig. 2). It was due to a growing anthropogenic

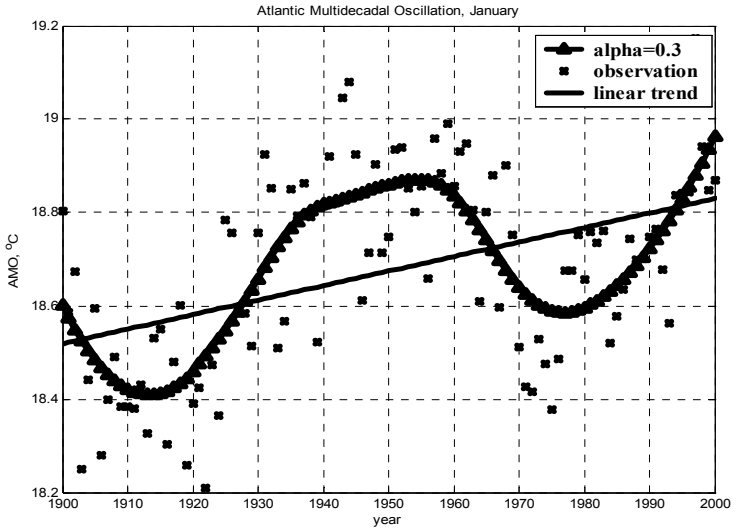

Fig. 1. An averaged North Atlantic SST (°C) – AMO nonlinear and linear trend for January: 1900–2000.

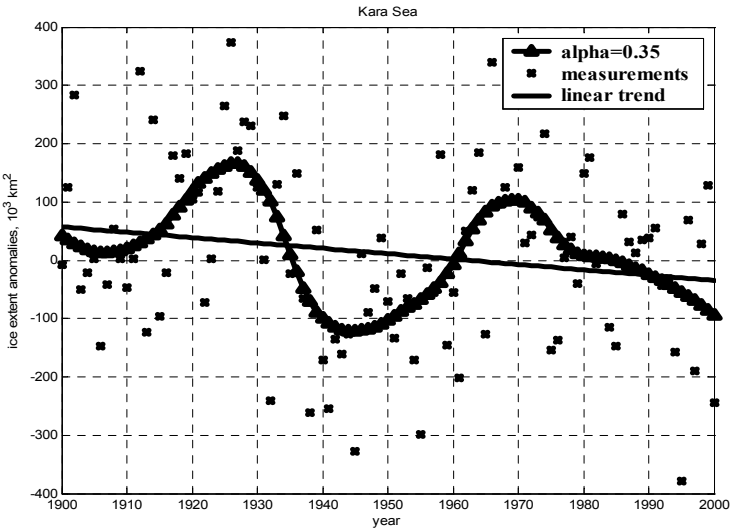

Fig. 2. Nonlinear and linear trend for Kara Sea ice extent anomaly (10^3 km^2) anomalies: August: 1900–2000.

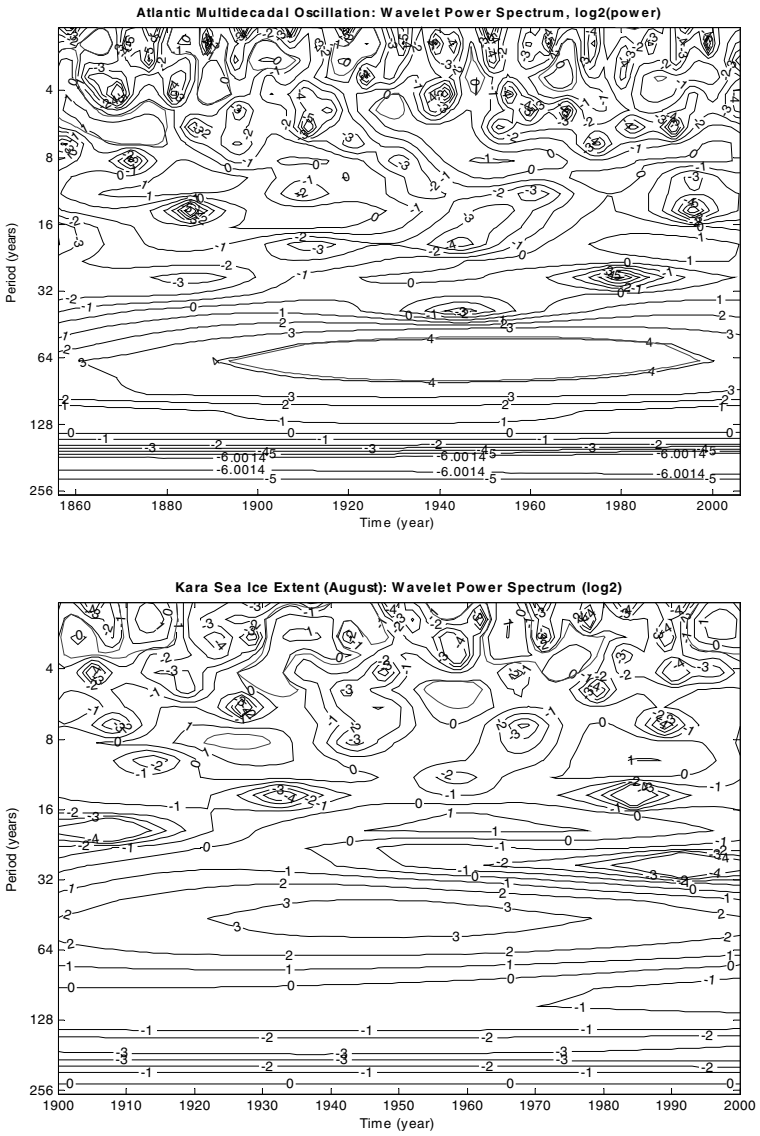

Fig. 3. Coherency in wavelet power spectrum ($\log_2$ scale) for climate series of: AMO winter values for 1856–2000 (*upper panel*) and ice extent September values in Kara Sea for 1900–2000 (*lower panel*).

factor. These periodicities might be found independently by wavelet analysis of both time series. The ice extent wavelet power spectrum (Fig. 3, lower panel) and its comparison with the AMO wavelet spectrum (Fig. 3, upper panel) confirm this important conclusion. Thus, it is the North Atlantic water temperature that is a major regulator of the ice extent in the Kara Sea. A similar result was obtained for the Barents Sea, but the ice extent values there were much lower and respective variability was in contrast higher. Moreover, its opposite phases are a physically evident and explainable phenomenon. Ice extent modulation gives an additional argument in favor of hypothesis that Atlantic waters are major contributor in Eastern Arctic ice melting during last decades.

Rapid increasing of SST in Kara and Laptev Seas

Despite of possible slow downing of Gulf Stream due to enhancement of water refreshment in Nordic Seas we found a strong positive trend in the August and September SST magnitudes spatially averaged over Kara Sea aqua in 1970s and since 1990 (Fig. 4) when ice melting was activated by arrival of warm Atlantic waters after neutral SST and ice extent phase in 1980s (Figs. 1, 2). It is necessary to note the most rapid SST increasing during last decade when temperature increment achieved 2°C. Spatial maps shows that the monthly SST contrasts between August 2006 and 2003 values exceeded 3°C in the central and eastern parts of Kara Sea. Changes occurred in Arctic Ocean actively impact on atmospheric processes in Northern Siberia.

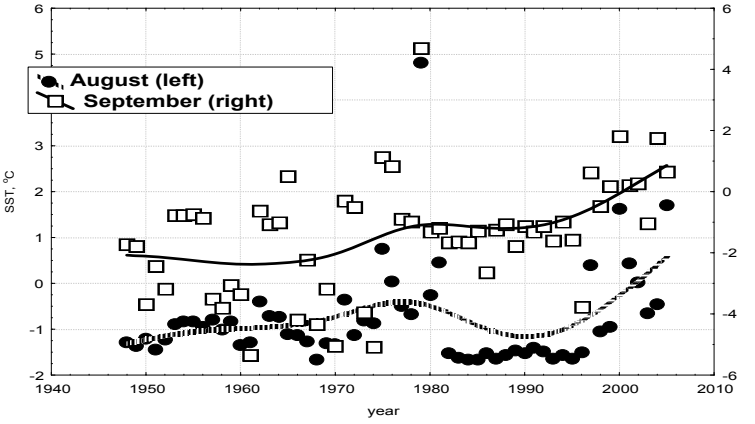

Fig. 4. Kara Sea SST (°C) trend for August (dotted line) and September (solid line): 1948–2005.

Modulation of the sea level pressure over northern Asia

Activation of air-sea energy exchange over water surface free of ice led to responding oscillations in sea level pressure (SLP) of atmosphere. Based on 1-month scale of the atmosphere-ocean adjustment we investigated the SLP October time series for a number of Siberian stations for last century. Smoothed SLP curve at Fig. 4 demonstrates an evident modulation of atmospheric pressure by ice extent in the end of summer (see Fig. 2). In fact, maximum in ice extent attributed to the end of 1920s corresponds to minimum in SLP at the same time. Similar correspondence is valid for early 1940s and late 1960s. Therefore, a high ice extent corresponded to a low SLP and vice versa. It was valid till the end of 1970s, when this relationship turned to opposite: the ice extent decreasing was corresponded to the SLP dropping.

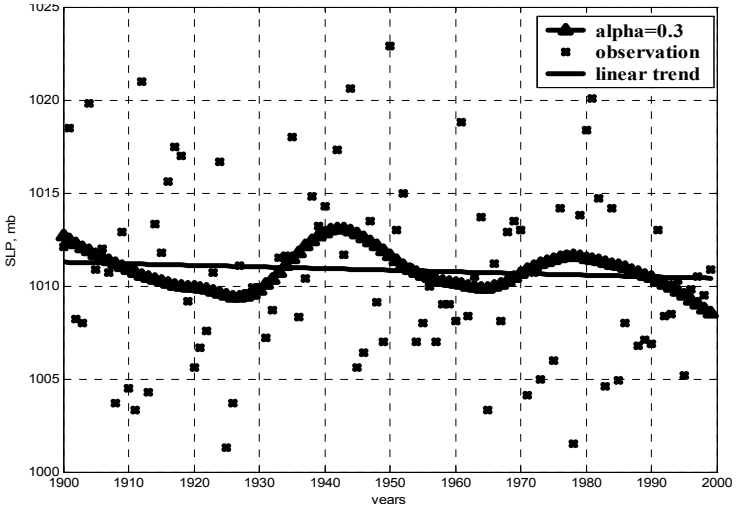

Fig. 5. The SLP (mb) nonlinear trend (station Berezovo: 63° N, 65° E) for October: 1900–2000.

The Arctic dipole and North Siberian oscillation

There is evident *asymmetry* in Arctic ice retreat (Belchansky et al. 2005). This process is occurred most actively in the Eastern Arctic and rather neutral in Western Arctic. During a second half of last century the SLP anomaly field in high latitudes had monopole structure centered at North Pole. In 1950s and 1960s it was a positive monopole, but in 1980s and 1990s – a negative monopole. Since the beginning of 21st century an appearance of *SLP dipole pattern* (see also Wu et al. 2005) was observed. This pattern has two pole of opposite signs: one in high latitudes of Eastern Hemisphere, other – in Western Hemisphere. Strongest SLP

dipole anomaly with account to amplitude was observed in October 2003–2006. One can deduce that there is a link between enhancement of air-sea energy exchange in Kara and Laptev Seas, on one hand, and appearance of *dipole structure* in SLP field in polar area, on other hand. *North Atlantic Oscillation (NAO)* index is related to the difference between Azores and Iceland SLP. A vast pool of no-freezing waters in high latitudes surrounds Iceland. Now days most part of Kara Sea is free of ice during late summer and early autumn. This fact gave us a hint on possibility of similar effect on atmospheric SLP. Therefore, we decided to investigate a new climate index – *North Siberian Oscillation (NSO*) as a twin to NAO. It is a normalized difference between Azores and station "Island Dixon" (in Kara Sea) SLP. September curves of NAO (dotted) and NSO (solid) are in a good agreement (Fig. 6). The NSO growth since the beginning of this century is even a more rapid than those of NAO. Latter might be explained by

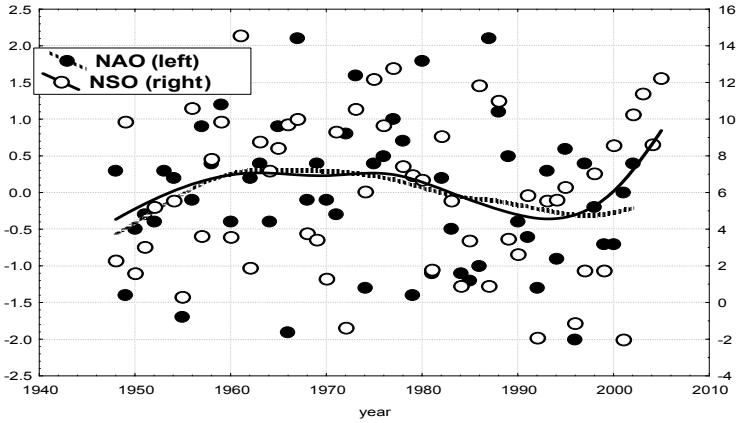

Fig. 6. Comparison of the September NAO (dotted line) and NSO (solid line).

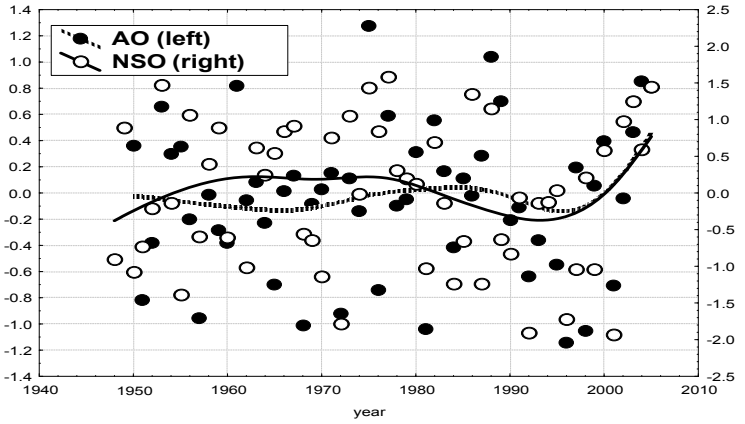

Fig. 7. Comparison of the September AO (dotted line) and NSO (solid line).

abrupt increasing of SST in Kara Sea (see Fig. 4) during last decade. Similar plots were drawn for other autumn and winter months. All of them demonstrated analogical behavior with NAO. It is known that NAO determines intensity of meridian circulation over North Atlantic. Below we will show that NSO plays now a similar role in Asia. NSO comparison with *Arctic Oscillation (AO)* index, which represents a coefficient with the first EOF in the high latitude SLP field expansion, demonstrates that there were two different periods: its resemblance in 1950–1995 and similarity occurred during last decade (Fig. 7). Both figures (Figs. 6 and 7) give substantial support to above assumption that rapid ice melting leads to fundamental changes in the atmospheric circulation regimes in Northern Asia.

Changes in atmospheric circulation regimes

Some experts (e.g. Wu et al. 2005) consider Atlantic water warming and ice extent reduction as major causes of recent changes in atmospheric circulation regimes in Northern Eurasia: appearance of long-lived low atmospheric pressure patterns during warm part of year and a high ones – during cold period over Arctic Shelf Seas. Deepest SLP depression was observed over Northern Siberia in September 2005 and October 2006 (Pokrovsky 2006). Low atmospheric pressure anomaly in early autumn led to appearance of a more strong meridian flow and as a consequence to delay in autumn development in Northern Eurasia. Extremes in anomalies of atmospheric pressure field, which spread over vast territory, prevents a normal zonal atmospheric flow across Siberia from west to east and can cause a flow of opposite direction in Eastern and Western Siberia. Inflow of warm and humid air masses from Pacific Ocean and South-East Asia is a main reason of sudden spring warming in Eastern Siberia. Catastrophic flood in Lena river basin, which was occurred in May 2001, is an example of dangerous consequence of circulation regime development related to a negative pressure anomaly. Extreme low and vast SLP anomaly last September–October (2006) caused a huge vortex spread over most part of Northern Asia. A winter of 2005/2006 demonstrated the extreme high atmospheric pressure and height field anomalies in troposphere, which blocked a normal zonal flow in Northern Eurasia and generated intensive cold air outbreaks to Eastern/Southern Europe and to Central Asia. As a result, a winter of 2005/2006 was most severe among others during last 50 years.

Modulation of the surface air temperature

Final target of our study was evolving of the *surface air temperatures (SAT)* in some areas of Northern Asia during last century. We selected several sites located in neighborhood of Kara and Laptev Seas. Figure 8 demonstrates a close link

between AMO trend (Fig. 1) and SAT autumn trend for one of North Siberian stations. The SAT trend reveals the same major features: increasing till 1940s and decreasing till 1970s.

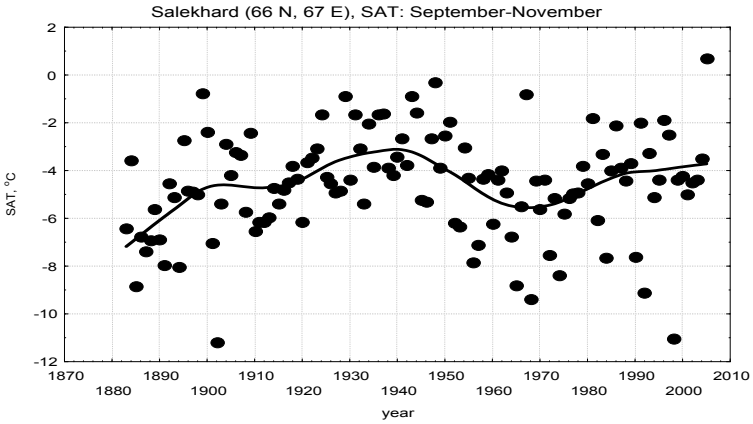

Fig. 8. The September–November SAT (°C) trend for a site Salekhard (66° N, 67° E).

Discussion and conclusion

Presented results proved that the Atlantic-Arctic climate system components are closely interrelated. Moreover, fluctuations in the Atlantic SST modulated corresponding oscillations in many other subsystems: Eastern Arctic ice extent, land surface pressure, SST in shelf seas, surface air temperatures in North Asia.

The key to the new climate change outlook is the natural cycle of ocean temperatures called the Atlantic Multidecadal Oscillation (AMO), which is closely related to the warm currents that bring heat from the tropics to the shores of Europe. The cause of the oscillation is not well understood, but our study proved that the cycle appears to come round about every 60–70 years. It may partly explain why temperatures rose in the early years of the last century before beginning to cool in the 1940s. One message from our study is that in the short term, you can see changes in the global mean temperature that you might not expect given the reports of the Intergovernmental Panel on Climate Change (IPCC). But in the long term, radiative forcing (the Earth's energy balance) dominates.

Modeling of climatic events in the oceans is difficult, simply because there is relatively little data on some of the key processes, such as the meridional overturning circulation (MOC) – sometimes erroneously known as the Gulf Stream – which carries heat northwards in the Atlantic. Only within the last few years have researchers begun systematically deploying mobile floats and tethered buoys that will, in time, tell us how this circulation is changing. Looking forward, our results can suggest a weakening of the MOC and a resulting cooling of north Atlantic

waters, which will act to keep temperatures in check around the world, much as the warming and cooling associated with El Nino and La Nina in the Pacific bring global consequences.

Recent observing data have led to a conclusion that a slowly fluctuating oscillation in Pacific Ocean temperatures had shifted into its cool phase, a condition that is also thought to exert an overall temporary cooling of the climate. Of course, these natural variations can also amplify warming, and that is likely to happen in future decades on and off as well. The global climate will continue to be influenced in any particular decade by a mix of natural variability and the building greenhouse effect.

This projection does not come as a surprise to climate scientists, though it may to a public that has perhaps become used to the idea that the rapid temperature rises seen through the 1990s are a permanent phenomenon. We have always known that the climate varies naturally from year to year and decade to decade. We can expect man-made global warming to be superimposed on those natural variations; and this kind of research is important to make sure we don't get distracted from the longer term changes that will happen in the climate (as a result of greenhouse gas emissions). It should also help the public and policy makers understand that a cool phase does not mean the overall theory of human-driven warming is flawed.

No doubt we need to have more data from the deep ocean, and we don't have that at present. But imagine the payoff of knowing with some certainty what the next 10 years hold in terms of temperature and precipitation – the economic impacts of that would be significant.

Acknowledgements

NATO ARW provides a financial support for the conference participation and publication of this proceedings volume.

References

Belchansky GI, Douglas DC, Eremeev VA, Platonov NG (2005) Variations in the Arctic's perennial sea ice cover: A neural network analysis of SMMR-SSM/I data, 1979–2004. Geophys Res Lett, 32, L09605, doi:10.1029/2005GL022395

Cleveland WS (1979) Robust locally weighted regression and smoothing scatterplots. J Am Stat Assoc, 74, 829–836

Enfield D, Mestas-Nunez A, Trimble P (2001) The Atlantic multidecadal oscillation and its relation to rainfall and river flows in the continental US. Geophys Res Lett, 28, 2077–2080

Goupillaud P, Grossman A, Morlet J (1984) Cycle-octave and related transforms in seismic signal analysis. Geoexploration, 23, 85–102

Gray ST, Graumlich LJ, Betancourt JL, Pederson GT (2004) A tree-ring based reconstruction of the Atlantic Multidecadal Oscillation since 1567 AD. Geophys Res Lett, 31, L12205, doi:10.1029/2004GL019932

Knight JR, Allan RJ, Folland CK, Vellinga M, Mann ME (2005) A signature of persistent natural thermohaline circulation cycles in observed climate. Geophys Res Lett, 32, L20708, doi: 10.1029/2005GL024233

Pokrovsky OM (2006) Recent Changes in atmospheric circulation regimes over northern Eurasia and suggestions to redesign the RAOB network. Proceedings of the Second THORPEX International Scientific Symposium, WMO/TD, 1355, 234–235

Pokrovsky OM, Timokhov LA (2005) The circulation regimes in the Arctic Ocean and the climate change in Northern Hemisphere. Proceedings of the Six International Conference on Global Change: Connection to Arctic (GCCA-6), Dec 12–13, 2005, Published by University of Tsukuba, Japan, 74–77

Pokrovsky OM, Makhotkina EL, Pokrovsky IO, Ryabova LM (2004) Land surface radiation budget response to global warming: Case study for European and Asian radiometric network. Proceedings of the ACIA International Scientific Symposium on Climate Change in Arctic, Reykjavik, Published by AMAP, Paper N 3.3, 1–5

Polyakov I, Johnson MA (2000) Arctic decadal and interdecadal variability. Geophys Res Lett, 27, 4097–4100

Polyakov IV, Alekseev GV, Bekryaev RV, Bhatt US, Colony R, Johnson MA, Karklin VP, Walsh D, Yulin AV (2003) Long-term ice variability in arctic marginal. Seas J Climate, 16, 2078–2075

Sutton RT, Hodson DLR (2005) Atlantic Ocean forcing of North American and European summer climate. Science, 309, 115–118

Tikhonov AN (1963) Inverse problem solution by regularization method. Rep Soviet Acad Sci, 153, N 1, 49–53 (in Russian)

Wahba G (1985) A comparison of GCV and GML for choosing the smoothing parameter in the generalized spline smoothing problem. Ann Stat, 13, 1378–1402

Wu B, Wang J, Walsh JE (2005) Dipole forcing and Arctic Sea ice motion. J Climate, 19, 210–225

Mesoscale atmospheric vortices in the Okhotsk and Bering Seas: results of satellite multisensor study

Leonid M. Mitnik

V.I. Il'ichev Pacific Oceanological Institute, Far Eastern Branch, Russian Academy of Sciences, Vladivostok, Russia, mitnik@poi.dvo.ru

Abstract

Winter mesoscale cyclones (MCs) are frequently formed over the northern Asian Marginal Seas. They are often associated with precipitation and severe winds causing ice drift and serious disturbance in fishery and transport operation at the sea. Mesocyclones are difficult to forecast because of their rapid evolution and movement. Climatological occurrence of mesoscale vortices in various areas is still poorly understood. They were investigated mainly in the Northern Atlantic Ocean, as well as in Gulf of Alaska and the Japan Sea in the Pacific Ocean. Favorable conditions for their development are also in the Bering and Okhotsk Seas and to the east of Kamchatka where MCs are frequently observed on satellite images. However, conventional network is here sparse and the published information on MCs is too limited. Thus the main sources of quantitative spatial data to examine these systems are satellite observations and fields of geophysical parameters retrieved from measurements conducted by various satellite sensors. The MCs were detected by screening Envisat ASAR archive images acquired over the Northwest Pacific in 2002–2006. High-resolution ASAR images of selected MCs were compared with satellite visible and infrared imagery, QuikSCAT-derived wind fields, surface analysis and upper-air analysis as well as with Aqua AMSR-E-derived fields of total atmospheric water vapor content V, total cloud liquid water content Q and wind speed W.

Introduction

Any cyclone to the north of the polar front which divides cold air to the north and warm air to the south, and the size of which less than 2,000 km is defined as a mesocyclone. Mesocyclones form over the sea during winter months when cold air mass moves across relatively warmer water. Polar lows, the most intensive MCs, are considered as a subtype. Up-to-date definition states: "A polar low is a small, but fairly intense maritime cyclone that forms poleward of the main

J.C.J. Nihoul and A.G. Kostianoy (eds.), *Influence of Climate Change on the Changing Arctic and Sub-Arctic Conditions*,

baroclinic zone (the polar front or other major baroclinic zone). The horizontal scale of the polar low is approximately between 200 and 1,000 km and surface winds near or above gale force" (Rasmussen and Turner 2003). (Some may span as little as 100 km). MCs are not often noted on the weather charts issued by local weather bureaus due to their small scales, short life time (typically between 12 and 36 h) and development in remote data sparse regions.

Satellites continue to be the most important source of data for study weather systems including mesocyclones especially for data-sparse regions. Analysis of satellite visible and infrared images revealed two main cloud patterns accompanying the polar lows: comma-shaped cloud patterns and spiral ones. Spiral polar lows have considerable similarity to tropical cyclones including the presence of a clear eye at the centre of the cloud vortex and a warm core. It is these features explain appearance of the term "arctic hurricane" as applied to polar low (Emanuel and Rotunno 1989).

Climatology

Individual polar lows can have fluxes of heat of up to 1,000 W/m^2 (Shapiro et al. 1987) that could trigger downward convection in the ocean. In connection with this the frequency of occurrence of mesocyclones, in particular, polar lows should be investigated to estimate the possible climatological importance of polar lows. Cold air vortices and polar lows occur in areas where cold air has an opportunity to flow over a water surface. Additionally, polar lows are most often associated with an upper-level cold core low or cold upper trough. Ice cover charts produced for example by National Snow Ice Data Center NSICD (http://www.nsidc.org/) and Sea Surface Temperature (SST) produced by several centers in combination with atmospheric characteristics can be used to gain an insight on the geographic and seasonal variations of areas favorable for MC development. Information on occurrences of MCs and PLs covers not all favorable areas.

The most detailed investigation of polar MCs was carried out for the Northeast Atlantic Ocean (Condron et al. 2006). Authors used the 40-year European Centre for Medium-Range Weather Forecasts (ECMWF) Re-Analysis dataset (ERA-40) to detect automatically MCs in mean sea level (MSL) pressure and 500-hPa geopotential height. It was mentioned that the ERA-40 provides some representation of features of scale ~125–500 km and accurate representation of features of scale >500 km. An overall total of 11,383 cyclone centers were revealed in the MSL pressure reanalysis (40 cyclones per 125,000 km^2) and their density distribution was constructed. The ERA-40 results for 2-year period (from 1 October 1993 to 30 September 1995) were compared to MCs found on NOAA AVHRR infrared images (Harold et al. 1999). 5370 mesoscale cloud patterns observed in more than one satellite image were selected for comparison. It was shown that MCs are under-represented in current reanalysis datasets such as

ERA-40. Up to 80% of cyclones larger than 500 km were detected in MSL pressure, up to 40% for 250-km-scale cyclones and only 20% for 100-km-scale cyclones (Condron et al. 2006).

At the same time a modal size of AVHRR-derived MCs was 100–150 km (Harold et al. 1999). The similar conclusion follows from the statistical analysis of polar mesoscale cyclones (PMCs) over the North European Basin using cloud cover distribution data for 1981–1995 (Mokhov et al. 2007). It was shown that the cumulative frequency distribution of mesocyclones is well approximated by an exponential function in a size range from 50 to 400 km. This result suggest that a substantial amount of heat, moisture and momentum flux at the air-sea interface is likely may be missing from the reanalysis (Condron et al. 2006). It is evident that there is a need both for a parameterization of MC activity below 500 km and for detailed satellite-based quantitative study of MCs to correctly model how the atmosphere affects rates of deep-water formation and the climate system.

Climatology of an important group of polar lows, the reverse-shear systems (Duncan 1978; Rasmussen and Turner 2003) was studied by Kolstad (2006). The ERA-40 reanalysis data set and two suggested criteria (reverse thermal shear and low static stability in the lower atmosphere) the wind direction at either 775 or 850 hPa relative to thermal wind) were used to quantify the climatological distribution of conditions favorable for development of the reverse-shear polar lows. Spatial distribution of the percentage of time during November to March from 1960–1961 to 1990–2000 with polar low potential shows a distinct maxima not only in the Norwegian Sea reaching into the Bering Sea (in a good agreement with conclusion by Noer and Ovhed (2003)) and to the west and south-west of Iceland but also in the North Pacific, in the Bering and Okhotsk Seas (Kolstad 2006).

In the Pacific Ocean, several detailed investigations of MCs and polar lows were carried out in the Gulf of Alaska (Businger 1987; Douglas et al. 1991; Shapiro et al. 1987; Young et al. 2005), in the Bering Sea (Bresch et al. 1997; Friedman et al. 2001; Young et al. 2005) and in the Japan Sea (Fu et al. 2004a; Tsuboki and Asai 2004; Ninomiya 1989 and papers cited there). Polar low climatology was studied in the Gulf of Alaska (Businger 1987). Climatology in the Northern Pacific was investigated by Yarnal and Henderson (1989) who interpreted satellite imagery for seven seasons between November and March, 1976/77–1983/84. Distribution of instant occlusion was determined: they concentrated in a large area in the Northeast Pacific and in two small areas in the Northwest Pacific where they were observed rarely. From above it follows that climatology of MCs, in particular, PLs was not investigated in details especially in the Western Bering Sea and in the Okhotsk Sea in spite of these weather systems are typical here that follows from screening of NOAA AVHRR and Terra and Aqua MODIS images.

Satellites and sensors

The potential of satellite retrievals for PL studies was demonstrated in many papers (Claud et al. 1993, 2004; Carleton et al. 1995; Heinemann 1995; Heinemann and Claud 1997; McMurdie et al. 1997; Mitnik et al. 1996, 2004, 2007; Moore and Vonder Haar 2003; Rasmussen and Turner 2003). Registration of warm core in polar lows from the measurements of brightness temperature at frequency 53.6 GHz by the Advanced Microwave Sounding Unit on a board of NOAA-15 (Moore and Vonder Haar 2003) and obtaining detailed distribution of sea surface wind from the X-band Real Aperture Radar (RAR) images acquired from Okean series satellites (Kalmykov 1996) were especially important to understand better PL structure and development. Strong correlation of the surface wind and cloudiness fields was revealed by joint analysis of RAR and infrared images of the mesoscale cyclones and cold air outbreaks with resolution of 1–2 km (Mitnik 1990; Mitnik et al. 1996).

Appearance of new passive and active microwave and optical sensors installed on recently launched satellites such as QuikSCAT, Terra, Envisat, Aqua and ADEOS-II stimulated their application for detailed study of structure and evolution of MCs (Chunchuzov et al. 2000; Gurvich et al. 2008; Mitnik et al. 2004; Sikora et al. 2000; Vachon et al. 2000; Young et al. 2005). The West Bering Sea and the Okhotsk Sea, for which information on mesoscale marine weather systems is very limited, were chosen for the case studies of MCs taking into account the future climatological compilation. In this study, a combination of the following three microwave sensors is used: the Advanced Microwave Scanning Radiometer (AMSR-E) of the Aqua satellite, the Advanced Synthetic Aperture Radar (ASAR) of Envisat satellite and the SeaWinds scatterometer of QuikSCAT. Taking into account an Envisat ASAR swath width 405 km the main attention was given to MCs the size less than 500 km. It corresponds to meso α (200–2,000 km) and meso β (20–200 km) scales (Orlanski 1975). Visible and infrared (IR) images were obtained from the Terra and Aqua spectroradiometer MODIS. All these sensors possess by the higher spatial resolution and the presence of additional spectral channels compare to similar instruments launched earlier such as SSM/I, ERS scatterometer, AVHRR. Due to the small-scale characteristics of polar lows, the reduction in spatial truncation errors provided by increased resolution is of primary importance. Optical images give an insight into condition on the upper boundary of the marine boundary layer of the atmosphere whereas the radar images – on its lower boundary. Characteristics of the whole layer can provide passive microwave measurements. This acquires distinctive importance in relation to the progress in high resolution simulation of the structure of mesoscale atmospheric vortices restoring fields of total water vapor content, snow content, liquid water content (Fu et al. 2004b).

The Aqua AMSR-E measures the brightness temperatures T_Bs at six frequencies ν = 6.925, 10.65, 18.7, 23.8, 36.5 and 89.0 GHz with vertical (V) and horizontal (H) polarization. Instant field of view (IFOV) increases with the decrease of frequency from approximately 3.5 × 6 km (cross track x along track) at 89.0 GHz to approximately 43 × 75 km at 6.925 GHz. AMSR-E antenna beam scans within swath width of 1,450 km, incidence angle is 55°. Sensitivity of microwave channels is ≈0.34 K at 6.925 GHz, ≈1.2–1.4 K at ν = 89.0 GHz and 0.6–0.7 K at other frequencies (Kawanishi et al. 2003).

AMSR-E measurements allow to visualize the structure of cloud liquid water content, precipitation, and surface winds, to reveal ice clouds, to retrieve fields of the total water vapor content V, total cloud liquid water content Q and sea surface wind W, to assist with the detection of developing mesoscale cyclones circulation centers, etc. Retrieval algorithms used for MC study were developed using simulated brightness temperatures (see below).

Envisat ASAR operates at C-band (wavelength is 5.6 cm). Wide swath mode regime (swath width is 405 km) is optimal for MC study. Spatial resolution of ASAR data is 75 × 75 m (Envisat Special Issue 2001). ASAR images map accurately the location of atmospheric fronts, the cyclone centers, reveal the fine-scale and mesoscale features of sea surface wind field in various weather systems, in the areas of organized roll and cell convection including regions where this convection does not expressed in cloud field.

QuikSCAT scatterometer provides indirect measurements of winds at the sea surface and is a powerful tool to assist in both the detection and intensity of polar low circulations. QuikSCAT is capable of measuring wind speeds between 0 and 20 m/s with a 2 m/s accuracy, and has a directional accuracy of about 20°. One thousand and eight hundred kilometer swath during each orbit provides ≈90% coverage of Earth's oceans every day. QuikSCAT-derived wind fields can be downloaded with a resolution of 25 × 25 or 12.5 × 12.5 km from http://manati.orbit.nesdis.noaa.gov/quikscat/. Polar areas are covered completely.

Simulation of the AMSR-E brightness temperatures and retrieval algorithm development

Microwave radiometers measure the outgoing emission of the underlying surface–atmosphere system in several frequencies ν and polarizations. The measured parameter is antenna temperature (brightness temperature $T_B(\nu)$ after calibration). Contribution of the underlying surface in the measured $T_B(\nu)$ is defined by the relation $T_B(\nu) = T_S\, \kappa(\nu)$ where T_S is the surface temperature and κ is the emissivity. For the frequencies between about 7 and 90 GHz used by AMSR-E, the emissivity of the sea surface can be calculated quite accurately (especially for calm water) from a model describing spectrum of the dielectric permittivity of water. The behavior of $\kappa(\nu)$ for the various forms of ice and snow is less accurately known,

and therefore often has to be empirically measured. IFOV of AMSR-E changes approximately between 5 and 60 km, implying that many different components of snow/ice/water can be present in one measurement. Atmospheric contribution to the $T_B(\nu)$ depends mainly from the values of total cloud liquid water content Q and total water vapor content V. Variable weather conditions are responsible for large $T_B(\nu)$ variations especially over the open ocean. A developed program of microwave radiative transfer allows computing the brightness temperatures $T_B^{V,H}(\nu)$.

The radiative transfer equation (RTE) is the basis for the development of retrieval algorithms of the ocean surface and atmospheric parameters. Modeling of AMSR-E measurements over the open ocean was carried out with an updated microwave radiative transfer program. The program and calculations of the brightness temperatures were described in (Mitnik and Mitnik 2003). Some modifications were made in the program. In particular, formulas for dielectric permittivity of saline and fresh water which are used in calculation of the sea surface emissivity and cloud absorption respectively were taken from (Meissner and Wentz 2004). Dependence of the sea surface emissivity on wind speed was also corrected in accordance with (Meissner and Wentz 2004). A contracted form of the RTE can be written as:

$$T_B^{V,H}(\nu,\theta,T_s,W) = [\kappa_w^{V,H}(\nu,\theta,T_s,W)T_s]\ \exp[-\tau(\nu)\sec\theta] + T^{\uparrow}_{Batm}(\nu,\theta) + T^{\downarrow}_{Batm}(\nu,\theta) \times$$
$$[1 - \kappa_w^{V,H}(\nu,\theta,t_s,W)]\exp[-\tau(\nu)\sec\theta] + T_{cos}[1 - \kappa^{V,H}(\nu,\theta,t_s,W)]\exp[-2\tau(\nu)\sec\theta] \quad (1)$$

where θ is an incidence angle, T_s is sea surface temperature (SST), W is sea surface wind speed, $\kappa_w^{V,H}$ is the water surface emissivity at the vertical (V) and horizontal (H) polarization, $T_s = t_s + 273.16$, where t_s is SST in Celsius degrees, $\tau(\nu)$ is the total atmospheric absorption, $T^{\uparrow}_{Batm}(\nu,\theta)$ and $T^{\downarrow}_{Batm}(\nu,\theta)$ are the upwelling and downwelling brightness temperatures of the atmosphere, respectively, $T_{cos} = 2.7$ K is brightness temperature of the cosmic background radiation.

To model atmospheric conditions observable in winter over the Okhotsk and Bering Seas the radiosonde (r/s) database was built up. Only r/s issued when SST $t_S \le 2$°C were included in the database. Total 410 cases measurements were selected: 69 sets from research vessels and 341 sets from six polar coastal and island stations. Every set consists of radiosonde, meteorological data (wind speed and direction, forms and amount of clouds) and the values of sea surface temperature. In the database, the total atmospheric water vapor content V varied from 0.63 to 24.5 kg/m^2, total cloud liquid water content Q did not exceed 0.3 kg/m^2 and wind speed $W \le 18.0$ m/s. R/s atmospheric profiles were complimented by the cloud liquid water content profiles as in (Mitnik and Mitnik 2003).

The $T_B^{V,H}(\nu)$, the oceanic and atmospheric contributions to $T_B^{V,H}(\nu)$, total absorption by atmospheric gases and clouds and other parameters were computed by numerical integration of the RTE for the whole input database. For each r/s, the T_Bs (ν) were computed for four values of sea surface wind and for r/s with cloudiness for two profiles of cloud liquid water content. As a result, the

dataset used for the algorithm development comprised of 2,730 scenes. The randomly Gaussian distributed radiometer noises were added to T_Bs. The standard deviation of the radiometer error distribution was set equal to the noise level 0.5 K for all AMSR-E channels. Spectra of $T_B^{V, H}$ (ν) computed for four r/s differing in V and Q values are presented in Fig. 1. Their analysis shows that the changes of atmospheric parameters that are observed during MCs passing result in the significant changes of the brightness temperatures compare to radiometer sensitivity.

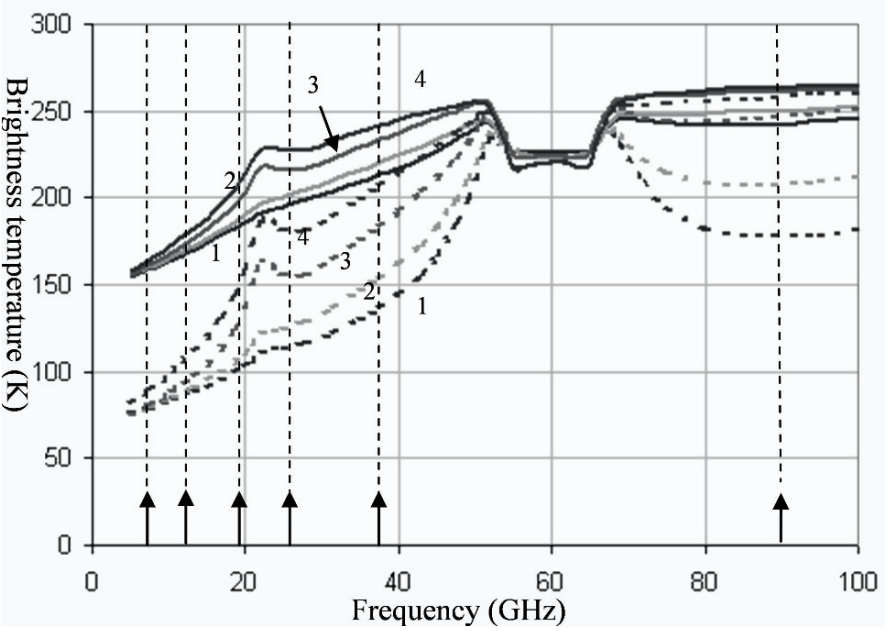

Fig. 1. Spectra of the brightness temperature of the atmosphere-ocean system with vertical (solid lines) and horizontal (dotted lines) polarization computed for cloudless atmosphere (1) and three cloudy atmospheres (2–4) with various values of total water vapor content V and total cloud liquid water content Q. Arrows mark AMSR-E frequencies. 1 – V = 2.8 kg/m^2, Q = 0 kg/m^2; 2 – V = 3.6 kg/m^2, Q = 0.14 kg/m^2; 3 – V = 13.8 kg/m^2, Q = 0.26 kg/m^2; 4 – V = 19.3 kg/m^2, Q = 0.56 kg/m^2.

Several versions of V and Q retrieval algorithms were constructed. They include linear and nonlinear regression, physically-based and Neutral Network-based algorithms (Mitnik and Mitnik 2003, 2006; Zabolotskikh et al. 2005, 2007). Fields of V and Q are important characteristics of the whole boundary layer as opposite to the visible and infrared images which represent a situation at the upper boundary of the marine boundary layer of the atmosphere and to the radar images, which represent a situation at its lower boundary. Knowledge of V and Q distributions in the area of origin and evolution of MCs can be used to improve their forecast as well as to validate the present high resolution models describing development of

the marine boundary layer of the atmosphere during cold air outbreaks (Liu et al. 2004, 2006) and polar lows (Fu et al. 2004a, b).

Data

The main sources of quantitative spatial data to examine MCs are satellite observations and fields of geophysical parameters retrieved from measurements conducted by various satellite sensors. The MCs were detected by screening wide swath mode ASAR archive images acquired over the Northwest Pacific in 2002–2007. The images were downloaded from an ESA web site (http://eoli.esa.int/). They represent the so-called quick look (QL) images and have the strongly reduced spatial and radiometric resolution. In spite of this they are valuable source of information on the features of spatial organization of the cyclones, the location of their centers, the areas of high surface winds, wind direction, the presence of sea ice. The ASAR precision processed images (PRI) have a spatial resolution of 75 × 75 m in wide swath mode that allowed studying the fine details of surface wind. The ASAR images cover the Japan, Okhotsk and Bering seas and the northwest Pacific Ocean between 40–62° N and 130–180° E. More than 3,000 QL and 320 PRI images are now in our database. SAR images of the MCs in different stage of development were selected for the study.

Each ASAR image of MC covering it completely or partly was compared with the microwave brightness temperatures measured by Aqua AMSR-E and ADEOS-II AMSR provided by EORC JAXA (http://sharaku.eorc.jaxa.jp/AMSR/index_e.htm/), with QuikSCAT-derived wind speed fields downloaded from website http://manati.wwb.noaa.gov/quikscat/ as well as with the Aqua and Terra MODIS visible and thermal infrared (IR) images downloaded from web site http://rapidfire.sci.gsfc.nasa.gov/, and the NOAA AVHRR images available from several web sites. Satellite images were compared also with the surface analysis maps and ice condition maps of the Japan Meteorological Agency (AMS).

Detailed quantitative analysis of structure and parameters of MCs was carried out to demonstrate the high potential of the present satellite sensors providing quantitative information on various marine weather systems. The presence of growing quantitative data can be used in the future for construction of more reliable climatology of MCs, which will allow estimating fields of atmospheric water vapor, cloud liquid water, sea surface wind, impact of wind field on the sea surface, etc. Earlier climatological compilations were based or on satellite visible/IR images showing only cloud structure (Yarnal and Henderson 1989; Harold et al. 1999) or on Re-Analysis dataset (ERA-40) that permits to reveal predominantly the large MCs (Condron et al. 2006; Kolstad 2006).

Mesoscale cyclones

Okhotsk Sea

3 January 2004 (Fig. 2). The most remarkable features visible on the Envisat ASAR image and shown in Fig. 2c are two cyclonic mesoscale lows located to the west of Kamchatka coast. Convective vortices are also well distinguished in a field of cloudiness on NOAA AVHRR, Terra and Aqua MODIS and GOES-9

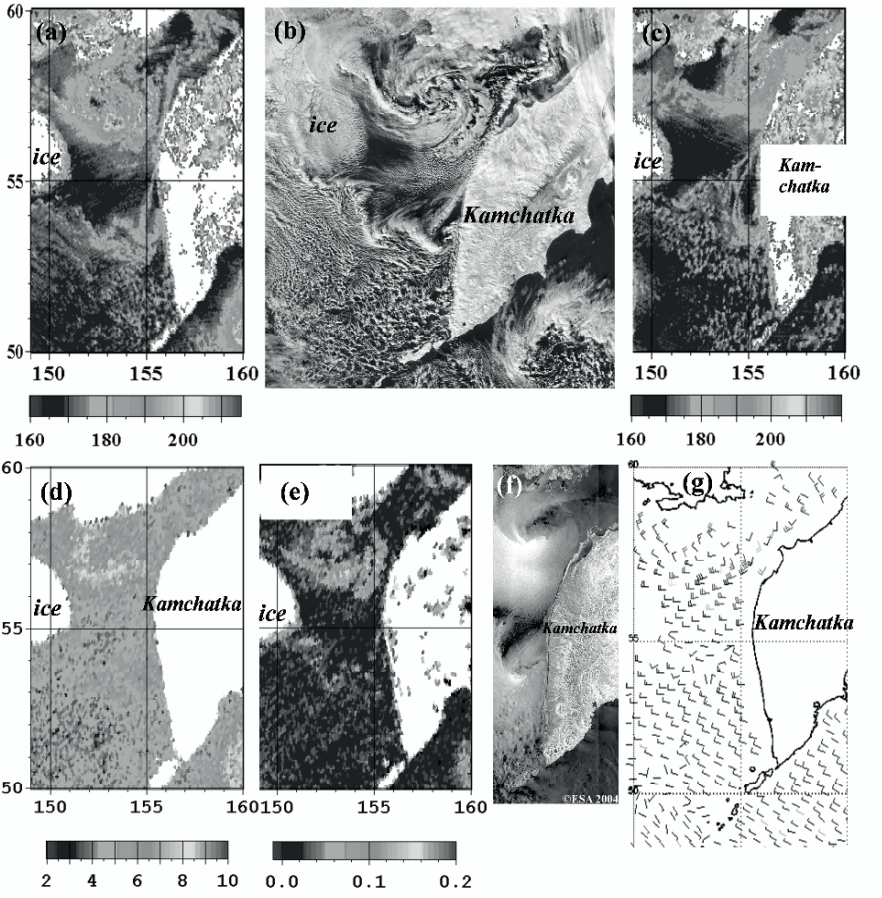

Fig. 2. Mesoscale cyclones over the Okhotsk Sea to the west of Kamchatka on 3 January 2004: (**a**) and (**c**) 89-GHz, H-polarization Aqua AMSR-E brightness temperature (Kelvin degrees) at 02:25 (**a**) and at 16:15 UTC (**c**); (**b**) Aqua MODIS visible image at 02:25; (**d**) total atmospheric water vapor content (in kg/m^2) and (**e**) total cloud liquid water content (in kg/m^2) retrieved from 23.8- and 36.5-GHz, V-polarization brightness temperatures at 02:25 UTC; (**f**) Envisat ASAR image at 11:13 UTC and (**g**) QuikSCAT-derived wind field at 08:37 UTC.

images. Aqua MODIS visible image taken at 02:25 UTC i.e. about 9 h before the Envisat data acquisition is given in Fig. 2b. Water clouds, increased total water vapor content and wind speed variations are responsible for lows' detection by Aqua AMSR-E before (at 02:25 UTC, Fig. 2a) and after (at 16:15 UTC, Fig. 2d) Envisat ASAR acquisition. Cyclonic circulation was also registered by QuikSCAT scatterometer (Fig. 2e). Maximum wind speed (12–15 m/s) was measured to the south of the large low. This is consistent with radar backscatter (brightness) variations on ASAR image. The total atmospheric water vapor content V and total cloud liquid water content Q were retrieved from T_B(23.8 V) and T_B(36.5 V) (Mitnik and Mitnik 2003). The maximum V and Q values located to the southeast, east and northeast from the cyclone center in the spiral bands' area reached 7–9 kg/m^2 and 0.12–0.14 kg/m^2 correspondingly. The width of the bands in Q-field was about 20–30 km. Typical values in the cyclonic eddy area were lower: V = 5–6 kg/m^2 and Q = 0.04–0.06 kg/m^2. Around the eddy, the V values decreased till 3.5–5 kg/m^2. At the eddy center V = 3.7–4.5 kg/m^2.

On the surface analysis map of the JMA for 3 January at 00:00 UTC the northern low the size of ≈300 km was outlined by 1,004-mb isobar and 12 h later it was outlined by 1,008-mb isobar. The southern low the size of ≈120 km was not mapped.

It is the last eddy in a chain extending from the ice edge in the central part of the Okhotsk Sea to the western Kamchatka coast. The whole chain was depicted in the cloud field on several satellite visible and IR images taken on 2–4 January. The chain is the northern boundary of the area with the mesoscale convective cells and rolls. They manifest themselves both in cloud field (Fig. 2b) and in field of the sea surface roughness (Fig. 2c). Lows are very dynamic structures and the best correspondence between the images taken by various sensors from different satellites is accomplished at small difference in data acquisition time. On ASAR image for 3 January 2004 at 11:12 UTC, the lows manifest themselves as the areas of the increased brightness (increased wind speed) spiraling around dark area (low wind speed) in their centers. The spiral structure of the eddy is detected also on MODIS and AMSR-E $T_B(\nu)$ images depicted in Fig. 2a, b, d. The centers of the eddy spirals look dark both on the ASAR image due to weak winds and on the NOAA and MODIS images due to low amount of clouds. The bright area south and southwest of the northern eddy center on the ASAR image results from severe winds. Wind speed decreased as the distance from the center increases. The width of this area is about 250 km. The brightest spiral bands with sharp wavelike edges imbedded in the area mark the atmospheric fronts' position near the sea surface. The width of transition zone dividing the area with low and high winds does not exceed 1–2 km. Very likely that the highest surface winds coincide with the convective cloud bands on MODIS image or somewhat shifted relative to them. The cloud bands are characterized by the increased brightness due to intense developed convection. AMSR-E-derived wind speed reached 15 m/s in a circle around the center and in the area south of it.

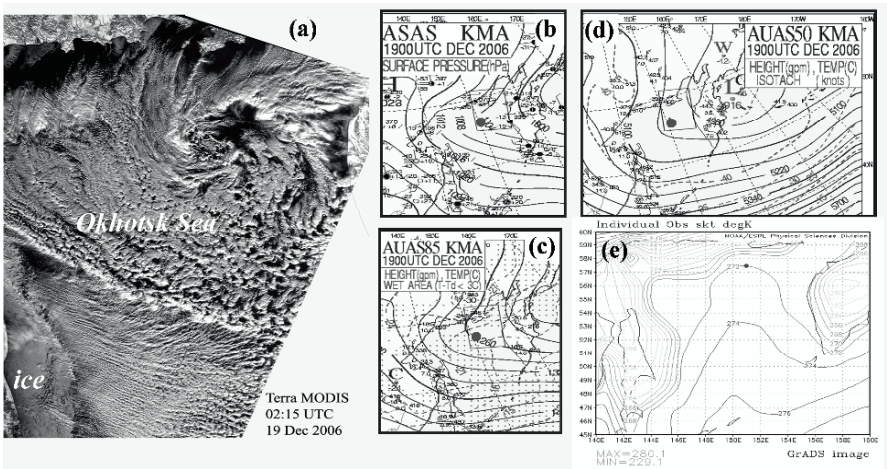

Fig. 3. Mesoscale cyclone in the Okhotsk Sea on 19 December 006: (**a**) Terra MODIS visible image acquired at 02:15 UTC, (**b**) surface analysis map, (**c**) and (**d**) thermobaric fields at 850 mb (**c**) and at 500 mb (**d**) of the KMA at 19 UTC and (**e**) reanalysis map of underlying surface temperature (isotherms are shown through 2 K) at 00 UTC. Red dot marks the center of mesocyclone.

19 December 2006 (Figs. 3–5). Envisat ASAR image acquired at 00:13 UTC (Fig. 5a) shows cyclonic eddy the size of approximately 400 km, which was not revealed on the surface analysis map of the Korean Meteorological Administration (KMA) (Fig. 3b). Terra MODIS visible image (Fig. 3a) taken in 2 h after ASAR image depicts its cloud system. The MC was formed to the northeast from intense cold air outbreak over the Okhotsk Sea near stationary tropospheric trough (Fig. 3c–e). Cloud rolls typical for cold outbreak are seen to the south-west of the trough (Fig. 3a). Low-gradient thermal trough that corresponds to the high-altitude trough spreads over the whole Okhotsk Sea (Fig. 3d). The cold center at 500 hPa absolute topography map AT500 near the northeast Kamchatka coast was outlined by –45°C isotherm. Thermobaric field at AT850 map (Fig. 3c) indicates the presence of baroclinic instability of the boundary layer of the atmosphere in a northern part of the sea, which was formed as a result of the large thermal contrasts between very cold land and the relatively warm sea surface. The largest closeness of the isotherms was observed near the coast (Fig. 3e). Axis of the thermal ridge at 850 mb level was directed from the south-east to the north-west. Cold trough coinciding with narrow cloud rows on the visible image extended from continent through the Okhotsk Sea. Still one small cold tongue from continental regions adjoin the northern sea coast, wedged in warmth ridge increasing thermal and baric gradients that favored strengthening northeast winds here. QuikSCAT-derived wind speed in the mesocyclone was 12–15 m/s (Fig. 4a, b).

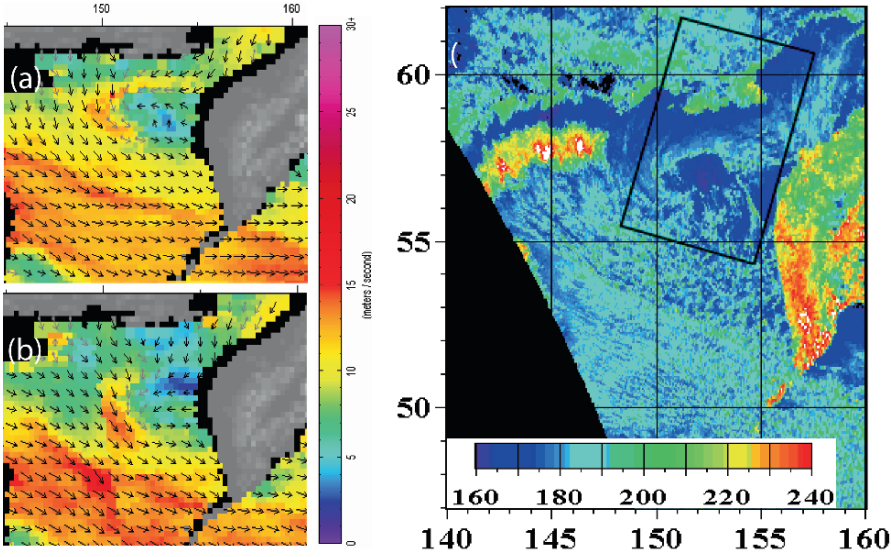

Fig. 4. Mesoscale cyclone over the Okhotsk Sea: (**a**) and (**b**) QuikSCAT-derived wind fields (**a**) on 18 December at 18:48 UTC and (**b**) on 19 December at 08:54 UTC; (**c**) 89-GHz, H-polarization Aqua AMSR-E brightness temperature on 19 December at 02:25 UTC. Dark box marks the boundaries of Envisat ASAR image shown in Fig. 5a.

Configuration and structure of MC cloud system on NOAA-17 AVHRR infrared image and brightness (sea surface wind) field on SAR image acquired with time difference of 8 min are in a good agreement (Fig. 5). Bright area ***1*** in a northern part of MC was caused by strong eastern and northeastern winds. It is confirmed by structure of thermobaric field in the boundary layer of the atmosphere (Fig. 3d). Bands of alternating brightness on SAR image (Fig. 5a), as well as cloud rows on IR image (Fig. 5b) also indicate northeastern wind direction. Disturbances in the area of eddy chain distinguished on visible image are clearly seen along the boundary of wind shift ***2***, which coincides with the internal boundary of a bright cloud band ***A*** on IR image. The size of eddies decreases from 70 to 10 km as the distance to the MC center decreases. Small dark patches ***3***, typical for the eddy centers where winds are weak are clearly seen in several places along wind shift line. Their sizes are approximately 9 × 2 and 5 × 1.5 km. Small-scale cloudless zones in the centers can be revealed on IR image (Fig. 5b) not so clearly due to their small sizes (Gurvich et al. 2008).

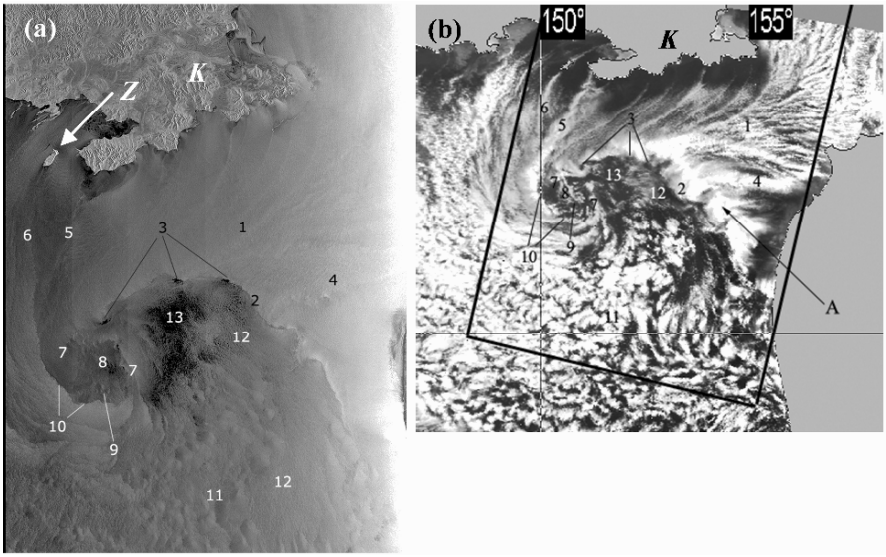

Fig. 5. Mesoscale cyclone over the Okhotsk Sea on 19 December 2006: (**a**) Envisat ASAR image at 00:13 UTC; (**b**) NOAA-17 AVHRR infrared image at 00:21 UTC. Dark lines mark the boundaries of ASAR image. ***K*** – Koni Peninsula, ***Z*** – Zav'yalova Island.

One more bright cloud band ***4***, formed likely as a result of interaction of air flow with mountains higher than 1,000 m extends from Kamchatka to the west. Disturbances of sea surface wind correlated with this cloudiness are small and their contrasts against the background on SAR image are small too. Vortex chain ***5*** extends to the center of MC from the western Koni Peninsula. Its structure manifests itself in brightness variations on SAR image. From this follows, that the organized convection covers the whole boundary layer of the atmosphere from its upper boundary (cloudiness) till the lower boundary (surface wind). A contrast band ***6***, which extends from Zav'yalova Island, is merged with vortex chain ***5***. All cloud bands approach each other and curving anticlockwise form a circle 7 the size of 70–80 km around the almost cloudless cyclone center. These features look as eye wall and eye in typhoon. On the SAR image, a circle-like zone of strong winds fringes the central area with weak winds where imprints of convective cells ***9*** the size of 5–8 km can be distinguished.

Structures ***5***, ***6*** and ***7*** in fields of cloudiness and narrow contrast bands in field of sea surface wind on the SAR image visualize process of isolation of the warmer marine air by cold continental air which curves around it. This phenomenon is similar to warm seclusion in a synoptic-scale cyclone (Sikora et al. 2000; Young et al. 2005; Montgomery and Farrell 1992). The boundary of wind shift ***10*** is identified with seclusion front. Seclusion is one of the factors favorable for formation of warm core in mesoscale cyclones. Bright large rain cells ***11*** are seen on IR image to the south of boundary ***2***. Thin gray-tone very small cells ***12*** are observed farther south up to the boundary ***2***. These cells manifest themselves

clearly on SAR image. Their diameters vary from 10–20 km for large cells to 1–2 km for small ones (Gurvich et al. 2008).

Sharp boundary of vortex-like structure in the field of brightness temperature $T_B^H(89)$ separates dry air in the centre of the cyclone from the surrounding wet air mass (not shown). *Large* rain cells to the south of cyclone are reliably detected: $T_B^H(89)$ increment reaches 43–48 K whereas the small cells almost do not appear due to very low Q values. A dark area ***13*** on SAR image (Fig. 5a) is caused by weak winds that are observed in the region where $V = 3.0$ kg/m^2 and $T_B^H(89) = 160$–170 K. Maximum values $V = 7.5$–9.0 kg/m^2 are marked along bright convective bands. Mesocyclone manifests itself in Q field too: average Q value equals to 0.05–0.07 kg/m^2. Only individual cloud inclusions are characterized by $Q = 0.11$ kg/m^2, suggesting that probability of precipitation is low.

Bering Sea

15 January 2006 (Figs. 6, 7). Small mesoscale cyclone in the southwestern Bering Sea, which was formed in a cold dry air in the rear of another deep cyclone, was detected by Aqua MODIS, Envisat ASAR and QuikSCAT SeaWinds on 15 January 2005. As opposite to the deeper cyclone, it was not revealed in pressure field on the surface analysis map of the JMA (not shown). Cyclone is clearly visible as the spiral-like structure just off the coast.

Commander Islands are seen at the bottom of the images. A cloudless area in the center of the cyclone is its eye (Fig. 6a) where weak winds are observed (Fig. 6b). Open and closed mesoscale convective cells typical for cold air outbreaks are clearly seen to the east of bright convective band both on the daytime (Fig. 6a) and nighttime (Fig. 6c) MODIS images taken with the time difference of 13.5 h.

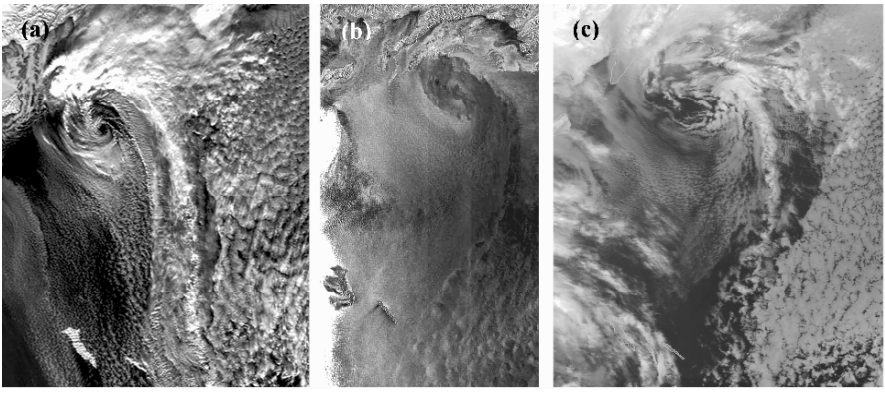

Fig. 6. Mesoscale cyclone over the southwestern Bering Sea on 15 January 2005: (**a**) and (**c**) Aqua MODIS image (**a**) visible at 00:55 UTC and (**c**) infrared at 14:25 UTC; (**b**) Envisat ASAR image at 10:21 UTC.

Circular and crescent imprints of the convective cells in the sea surface roughness as in the lower right of the ASAR image (Fig. 6b) are in close agreement with model calculations (Mitnik 1990, 1992). Several curvilinear features that spiral in towards the eye as well as the small-scale convective cells are distinguished to its southwest and south on all images (Fig. 6).

The cloudless center, convective spiral band, which extends far to the south, the mesoscale linear and cellular features to the east of the band are reliably detected on the AMSR-E 89-GHz image at horizontal polarization having a spatial resolution of 5 × 5 km (not shown). Variations of the brightness temperature $T_B^H(89)$ in the cyclone's area exceed 60 K. From a comparison of MODIS infrared and AMSR-E $T_B^H(89)$ images acquired simultaneously it follows that the maximum $T_B^H(89)$ values (>210 K) are observed in the convective bands near the cyclone's center. The lowest $T_B^H(89)$ values (<170 K) were measured over cloudless area to the south of the center.

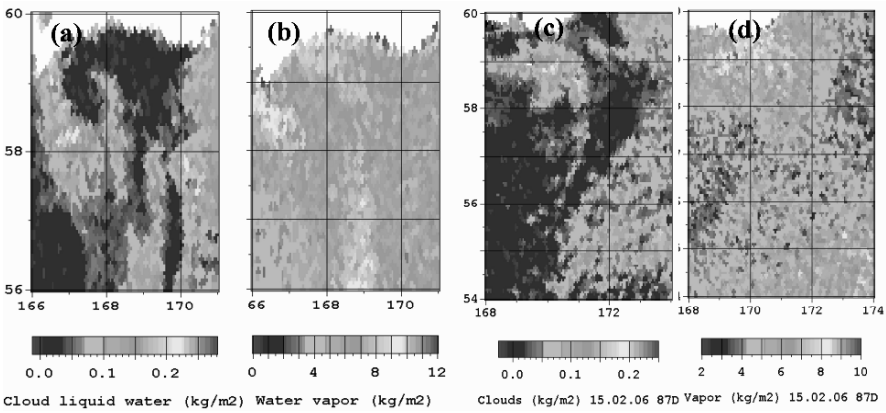

Fig. 7. Fields of total cloud liquid water content (in kg/m^2) (**a**) and (**c**) and total atmospheric water vapor content (in kg/m^2) (**b**) and (**d**) derived from Aqua AMSR-E measurements taken on 15 January 2005 at 00:55 UTC (**a**) and (**b**) and at 14:55 UTC (**c**) and (**d**).

The low is also detected as cyclonic structure in AMSR-E retrievals showing a distinct mesoscale signal in the fields of total cloud liquid water content Q and total water vapor content V (Fig. 7). Fields of Q and V were derived by application of algorithm (Mitnik and Mitnik 2003) to the measured brightness temperatures at 23.8 and 36.5 GHz at vertical polarization. Spiral structure is better expressed at 00:55 UTC (Fig. 7a, b) than at 14:25 UTC (Fig. 7c, d) that very likely reflects dissipation of the cyclone. Analysis of the brightness temperatures at all AMSR-E channels and the results of modeling allows to conclude that probability of precipitation is high in the spiral bands near the center where $Q > 0.15$ kg/m^2. Mesoscale organized convection manifests itself in mesoscale variations of Q and V (Fig. 7c, d).

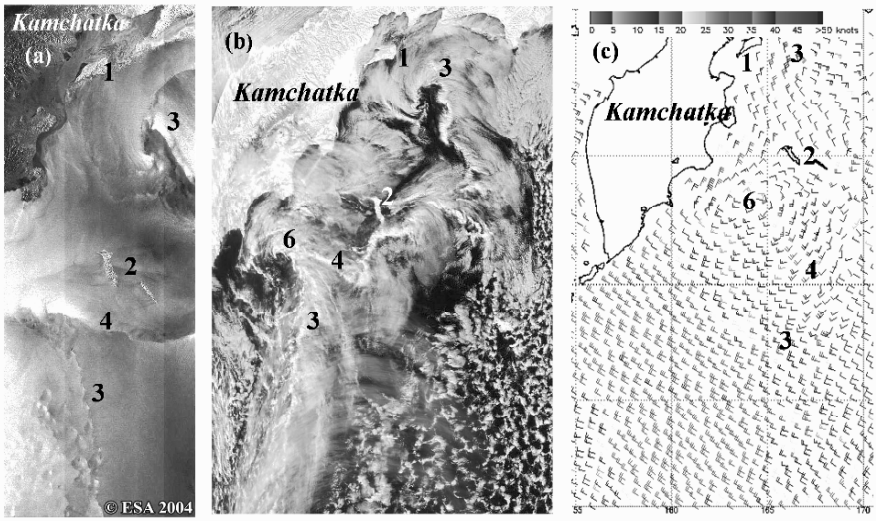

Fig. 8. Mesoscale cyclone over the Southwest Bering Sea on 21 February 2004: (**a**) Envisat ASAR image at 10:21 UTC; (**b**) Aqua MODIS visible image at 01:35 UTC and (**c**) QuikSCAT-derived wind field at 09:09 UTC.

21 February 2004 (Fig. 8). Cold air advection on the warmer sea surface in combination with influence of orography were responsible for intensive convective activity to the east of Kamchatka Peninsula on 21–22 February that was registered by Envisat ASAR and other satellite sensors. Envisat ASAR image acquired on 21 February at 10:34 UTC depicts the well-developed mesoscale cyclone in the Southwest Bering Sea (Fig. 8a). Kamchatka Peninsula, Karaginsky Island 1 and Commander Islands 2 are visible both on ASAR and on Aqua MODIS visible images. In spite of the time difference of 9 h, a good agreement is observed between cloud field and the radar signatures, which are determined mainly by the sea surface wind field. It may be concluded that synoptic situation changed slowly during this period. It follows also from the surface analysis maps of the Japan Meteorological Agency for 00:00 and 12 UTC on 21 February.

The most striking features of the ASAR image are associated with the polar low 3 and with the sharp frontal boundaries 4 and 5 of the second mesoscale cyclone. Its center 6 was located to the south from the first one (Fig. 8b) and to the west of ASAR swath. The second cyclone with the minimum central pressure 990 mb was shown on the weather maps of the JMA as opposite to the first one. The ASAR image illustrates, in detail, the spiral-form structure of the surface wind field around the eye of the low, wave-like features of the frontal boundaries, the zones with the increased wind speed and other features, which were revealed partially earlier (Chunchuzov et al. 2000; Mitnik et al. 1996). The surface wind convergence zones are characterized by sharp wind field gradients across the frontal boundary that converges toward the eye. QuikSCAT-derived wind field was obtained at 09:09 UTC (Fig. 8c). The centers of both cyclones and the sharp frontal boundaries are clearly distinguished in Figure 8c and correspond to the brightness field of ASAR image.

Discussion and conclusions

The clearly surface manifestations and accurate location of the mesoscale cyclones, frontal boundaries, wavelike disturbances on the fronts, mesoscale convective cells and rolls, etc. were found on many Envisat ASAR images of the Northwest Pacific Ocean. Surface imprints of the atmospheric features can indicate wind direction needed for wind speed retrieval with C-band SCAT model CMOD4 or CMOD5.

AMSR-E retrievals showed the distinct features in the fields of total cloud liquid water content and total atmospheric water vapor content correlated with MODIS visible/infrared images and radar signatures. The MC areas were characterized by appearance of water clouds with low and moderate Q values 0.05–0.25 kg/m^2 and by the higher V values against the surrounding areas. The frontal structure of the

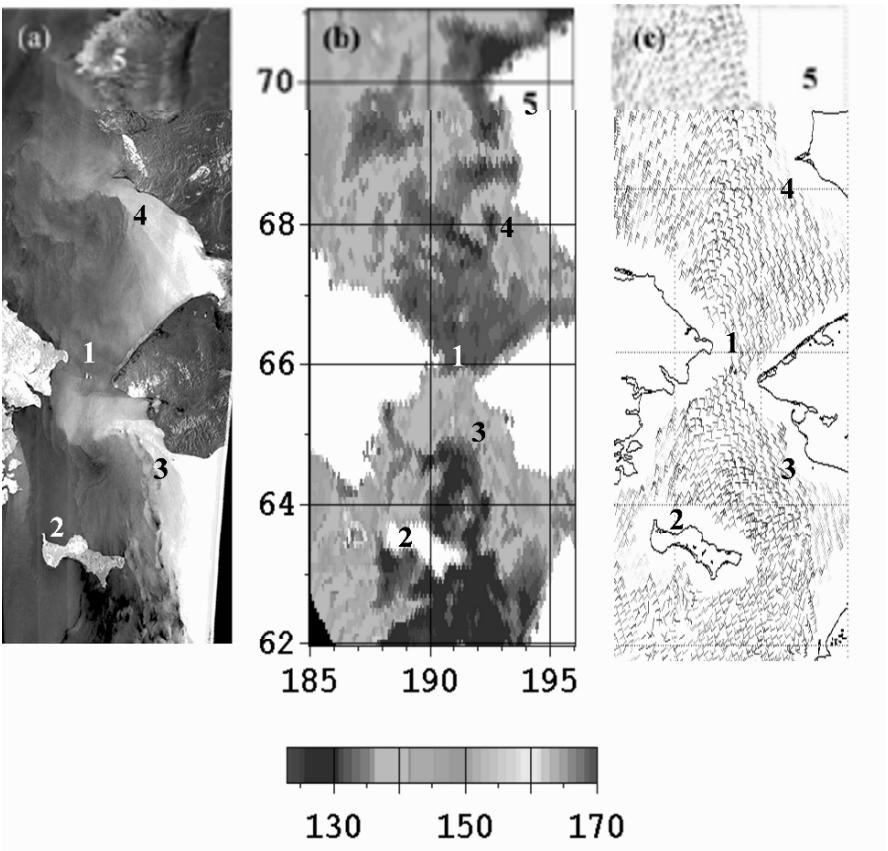

Fig. 9. Mesoscale vortices in the Bering Strait area on 12 November 2007: (**a**) Envisat ASAR image at 21:46 UTC, (**b**) 36-GHz, H-polarization Aqua AMSR-E brightness temperature at 23:00 UTC and (**c**) QuikSCAT-derived wind field at 16:43 UTC. 1 – Bering Strait, 2 – St. Laurent Island, 3 – vortex to the south of the strait, 4 – vortex to the north of the Strait, 5 – sea ice.

most intense MCs was depicted by position of maximum Q values near frontal boundaries and high V gradients. Remarkable degree of similarity between ASAR, visible/infrared and 89-GHz brightness temperatures was found.

Individual ASAR images and time series of visible/infrared images, microwave radiometer and scatterometer measurements allowed to study the life circle of the most intense MCs. Incorporating data from multiple satellite platforms improves the temporal resolution through employment of a greater number of satellites and increases the amount and kind of spatial quantitative information collected. However, the detection of severe or violent MCs over the ice-free ocean depends mainly on passive and active microwave images and their quantitative estimates.

The continuing thawing of sea ice in the Arctic Ocean that is observed in the recent years increases the ice-free period. The mesoscale cyclones can be formed over the new areas of the open water that can accompany by additional release of carbon dioxide in the atmosphere due to coastal erosion caused by strong winds. Quantitative spatial data on the various weather systems in the Arctic Ocean can be obtained mainly from space since conventional observations are scarce and carried out at several coastal stations and islands.

Figure 9a shows two mesocyclones on Envisat ASAR image acquired on 12 November 2007 at 21:46 UTC over the Bering Strait area. In the previous years this area was mostly ice-covered in the middle of November. One MC is located to the south of the Strait and another to the North of it. Frontal boundaries and the zones of strong winds along the coast are distinguished very clearly on ASAR image. Strong winds were also measured by QuikSCAT scatterometer 5 h before ASAR sensing, however, wind retrieval near the coast is impossible (Fig. 9c). Both mesoscale weather systems were also detected by Aqua AMSR-E at 14 and 23 UTC (Fig. 9b). They were characterized by values of $V = 7–9$ kg/m^2 and $Q = 0.08–0.11$ kg/m^2.

The detailed mesoscale and submesoscale variations of oceanic and atmospheric parameters in the area of MCs are the subject to further careful and rigorous investigation. The multispectral sensors onboard today's satellite systems offers new opportunities to improve understanding of many problems associated with MCs. The passive and active microwave sensors play a crucial role in acquisition of their quantitative characteristics that are needed, in particular, both for monitoring and modeling of mesoscale cyclones.

Acknowledgments

This study has been carried out within ESA Envisat project AO-ID-391 and ESA-IAF Bear project AO-2775. This work is partly supported by RFBR Projects: 06-05-65177-a and 06-05-96076-p_vostok_a. Aqua AMSR-E measurements were provided the Japan Aerospace Exploration Agency (JAXA) within the cooperation between the JAXA and the POI FEB RAS (project AD2M-3RA-UF002).

References

Bresch JF, Reed RJ, Albright MD (1997) A polar low development over the Bering Sea: Analysis, numerical simulation, and sensitivity experiments. Mon Weather Rev, 125: 3109–3130

Businger S (1987) The synoptic climatology of polar low outbreaks over the Gulf of Alaska and the Bering Sea. Tellus, 39A: 307–325

Carleton AM, McMurdie LA, Katsaros KB, Zhao H, Mognard NM, Claud C (1995) Satellite-derived features and associated atmospheric environments of Southern Ocean mesocyclone events. Global Atmos Ocean Syst, 3: 209–248

Chunchuzov I, Vachon PW, Ramsay B (2000) Detection and characterization of mesoscale cyclones in RADARSAT synthetic aperture radar of the Labrador Sea. Can J Remote Sens, 26: 213–230

Claud C, Mognard NM, Katsaros KB, Chedin A, Scott NA (1993) Satellite observations of a polar low over the Norwegian Sea by Special Sensor Microwave/Imager, Geosat and TIROS-N Operational Vertical Sounder. J Geophys Res, 98: 14,487–14,506

Claud C, Heinemann G, Raustein E, McMurdie L (2004) Polar low le Cygne: Satellite observations and numerical simulations. Q J R Meteorol Soc, 130: 1075–1102

Condron A, Bigg GR, Renfrew IA (2006) Polar mesoscale cyclones in the Northeast Atlantic: Comparing climatologies from ERA-40 and satellite imagery. Mon Weather Rev, 134: 1518–1533

Douglas MW, Fedor L, Shapiro MA (1991) Polar low structure over the Northern Gulf of Alaska based on research aircraft observations. Mon Weather Rev, 119: 32–54

Duncan CN (1978) Baroclinic instability in a reversed shear flow. Meteorol Mag, 107: 17–23

Emanuel KA, Rotunno R (1989) Polar lows as arctic hurricanes. Tellus, 41A: 1–17

Envisat Special Issue (2001) ESA Bulletin, No. 106, 168 pp

Friedman KS, Sikora T, Pichel WG, Clemente-Colon P, Hufford G (2001) Using spaceborne synthetic aperture radar to improve marine surface analyses. Weather Forecast, 16: 270–276

Fu G, Niino H, Kimura R, Kato T (2004a) A Polar low over the Japan Sea on 21 January 1997. Part I: Observational analysis. Mon Weather Rev, 132: 1537–1551

Fu G, Guo J, Zhang M (2004b) High-resolution simulation and analysis of the mature structure of a polar low over the Sea of Japan on 21 January 1997. Adv Atmos Sci, 21: 597–608

Gurvich IA, Mitnik LM, Mitnik ML (2008) Mesoscale cyclogenesis over Far Eastern Seas: Investigation on the basis of satellite microwave radiometric and radar measurements. Investigation of the Earth from Space (Issledovanie Zemli iz Kosmosa), N 5: 58–73 (in Russian)

Harold JM, Bigg GR, Turner J (1999) Mesocyclone activity over the North-East Atlantic. Part 1: Vortex distribution and variability. Int J Climatol, 19: 1187–1204

Heinemann G (1995) TOVS retrievals obtained with the 3I-algorithm. A study of a meso-scale cyclone over the Barents Sea. Tellus, 47A: 324–330

Heinemann G, Claud C (1997) Report of a workshop on 'Theoretical and Observational Studies of Polar Lows' of the European Geophysical Society Polar Lows Working Group. Bull Am Meteorol Soc, 78: 2643–2658

Kalmykov AI (1996) Real-Aperture Radar (RAR) imaging from space. Radio Science Bulletin, No. 276: 13–22

Kawanishi T, Sezai T, Ito Y, Imaoka K, Takeshima T, Ishido Y, Shibata A, Miura M, Inahata H, Spencer RW (2003) The Advanced Microwave Scanning Radiometer for the Earth Observing System (AMSR-E), NASDA's contribution to the EOS for global energy and water cycle studies. IEEE Trans Geosci Remote Sens, 41: 184–194

Kolstad EW (2006) A new climatology of favourable conditions for reverse-shear polar lows. Tellus, 58A: 344–354

Liu AQ, Moore GWK, Tsuboki K, Renfrew IA (2004) A High-resolution simulation of convective roll clouds during a cold-air outbreak. Geophys Res Lett, 31: L03101, doi:10.1029/2003GL018530

Liu AQ, Moore GWK, Tsuboki K, Renfrew IA (2006) The effect of the sea ice zone on the development of boundary-layer roll clouds during cold air outbreaks. Bound Layer Meteorol, 18: 557–581

McMurdie LA, Claud C, Atakturk S (1997) Satellite-derived characteristics of spiral and comma-shaped southern hemisphere mesocyclones. J Geophys Res, 102: 13,889–13,905

Meissner T, Wentz FJ (2004) The complex dielectric constant of pure and sea water from microwave satellite observations. IEEE Trans Geosci Rem Sens, 42: 1836–1849

Mitnik LM (1990) Polar lows, convective eddies and chains of mesovortices. In: Radar Sensing of the Earth's Surface from Space, eds Mitnik LM and Viktorov SV, Hydrometeoizdat, Leningrad, pp 100–105 (in Russian)

Mitnik LM (1992) Mesoscale coherent structures in the surface wind field during cold air outbreaks over the Far Eastern seas from the satellite side looking radar. La Mer, 30: 287–296

Mitnik LM, Mitnik ML (2003) Retrieval of atmospheric and ocean surface parameters from ADEOS-II AMSR data: comparison of errors of global and regional algorithms. Radio Sci, 38: 8065, doi: 10.1029/2002RS002659

Mitnik LM, Mitnik ML (2006) Retrieval of total water vapor content and total cloud liquid water content over the ocean by microwave sensing from DMSP, TRMM, AQUA and ADEOS-II satellites. Investigation of the Earth from Space (Issledovanie Zemli iz Kosmosa), N 4: 34–41 (in Russian)

Mitnik LM, Hsu M-K, Mitnik ML (1996) Sharp gradients and mesoscale organized structures in sea surface wind field in the regions of polar low formation. Global Atmos Ocean Syst, 4: 335–361

Mitnik LM, Mitnik ML, Dubina VA (2004) Marine weather systems: Study with ADEOS-II AMSR, Aqua AMSR-E and Envisat ASAR. Gayana, 68: 389–395

Mitnik M, Mitnik L, Gurvich I (2007) Using Envisat ASAR for the study of winter mesoscale cyclones in the Asian Marginal Seas. Proc Envisat Symp 2007, 23–27 April 2007, Montreux, Switzerland. ESA Publication SP-636

Mokhov II, Akperov MG, Lagun VE, Lutsenko EI (2007) Intense arctic mesocyclones. Izvestiya. Atmos Ocean Phys, 43: 259–265

Montgomery MT, Farrell BF (1992) Polar low dynamics. J Atmos Sci, 49: 2484–2505

Moore RW, Vonder Haar TH (2003) Diagnosis of a polar low warm core utilizing the Advanced Microwave Sounding Unit. Weather Forecast, 18: 700–711

Ninomiya K (1989) Polar comma cloud lows over the Japan Sea and the Northwestern Pacific in winter. J Meteorol Soc Jpn, 67: 83–97

Noer G, Ovhed M (2003) Forecasting of polar lows in the Norwegian and the Barents Sea. Proc 9th Meeting of the EGS Polar Lows Working Group, Cambridge, UK

Orlanski I (1975) A rational subdivision of scales for atmospheric processes. Bull Am Meteorol Soc, 56: 527–530

Rasmussen E, Turner J (2003) Polar Lows: Mesoscale Weather Systems in the Polar Regions. Cambridge University Press, Cambridge, 612 pp

Shapiro MA, Fedor LS, Hampel T (1987) Research aircraft measurements of a polar low over the Norwegian Sea. Tellus, 39A: 272–306

Sikora TD, Friedman KS, Pichel WG, Clemente-Colon P (2000) Synthetic aperture radar as a tool for investigating polar mesoscale cyclones. Weather Forecast, 15: 745–758

Tsuboki K, Asai T (2004) The multi-scale structure and development mechanism of mesoscale cyclones over the Sea of Japan in winter. J Meteorol Soc Jpn, 82: 597–621

Vachon PW, Adlakha P, Edel H, Henschel M, Ramsay B, Flett D, Rey M, Staples G, Thomas S (2000) Canadian progress toward marine and coastal applications of Synthetic Aperture Radar. Johns Hopkins APL Tech Digest, 21: 33–40

Yarnal B, Henderson G (1989) A satellite-derived climatology of polar-low evolution in the North Pacific. Int J Climatol, 9: 551–566

Young GS, Sikora TD, Winsted NS (2005) Use of synthetic aperture radar in finescale surface analysis of synoptic-scale front at sea. Weather Forecast, 20: 311–327

Zabolotskikh EV, Bobylev LP, Mitnik LM, Mitnik ML, Johannessen OM (2005) Atmospheric total water vapor content retrievals using Aqua AMSR-E data: Theoretical and experimental results. Proc 31st Intern Symp Rem Sens Environment, 20–24 June 2005, St Petersburg, Russia (on CD)

Zabolotskikh EV, Bobylev LP, Mitnik LM, Mitnik ML, Johannessen OM (2007) Algorithms for water vapor and liquid water retrievals over the Arctic Ocean from SSM/I and AMSR-E measurement data. Proc 5th All-Russian Conf "Current Problems of Remote Sensing of the Earth from Space", 12–16 Nov 2007, Moscow, Russia (on CD)

Recent sea ice ecosystem in the Arctic Ocean: a review

Igor A. Melnikov

P.P. Shirshov Institute of Oceanology, Russian Academy of Sciences, Moscow, Russia, migor@online.ru

Abstract

Recent global warming in the Arctic Ocean predicts shifting of ice-edge to the north, decreasing of sea-ice thickness and surface, and increasing of ice-open areas. This scenario suggests increasing of biological productivity and duration of vegetation period, and intensification of regeneration processes in the sea ice-upper ocean system. However, at present the evidence of impacts of global change on the sea ice ecosystem is sparse or uncertain, though there are fragmentary indications of recent changes. As established now, the biological community response to global change is most likely in the regions, where the sea ice retreat is rather remarkable, e.g., in the region of Beaufort Gyre. Assessment of the recent sea-ice ecosystem dynamic and modeling its potential changes in the Central Arctic Ocean will allow estimating and forecasting potential changes within the sea ice-upper water system and consequent ecological effects on higher trophic levels including birds, marine mammals and benthic organisms.

Introduction

During the last decades, a clear temperature trend towards warming is observed in the Arctic. As a result of warming, the multiyear ice area decreases at least twice, but the seasonal ice area is increasing rapidly exceeding 50% of the Arctic Ocean area in 2007. The ice-cover thickness is also decreased from 3–5 m thick in middle 70th (Busuev 1968; Koerner 1973; Wadhams 1983) to less than 2 m thick in last decade (Perovich et al. 1999; Melnikov 2007, 2008). As a consequence of sea ice melting, a temperature increase and freshening of surface arctic water were also detected (Carmack et al. 1995; Serreze and Maslanik 1997; Morrison et al. 1998; McPhee et al. 1998; etc.) as well as changes in the composition and structure of the sea ice-associated biological communities (Melnikov et al. 1998,

J.C.J. Nihoul and A.G. Kostianoy (eds.), *Influence of Climate Change on the Changing Arctic and Sub-Arctic Conditions*,

2001, 2002; Melnikov 2000; Melnikov and Kolosova 2001). Remarkable changes were occurred in quality and quantity composition of the sea ice biota in comparison to composition in the middle of 70th. So, the total number of sea ice algae in 1975–1982 consists of 172 species (Melnikov 1989) and about 30 species during the last decade (Melnikov 2008). Diatoms were dominated both by species and number in sea ice phytocenoses but recently their domination is decreased and changed by prevalence of other algal groups. Composition of sea ice fauna is also changed: protozoans and sea ice-associated invertebrate animals like acarians, nematodes, turbellarians, rotatorians, copepods and amphipods were numerous in ice of 70th but they are very rare found in ice of last decade and met very often as dead fragments of tintinnides, nematodes, and skins of copepods.

The observed changes allow setting questions related to the response of the sea ice ecosystem to global warming, of which the most important are as follows:

1. How do the physical–chemical properties of sea ice and sea water contacting it change?
2. How does the species composition and structure of biological communities change?
3. What is the dynamics and direction of these processes?

In this review, the main attention will be focused on two major components of the Arctic sea ice cover – multiyear (MY) and seasonal or first year (FY) sea ice as well as the upper ocean system. In this formulation, by the "upper ocean" definition, it means the water of the mixed layer above the pycnocline with a thickness of 0–30 (50) m, whose characteristics and dynamics are interrelated with the sea ice cover.

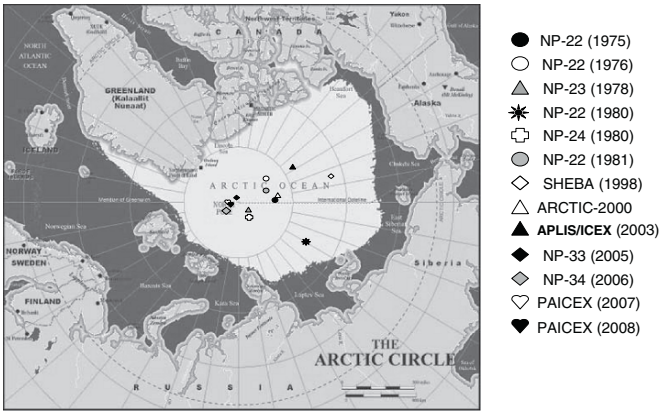

Fig. 1. Map of study areas, where the cryobiological investigations were carried out. Points are the start positions of ice camps drift: North Pole-22 (1975–1981, 83N, 177W); North Pole-23 (1978, 77N, 165E); North Pole-24 (1980, 87N, 125E); SHEBA (1997–1998, 75N, 170W); "Arctic-2000" (2000, 82N, 170E); ARLIS/ICEX (2003, 73N, 148W); North Pole-33 (2005, 85N, 156E); North Pole-34 (2006, 87N, 105E); PAICEX (2007, 89N, 26E) and PAICEX (2008, 89N, 06E).

This review is based on materials obtained in Arctic Ocean expeditions (Fig. 1): North Pole (NP) drifting stations (1975–1982); SHEBA (Surface Heat Budget of the Arctic Ocean), 1997–1998; "Arctic-2000"; ICEX (Ice Camp Expedition), 2003; NP-33 and 34, 2004–2006; PAICEX (PanArctic Ice Camp Expedition), 2007–2008, as well as on the data available from literature sources. The main focus will be done on comparison of data obtained at the North Pole stations during the period of the middle 70th which is considered as a pre-melting period of sea ice cover in the Arctic Ocean and steady-stable existence of sea ice ecosystem, and on data from SHEBA expedition in 1997–1998 and last decade expeditions when observed an intensive melting sea ice and degradation of sea ice ecosystem.

Sea ice extent and thickness

In the middle of 70th the total extent of sea ice area in the Arctic Ocean varies from a minimum of about 6.9 million square kilometer in September to a maximum of about 8.3 million square kilometer in March (Atlas 1980) and within this ocean, the multi-year sea ice is a key dominant environmental feature. According to the data of ice satellite observations in 1973–1976 (NASA 1987), the MY ice occupied up to

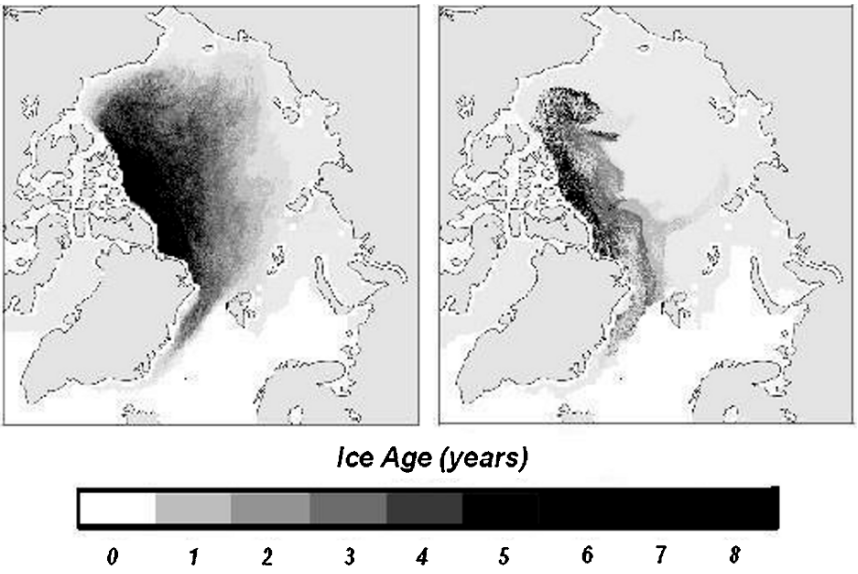

Fig. 2. Arctic Sea ice age and extent in February 2008 (right) compared to the average for 1985–2000 (left). The area and thickness of sea ice that survives the summer has been declining over the past decade. Whereas perennial ice used to cover 50–60% of the Arctic, it covered less than 30% in 2008—down 10% from 2007. The ice that remains is also getting younger. In the mid- to late 1980s, over 20% of Arctic sea ice was at least six years old; in February 2008, just 6% ice was six years old or older (Source: http://nsidc.org/data/seaice_index/n_plot.html).

80% of the Arctic Basin area and interannual variability of this area does not exceed 2% (Carsey 1982). In that pre-melting period, the seasonal ice occupies 6–17%, and ice-free water is 3–24%, respectively, depending on space and time.

The observations during the last decade have recorded a significant decrease of the sea ice extent (Fig. 2) from 7 to 5.32 million square kilometer and 4.14 million square kilometer for September 2000, 2005 and 2007, correspondingly, that is to be melting faster than predicted by any of the 18 computer models used by the Intergovernmental Panel on Climate Change (Stroeve et al. 2007). Two facts are primarily of interest: (1) the ice edge has been significantly displaced northward approximately by 2–3°, which confirms satellite information about the ice cover area decrease (Cavaliere et al. 1997), and (2) the sea ice thickness has noticeably changed. According to data of different authors who carried out ice thickness measurements in the Arctic Basin in the 1960s, the mean equilibrium thickness of non-deformed ice in the Amerasian sub-basin comprised about 3 m (Busuev 1968; Koerner 1973; Wadhams 1983). Based on data obtained at NP-22 and AIDJEX ice stations that drifted in the Beaufort Gyre in 1975–1976, the ice thickness after summer melting was 2–3 m (Melnikov 1989; McPhee et al. 1998). Twenty years later in October 1997 during the ice camp SHEBA expedition in the same region of the Beaufort Gyre the average ice thickness was 1.5 m. PAICEX observations during the IPY in the North Pole region shown that the average ice thickness was 177.1 cm ± 13.2 (n = 133) and 181.4 cm ± 13.3 (n = 203) in April 2007 and 2008, correspondingly (Table 1) (Melnikov 2007, 2008a). The occurrence of seasonal ice was increased from 37% in 2007 to 68% in 2008 (group of ice 180– 200 cm thick), but the multiyear ice (group of ice 240–300 cm) in April 2008 was not met at all by 203 direct thickness measurements along 23 km transect (Fig. 3).

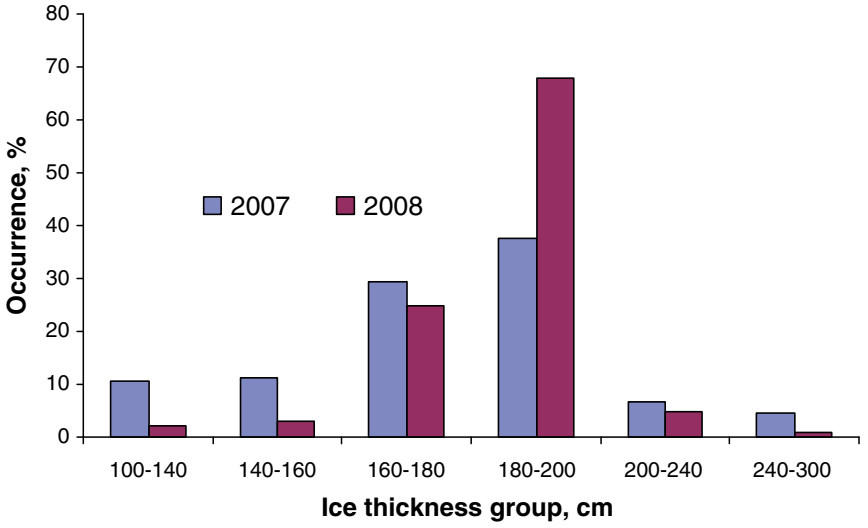

Fig. 3. Occurrence of ice thickness size groups in the North Pole area. Data from observations at PAICEX 2007 and 2008 (Melnikov 2007, 2008).

Table 1. Average sea ice thickness in the nearby North Pole area (PAICEX, April 2007 and 2008).

Ice thickness profiles "PAICEX", April 2007				
	Number of		Average thickness (cm)	
Direction	measurements	Distance (m)	Ice	Snow
West	25	4,000	174	24
East	28	3,400	181	26
South	31	4,700	185	24
North	36	4,000	170	26
Total	119	16,100	178	25
Ice thickness profiles "PAICEX", April 2008				
	Number of		Average thickness (cm)	
Direction	measurements	Distance (m)	Ice	Snow
West	40	4,200	185	6
East	51	4,800	182	6
South	52	7,100	181	4
North	60	6,400	179	5
Total	203	22,500	182	5

Physical-chemical variables

The thickness and salinity are main physical factors accentuating differences between MY and FY ice. It is common knowledge that the older ice is the thicker and the fresher it is, and vice versa. Salinity values reflect a typical vertical distribution characteristic of seasonal ice within 5–8 ‰ through the whole ice mass in ice as thick as 180–200 cm and perennial ice within values varying from 0.1–0.5‰ in the upper layer to 2–3‰ in the lower layer in ice as thick as 240–300 cm (Fig. 4). The reason for a lower salinity of the MY ice consists in that this ice recurrently passed the ice melting stage. In the result of intravolumetric melting, the porosity is intensified so that the brine cells are being diluted with the melt water drain downward by the force of gravity, thereby promoting more active rejection of the salts. In winter, the salinity of the MY ice increases in comparison with the ice salinity in summer by the growth of a new ice layer with the increased salinity from beneath which increases the salinity of the entire thickness of the MY ice on the whole. The reason for a higher salinity of FY ice consists in that, from one hand, at the initial moment of ice formation, some salts are retained in the intercrystalline spaces, therefore high salinity values are observed in the upper layers and, from another hand, this ice is formed in winter and it has not passed the summer melting stage.

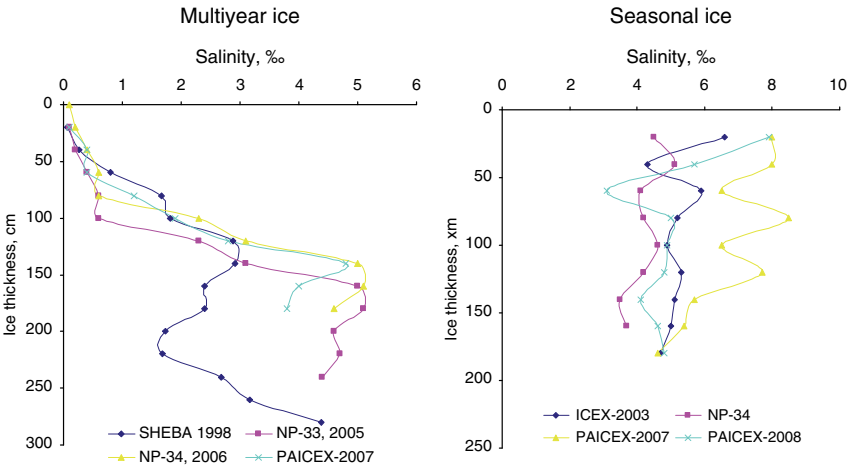

Fig. 4. Vertical distribution of salinity in multiyear and seasonal sea ice thickness for the period 1998–2008 in the Central Arctic Ocean.

Physical and chemical variables of the MY and FY are presented in Table 2. Mean SHEBA values of the MY ice salinity are about half those of NP-22, but the FY values are twice as high. The most curious feature of the SHEBA ice samples is very low concentrations of silicate in the MY and FY sea ice, an order of magnitude less than at the NP-22: 3.76 μM/l and 2.18 μM/l in the MY and FY ice at the NP-22, and 0.40 μM/l and 0.28 μM/l at the SHEBA, respectively. The main feature of chlorophyll *a* concentrations in the ice cores is the two-fold decrease in SHEBA multi-year ice compared to NP-22, and three-fold increased chlorophyll *a* concentrations in first-year ice. Such a large discrepancy can be caused by a loss of silicate with melt water due to its active export from ice to the underlying sea water as a result of active intra-volumetric ice melting in the summertime at SHEBA station while at NP-22 such strong melting was not observed. The loss of silicate with melt water can in turn be a cause for a significant decrease in the numbers of diatoms (main silicate consumers during photosynthesis), which we observed at SHEBA station and did not observe at NP-22. The main peculiarity in the distribution of chlorophyll *a* in the MY and FY ice strata is its twofold decrease in MY ice at SHEBA and a threefold increase in FY ice as compared with a similar concentration of chlorophyll *a* in ice at NP-22. Throughout winter, the concentration of chlorophyll *a* under m^2 of MY ice at SHEBA station did not experience any significant changes. From October to February, the concentrations varied within 0.3–0.5 mg/m^2. In March, the concentration has increased to a value of 1.2 mg/m^2 (spring maximum of alga blooming) and then comprised again the values observed in winter. A noticeable increase of chlorophyll *a* concentration was observed in summer in July–August when its concentration has increased to 2 mg/m^2 (summer maximum). In autumn (September), the concentration of chlorophyll

Table 2. Summary of ice thickness, date of sampling and position, physical and chemical variables of MY and FY ice cores at the NP-22 and SHEBA ice camps. Data are mean ±1SD.

Core #	Thick (cm)	Sampling date	Latitude	Longitude	Salinity (‰)	Silicate (μM/l)	Chl *a* (μg/l)
			NP-22, multi-year ice				
1	404 (11)	15 Feb 80	77° 53'N	153° 49'E	2.02±1.69	6.1±2.11	0.45±0.44
2	350 (9)	11 Mar 80	78° 17'N	153° 35'E	2.42±1.43	2.6±0.53	0.23±0.18
3	163 (5)	31 Mar 80	78° 21'N	153° 07'E	5.60±2.14	3.51±4.05	0.18±0.22
4	199 (6)	01 Apr 80	78° 22'N	153° 01'E	5.07±0.48	2.21±0.43	0.09±0.01
5	162 (5)	04 Apr 80	78° 22'N	152° 30'E	5.52±0.86	3.93±0.5	0.06±0.04
6	339 (11)	18 Apr 80	78° 35'N	151° 52'E	3.17±0.56	3.2±1.33	0.61±0.34
7	211 (4)	20 Apr 80	78° 39'N	151° 48'E	4.86±4.21	4.68±2.39	0.24±0.18
				Mean:	4.09±1.62	3.76±1.62	0.35±0.20
			NP-22, first-year ice				
1	104 (3)	23 Jan 80	77° 40'N	154° 99'E	0.99±0.09	1.90±0.69	0.05±0.01
2	114 (4)	01 Feb 80	77° 48'N	153° 54'E	0.84±0.19	ND	ND
3	129 (4)	26 Feb 80	78° 05'N	154° 36'E	0.88±0.22	1.98±0.33	0.09±0.07
4	167 (4)	28 Feb 80	78° 07'N	153° 54'E	1.28±0.25	2.67±0.70	0.06±0.03
				Mean:	0.99±0.19	2.18±0.57	0.06±0.03
			SHEBA, multi-year ice				
1	244 (10)	27 Oct 97	75° 17'N	143° 31'W	ND	ND	0.12±0.08
2	235 (12)	12 Nov 97	76° 09'N	146° 26W'	1.43±0.96	0.12±0.16	0.24±0.19
3	185 (9)	28 Nov 97	75° 07'N	147° 33'W	1.67±1.08	0.16±0.14	0.09±0.15
4	216 (11)	10 Dec 97	75° 44'N	150° 25'W	2.16±1.36	ND	0.31±0.53
5	178 (9)	29 Dec 97	75° 17'N	149° 59'W	2.62±1.60	0.72±0.43	0.13±0.05
6	177 (9)	12 Jan 98	74° 51'N	150° 25'W	2.97±1.87	0.74±0.37	0.11±0.05
7	260 (13)	27 Jan 98	74° 51'N	155° 38'W	2.10±1.30	0.46±0.27	0.31±0.32
8	281 (14)	18 Feb 98	74° 54'N	157° 50'W	2.55±1.58	0.35±0.22	0.05±0.04
9	417 (21)	09 Mar 98	75° 28'N	160° 18'W	2.08±0.95	0.08±0.05	0.17±0.13
10	287 (15)	29 Apr 98	75° 57'N	166° 13'W	2.50±2.02	0.45±0.37	0.09±0.09
11	291 (14)	25 May 98	76° 24'N	167° 11'W	0.94±0.50	0.56±0.18	0.11±0.13
				Mean:	2.10±1.32	0.40±0.24	0.16±0.16
			SHEBA, first-year ice				
1	62 (6)	19 Oct 97	75° 20'N	144° 29'W	0.41±0.19	ND	0.20±0.07
2	66 (6)	27 Oct 97	75° 17'N	143° 31'W	0.58±0.32	ND	0.46±0.50
3	77 (7)	11 Nov 97	76° 09'N	146° 23'W	1.74±0.89	0.08±0.01	0.13±0.10
4	79 (8)	26 Nov 97	76° 13'N	147° 43'W	3.03±1.85	0.36±0.27	0.41±0.25
5	116 (6)	12 Dec 97	75° 41'N	150° 44'W	2.42±1.54	ND	0.14±0.09
6	95 (9)	27 Dec 97	77° 17'N	149° 57'W	2.86±1.56	0.44±0.26	0.10±0.11
7	137 (7)	11 Jan 98	74° 53'N	150° 12'W	2.86±1.62	0.45±0.19	0.05±0.02
8	150 (8)	24 Jan 98	74° 38'N	153° 25'W	3.42±1.99	0.14±0.05	0.06±0.04
9	132 (7)	16 Feb 98	74° 53'N	157° 50'W	3.31±1.58	0.11±0.03	0.13±0.07
10	171 (9)	09 Mar 98	75° 28'N	160° 18'W	3.39±1.75	0.05±0.03	0.12±0.08
11	142 (7)	29 Apr 98	75° 57'N	166° 13'W	ND	0.25±0.09	0.18±0.16
12	138 (7)	25 May 98	76° 24'N	167° 11'W	ND	0.67±0.28	0.20±0.16
				Mean:	2.4±1.33	0.28±0.13	0.18±0.13

a has dropped to the values recorded during the previous autumn period, i.e. about 0.4 mg/m^2. The revealed chlorophyll *a* dynamics reflects the winter and summer stage of succession of ice flora where 17 species of the group of Bacillariophyta, 5 – Dynophyta and by 1 species, correspondingly, from the groups of Silicoflagellatae, Chlorococcales and Chrysophyta were recorded. Among the diatoms, *Cylinrotheca*

closterium, *Leptocylindrus minimus*, *Navicula vanhoeffenii* and *Nitzscia neofrigida* dominated 57 (63% of the numbers of cells) and among Chrysophyta – *Groenlandiella brevispina* (31%).

Sea ice biota

Vertical distribution. The species composition of the sea-ice communities is not uniform. Within the sea ice thickness it was found out the strict vertical zonation in their distribution within the sea-ice thickness.

The bottom sea-ice surface is colonized by the cryopelagic algae formed mass aggregations of benthic- and plankto-benthic types as well as by the algae developed on the under-ice platelets. Diatoms are the most abundant species with a domination of *Melosira arctica*, *Chaetoceros karianus*, *Gomphonema exiguum* (benthic type), *Fragilaria striatula*, *Comphonema kamtschaticum*, *Navicula vanhoeffenii*, *Nitzschia sigma* (plankto-benthic type), and *Navicula kariana*, *N. spicula*, *Gomphonema exiguum* (cryophilic microphytobenthos type). It was found out the very high resemblance between the species composition of all algae communities developed in this biotope. Cryopelagic fauna count the 48 species with a domination of *Arthropoda* (81% of the total species number). There are distinguished two dominant and one secondary ecological groups: (1) the autochthonous fauna including 12 species (*Amphipoda* – 6 species, *Copepoda* – 2, *Mysidacea* – 1, *Polychaeta* – 1, and *Osteichtyes* – 2), (2) the allochthonous fauna including 9 species of *Copepoda*, and (3) the group of the xenocryobiontic fauna. The list of algae developed in the sea-ice interior consists of 171 species (*Bacillariophyta* – 148 species, *Chlorophyta* – 20, *Silicoflagellatae* – 2, *Dinophyta* – 1, and *Cyanophyta* – 1). The obvious predominance of the pennate (136 species or 89% of all diatoms) compared with the centric (12 species or 11%) diatoms is the main peculiarity of the sea-ice flora. The existence of the fresh-water green algae (*Chlorophyta*) is a second peculiarity of the sea-ice phytocoenosis. Two different floristic communities develop independently within the sea-ice interior: (1) the fresh-water algae community of the upper layers and (2) the sea algae community of the lower layers. Cryointerstitial faunistic community consists of two ecological groups: (1) the autochthonous fauna (*Nematoda*, *Turbellaria*, *Acarina*, and *Protozoa*) and (2) the allochthonous fauna represented by juvenil amphipods *Apherusa glacialis* and juvenil harpacticoid copepods *Tisbe furcata*. Animals of both groups occupy the lower layer of the sea ice. Habitants of the upper sea-ice surface are mainly represented by the freshwater green algae (*Chlorophyta*) between which *Chlamydomonas nivalis* and *Ancylonema nordenskioeldii* dominate. Representatives of other groups (*Cyanobacteria*, *Chrysophyta*, and *Fungy*) are subdominant. Diatoms, which are abundant on the bottom sea-ice surface and within the sea-ice interior, do not develop in this biotope. Invertebrate fauna was not observed.

Flora. The total list of ice algae identified at NP-22 and SHEBA stations numbers 102 taxa among which 84 species or 76% of the total numbers were revealed at NP-22 station while at SHEBA – only 26 species or 23%, respectively (Table 3; Melnikov et al. 2001). The dominance of marine diatoms over the other groups of algae is the most important feature of the sea ice phytocenoses of NP-22. Freshwater algae (mainly from the group of Chlorophyta) were observed at NP-22 only in melt water of puddles developing in the summer period at the upper surface of multiyear ice or in the upper sections of this ice. The most important feature of the phytocenoses of multiyear and first-year ice of SHEBA station is a significant dominance of freshwater algae of the Pyrrophyta and Chlorophyta groups over the marine diatom algae with the former being distributed over the vertical strata of both multiyear and first-year ice.

Fauna. The most important and curious characteristic of sea ice from SHEBA station is a complete absence of interstitial fauna. Whereas in the multiyear ice strata of NP-22, such groups as Tintinnoidea, Acarina, Nematoda, Turbellaria, Copepoda and Amphipoda in numbers of tens of thousands individuals per square meter were noted (Table 4; Melnikov 1989) there was not a single living individual from the enumerated groups in the ice samples from SHEBA station (Melnikov et al. 2001). In all investigated samples, single shells of dead foraminifers, fragments of tintinnides and nematodes, and skins of copepods were detected.

Table 3. Number of algal species presents within sea ice interior in samples collected from the ice camps NP-22 (winter 1979–1980) and SHEBA (winter 1997–1998), Beaufort Gyre, Canadian Basin of the Arctic Ocean.

Taxon	NP-22	SHEBA
Bacillariophyta	79	18
Dinophyta	NO	5
Chrysophyta	NO	1
Chlorophyta	NO	1
Silicoflagellatae	5	1

NO – not observed.

Table 4. Species number of fauna associated with the sea ice interior in samples from the ice camps NP-22 (winter 1979–1980) and SHEBA (winter 1997–1998), Beaufort Gyre, Canadian Basin of the Arctic Ocean.

Taxon	NP-22	SHEBA
Protozoa	3	NO
Foraminifera	1	1
Acarina	1	NO
Nematoda	2	NO
Turbellaria	1	NO
Harpacticoida	1	NO
Amphipoda	1	NO

NO – not observed.

A comparative analysis of data obtained at NP-22 and SHEBA allows to make the following conclusions:

- Populations of ice diatom algae identified in all types of sea ice during the SHEBA station drift have low numbers both in respect of the numbers of species and the numbers of cells;
- Freshwater algae identified earlier at NP-22 only within the upper surface of multiyear sea ice are currently distributed throughout the entire sea ice strata (SHEBA);
- Populations of invertebrates such as nematodes, copepods, amphipods and turbellarian dominating both by the numbers and the biomass in the multiyear ice strata during the NP-22 station drift (1979–1980) were not observed at all in sea ice samples in the SHEBA expedition (1997–1998).

The changes revealed in the composition and structure of the communities inhabiting sea ice could be probably attributed to increasing melting of the ice cover for the last two decades. I consider several factors determining these changes among which the most important are the following: 1) draining of fresh melt water through the ice strata; 2) accumulation of freshwater under the ice; and 3) formation of a sharp pycnocline in 25–30 m depths weakening vertical water mixing. Ie suppose that the modern "upper ocean – sea ice" ecosystem modifies due to these acting factors from a typically marine to brackish-water ecological system.

Discussion and conclusions

The sea-ice cover of the Arctic Ocean is a multi-component natural complex comprising the ice layers which differ from each other in the age, thickness, mobility and other features. The main component of the sea-ice cover in the central deep-sea Arctic Basin is represented by the MY ice which dominates over the ice of other age groups in respect to the area and volume. The FY ice which is formed mainly in winter in open water on the area of the Arctic Seas after summer ice melting partially compensates for the loss of the ice during its drift from the Arctic Basin into the Northern Atlantic Ocean regions. The young ice and ice-free areas (ponds, cracks, polynyas, and leads) comprise a small area of the basin.

It is well known that the arctic sea ice is a fine and sensitive climate indicator: the warmer it is the more intense is melting and vice versa, the colder it is, the more intense and stronger is the growth of its thickness. At that climatic and hydrological level, the sea-ice cover is a stable natural formation. The main reason for its stability consists in the existence of a thin stratified surface layer precluding the contact of the sea ice with warm Atlantic water. The mechanism regulating the average equilibrium thickness as well as the peculiarities of the large-scale ice circulation, and the system maintaining the equilibrium sea-ice budget contribute to the stability of the ice cover in the geographical scales of the ocean.

The observations during the last two decades have recorded a significant decrease of the ice cover area and thickness in the Arctic Ocean due to global climate warming in the Northern hemisphere. How does it influence the species composition and structure of sea ice ecosystems?

Studies carried out over the past decade revealed appreciable changes in the qualitative and quantitative composition of the biota in the Arctic sea-ice compared to the composition in the mid-1970s. The total list of ice algae identified for the period of 1975–1982 comprises 172 taxa (Melnikov 1989) and about 30 species identified in 1997–2008 (Melnikov et al. 2002; Melnikov 2005, 2008b). The prevalence of sea diatoms was a significant feature of sea ice phytocoenosis in the 1970s, and their domination greatly decreased in the past decade, while other groups are growing in importance. The ice fauna composition has changed as well. Such mass representatives of protozoans and invertebrates as foraminifers, tintinninids, mites, nematodes, turbellarians, rotifers, copepods, and amphipods inhabiting the ice mass in the 1970s (Melnikov 1989) were rarely encountered in the past decade or were found as individual body fragments of these organisms. To appreciate the causes of the revealed differences, we must take a closer look at the composition and dynamics of the Arctic Ocean recent sea-ice cover, as well as at peculiarities of the formation and function of the MY and FY sea-ice ecosystems.

Under conditions of a stable climate, perennial sea ice represents an integral ecological system stable in time with a constant species composition of the flora and fauna (Melnikov 1989). The system stability persists due to average equilibrium thickness supported by summer ice thawing from above and winter compensation ice growth from below (Zubov 1945). This property, which can be referred to as sea ice cover homeostasis, the ability to retain its average equilibrium thickness, is of great ecological significance. It is expressed in the fact that the vertical structure of biological communities inhabiting it persists due to the action of two flows in different directions: (1) the motion of the crystalline structure from the bottom upwards due to thermodynamic ice thawing and ice formation, (2) the passive and/or active counter motion of organisms from the top down. In winter, ice grows from below on existing ice, the thickness of which after summer thawing is preserved at 2 m, and organisms, which inhabit these layers building-up from below, reside in conditions of mild temperatures close to the seawater temperature (about –2°C), which promotes their survival in the winter period. The balanced relationship between regions of perennial ice production and evacuation from the basin, as well as peculiarities of ice circulation along with mechanisms maintaining a constant species composition of ice organisms within the vertical crystalline structure, determines the stability of the perennial ice ecosystem in the Arctic Ocean.

By contrast, seasonal ice is a dependent ecosystem unstable with time, the life-time of which is determined by a complex of environmental factors, the temperature being regarded as the most significant among them. Seasonal ice formation begins in open water at a low air temperatures. In the course of formation of first layers, planktonic organisms in the water at the moment are mechanically entrained

into the ice crystalline structure of the lower growing layer. As the qualitative and quantitative composition of plankton in water is poor in the autumn–winter period, the amount of organisms entrained in ice appears to be small. Those organisms, which were mechanically entrained into ice, appear under conditions of intense cooling since the surface is in contact with air, the temperature of which decreases down to minus 30–40° C, and some of them survive but most of the organisms die because of sharp cooling. It is likely that because of this some isolated cells of algae and protozoans, as well as individual representatives of invertebrates, mechanically captured into the ice structure during its growth in winter are found in the ice mass in the spring period during the maximal ice development. In the autumn period, conditions for the formation of what is called infiltration ice may emerge at a low air temperature and intense snow accumulation on the ice. When the ice is thin and the snow weight becomes substantial relative to the weight of the ice, the ice appears to be submerged below the sea level, so that seawater along with cells of planktonic algae rises through the capillary system to the ice–snow boundary. As snow is a good heat insulator and light is still sufficient for photosynthesis to proceed, favorable conditions are created in this layer for alga development. The biomass of algae and concentration of the organic matter synthesized by them exceed in this layer by many times the same parameters in water below the ice. Such ice was encountered for the first time during the expedition "Arctic-2000" at the icebreaker *Akademik Fedorov* in the Canadian sector of the Arctic Ocean at 82°N and 170°W in September 2000 (Melnikov 2004). The formation of infiltration ice is a typical Antarctic phenomenon (Buinitskii 1973), and direct testimony to further development of infiltration ice in the Arctic Ocean is unavailable nowadays. However, it may be inferred that the phenomenon would continue in the future in view of the growing role of seasonal ice and increasing snowfall in the Arctic regions.

In comparing mechanisms for the formation of sea ice of these two types, it may be concluded that the main cause of the differences revealed between the composition of biological sea ice communities in the 1970s and the last decade is that the two MY and FY sea-ice ecosystems considered and compared were different in the structure and function. Indeed, in the first case, the constant species composition of algae and the invertebrate fauna was maintained by mechanisms forming the average equilibrium thickness, as well as by processes of colonization and evolution of organisms within the vertical crystalline structure of ice. Predominant were benthic-type algae adapted to dwelling in a solid substrate and capable of moving in narrow intercrystalline spaces of ice. In the second case, the species composition of the ice flora was formed directly from water and mainly represented by typical planktonic forms making up long chains from cells and mainly evolving in the lower layer of ice or on its lower surface (Melnikov 1989).

Hence, two MY and FY ice ecosystems different in composition and function coexist in the recent Arctic sea-ice cover As the share of the first ecosystem is dynamically decreasing and the share of the second ecosystem is simultaneously increasing, a gradual reorganization in the ecosystem of the Arctic Ocean pelagic

region is taking place at present. If such a dynamics is retained, it may be inferred that in the course of time the marine Arctic regions will gain features of the marine Antarctic regions. Indeed, the sea ice cover in the Southern Ocean disappears in summer and reappears in winter. Seasonal ice predominates and occupies more than 80% of the sea-ice cover area for eight months, whereas perennial ice occupies less than 20% of the area (NASA 1987). Seasonal ice develops in the Southern Ocean north of 70°S. There is no long polar night at these latitudes and light is sufficient for maintaining photosynthesis of the ice flora (Melnikov 1998). The total organic material of the Antarctic regions is produced mainly by phytoplankton in summer and partially by the flora of infiltration ice in winter. By contrast, the whole Arctic sea-ice cover is located north of 70°N, and all the biological communities evolve under more severe conditions. In central regions constantly covered with sea ice, the total organic production is combined from the production created by algae of perennial ice (>90%) and production of algae of seasonal ice and phytoplankton, which account for less than 10% (Melnikov 1989). The phytoplankton organic production makes up 97–99% in regions where seasonal ice predominates, for instance, in Arctic seas, which become free of ice in summer (Subba Rao and Platt 1984). At present, the function of the pelagic ecosystem in the central regions of the Arctic Ocean is being rearranged and is passing into conditions of seasonal development of the sea-ice cover; therefore, organic production by phytoplankton should be growing and the contribution of the sea ice flora should be decreasing. Such a cycle of evolution may result in reorganization of the whole lower trophic structure of the ocean and, probably, may affect all higher chains of the trophic structure, fishes, birds, and mammals included.

Recent decreasing of sea ice extent and thickness is not a fact of the complete disappearance of sea ice cover in the Arctic Ocean. In fact, it observes a reduction of MY ice surface that it leads to increasing of ice-free areas where FY ice is formed in winter. Now we observe the intensive process in reconstruction of sea-ice cover from domination of MY ice onto domination of seasonal ice. If this dynamic will be continued the Arctic Ocean will be getting similar to the Southern Ocean where seasonal ice is a dominant component reaching more 80% of its surface (NASA 1983), by another words, in time marine Arctic is getting more features of marine Antarctic.

Acknowledgments

This research was supported by the Russian Foundation for Basic Research (grant #08-05-00219).

References

Atlas of Oceans (1980) Arctic Ocean. Glav Red Atlasov Okeanov, VMF USRR, 184 pp
Buinitskii VKh (1973) Sea Ice and Icebergs of Antarctic Regions (LGU, Leningrad) 255 pp
Buzuev AY (1968) Certain statistical particularities in the multi-year ice thickness distribution. Trudi AANII, 287: 76–84
Carmack EC, Macdonald RW, Perkin RG, McLaughlin FA, Pearson RJ (1995) Evidence for warming of Atlantic water in the southern Canadian Basin of the Arctic Ocean: Results from the Larson-93 expedition. Geophys Res Lett, 22: 1061–1064
Carsey FD (1982) Arctic sea ice distribution at the end of summer 1973–1976 from satellite microwave data. J Geophys Res 87: 5809–5835
Cavaliere DJ, Gloersen P, Parkinson CL, Comiso JC, Zwally HJ (1997) Observed hemispheric asymmetry in global sea ice changes. Science, 278: 1104–1106
Koerner RM (1973) The mass balance of the sea ice of the Arctic Ocean. J Glaciol, 12(65)
McPhee M, Stanton TP, Morison JH, Martinson DG (1998) Freshening of the upper ocean in the arctic: Is perennial sea ice disappearing? Geophys Res Lett, 25: 1729–1732
Melnikov IA (1989) The Arctic Sea Ice Ecosystem. P.P. Shirshov Institute of Oceanology, Moscow, 190 pp
Melnikov IA (1998) Winter production of sea ice algae in the western Weddell Sea. Journal of Marine Systems, 17(1–4): 195–206
Melnikov I, Sherr B, Wheeler P, Welch H (1998) Preliminary biological and chemical oceanographic evidence for a long-term warming trend in the Arctic Ocean (current materials of the SHEBA Ice Camp, Beaufort Sea). In: Proceedings of the Arctic Change Workshop, Seattle, University of Washington, Washington, DC, June 1997, Report #8, August 1998, 60 pp
Melnikov IA (2000) The Arctic Sea Ice Ecosystems and Global Warming. In: Huntington, HP (ed.). *Impacts of Changes in Sea Ice and Other Environmental Parameters in the Arctic*. Report of the Marine Mammal Commission Workshop, 15–17 February 2000, Girdwood, Alaska, pp 72–82
Melnikov IA, Zhitina LS, Kolosova EG (2001) The Arctic Sea Ice Biological communities in recent environmental changes. In: Mem Natl Inst, Polar Res, Spec Issue, 54: 409–416
Melnikov IF, Kolosova EG (2001) The Canada Basin zooplankton in recent environmental changes in the Arctic Ocean. In: Proceedings of the Arctic Regional Centre, v.3, pp 165–176
Melnikov IA, Kolosova EG, Welch HE, Zhitina LS (2002) Sea ice biological communities and nutrient dynamics in the Canadian Basin of the Arctic Ocean. Deep-Sea Res, Part 1. 49: 1623–1649
Melnikov IA (2004) Sea ice export as an indicator of changing Arctic Ocean ecology. In: Skreslet S (ed.), Jan Mayen Island in Scientific Focus, 113–122
Melnikov IA (2005) Sea ice and upper ocean ecosystem in recent climate change in the Arctic. Marine Biology, 31(1): 3–10
Melnikov IA (2007) Panarctic ice camp expedition. Oceanology, 47(6): 952–954
Melnikov IA (2008a) Studies from the drifting ice station in April 2008. Oceanology, 48(6): 889–891
Melnikov IA (2008b) Recent Arctic Sea-Ice Ecosystem: Dynamics and Forcast. Doklady Akademii Nauk, 423(5): 817–820
Morison J, Steele M, Anderson R (1998) Hydrography of the upper Arctic Ocean measured from the Nuclear Submarine USS Pargo. Deep-Sea Res, Part 1, 45: 15–38
NASA SP-459 (1983) Antarctic Sea Ice, 1973–1976: Satellite Passive-microwave observations (NASA Sci. Tech. Info. Branch, Washington), 206 pp
NASA SP-489 (1987) Arctic Sea Ice, 1973–1976: Satellite Passive-microwave observations (NASA Sci. Tech. Info. Branch, Washington), 296 pp

Perovich DK, Andreas EL, Curry JA, Eiken H, McPhee MG, Morison J, Moritz RE, Pinkel R, Tucker WB (1999) Year on Ice Gives Climate Insights. EOS. 80(41): 481–486
Stroeve J, Holland MM, Meier W, Scambos T, Serreze M (2007) Arctic Sea ice decline: Faster than forecast. Geophys Res Lett, 34: L09501, doi:10.1029/2007GL029703
Subba DV, Platt T (1984) Primary production of arctic waters. Polar Biology, 3(4): 191–201
Wadhams P (1983) Sea ice thickness distribution in Fram Strait. Nature, 305(5930): 108–111
Zubov NN (1945) Arctic Ice. Izd Glavsevmorputi, Moscow, 360 pp

The effects of irradiance and nutrient supply on the productivity of Arctic waters: a perspective on climate change

Jean-Éric Tremblay and Jonathan Gagnon

Département de Biologie and Québec Océan, Pavillon Alexandre-Vachon, Université Laval, Québec, QC, Canada G1V OA6, Jean-Eric.Tremblay@bio.ulaval.ca

Abstract

A previous analysis of published data suggested that annual, pelagic primary production in the Arctic Ocean is related linearly to the duration of the ice-free period, presumably through cumulative exposure to solar irradiance. However, the regions with the longest ice-free periods are located in peripheral seas and polynyas where nutrient supply by advection or the vertical mixing induced by winds and convection can be extensive. The ensuing replenishment of nutrients drives primary production to levels unattained in the strongly stratified interior (e.g. the Beaufort Sea), with the exception of upwelling areas. A reanalysis of published data showed no relation between cumulative production and incident solar radiation during the growth season. We propose that changes in annual primary production per unit area in seasonally ice-free waters are controlled primarily by the environmental forcing of nitrogen supply. Incidental changes in light regime should mostly affect the timing and, possibly, the species composition of the main production pulse(s) in the upper mixed layer and, underneath, the ability of phytoplankton to exploit nutrients in the lower euphotic zone. While the ongoing rise in the supply of heat and freshwater to the Arctic Ocean should bolster vertical stratification and further impede the mean upward supply of nutrients, episodic yet direct atmospheric forcing of the upper ocean may act in synergy with a prolonged exposure to light and greatly augment pelagic productivity.

Introduction

The physical environment of the Arctic Ocean is changing rapidly and profoundly (ACIA 2005). The most spectacular manifestation is the decline in the minimum extent of sea ice in September and the thinning of the multi-year ice that remains

J.C.J. Nihoul and A.G. Kostianoy (eds.), *Influence of Climate Change on the Changing Arctic and Sub-Arctic Conditions*,

(Kwok et al. 2007; Maslanik et al. 2007; Stroeve et al. 2008). The ice cover is becoming essentially seasonal and, in some region, melts increasingly early or forms increasingly late (Lemke et al. 2007). River discharge is on the rise, augmenting freshwater content and the loading of organic and inorganic matter into the coastal zone (Peterson et al. 2006). The intensity and frequency of extreme wind events increased in several regions (Zhang et al. 2004), which will impact upper ocean dynamics under a reduced-ice scenario.

Quantifying and predicting the response of marine primary production to these alterations is a prerequisite to understand their impacts on Arctic food webs, biogeochemical cycles and air-sea fluxes of climate-active gases. One obvious consequence of the ongoing changes is that the amount of light reaching the ocean surface increases. Much less obvious is how this energy subsidy interacts with concomitant perturbations of the water column to alter the magnitude and species composition of pelagic primary production. Autotrophic growth requires light, but it also necessitates nutrients whose inventories are limited in the upper ocean. The ideal mixture of nutrients for growth varies across phytoplankton taxa and the ratios of the different nutrients differ widely among the source waters that pervade the Arctic Ocean (Tremblay et al. 2002b). A fraction of these nutrients is recycled locally by biological activity (i.e. excretion, decomposition) but changes in overall productivity must be sustained by allochthonous nitrogen (N) subsidies to the euphotic zone. This input may originate from deep waters as nitrate, from the atmosphere as N_2 or from precipitation and rivers as inorganic or organic N.

In the present context of rapid change, it is worth asking if generalizations can be made from the data gathered in the last 50 years to help bracket predictions and provide a perspective for the future. A few reviews of primary production have been published for Russian Seas (Vetrov and Romankevich 2004), the Arctic in general (e.g. Sakshaug 2004; Legendre et al. 1992; Smith and Sakshaug 1990) and polynyas (Arrigo 2007; Tremblay and Smith 2007). These reviews document the diversity and complexity of Arctic marine ecosystems, contrasting regions where ice dynamics and physical oceanography differ broadly (see also Carmack and Wassmann 2006).

In an effort to synthesize pan-Arctic data, Rysgaard et al. (1999) obtained a positive correlation between annual primary production and the duration of the ice-free period. Taken at face value, this relationship suggests that primary production would, in the future, increase in direct proportion with the lengthening of the ice-free season. Here we assess whether the correlation proposed by Rysgaard et al. (1999) has predictive value by investigating the causal, underlying factors. We begin by considering the role of irradiance and nutrients separately and conclude with a few perspectives and hypotheses for future research.

Data mining

Our review of the literature considered the studies used by Rysgaard et al. (1999), Sakshaug (2004) and Vetrov and Romankevich (2004) in addition to recent work in Baffin Bay and the Beaufort Sea (Klein et al. 2002; Simpson et al. 2008). The synthesis published by Rysgaard et al. (1999) reported annual values of primary production but none of the contextual physical and chemical parameters needed for an in-depth analysis of controlling factors. The latter requires information on the bathymetry of sampling stations, nutrient supply and the date of the first and last seasonal measurement of primary production (needed to estimate incident irradiance during the measurement period).

Albeit informative in their own right, several of the studies considered were excluded from the analysis because they were deemed non comparable. Sampling sites with bottom depths and salinities of less than 5 m and 5‰, respectively (Horner and Schrader 1982; Kangas et al. 1993; Meskus 1976) belong to neritic, intertidal or fluvial ecosystems and were dismissed. Model results were also discounted (e.g. Slagstad and Støle-Hansen 1991; Taguchi 1972; Wassman et al. 2006) as they cannot be considered on the same footing as actual measurements in first analysis.

Two levels of data synthesis were produced. Level 1 concerns only those studies where populated time series (i.e. measurements made at frequent time intervals in a constrained region or water mass) of primary production were available. Time series that did not resolve the peak and tail ends of the main production pulse (Grainger 1980 – for 1968; Walsh et al. 1989; Alexander 1974; McRoy and Goering 1976; Nielsen and Hansen 1999) were excluded from the level 1 data base. For purposes of concision, clarity and comparison, the time courses are reported and compared as cumulative primary production (ΣP) values obtained by leap-frog integration between successive time points. Level 2 gives annual primary production values estimated by interpolation and/or extrapolation, preferably by the authors themselves or by us when the calculation was not done originally. In some cases this was done by combining data from 2 or more years. We assume that the level of confidence attached to the different estimates is much higher for level 1 than for level 2 since extrapolations do not take into account possible changes in the time courses when measurements stopped long before the ice cover was re-established. The number of studies considered for level 1 (9 studies and 13 distinct time courses) is lower than the number of studies considered for level 2 (n = 12).

In most studies, data on incident or underwater solar radiation are either not provided or not usable for comparative purposes. Daily averages of incident short-wave radiation (W m^{-2}) corrected for cloud cover were retrieved from the NCEP/NCAR reanalysis. For each time series, cumulative radiation at the sea surface was calculated by multiplying daily averages in watts per square meter by 86,400 s and summing these daily doses over 60 days or the full time course.

Unless stated otherwise, results are expressed in GJ (Giga Joules) m^{-2}. Information on the initial concentrations of nutrients prior to the growth season was absent from a few studies. In these cases, concentrations were taken from anterior or posterior studies in the area or from the World Ocean Database 2005 (Boyer et al. 2006).

General properties of the data set

The general location of the studies used for level 1 and 2 analyses is shown in Fig. 1 and the characteristics of the each sampling site are given in Table 1. The study sites cluster in the western Arctic, an unintended regional bias, and range broadly in latitude (60–82.5° N) depth (15–450 m, taken as the average for a given sampling region) and year day of the first measurement of primary production (from late March to early July).

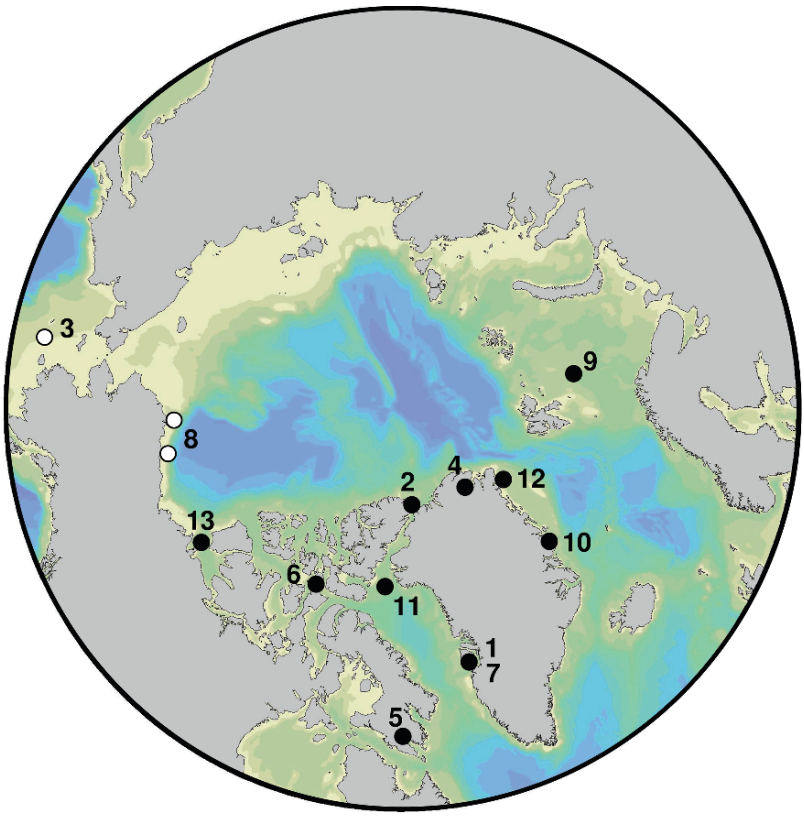

Fig. 1. Map of the sampling sites used for the analysis of detailed time series (black circles) and annual estimates (all symbols) of primary production. Numbers refer to the studies described in Table 1.

Table 1. General characteristics of the studies retained for level 1 and 2 analyses. Missing values (-) in the Start and End columns indicate that no time course data on primary production are available (only annual estimates).

ID	Year	Location	Latitude (°N)	Longitude (°W or °E)	Depth (m)	Start (year day)	End (year day)	Reference
1a	1959	Disko Bay (W. Greenland)	69.250	53.567° W	30	129	141	Petersen 1964
1b	1960	Disko Bay (W. Greenland)	69.250	53.567° W		93	165	Petersen 1964
2	1959	Dumbell Bay (Lincoln Sea)	82.517	62.167° W	25	172	66	Apollonio 1980
3	1968	Bering Sea	60.000	170.000° W	100	-	-	McRoy and Goering 1976
4	1968	N. Greenland	82.167	31.233° E	26	-	-	Andersen 1981
5a	1968	Frobisher Bay	63.667	68.450° W	50	176	110	Grainger 1980
5b	1969	Frobisher Bay	63.667	68.450° W		167	82	Grainger 1980
6	1971	Resolute Bay	74.684	94.868° W	15	181	102	Welch and Kalff 1975
7a	1973	Disko Bay (W. Greenland)	69.167	53.500° W	50	171	119	Andersen 1977
7b	1974	Disko Bay (W. Greenland)	69.167	53.500° W		138	168	Andersen 1977
7c	1975	Disko Bay (W. Greenland)	69.167	53.500° W		81	77	Andersen 1977
8a	1976	Beaufort Sea	71.000	148.000° W	30	-	-	Carey 1978
8b	1977	Beaufort Sea	71.000	148.000° W		-	-	Carey 1978
8c	1976	Chuckchi Sea	71.800	156.000° W	40	-	-	Carey 1978
8d	1977	Chuckchi Sea	71.800	156.000° W		-	-	Carey 1978
9	1982	Barents Sea	76.000	32.500° E	200	98	181	Rey et al. 1987
10	1996	Young Sound (E. Greenland)	74.310	20.251° W	35	174	100	Rysgaard et al. 1999
11	1998	NE. Baffin Bay	76.000	74.000° W	450	98	104	Klein et al. 2002
12	1993	NE. Greenland Sea	80.230	13.000° W	200	-	-	Klein et al. 2002
13	2004	SE. Beaufort Sea	70.807	125.393° W	250	152	84	Simpson et al. in press

Although the date of the first measurement differs broadly among studies, the different time courses (level 2) were plotted with a common time origin in order to directly compare the influence of time on ΣP (Fig. 2). One striking result is that in the most productive systems ΣP tends to reach an asymptote whereas in the others it generally increases in a roughly linear fashion. The latter observation challenges the general notion that Arctic systems are strongly pulsed in time with a peak period of production lasting only a few weeks. Another noteworthy aspect of Fig. 2 is that although the initial rates of increase vary, the time courses rapidly assume their final, relative rank. Such layering implies the absence of a single time continuum along which ΣP values lay as the duration of the open water period increases. In other words, the level of primary production in these systems is largely conditioned or set at the beginning and overall differences in ΣP are not explained by the duration of the open water period *per se*. As much as 85% of the variability in ΣP end points is predictable after only 60 days, despite measurement periods lasting from 3 to 8 months.

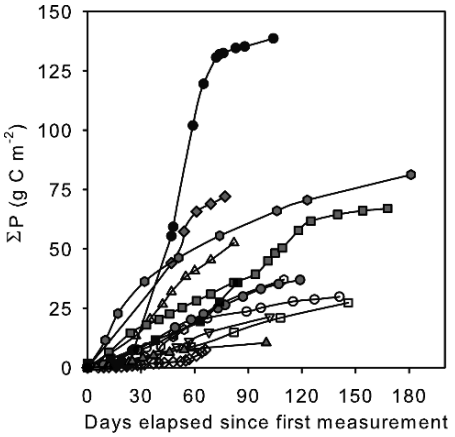

Fig. 2. Time courses of cumulative primary production (ΣP), starting on the first day of measurement for each time series. The different symbols refer to the ID numbers of the distinct studies and sampling years given in Table 1: 1a (open circle), 1b (open square), 2 (open diamond), 5a (open hexagon), 5b (open triangle), 6 (open inverted triangle), 7a (gray circle), 7b (gray square), 7c (gray diamond), 9 (gray hexagon), 10 (gray triangle), 11 (black circles), and 13 (black square).

The role of irradiance

The ice cover and extreme solar cycle impose severe constraints on primary production. These limits are most severe toward the pole, where the vanishing multi-year ice conspires with the polar night to make photosynthesis impossible throughout most of the winter. Conditions are less stringent at lower latitudes where variable ice dynamics and irradiance regimes create a host of transient

niches for primary producers. The replacement of multi-year ice by seasonal ice is likely to create a more favourable light climate at higher latitudes. Light plays two roles in this respect. It determines when net phytoplankton growth is possible and how much cumulative energy is available for photosynthesis during the course of the growth season.

Once light has reached the water its availability for phytoplankton is determined by a combination of factors that includes mixing, which sets the mean irradiance seen by the cells and affects water transparency via sediment re-suspension on shallow shelves (e.g. Forest et al. 2008), the biomass of phytoplankton and horizontal inputs of dissolved and particulate organic matter in coastal regions. The interplay between incident irradiance, water transparency and mixing depth in determining the potential for phytoplankton growth has been the subject of empirical considerations that will not be repeated here (Nelson and Smith 1991; Sakshaug and Slagstad 1991). It is noteworthy that the data sets used in our analysis seldom include the information needed to estimate mean irradiance in the mixed layer.

Onset of the productive season

Net primary production is considered possible only when phytoplankton have enough light for positive growth, generally in accordance with Sverdrup's critical depth model as revised by Smetacek and Passow (1990). Although communities located at the ice-water interface or at the top of the euphotic zone may not be vigorously mixed, they require enough light to outgrow losses, i.e. irradiance must be higher than the compensation light intensity below which the sum of phytoplankton respiration and other losses (grazing, lysis and sinking) exceeds the gain of carbon by photosynthesis. Recent empirical estimates indicate that the compensation irradiance of diatom communities in the Arctic is similar to the mean for the north Atlantic (1.3–1.9 mol quanta m^{-2} day^{-1}; Tremblay et al. 2006b).

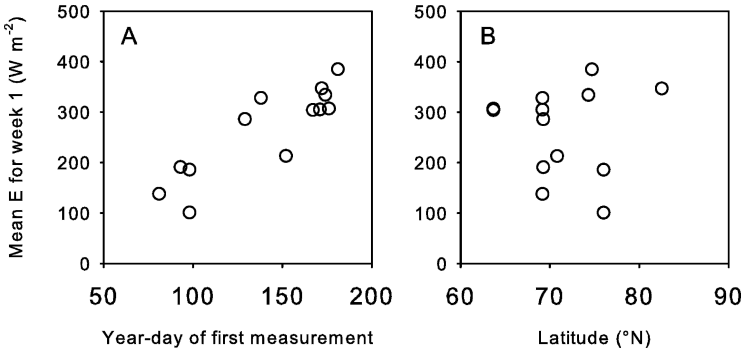

Fig. 3. Relationship between the mean, downwelling short-wave radiation at the sea surface during the first week of measurements and (**A**) the year-day of the first measurement, and (**B**) the latitude of the sampling site.

Not surprisingly, the locations that open early during the year receive much less irradiance initially (Fig. 3A). The mean incident short-wave radiation at the surface during the first week of measurement is independent of latitude (Fig. 3B), indicating that the onset of the productive period is controlled essentially by regional oceanic processes and ice dynamics instead of the solar cycle. Once there is enough light for net growth the initial rate of development of a bloom should depend on the exposure of micro-algae to irradiance and their ability to harvest this light efficiently, which is influenced by the physiological state of the cells and, possibly, temperature (Tremblay et al. 2006b).

Cumulative irradiance

The pattern shown in Fig. 4A is counter-intuitive. The systems with the highest levels of primary production after 60 days (the point where all systems can be compared) received much less light than the least productive ones. This results is consistent with the inability of diatoms to harvest light immediately after an abrupt switch from near complete obscurity to full sunlight after rapid ice ablation (Tremblay et al. 2006b), a problem that is likely to be most acute in systems that open late and close to the summer solstice.

How the algae respond to light at the onset of the growth season presumably depends on how fast the transition occurs, but also on the different photoadaptation and photoacclimation strategies of the seed organisms present (Sakshaug and Slagstad 1991). The photoinhibition of planktonic algae has sometimes been regarded as an experimental artefact of incubations, whereby the cells are contrived to remain under high light for longer than they do under mixed, *in situ* conditions. The advent of rapid, non-intrusive active fluorescence techniques showed that photoinhibition is often severe in these communities, even when exposed to light flashes of a few micro-seconds. In fact, this short-term photoinhibition is often more acute than is apparent from incubations spanning a few hours to a day (either *in situ* or simulated *in-situ*), suggesting that in the latter, the algae have some time to adjust and recover, which does not intervene during near-instantaneous measurements.

As expected, the apparent negative effect of irradiance disappears when considering time courses in their entirety. Nevertheless, the total amount of radiation (ΣE) received during the time courses bears no relationship to ΣP, either for the duration of each time course (Fig. 4B) or on an annual basis (Fig. 4C). Note also that in Fig. 4B, ΣP ranges by an order of magnitude for ΣE values of 1.5–2.1 GJ m^{-2}. Although rigorous comparisons based on mean irradiance in the mixed layer are not possible in retrospect, it is clear that differences in irradiance dose are by far insufficient to account for the range of ΣP across seasonally-open systems.

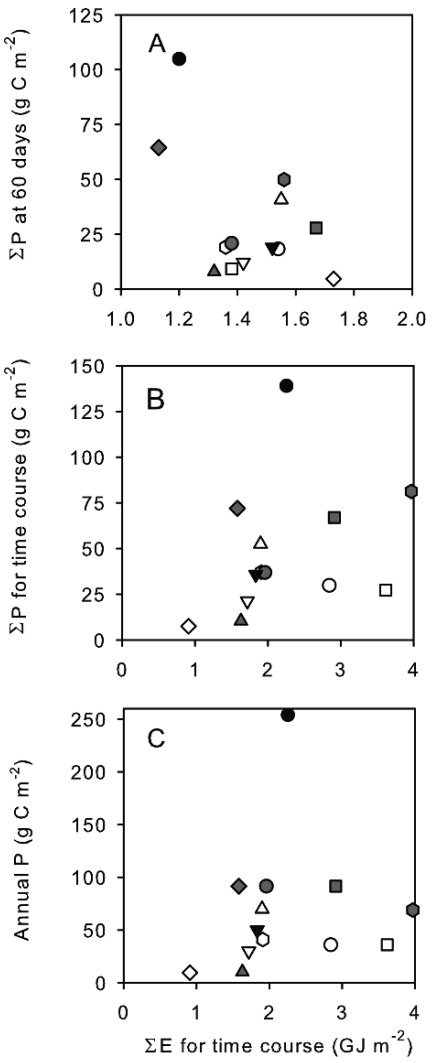

Fig. 4. Relationships between cumulative primary production (ΣP) and cumulative downwelling, short-wave radiation at the sea surface (ΣE) for (**A**) the first 60 days of each time course, (**B**) the total duration of each time course, and (**C**) 1 year for ΣP with ΣE calculated for the time course only (**B**). Symbols as per Fig. 2.

The role of nutrients

Allochthonous nitrate

Nutrients are supplied to the upper Arctic Ocean by a variety of processes that operate at different scales of time and space. Horizontal inputs are provided by rivers and currents originating from adjacent seas. Advection is especially important immediately downstream of gateways to the Pacific and Atlantic, where it can support intense primary production, especially in the Chukchi Sea. Surface waters reside in the central Arctic for ca. 10 years and, unless their transit occurs exclusively under multi-year ice, labile nutrients are readily consumed at the periphery during the first year. This scenario also applies to the inorganic nutrients delivered by major rivers. For example, the Mackenzie River supplies a lot of silicate to the Arctic Ocean, but any residual, inorganic phosphate and nitrogen is exhausted before the freshwater plume advances into the sea (Emmerton et al. 2008; Simpson et al. 2008).

Denitrification over the shallow shelves of the subarctic Pacific Ocean and the Arctic, in combination with high silicate loading by rivers insures that phosphorus and silicon remain in excess, especially where Pacific waters dominate. Nitrogen is the primary yield-limiting nutrient in the Arctic as it was exhausted first in all blooms investigated so far (Kattner and Budeus 1997; Simpson et al. 2008; Tremblay et al. 2002b, 2008), even in the Barents Sea where concentrations of silicate and phosphate are relatively low (Reigstad et al. 2002).

Physical singularities episodically subsidize a given region with nutrients. These singularities can take the form of internal waves, storms that erode the halocline, shelf-break upwelling and dynamic instabilities caused by bathymetry or convection (Mathis et al. 2007; Williams et al. 2006; Zhang et al. 2004; Tremblay et al. 2002a). The incidence and strength of upwelling events and halocline perturbations are presumably increasing with the rising frequency and intensity of cyclones (Yang et al. 2004) and the retreat of the perennial ice pack beyond the shelf break (Carmack and Chapman 2003). It is not currently possible to assess or forecast the net result of changes in the mean *versus* episodic deliveries of nutrients on the magnitude and species composition of primary production.

The total availability of nutrients to primary producers is the sum of the initial inventory in the euphotic zone (end of winter) and any inputs that occur once the growth season is initiated. Because these subsidies are difficult to quantify and were seldom considered in the papers used for level 1 and 2 analyses, we evaluated only the initial inventories of nutrients present at or prior to the onset of the growth season.

It is clear from the depth distribution of studies (Table 1) that vertical integration must be standardized for comparison. Time series obtained over deep waters indicate that pronounced seasonal nutrient deficits frequently extend to 50–75 m (Tremblay et al. 2002a; Smith et al. 1997), due to either episodic vertical mixing

during the growth season or the ability of phytoplankton to thrive within subsurface chlorophyll maxima (Tremblay et al. 2008). In this view, systems with bottom depths of less than 50 m cannot yield the same new production because of their limited nutrient inventories and the vertical proximity or overlap between sediment denitrification and the euphotic zone. In Young Sound, as example, the shallow bottom (35 m) and associated denitrification limit nitrate concentrations to 2 μM during winter (total spring time inventory of 70 mmol m^{-2}) (Rysgaard et al. 2004). Phytoplankton in waters less than 40 m in depth typically have access to initial nitrate inventories of 150 ± 135 mmol m^{-2}, whereas those in deeper waters can potentially tap into as much as 1,000 mmol m^{-2} (Fig. 5). In order to perform a legitimate comparison of the nutrients available to phytoplankton, late-winter inventories were estimated for the upper 75 m over deep waters or for the whole water column at sites shallower than 75 m.

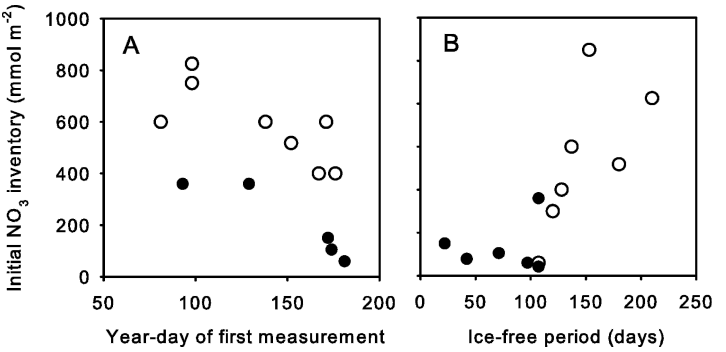

Fig. 5. Relationship between the initial concentration of nitrate at the onset of the growth season and (**A**) the year-day of the first measurement for level 1 and 2 data, and (**B**) the estimated duration of the ice-free period for all data. Closed and open circles indicate bottom depths of less or more than 30 m, respectively.

Although the shallowest waters have the smallest nitrate inventories, bathymetry alone explains 30% ($p < .05$) of the overall variability in the initial availability of nitrate, indicating that physical processes play a determinant role at deep sites. As example, systems located in the Atlantic sector of the Arctic (e.g. eastern North Water and Barents Sea, i.e. studies 9 and 11 in Table 1) are usually advantaged by the greater susceptibility of surface waters to vertical mixing relative to the strongly stratified Pacific-derived waters (e.g. Gulf of Amundsen, study 13 in Table 1) (see also Tremblay et al. 2008). Overall, the initial nitrate inventory shows a negative relationship ($r^2 = .36$, $p < .05$) with the year-day of the first measurement (Fig. 5A) and a positive one ($r^2 = .41$, $p < .01$) with the estimated duration of the ice-free season (Fig. 5B). This pattern implies that systems where surface waters are exposed to the atmosphere for a longer time experience a larger nitrogen load. The likely cause of this effect is that systems with a long ice-free period such as the North

Water or the Barents Sea are exposed to storms during late winter or autumn and convection that erode the weak vertical stratification and replenish nutrients (Tremblay et al. 2002a). Waters that open in late spring or summer (e.g. the Northeast Water) when winds are weak and the sun induced melt-water stratification is strong see little vertical replenishment of nutrients on an annual basis (Kattner and Budeus 1997). Parts of the Barents Sea that lay along storm tracks in summer also experience significant nutrient renewal where haline stratification is moderate (Sakshaug and Slagstad 1992; Wassman et al. 2006). In extreme cases, even the strong stratification that characterizes waters of the Canada Basin can be overturned, thus providing an ample supply of nutrients to an otherwise impoverished upper euphotic zone. This condition was observed in northwest Baffin Bay, but the underlying mixing process has yet to be confirmed (Tremblay et al. 2002b).

The initial inventory of nitrate in the upper 75 m proved to be a reasonably robust predictor of ΣP at 60 days ($r^2 = .53$, $p < .01$; Fig. 6A) and at the end of each time course ($r^2 = .69$, $p < .001$; Fig. 6B). These relationships explain why annual production can be predicted from cumulative values after 60 days, i.e. the overall level of primary production is largely pre-determined by the initial nutrient load although light may influence the initial rates of drawdown. The relationship between nitrate loading also held for annual P, but this time the North Water clearly stood out as a positive anomaly. Removing this outlier from the analysis yields a very robust correlation ($r^2 = .78$, $p < .0001$; Fig. 6C). The anomalously high level of annual primary production in the North Water was caused by episodic mixing, a fall bloom and continued productivity through October (Garneau et al. 2007; Klein et al. 2002), which underscores how the initial inventories of nitrate provide only a limited view of nitrogen supply in some systems. Another example of this limitation is found in some regions of the Bering Sea, where persistent nutrient renewal leads to unusual productivity levels similar to and higher than those observed in the North Water (e.g. Sambrotto et al. 1984; Springer et al. 1996). Clearly, the inshore portions of shallow Arctic shelves do not experience a significant late-season, vertical re-supply of nitrate simply because the deep reservoir is absent. At the shelf break or in deeper regions, episodic mixing and upwelling may augment primary productivity far beyond the levels expected from initial conditions. It follows that, on a regional basis, the effects of climate change on primary productivity will greatly depend on bathymetry and distance from the shelf break, rivers and the adjacent Pacific and Atlantic oceans.

A multiple regression model that included ΣE in addition to the inventory of nitrate only slightly improved the prediction of ΣP, and the partial coefficient for the effect of irradiance was not significant (not shown). It is clear in this context that nitrogen loading is the primary control on the productivity of Artic waters. Considering the few studies were temperature data were available, we were unable to find a relationship between temperature and the initial increase in ΣP (see also Tremblay et al. 2006b).

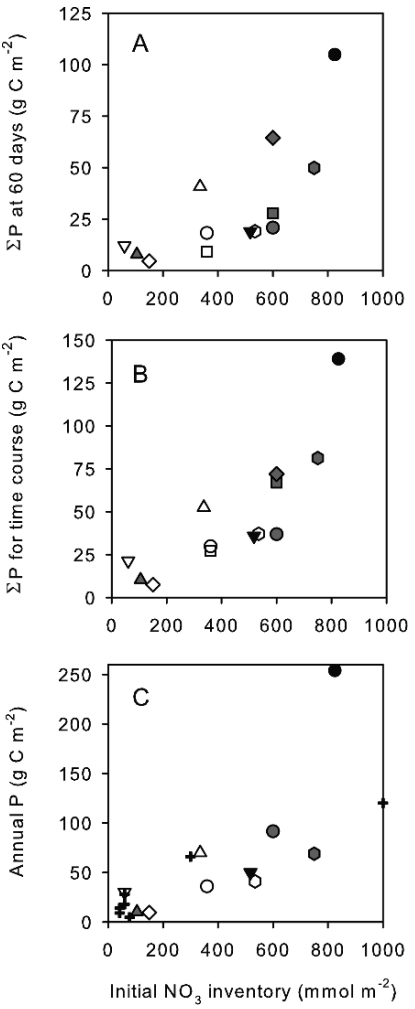

Fig. 6. Relationships between the initial concentration of nitrate at the onset of the growth season and ΣP for (**A**) the first 60 days of each time course, (**B**) the total duration of each time course, and (**C**) 1 year. Symbols as per Fig. 2 except for panel C where crossesrepresent studies for which annual estimates but no time courses are available (ID 3, 4, 8a–d, and 12 in Table 1).

The contribution of new and regenerated production

The allochthonous N assimilated by autotrophs (i.e. new production) is eventually channeled into waste or lost by transport or sinking. Some of the waste products that remain in the euphotic zone can be re-used directly or readily broken down

into usable N forms by photochemistry or bacteria. The N thus recycled drives regenerated production, which contributes to total primary production but cannot sustain net increases in the yield of organic matter, ecosystem productivity and vertical carbon export (Dugdale and Goering 1967; Eppley and Peterson 1979). The relative importance of new and regenerated production must be resolved to understand what drives pan-Arctic differences in total production and what these changes signify for the yield of harvestable resources and air-sea fluxes of climate-active gases.

As the duration of the ice-free season increases, there is a distinct possibility that ΣP also does simply because N cycles more times in the euphotic zone. To investigate this possibility it is useful to consider published estimates of the *f*-ratio, i.e. the ratio of allochthonous N uptake to total N uptake. Ideally, the uptake of all sources of allochthonous and recycled N should be considered in the *f*-ratio, but only the net uptake of nitrate, ammonium and, sometimes, urea are routinely estimated.

Comparable, populated time series of the *f*-ratio that resolve a major portion of the growth season remain extremely rare. This data is available for the North Water (*f*-ratio = 0.58; Tremblay et al. 2006a) and the Northeast Water (*f*-ratio = 0.65; Smith et al. 1997), where repeated measurements were made over a similar period of ca. 3 months starting in spring. These *f*-ratios are remarkably similar despite the threefold difference in initial nitrate inventories and the fourfold difference in annual production between the two systems (252 g C m^{-2} for the North Water versus 66 g C m^{-2} for the Northeast Water). The comparison shows that regenerated production accounts for a substantial share of total primary production, but is merely proportional to new production and the supply of allochthonous N. Since the two systems were characterized by negligible inventories of ammonium and urea at the onset of the growth season, a transformation of the *f*-ratio, $(1 - f)/f$, can be used to estimate the number of times the N initially bound in nitrate was recycled during the 3-month period, which yields low values of 0.6–0.7 . In the North Water, a net amount of 920 mmol N m^{-2} was consumed between 23 April and July 1 (Tremblay et al. 2006a). By then, only 100 mmol N m^{-2} remained as PON and 22 mmol N m^{-2} as ammonium + urea in the euphotic zone (Tremblay et al. 2002a, 2006a). This rough budget implies that up to 87% of the N initially taken up as nitrate resided in the euphotic zone for less than 68 days, which is short relative to the duration of the ice-free period (ca. 6 months). In this view, a protracted ice-free season should promote regenerated production insofar as there is a continual or pulsed supply of external N to maintain it.

Implications, perspectives and future research

Assessments of the current and future productivity of the Arctic Ocean should distinguish between rate and yield-limiting processes, and between new and regenerated production. Light and the physiological state of phytoplankton influence

the rate at which nutrients are consumed early (Tremblay et al. 2006b) and late (Garneau et al. 2007) in the year, whereas the supply of external nitrogen to the euphotic zone sets the upper yield of organic matter production (Tremblay et al. 2006b). Offshore, the ablation of multi-year ice will initially increase new production per unit area where residual nutrients linger, but the stimulation will lessen in subsequent years unless the new physical regime promotes recurrent nutrient renewal through vertical mixing, upwelling or eddy genesis. Over shallow shelves with a limited inventory of inorganic N and a secular, seasonal ice cover, it is doubtful that a protracted ice-free period will augment new production per unit area away from shelf breaks, rivers and adjacent oceans. In essence, the greater extent of seasonally-open water should increase basin-scale primary production but, beyond the initial transition from multi-year to seasonal ice, cannot in and off itself lead to a sustained, order-of-magnitude increase in ΣP per unit area (c.f. Rysgaard et al. 1999) in currently unproductive areas.

The environmental changes at work in the Artic may very well alter the upward supply of N to the euphotic zone. Whether these alterations result in a subsidy or an impoverishment in a given region will largely depend on how changes in the fresh-water balance interact with atmospheric forcing of the upper ocean. While warming, precipitation and the increasing delivery of freshwater should increase vertical stratification and further curtail the upward flux of nutrients in the coastal zone, evaporation and the export of multiyear ice offshore are conducive to salinization (Polyakov et al. 2007), which by weakening stratification of the surface layer could make it more susceptible to mixing by storms. This susceptibility is also increased by the contraction of the ice-covered period, which submits surface waters to direct wind forcing during early spring or late fall (e.g. Tremblay et al. 2002a).

The role of advection and rivers as direct, horizontal sources of nutrients remains difficult to assess. Historically, rivers did not deliver large amounts of inorganic N and phosphorous to the Arctic Ocean, but rising discharge and contributions of melted permafrost to affluent waters may increase nutrient load in coastal waters (Frey et al. 2007; McClelland et al. 2007). This subsidy, however, is likely to be local in nature since inorganic nutrients are readily consumed inshore. The scenario may differ for dissolved organic nitrogen (DON) that escapes early consumption and potentially sustains a portion of primary production in coastal waters.

Recent data from the southeast Beaufort Sea shows that the net depletion of inorganic phosphorus and dissolved inorganic carbon (DIC) continues after nitrate is exhausted (Simpson et al. 2008; Tremblay et al. 2008), which suggests that autotrophs have access to an alternate source of allochthonous N. Some of the DON supplied by rivers can be used directly by some phytoplankton or made available by photochemical or bacterial attack of non-readily labile compounds (e.g. Vahatalo and Zepp 2005). New evidence implies that the input and biological availability of dissolved organic matter during the spring freshet is higher than previously thought on the basis of summer data (Holmes et al. 2008). The excess phosphorus and low availability of nitrate in the high Arctic also makes it a fertile ground for N_2 fixation. Yamamoto-Kawai et al. (2006) suggested that the excess

phosphorus sustains N_2 fixation downstream in the North Atlantic, but it might also be so within the Arctic proper, especially when and where conditions (e.g. temperature) are favourable for diazotrophs. This hypothesis remains to be confirmed experimentally, but it is plausible that regional N_2 fixation will gain in importance as the upper Arctic warms and becomes more stratified.

Much of the literature dealing with river discharge understandably focuses on dissolved organic carbon (DOC) inputs and their impact on ocean biogeochemistry, including the heterotrophic and photochemical release of DIC (e.g. Bélanger et al. 2006). The effect of this release on air-sea fluxes of CO_2, however, could be mitigated by the incidental increase of net primary production resulting from a relaxation of N limitation. It is possible, however, that declining water transparency could trigger a shift from nutrient limitation to light limitation over shallow shelves. An integrated study of these aspects in addition to N_2 fixation, nitrification and sediment denitrification is warranted given their potential impact on the air-sea exchange of CO_2 and N_2O (e.g. Duce et al. 2008).

Ongoing changes in the physical environment will probably affect taxonomic dominance during production pulses (e.g. Arrigo et al. 1999; Walsh et al. 2004), but this topic remains severely understudied in the Arctic. Apart from peripheral seas (i.e. Bering, Barents, Labrador and Greenland), where *Emiliana huxleii* or colonies of *Phaeocystis pouchetii* can reach high biomasses, documented phytoplankton blooms in the interior of the Arctic Ocean have been dominated by diatoms so far. No satisfactory explanation has been proposed for this geographical segregation but, as in the Southern Ocean, distinct adaptations to light regime (Arrigo et al. 2007) possibly play a part. More research is needed on this question since changes in taxonomic dominance have profound consequences for food webs, biogeochemical fluxes and climate feedbacks (e.g. Tozzi et al. 2004).

Another unknown is how recurrent reductions in the duration of the seasonal ice cover and the production of ice algae will affect sympagic-pelagic-benthic interactions. Algae from the water column can either be trapped in new ice or colonize the bottom of thicker first-year ice during winter and spring, but the converse is much less obvious. On the one hand, there is evidence that ice algae, when released from the ice, sink promptly to the bottom and provide food to benthic communities, especially over shallow continental shelves (Legendre et al. 1992). On the other hand, retention of sloughed ice algae in the upper water column has been observed (Michel et al. 1993) and inferred to provide significant energy to pelagic grazers on the basis of carbon budgets (Michel et al. 1996). The extent to which ice-grown algae currently seed and shape pelagic blooms is an open question. Although it may not affect the overall yield of organic matter during the growth season, a change in the timing and species composition of pelagic blooms is likely to alter food webs and the success of herbivores with less flexible life histories.

In conclusion, this review showed that the positive correlation between the duration of the ice-free period and annual primary production observed by Rysgaard et al. (1999) does not have predictive power per se. This correlation was essentially

driven by bathymetry and the differential susceptibility of distinct oceanic provinces to vertical mixing. The productivity of shallow or strongly stratified Arctic waters will not catch up with that of weakly stratified or upwelling-prone regions simply because the duration of the growth season increases. Such an increase will of course modulate annual productivity within a given body of water, notably by increasing production in the subsurface chlorophyll maximum, but the change will not measure up to the order-of-magnitude range in ΣP observed at the pan-arctic scale. Almost any short-term response is possible within this envelope, as recently shown by Arrigo et al. (2008) for the 2007 growth season. However, sustained increases in primary production per unit area will only occur where the greater exposure of surface waters to solar radiation is matched by annually recurring nutrient subsidies. Whether this occurs or not essentially depends on the net result of concomitant changes in the freshwater balance, horizontal nutrient loading and atmospheric forcing of the upper Arctic Ocean.

Acknowledgments

We thank Danny Dumont for his timely help with the NCEP reanalysis of solar radiation data. This work was supported by grants to JET from the Natural Sciences and Engineering Research Council of Canada and the ArcticNet Network Center of Excellence, and is a contribution to the programs of Québec Océan and the Canada Research Chair on the Response of Arctic Marine Ecosystems to Climate Change.

References

ACIA (2005) Scientific Report: Arctic Climate Impact Assessment. Cambridge University Press, Cambridge

Alexander V (1974) Primary productivity regimes of the nearshore Beaufort Sea, with reference to potential roles of ice biota. In: Reed JC, Sater JE (eds.) The Coast and Shelf of the Beaufort Sea, The Arctic Institute of North America, Calgary

Andersen OGN (1977) Primary production, illumination and hydrography in Jorgen Bronlund Fjord, North Greenland. Medd om Grønland 205:1–27

Andersen OGN (1981) The annual cycle of phytoplankton primary production and hydrography in the Disko Bugt area, West Greenland. Medd om Grønland 6:3–65

Apollonio S (1980) Primary production in Dumbell Bay in the Arctic Ocean. Mar Biol 61:41–51

Arrigo KR (2007) Physical control of primary production in Arctic and Antarctic polynyas. In: Barber DG, Smith WOJ (eds.) Polynyas: Windows into the World, Elsevier, Oceanography Series, Amsterdam

Arrigo KR, Robinson DH, Worthen DL, Dunbar RB, DiTullio GR, VanWoert M, Lizotte MP (1999) Phytoplankton community structure and the drawdown of nutrients and CO2 in the Southern Ocean. Science 283:365–367

Bélanger S, Xie HX, Krotkov N, Larouche P, Vincent WF, Babin M (2006) Photomineralization of terrigenous dissolved organic matter in arctic coastal waters from 1979 to 2003: Interannual variability and implications of climate change. Global Biogeochem Cycles. doi: 10.1029/2006GB002708

Carey AG, Jr. (1978). Marine biota. In: Environmental Assessment Alaskan Continental Shelf Interim Synthesis, Beaufort/Chuckchi, NOAA, Boulder, CT

Carmack E, Chapman DC (2003) Wind-driven shelf/basin exchange on an arctic shelf: The joint roles of ice cover extent and shelf-break bathymetry. Geophys Res Lett. doi: 10.1029/2003GL017526

Carmack E, Wassmann P (2006) Food webs and physical-biological coupling on pan-Arctic shelves: Unifying concepts and comprehensice perspectives. Prog Oceanogr 71:446–477

Duce RA, LaRoche J, Altieri K, Arrigo KR, Baker AR, Capone DG, Cornell S, Dentener F, Galloway J, Ganeshram RS, Geider RJ, Jickells T, Kuypers MM, Langlois R, Liss PS, Liu SM, Middelburg JJ, Moore CM, Nickovic S, Oschlies A, Pedersen T, Prospero J, Schlitzer R, Seitzinger S, Sorensen LL, Uematsu M, Ulloa O, Voss M, Ward B, Zamora L (2008) Impacts of atmospheric anthropogenic nitrogen on the open ocean. Science 320:893–897

Dugdale RC, Goering JJ (1967) Uptake of new and regenerated forms of nitrogen in primary productivity. Limnol Oceanogr 12:196–206

Emmerton CA, Lesack LFW, Vincent WF (2008) Mackenzie River nutrient delivery to the Arctic Ocean and effects of the Mackenzie Delta during open water conditions. Global Biogeochem Cycles doi: 10.1029/2006GB002856

Eppley RW, Peterson BJ (1979) Particulate organic matter flux and planktonic new production in the deep ocean. Nature 282:677–680

Forest A, Sampei M, Makabe R, Sasaki H, Barber D, Gratton Y, Wassmann P, Fortier L (2008) The annual cycle of particulate organic carbon export in Franklin Bay (Canadian Arctic): Environmental control and food web implications. J Geophys Res. doi: 10.1029/2007JC004262

Frey KE, McClelland JW, Holmes RM, Smith LC (2007) Impacts of climate warming and permafrost thaw on the riverine transport of nitrogen and phosphorus to the Kara Sea. J Geophys Res. doi: 10.1029/2006JG000369

Garneau ME, Gosselin M, Klein B, Tremblay JE, Fouilland E (2007) New and regenerated production during a late summer bloom in an arctic polynya. Mar Ecol-Prog Ser 345:13–26

Grainger EH (1980) Primary production in Frobisher Bay, Arctic Canada. In: Dunbar MJ (ed.) Marine Production Mechanisms, Cambridge University Press, Cambridge

Holmes RM, McClelland JW, Raymond PA, Frazer BB, Peterson BJ, Stieglitz M (2008) Lability of DOC transported by Alaskan rivers to the Arctic Ocean. Geophys Res Lett. doi: 10.1029/2007GL032837

Horner R, Schrader GC (1982) Relative Contributions of Ice Algae, Phytoplankton, and benthic microalgae to primary production in nearshore regions of the Beaufort Sea. Arctic 35:485–503

Kangas P, Alasaarela E, Lax HG, Jokela S, Storgaard-Envall C (1993) Seasonal variation of primary production and nutrient concentrations in the coastal waters of the Bothnian Bay and the Quark. Aqua Fenn 23:165–176

Kattner G, Budeus G (1997) Nutrient status of the Northeast Water Polynya. J Mar Syst 10:185–197

Klein B, LeBlanc B, Mei ZP, Béret R, Michaud J, Mundy CJ, von Quillfeldt CH, Garneau ME, Roy S, Gratton Y, Cochran JK, Belanger S, Larouche P, Pakulski JD, et al. (2002) Phytoplankton biomass, production and potential export in the North Water. Deep-Sea Res II 49:4983–5002

Kwok R, Cunningham GF, Zwally HJ, Yi D (2007) Ice, Cloud, and land Elevation Satellite (ICESat) over Arctic Sea ice: Retrieval of freeboard. J Geophys Res 112:doi: 10.1029/2006JC003978

Legendre L, Ackley SF, Dieckmann GS, Gulliksen B, Horner R, Hoshiai T, Melnikov IA, Reeburgh WS, Spindler M, Sullivan CW (1992) Ecology of sea ice biota. 2. Global significance. Polar Biol 12:429–444

Lemke P, Ren J, Alley RB, Allison I, Carrasco J, Flato G, Fujii Y, Kaser G, Mote P, Thomas RH, Zhang T (2007). Observations: Changes in snow, ice and frozen ground. In: Solomon S et al. (eds.) Climate Change 2007: The Physical Science Basis Contribution of Working Group I to the Fourth Assessment Report of the Intergovernmental Panel on Climate Change, Cambridge University Press, Cambridge, UK/New York

Maslanik J, Fowler C, Stroeve J, Drobot S, Zwally HJ, Yi D, Emery WJ (2007) A younger, thinner arctic ice cover: Increased potential for rapid extensive sea ice loss. Geophys Res Lett. doi:10.1029/2007/GL032043

Mathis JT, Pickart RS, Hansell DA, Kadko D, Bates NR (2007) Eddy transport of organic carbon and nutrients from the Chukchi Shelf: Impact on the upper halocline of the western Arctic Ocean. J Geophys Res. doi: 10.1029/2006JC003899

McClelland JW, Stieglitz M, Pan F, Holmes RM, Peterson BJ (2007) Recent changes in nitrate and dissolved organic carbon export from the upper Kuparuk River, North Slope, Alaska. J Geophys Res-Biogeosci. doi: 10.1029/2006JG000371

McRoy CP, Goering JJ (1976) Annual budget of primary production in the Bering Sea. Mar Sci Commun 2:255–267

Meskus E (1976) The primary production in the northeastern Bothnian Bay. Acta Univ Oulu A 42:55–62

Michel C, Legendre L, Therriault JC, Demers S, Vandevelde T (1993) Springtime coupling between ice algal and phytoplankton assemblages in southeastern Hudson Bay, Canadian Arctic. Polar Biol 13:441–449

Michel C, Legendre L, Ingram RG, Gosselin M, Levasseur M (1996) Carbon budget of sea-ice algae in spring: Evidence of a significant transfer to zooplankton grazers. J Geophys Res 101:18345–18360

Nelson DM, Smith WO (1991) Sverdrup revisited - Critical depths, maximum chlorophyll levels, and the control of Southern-Ocean productivity by the irradiance-mixing regime. Limnol Oceanogr 36:1650–1661

Nielsen TG, Hansen BW (1999) Plankton community structure and carbon cycling on the western coast of Greenland during the stratified summer situation. 1. Hydrography, phytoplankton and bacterioplankton. Aquat Microb Ecol 16:205–221

Petersen GH (1964) The hydrography, primary production, bathymetry, and "Tagsâq" of Disko Bugt, West Greenland. Medd om Grønland 159:1–45

Peterson BJ, McClelland J, Curry R, Holmes RM, Walsh JE, Aagaard K (2006) Trajectory shifts in the Arctic and Subarctic freshwater cycle. Science 313:1061–1066

Polyakov IV, Alexeev VA, Belchansky GI, Dmitrenko IA, Ivanov VV, Kirillov SA, Korablev AA, Steele M, Timokhow LA, Yashayaev I (2007) Arctic Ocean freshwater changes over the past 100 years and their causes. J Climate 21:364–384

Reigstad M, Wassmann P, Riser CW, Oeygarden S, Rey F (2002) Variations in hydrography, nutrients and chlorophyll a in the marginal ice-zone and the Central Barents Sea. J Mar Syst 38:1–2

Rey F, Skjoldal HR, Slagstad D (1987) Primary production in relation to climatic changes in the Barents Sea. In: Loeng H (ed.) The Effect of Oceanographic Conditions on the Distribution and Population Dynamics of Commercial Fish Stocks in the Barents Sea, Proceedings of the 2nd Soviet-Norwegian Symposium, Institute of Marine Research, Bergen

Rysgaard S, Nielsen TG, Hansen BW (1999) Seasonal variation in nutrients, pelagic primary production and grazing in a high-arctic coastal marine ecosystem, Young Sound, northeast Greenland. Mar Ecol Prog Ser 179:13–25

Rysgaard S, Glud RN, Risgaard-Petersen N, Dalsgaard T (2004) Denitrification and anammox activity in arctic marine sediments. Limnol Oceanogr 49:1493–1502

Sakshaug E (2004) Primary and secondary production in the Arctic Seas. In: Stein R, Macdonald RW (eds.) The Organic Carbon Cycle in the Arctic Ocean, Springer, Berlin

Sakshaug E, Slagstad D (1991) Light and productivity of phytoplankton in polar marine ecosystems - A physiological view. Polar Res 10:69–85

Sakshaug E, Slagstad D (1992) Sea ice and wind: Effects on primary productivity in the Barents Sea. Atmos Ocean 30:579–591

Sambrotto RN, Goering JJ, McRoy CP (1984) Large yearly production of phytoplankton in the Western Bering Strait. Science 225:1147–1150

Simpson K, Tremblay J-E, Gratton Y, Price NM (2008) An annual study of nutrient distribution in the southeastern Beaufort Sea, Mackenzie Shelf and Amundsen Gulf. J Geophys Res. doi: 10.1029/2007 JC004462

Slagstad D, Støle-Hansen K (1991) Dynamics of plankton growth in the Barents Sea: Model studies. Polar Res 10:173–186.

Smetacek V, Passow U (1990) Spring bloom initiation and Sverdrup's critical-depth model. Limnol Oceanogr 35:228–234

Smith W, Jr., Gosselin M, Legendre L, Wallace D, Daly K, Kattner G (1997) New production in the Northeast Water Polynya: 1993. J Mar Syst 10:199–209

Springer AM, McRoy CP, Flint MV (1996) The Bering Sea Green Belt: Shelf-edge processes and ecosystem production. Fish Oceanogr 5:205–223

Stroeve J, Sereeze M, Drobot S, Gearheard S, Holland MM, Maslanik J, Meier T, Scambos TA (2008) Arctic Sea ice extent plummets in 2007. EOS Transactions. Am Geophys Union 89:13–14

Taguchi S (1972) Mathematical analysis of primary production in the Bering Sea in summer. In: Takenouchi A (ed.) Biological Oceanography of the Northern North Pacific Ocean, Idemitsu Shoten, Tokyo

Tozzi S, Schofield O, Falkowski PG (2004) Historical climate change and ocean turbulence as selective agents for two key phytoplankton functional groups. Mar Ecol Prog Ser 274:123–132

Tremblay JE, Smith WOJ (2007). Primary production and nutrient dynamics in polynyas. In: Barber DG, Smith WOJ (eds.) Polynyas: Windows to the World, Elsevier, Oceanography Series, Amsterdam

Tremblay JE, Gratton Y, Fauchot J, Price NM (2002a) Climatic and oceanic forcing of new, net and diatom production in the North Water Polynya. Deep-Sea Res II 49:4927–4946

Tremblay JE, Gratton Y, Carmack EC, Payne CD, Price NM (2002b) Impact of the large-scale arctic circulation and the North Water Polynya on nutrient inventories in Baffin Bay. J Geophys Res. doi: 10.1029/2000JC000595

Tremblay JE, Hattori H, Michel C, Ringuette M, Mei Z-P, Lovejoy C, Fortier L, Hobson KA, Amiel D, Cochran JK (2006a) Trophic structure and pathways of biogenic carbon flow in the eastern North Water Polynya. Prog Oceanogr 71:402–425

Tremblay JE, Michel C, Hobson KA, Gosselin MG, Price NM (2006b) Bloom dynamics in early-opening waters of the Arctic Ocean. Limnol Oceanogr 51:900–912

Tremblay JE, Simpson K, Martin J, Miller L, Gratton Y, Barber D, Price NM (2008) Vertical stability and the annual dynamics of nutrients and chlorophyll fluorescence in the coastal, southeast Beaufort Sea. J Geophys Res. doi: 10.1029/2007JC004547

Vahatalo AV, Zepp R (2005) Photochemical mineralization of dissolved organic nitrogen to ammonium in the Baltic Sea. Environ Sci Technol 39:6985–6992

Vetrov AA, Romankevich EA (2004) Biological production of the Arctic Seas of Russia. In: Vetrov AA, Romankevich EA (eds.) Carbon Cycle in the Russian Arctic Seas, Springer, New York.

Walsh JJ, McRoy CP, Coachman LK, Goering JJ, Nihoul JJ, Whitledge TE, Blackburn TH, Parker PL, Wirick CD, Shuert PG, Grebmeier JM, Springer AM, Tripp RD, Hansell DA, Djenidi S, Deleersnijder E, Henriksen K, Lund BA, Andersen P, Mullerkarger FE, Dean K (1989) Carbon and nitrogen cycling within the Bering Chukchi Seas - source regions for organic-mjatter effecting AOU demands of the Arctic Ocean. Prog Oceanogr 22:277–359

Walsh JJ, Dieterle DA, Maslowski W, Whitledge TE (2004) Decadal shifts in biophysical forcing of arctic marine food webs: Numerical consequences. J Geophys Res. doi: 10.1029/2003JC001945

Wassman P, Slagstad D, Wexels Riser C, Reigstad M (2006) Modelling the ecosystem dynamics of the Barents Sea including the marginal ice zone II. Carbon flux and interannual variability. J Mar Syst 59:1–24

Welch HE, Kalff J (1975) Marine metabolism at Resolute Bay, Northwest Territories. Proceedings of the Circumpolar Conference on Northern Ecology. Part II, NRC, Ottawa

Yamamoto-Kawai M, Carmack E, McLaughlin F (2006) Nitrogen balance and arctic throughflow. Nautre 443:43

Yang J, Comiso J, Walsh D, Krishfield R, Honjo S (2004) Storm-driven mixing and potential impact on the Arctic Ocean. J Geophys Res. doi: 10.1029/2001JC001248

Zhang X, Walsh JE, Zhang J, Bhatt US, Ikeda M (2004) Interannual variability of arctic cyclone activity, 1948–2002. J Climate 17:2300–2317

Bibliography

Simpson KG, Tremblay JE, Price NM (2009) Nutrient dynamics in the Amundsen Gulf and Cape Bathurst Polynya: 1. New production in spring inferred from nutrient draw-down. Mar Ecol Prog Ser (in press)

Smith WO, Jr. (1995) Primary productivity and new production in the Northeast Water (Greenland) Polynya during summer 1992. J Geophys Res 100:4357–4370

Production of phytoplankton in the Arctic Seas and its response on recent warming

Alexander A. Vetrov and Evgeny A. Romankevich

P.P. Shirshov Institute of Oceanology, Russian Academy of Sciences, Moscow, Russia, vetrov@ocean.ru, romankevich@mail.ru

Abstract

New maps of the mean monthly distribution of the primary production in the Arctic Seas of Russia (Barents, Kara, Laptev, East Siberian, and Chukci Seas) were compiled using joint processing of CZCS (1978–1986), SeaWiFS (1998–2007), MODIS (2002–2007) satellite data, and field measurements. The annual production of phytoplankton is estimated at $163 \cdot 10^6$ t of C per year. Flux of organic carbon to seafloor is estimated at $68 \cdot 10^6$ t of C per year. The trends of the production changes within 1998–2007 were considered in the Greenland, Norwegian, Barents, Kara, Laptev, East Siberian, and Chukchi seas using satellite and field data. In these seas positive trends of summary production of phytoplankton were revealed, which range from 3.7% to 18% per year with respect to the values averaged over the period of the observations.

Introduction

The transformation of the mineral form of carbon into the organic form by algae in the process of photosynthesis represents one of the principal elements of the carbon cycling in the ocean. The primary production that is formed provides energy for all the subsequent heterotrophic levels of life. Carbon cycle controls many parameters of the biosphere functioning: fluxes and geochemistry of almost all chemical elements; fluxes of greenhouse gases N_2O, CH_4, CO_2; bioproductivity, biomass and in many cases biodiversity of marine communities; weathering, halmirolysis, authigenic mineral formation; microbiological activity. Organic matter (OM) serves as a source of energy for all lithogeochemical processes of sedimentation and diagenesis. Unclosed (unbalanced in system: synthesis–destruction–burial) carbon

J.C.J. Nihoul and A.G. Kostianoy (eds.), *Influence of Climate Change on the Changing Arctic and Sub-Arctic Conditions*,

cycle realizes accumulation in bottom sediments organic matter initial for oil and gas formation and has the potential to influence the climate system through feedback pathways involving responses in terrestrial and marine systems.

The most direct method for primary production measurements is the radiocarbon method based on the consideration of the increments of the phytoplankton biomass in the course of the CO_2 fixing. These kinds of measurements are very laborious and therefore not numerous. Because of the obvious lack of expeditionary data, in order to quantitatively estimate the primary production in the Arctic seas, one has to apply indirect estimation methods using empirical relations between the primary production and chlorophyll content in the water. The measurements of the latter are more abundant; meanwhile, in the Arctic seas, the season of direct measurements is usually restricted to August–September.

Additional information about the intensity of photosynthesis in seawater may be obtained from the satellite scanning of the ocean color. Owing to the significant distance of satellites from the surface of the sea, it is feasible to cover the entire World Ocean with continuous measurements. The disadvantages of the satellite method are also related to the great distance of satellites from the sea, since the solar irradiance that is reflected by seawater and reaches the satellite comprises only a few percent of the incident irradiance. Special algorithms were elaborated that help to separate the signal corresponding to the chlorophyll content in the water from the solar irradiance reflected by the sea surface and attenuated by the atmospheric aerosols. In the Arctic seas, the separation of this kind of signal is related to additional difficulties caused by the low sun standing, enhanced cloudiness, and intensive runoff of organic and particulate matter to the sea by Siberian Rivers (Artem'ev et al. 2003; Burenkov et al. 2001; Kopelevich et al. 2003). Nevertheless, despite the numerous assumptions accepted for conversion of the data on the surface water color to chlorophyll concentrations and the insufficient development of special algorithms for Arctic coastal regions, satellite data verified with respect to direct chlorophyll measurements should be used in order to cover large areas and to increase the observation frequency.

Materials and methods

The maps of the chlorophyll distribution in the Arctic Seas of Russia based on the processing of field data and those obtained using a CZCS satellite radiometer (Vetrov and Romankevich 2004), regardless of the long observation period (1978–1986), have significant gaps (about half of the sea area) caused by the permanent cloudiness partly covering the sea. In this paper, in order to complement the maps of the chlorophyll distribution in the Arctic Seas and to estimate its primary

production, we analyzed the satellite data of third level with chlorophyll concentrations averaged over 8-day-long intervals over 0.7° × 0.7° areas obtained with the help of SeaWiFS (1998–2007) and MODIS (2002–2007) radiometers together with the data of field measurements (Fig. 1).

The determinations of the chlorophyll contents in the surface waters were performed following the standard scheme (Vedernikov et al. 1990; Vetrov 2008). It included separation of particulate matter from the seawater (1–10 l) over GF/F glass-fiber filters with a pore size of about 0.7 μm, extraction of chlorophyll from the particulate matter, and measurements of the concentration of chlorophyll *a* in the eluent from the absorption and fluorescence spectra obtained with a Fluorat-02 Panorama spectral fluorometer. A comparison of the satellite data with the results of field measurements allowed us to insert a correction into satellite data that has a circumcontinental character.

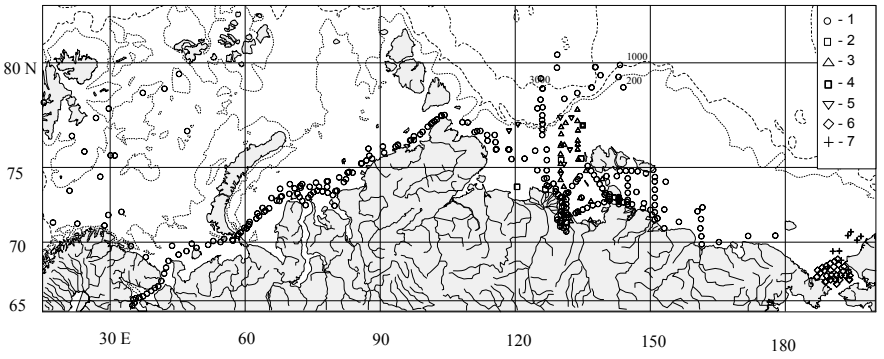

Fig. 1. Location of field measurements of chlorophyll used for verification of satellite data. 1 – our data; 2 – Juterzenka and Knickmeier 1999; 3 – Heiskanen and Keck 1996; 4 – Gleitz and Grossmann 1997; 5 – Tuschling 2000; 6 – Bidigare et al. 1992; 7 – Hameedi 1978.

Primary production

The maps of the production of phytoplankton in the Arctic Seas (Fig. 2) were calculated using the new maps of the chlorophyll distribution and the empiric relations between the chlorophyll concentration in the surface waters and the primary production in the water column (Table 1) established on the basis of direct parallel measurements of the primary production and chlorophyll content in the Arctic Seas (Vinogradov et al. 2000; Vetrov et al. 2008).

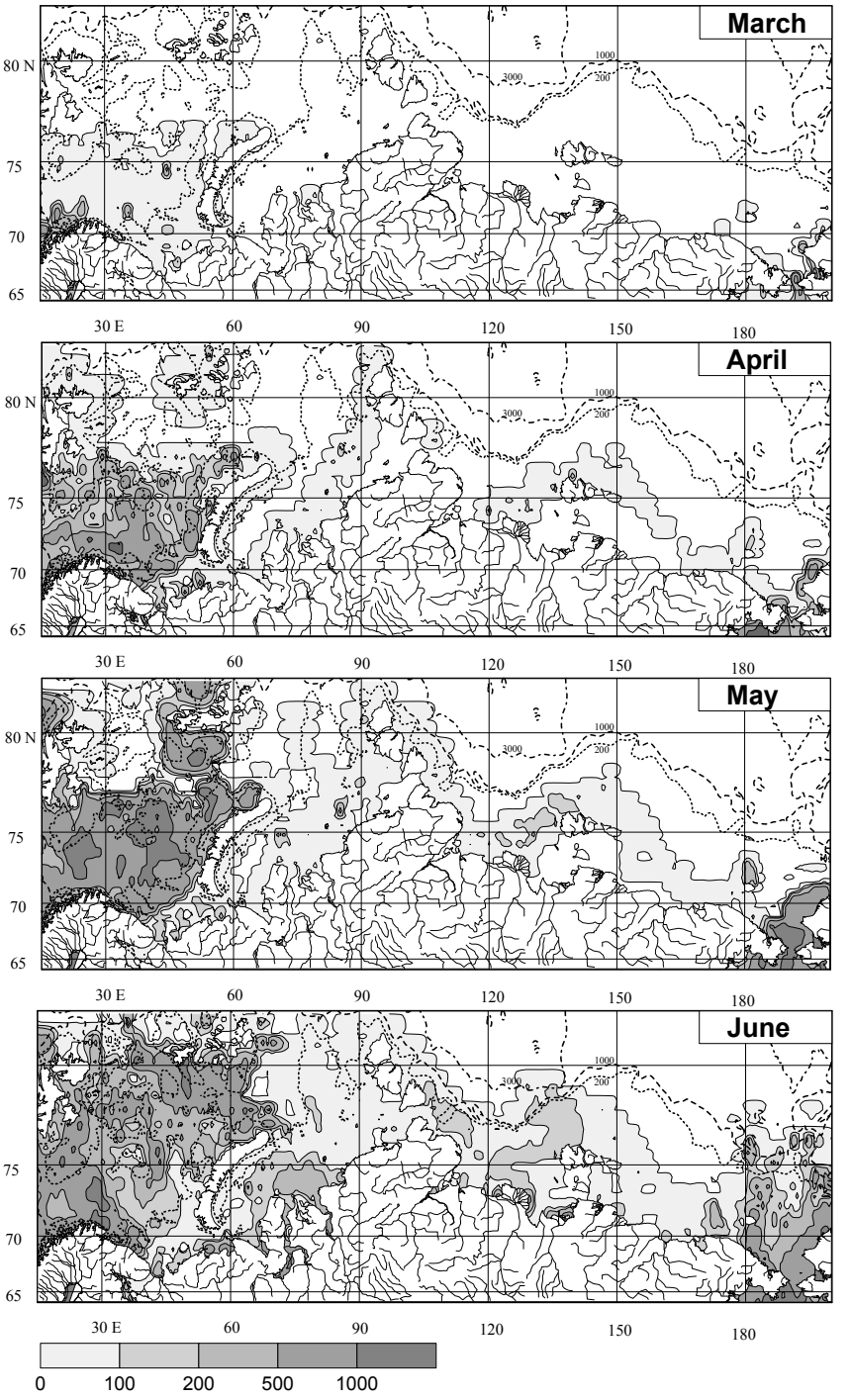
March
April
May
June
80 N
75
70
65
30 E
60
90
120
150
180
1000
3000
200
0
100
200
500
1000

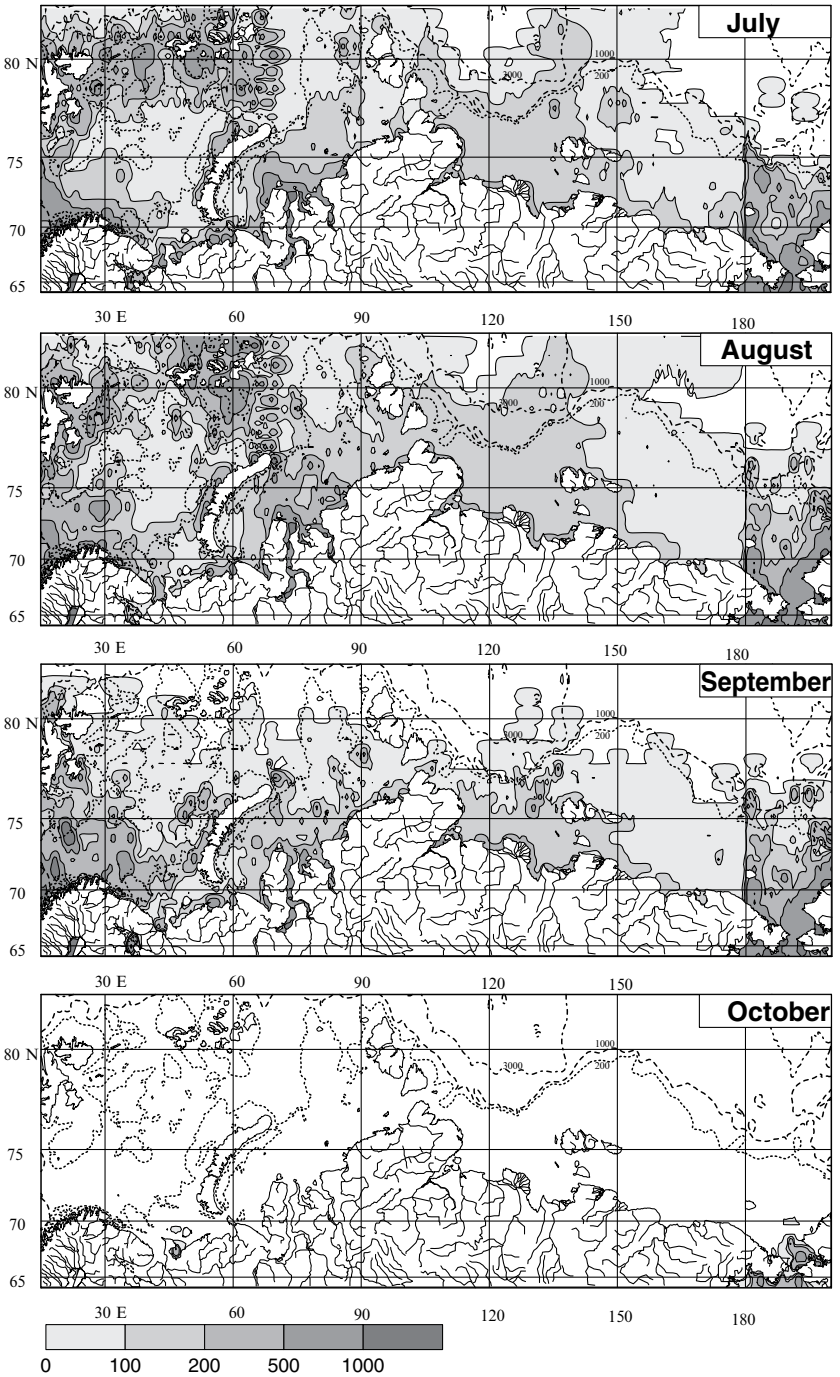

Fig. 2. Distribution of production of phytoplankton in the Arctic Seas, mg C m^{-2} per day.

Table 1. Mean values of primary production in water column (mg/m^2 per day) for zones with different chlorophyll "a" concentration in surface water (mg/m^3).

Range C_{chl} (mg/m^3)	Kara, Pechora and East Siberian[a]	Barents and Chukchi [a]	Laptev
<0.1	40	20	20
0.1–0.3	50	60	60
0.3–0.5	60	140	90
0.5–1.0	70	350	120
1–3	120	900	150
3–6	350	1,300	350
>6	1,000	1,800	1,000

[a]Vinogradov et al. 2000

In the Barents which is underwent to influence of atlantics water active vegetation of phytoplankton starts in March (Fig. 3). The maximums of both summary and specific primary production are observed in May–June during the period of high insolation and ice melting. In July, their values drastically decrease, nevertheless keeping on rather high level, which seems to be related to reduce of nutrients and eating away of phytoplankton by herbivorous grazers. High value of primary production remains also in autumn that is related to the decrease in the rate of the zooplankton metabolism, whereas for phytoplankton, the life conditions remain favorable due to mixing of water. In the Kara, Laptev and East Siberian seas, characterized by shorter vegetation period, which starts in April, single maximum of primary production is observed. In the Chukchi Sea, the phytoplankton bloom commences in May, and keeps high level to the end of September due to the penetration of the comparatively warm waters of the Anadyr Current enriched in nutrients into this area.

Annual production of phytoplankton (Fig. 4) is estimated taking into account all months of the year including nonproductive ones. The annual production of phytoplankton in the Russian Arctic Seas estimated using the maps compiled comprises $163 \cdot 10^6$ t of C per year, which is 1.3 times higher than the previous estimate ($126 \cdot 10^6$ t of C per year) based on the CZCS data (Vetrov and Romankevich 2004). The most total production of phytoplankton per year is estimated in the Barents Sea, but most annual production per day in the Chukchi Sea (Table 2). These seas are classified as mesothrophic (500 > PP > 100 mg/m^2 per day). Kara, Laptev and East Siberian seas are oligothrophic (PP < 100 mg/m^2 per day).

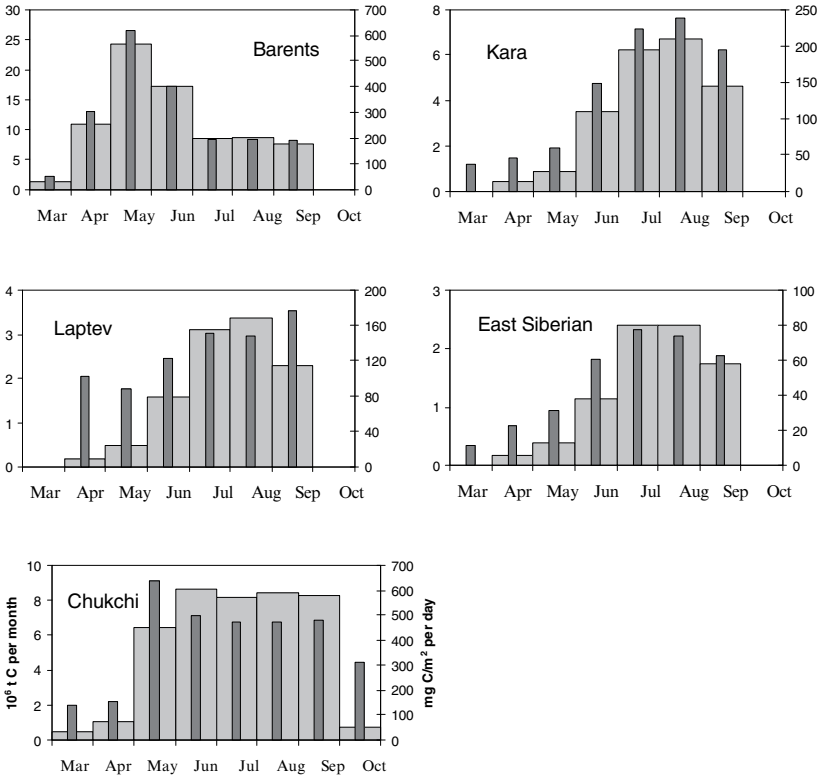

Fig. 3. Season variation in the primary production; light – mg C m^{-2} per day, dark – 10^6 t C per month.

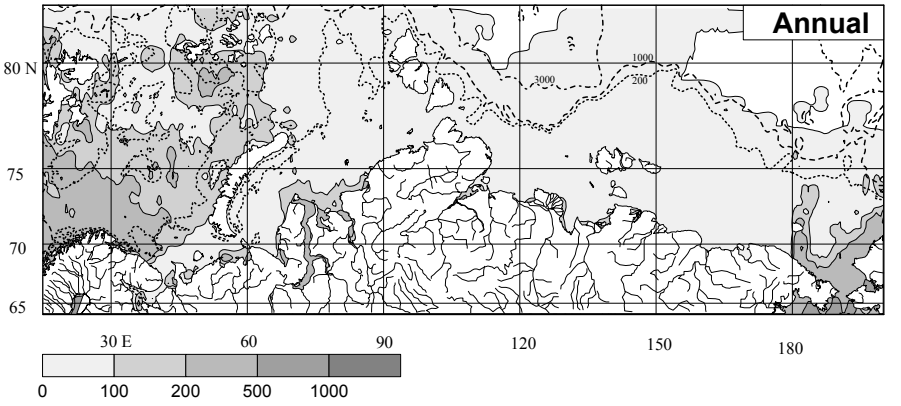

Fig. 4. Annual production of phytoplankton in the Arctic Seas, mg C m^{-2} per day.

Table 2. Production of phytoplankton of the Arctic Seas of Russia (ASR).

The sea	Annual production (10^6 t C year^{-1})	Mean annual production (mg C/m^2 per day)	Flux of organic carbon to seafloor (10^6 t C year^{-1})
Barents	78.5	152	22
White	1.5	46	0.9
Kara	22.3	70	11.6
Laptev	11	41	5.2
East Siberian	8.2	25	4.3
Chukchi	42	200	24
ASR as a whole	163.5		68

Based on the new map of the mean annual primary production (Fig. 3), we compiled a map of the mean annual C_{org} flux toward the bottom (Fig. 5). The calculations were performed with the use of the empiric relation $F_c = 33 \cdot PP/Z$ between the C_{org} flux to the sea bottom F_c, the value of the primary production in the water column PP, and the sea depth Z (Tseitlin 1993). At sea depths less than 50 m, the Z value was accepted to be 50 m. Main part of OM is dissolved and decomposes by bacteria during sinking. Nevertheless rather considerable part of OM reaches seafloor due to predomination of shallow waters in the Arctic Seas (Table 2).

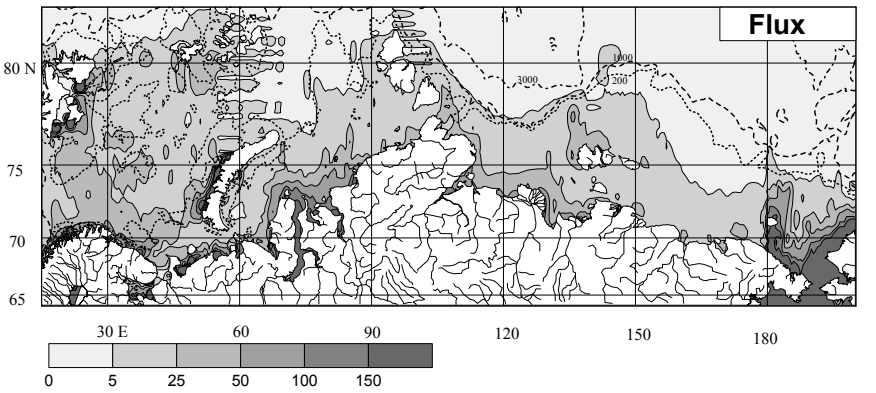

Fig. 5. Flux of organic carbon to seafloor in the Arctic Seas, mg C m^{-2} per day.

Response on recent warming

To estimate response of production of phytoplankton on climate warming in the Arctic Seas we have considered their trends for 1998–2007 using satellite data SeaWiFS and MODIS on chlorophyll value averaged over 8 days.

The interannual variations in the primary production and the trend of its changes may be characterized by its average value over the test areas (mg C/m^2 per day) and by the total production for each of the test areas (t C/day). The average value of the primary production for the test areas was calculated with the formula $PP = \Sigma(PP_{0.7} \times S_{0.7})/\Sigma S_{0.7}$, where $PP_{0.7}$ is the primary production in a 0.7° × 0.7° cell, and $S_{0.7}$ is the cell area with account for the latitude. We considered only the cells for which the data on chlorophyll were obtained. Thus, the influence of the clouds that covered the water surface on the final result was partially eliminated, as well as the decrease in the test area caused by ice.

The total production over the test areas was calculated with the formula $PP = \Sigma(PP_{0.7} \times S_{0.7})$. In this case, the decrease in the area due to the ice cover is included automatically, but the result is more distorted because of the clouds. This kind of distortion is somewhat decreased because the data on chlorophyll we used were averaged over 8 days of surveys. Thus, if a 0.7° × 0.7° sea area was partially opened for surveying during at least one satellite path, the value of the concentration measured is ascribed to the entire 8-day time interval in this area. The number of sites scanned this way over the test area in 8-day intervals (Fig. 6) tends to a significant increase, which points to the increase in the open water space in these tests areas and to the increase in the number of clear days.

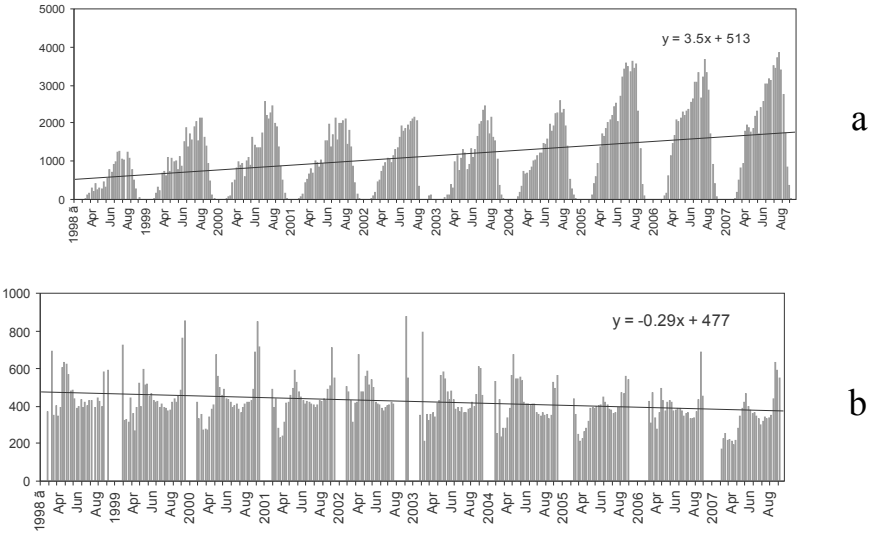

Fig. 6. Number of observations (**a**); and primary production, mg C m^{-2} per day (**b**) in the Arctic Seas as a whole (Greenland, Norwegian, Barents, Kara, Laptev, East Siberian, and Chukchi).

The trends of the average values of the primary production in the test areas were estimated exclusively using the actual data of the satellite surveys with no designation of zero values to the winter phase of photosynthesis and to the periods of data gaps caused by continuous cloudiness.

The trend of average value of primary production (mg C/m^2 per day) is negative for the Arctic Seas as a whole (Fig. 6). Negative values are observed for the Greenland, Norwegian and Chukchi seas (Table 3). For other seas there are no perceptible tendencies of primary production change. On the contrary total production of phytoplankton (t C per day) has positive trend for all seas (Fig. 7; Table 3). The difference in the trends of the daily total primary production and its average values in the test areas may be explained by the decrease in the ice covered areas and the gradual increase in the vegetation period caused by the climate warming. Thus total primary production grows but its average value can decrease because of involving northern parts of the sea characterized by small value of primary production.

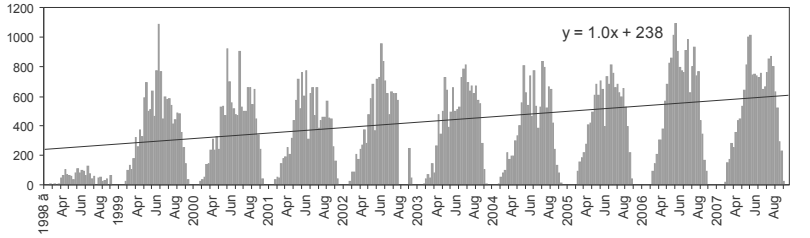

a

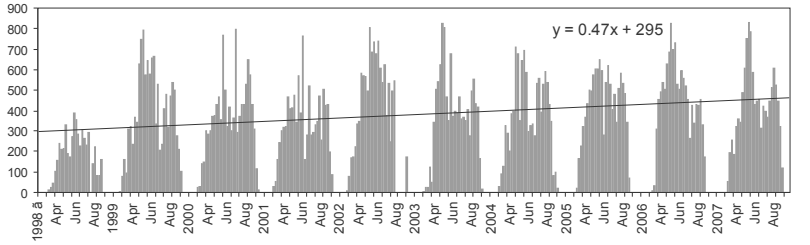

b

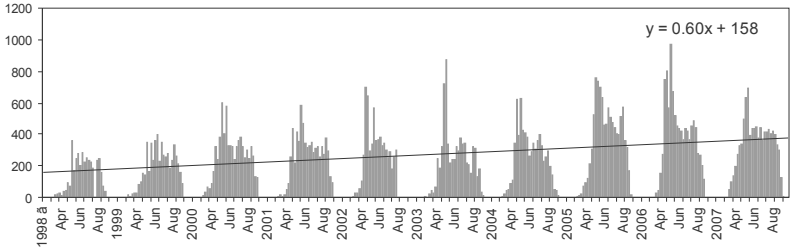

c

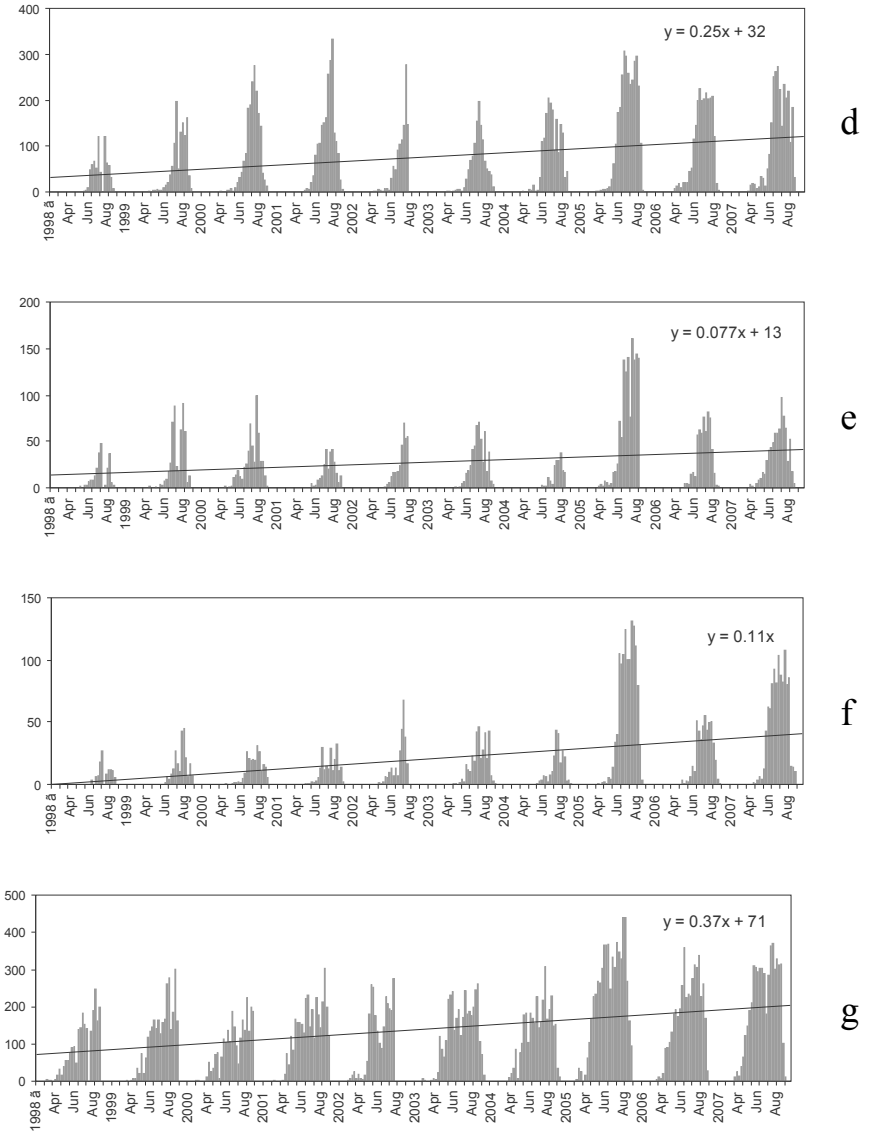

Fig. 7. Total production of phytoplankton, 10^3 t C per day in the Greenland (**a**), Norwegian (**b**), Barents (**c**), Kara (**d**), Laptev (**e**), East Siberian (**f**), and Chukchi (**g**) seas.

Table 3. Trends of primary production and flux of organic carbon to seafloor in the Arctic Seas (% year^{-1} from mean value for period of observation).

Sea	Number of observations	Average primary production (PP)	Summary PP for year	Flux to seafloor
Greenland	11.5	–2.3	7.8	5.8
Norwegian	7.6	–2.8	3.7	1.7
Barents	8.5	0.7	8.1	6.1
Kara	14.6	0.4	10.7	4.8
Laptev	10.7	0.6	10.7	9.2
East Siberian	19.4	–0.7	18.6	18
Chukchi	12.4	–3.7	9.6	5.5

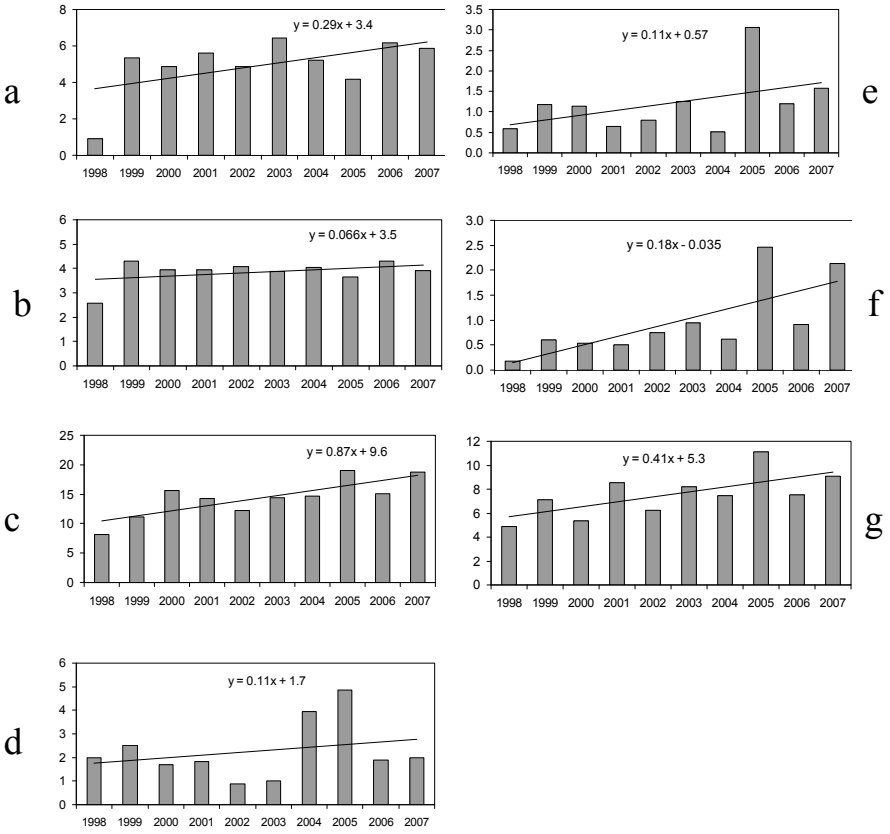

Fig. 8. Flux of organic carbon to seafloor, 10^3 t C year^{-1}, in the Greenland (**a**), Norwegian (**b**), Barents (**c**), Kara (**d**), Laptev (**e**), East Siberian (**f**), and Chukchi (**g**) seas.

Growth of primary production leads to increase of organic carbon flux to seafloor (Fig. 8). In some cases, trend of organic carbon flux to seafloor does not conform to that of the trends of the annual primary production. This is related to the annual variations of the primary production distribution over the test areas, and, if the increase in the annual primary production is accompanied by a displacement of the maximum photosynthesis activity to the seaward part of the test area, a lesser part reaches the bottom because of the great depths in these regions.

Analysis of trends of primary production in condition of open water with lest influence of ice conditions at polygons in the Barents, Kara and Chukchi seas (Vetrov and Romankevich 2008) also shows in some case negative trend of average primary production and positive trend of total primary production and organic carbon fluxes to seafloor for all polygons.

Conclusions

To summarize, one may note that the primary production of phytoplankton in the Arctic seas, sensitively responds not only to well-pronounced seasonal variations in the environment but also to the interannual changes. One may note the general trend of the primary production increase in the test areas in 1998–2007. The higher values of the total production trends and the greater number of observations, probably, are mainly caused by the gradual increase of the open water period. Because the phytoplankton primary production is the principal source of the autochthonous OM, the flux of organic carbon to seafloor and its burial in the bottom sediments varies with the changes in the organic matter produced by photosynthesis. Respectively, greater or smaller amounts of carbon dioxide are removed from the atmosphere, which is of considerable importance for the processes of climate formation. The process of the carbon burial in the bottom sediments acts as a negative feedback in the processes of climate change. However in concern to global climate processes burial of organic carbon in bottom sediments in the Arctic Seas (107 t C $year^{-1}$; Vetrov and Romankevich 2004) is three order of values as low as technogenic emission of CO_2 to atmosphere and 400 times as less as raise of CO_2 in atmosphere.

Acknowledgments

The authors are grateful to the GSFS DAAC and the NASA GES DISK DAAC for the SeaWiFS and MODIS data they provided. This study was supported by the Russian Foundation for Basic Research (project nos. 06-05-6405 and 06-05-08039-OFI); Presidium Russian Academy of Sciences (Program “Fundamentals of oceanic processes in sub polar regions. VI-5. Polar branch of carbon cycle.), and by the Program of the President of the Russian Federation for the Support of Leading Scientific Schools (grant nos. NSh-1902.2003.5, NSh-5329.2006.5 and NSh-4687.2008.5).

References

Artem'ev VA, Burenkov VI, Grigor'ev AV, et al. (2003) Optics. In: Romankevich EA (ed) *The Pechora Sea, system studies*. MORE, Moscow, 117–140 (in Russian)

Bidigare RR, Ondrusek ME, Brooks JM (1992) Phytoplankton pigment distributions in surface waters. In: Izrael YA, Tsyban' AV Ecosystem study of the Bering and Chukchi Seas, 3rd edn. Gidrometeoizdat, St Petersburg, 250–269 (in Russian)

Burenkov VI, Vedernikov VI, Ershova SV, et al. (2001) Application of the ocean color data gathered by the SeaWiFS satellite scanner for estimating the bio-optical characteristics of waters in the Barents Sea. Oceanology, **41**(4): 461–468 (Okeanologiya **41**(4): 485–492)

Gleitz M, Grossmann S (1997) Phytoplankton primary production and bacterial production. Ber Polarforschung, 226: 92–94

Hameedi MJ (1978) Aspects of water column primary productivity in the Chukchi Sea during summer. Mar Biol, 48(1): 37–46

Heiskanen A-S, Keck A (1996) Distribution and sinking rates of phytoplankton, deitritus, and particulate biogenic silica in the Laptev Sea and Lena River (Arctic Siberia). Mar Chem, 53: 229–245

Juterzenka KV, Knickmeier K (1999) Chlorophyll: a distribution in water column and sea ice duting the Laptev Sea freeze-up study in Autumn 1995. In: Kassens H et al. (eds) Land-ocean systems in the Siberian Arctic: dynamics and history. Springer, Berlin, 153–160

Kopelevich OV, Burenkov VI, Vazyulya SV, et al. (2003) An Assessment of the photosynthetically active radiation balance in the Barents Sea from the data of the SeaWiFS satellite color scanner. Oceanology, **43**(6): 786–796 (Okeanologiya, **43**(6): 834–845)

Tseitlin VB (1993) Correlation between the primary production and the vertical organic matter flux in mesopelagic zones of the ocean. Oceanology, **33**(2): 189–192 (Okeanologiya **33**(2): 224–228)

Tuschling K (2000) Phytoplankton ecology in the arctic Laptev Sea – a comparison of three seasons. Ber Polarforschung, 347: 1–144

Vedernikov VI, Sukhomlin AV, Shaposhnikova MG (1990) Primary production and chlorophyll in the central regions of the Pacific Ocean in January–April 1987. In: *Ecosystems of the eastern boundary currents and central regions of the Pacific Ocean.* Nauka, Moscow, 80–99 (in Russian)

Vetrov AA (2008) Chlorophyll, primary production, and organic carbon fluxes in the Kara Sea. Oceanology, 48(1): 33–42 (Okeanologiya **48**(1): 38–47)

Vetrov AA, Romankevich EA (2004) *Carbon cycle in the Russian Arctic Seas.* Springer, Berlin.

Vetrov AA, Romankevich EA (2008) Interannual variability of the primary production and organic carbon fluxes in the Arctic Seas of Russia. Oceanology, 48(3): 362–370 (Okeanologiya **48**(3): 371–380)

Vetrov AA, Romankevich EA, Belyaev NA (2008) Chlorophyll, primary production, fluxes, and balance of organic carbon in the Laptev Sea. Geochemistry Int, 46(10): 1055–1063 (Geokhimiya **46**(10): 1122–1130)

Vinogradov ME, Vedernikov VI, Romankevich EA, Vetrov AA (2000) Components of the carbon cycle in the Russian Arctic Seas: primary production and flux of Corg from the photic layer. Oceanology, 40(2): 204–215 (Okeanologiya 40(2): 221–233)

Reconstruction of oceanic circulation using mineralogical and isotopical (Nd/Pb) signatures of deep sea sediments: the case study of the northern North Atlantic and some perspectives for the Arctic

Nathalie Fagel

UR AGEs Argiles, Géochimie et Environnements sédimentaires, Department of Geology, University of Liege, B-4000 Liege, Belgium, Nathalie.Fagel@ulg.ac.be

Abstract

This work aims to reconstruct the evolution of deep ocean circulation patterns in the North Atlantic during the last 10–100 kyr using abiotic proxies. Nd and Pb isotopic ratios have been measured on the clay-sized fraction of two sediment cores drilled in the Labrador Sea off southern Greenland (MD99-2227, ODP646). At present this site is under the influence of the Western Boundary Undercurrent that drives the water masses involved in the formation of the North Atlantic Deep Water. Based on an identification of regional sources areas sedimentary isotopic signatures allow to determine the origin of the particles driven by the North Atlantic deep currents: any change in the sediment supplies reflects a relative change in the contribution of the deep water masses. Our isotopic dataset emphasizes several main changes in the relative contribution of the two major components of North Atlantic Deep Water, i.e. the North East Atlantic Deep water (NEADW) and the Denmark Strait Overflow Water (DSOW) throughout the last 12 kyr, and especially during the Late Holocene. The inception of the modern deep circulation seems to be quite recent, occurring during the last 3 kyr. Over glacial/interglacial time-scale deep current variability is less pronounced and/or partly masked by variable proximal supplies. Labrador Sea results emphasize that the application of mineralogical and isotopical tools on sediments allow to monitor variability in sedimentary supplies driven by deep currents. This *indirect* approach is further promising to identify deep currents pathways and reconstruct past circulation.

Introduction

The deep water formation is a critical component of the climate system (Fig. 1). In particular in the northern North Atlantic the production rate of North Atlantic Deep Water (NADW) is one of the puzzle in understanding the oceanic influence

J.C.J. Nihoul and A.G. Kostianoy (eds.), *Influence of Climate Change on the Changing Arctic and Sub-Arctic Conditions*,

in climate changes (Broecker and Denton 1989). Variations in atmospheric CO2 concentrations have been related to Pleistocene glacial to interglacial changes in the exportation of NADW to the Southern Ocean (e.g., Boyle and Keigwin 1987).

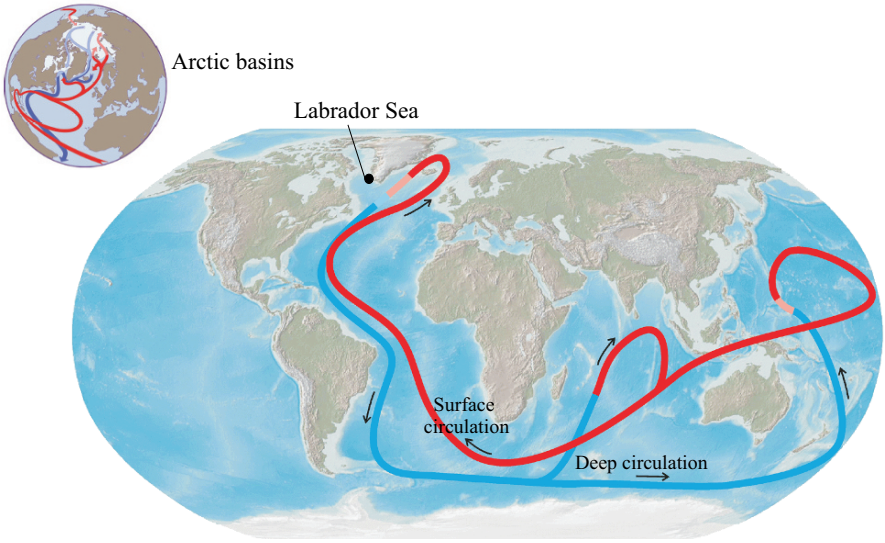

Fig. 1. The global ocean circulation pattern. (Lower panel modified from Broecker and Denton 1989.) The Labrador Sea is one of the areas of formation of North Atlantic Deep Water (NADW). NADW takes part of the thermohaline circulation and therefore it is a key factor for the regulation in the Earth's climate. The upper panel emphasizes the role of the arctic basins in the global thermohaline circulation. Major features of North Atlantic and Arctic Ocean circulation: red arrows: warm water from lower latitudes entering the arctic; blue arrows: export of colder water from the arctic; shaded white: average area covered by sea ice. (Figure courtesy of G. Holloway, Institute of Ocean Sciences, Sidney, British Columbia. For more information see http://www-sci.pac.dfo-mpo.gc.ca/osap/.) http://nsidc.org/arcticmet/factors/land_sea_distribution.html. Accessed 23 June 2007.

Most paleoceanographic reconstructions derived from biogenic proxies (benthic fauna species distribution, elemental chemical ratios, carbon or oxygen isotopic composition of benthic assemblages) that are sensitive to ocean ventilation and water mixings (for a synthesis see e.g., Boyle 1995; Hillaire-Marcel and de Vernal 2007). Sedimentary abiotic components like magnetic properties, clay mineral assemblages or long period isotopic composition of clays were less investigated, even they bring indirect information on past circulation tracing the origin of the particles driven by the water masses (Fagel and Hillaire-Marcel 2006).

In this study, mineralogy and isotopic composition (Nd, Pb) of Labrador Sea deep sea sediments are coupled to reconstruct deep circulation patterns in northern North Atlantic. Since the 1960s clay mineralogy has been used as a tracer of provenance and transport mechanisms in studies of the world oceans in which the mineralogy of the fine detrital fraction generally reflects the intensity of continental weathering in the source areas (e.g., Biscaye 1965; Chamley 1989). Radiogenic

isotopes of the detrital sedimentary fraction are also used to trace sediment provenance (e.g., Goldstein and O'Nions 1981). Radiogenic signature can therefore be used as indirect paleoceanographic tracers (Fagel et al. 2004, Paleoceanography and references therein; Fagel 2007). In this approach both clay mineralogy and isotope signatures constitute fingerprints of regional continental source-areas: they are proxies for deep current supplies. Changes in their relative contribution through time bring further information on the deep circulation pathways: they constitute indirect proxies for oceanic circulation.

Such approach has been applied on two cores from the deep Labrador Sea basin. Cores MD99-2227 and ODP646 were retrieved off Southern Greenland, at 3,460 m, at the inlet of deep circulation gyre into Labrador Sea (Figs. 1, 2). In both cores we focus on the clay-size fraction of the sediments: due to its cohesive behaviour, this fraction is less sensitive to winnowing after deposition (McCave et al. 1995). Clay minerals have been identified by X-ray diffraction analysis (Moore and Reynolds 1989); Nd isotopes have been measured by TIMS (Geotop, Montreal, Canada) and Pb isotopes have been measured by TIMS and/or MC-ICP-MS (DSTE, Brussels, Belgium). For the full analytical procedures, see Fagel et al. (1997), Innocent et al. (1997), Fagel et al. (2004), respectively.

In term of time window North Atlantic paleoceanography has been mainly investigated over the Last Glacial. Here different time-scales have been investigated: samples from core MD99-2227 allow to investigate Holocene variability (OIS 1-2) whereas glacial/interglacial cycles were investigated with ODP material. Age model are derived from oxygen isotope and paleomagnetic stratigraphies, constrained by 14C AMS dating (details in Fagel et al. 2004; Fagel and Hillaire-Marcel 2006). By comparing the Last Glacial with previous glacial/interglacial cycle we would like to document short term and long term variability in order to test the still debate representativity of last climate cycle for the whole Pleistocene (e.g., Raymo et al. 2004).

Present distribution of deep water masses in northern North Atlantic

In the modern North Atlantic, the deep circulation is driven by a contour-flowing bottom current, the Western Boundary Undercurrent (WBUC), which carries the main water masses involved in the formation of the North Atlantic Deep Water (NADW) along a counterclockwise gyre through the marginal North Atlantic basins (Fig. 2). These water masses include: (a) the Northeast Atlantic Deep Water 1 (NEADW1) flowing from East to West and bathing the shallower parts of Reykjanes Ridge; (b) the deeper Northeast Atlantic Deep Water 2 (NEADW2) whose circulation is constrained by the morphology of Reykjanes Ridge, and flowing from the Northeast Atlantic through the Charlie-Gibbs Fracture Zone into the Irminger Basin where it forms a counterclockwise gyre along the ridge and the

Greenland Margin; (c) the Denmark Strait Overflow Water (DSOW) that consists of cold surface waters from the Greenland and Norwegian seas that sink below 2,700 m along the Eastern Greenland Margin to fill most of the deepest parts of the Irminger and Labrador basins; (d) the Labrador Sea Water (LSW) characterized by cold water flowing from Davis Strait (Davis Strait Overflow, DSO) southwards along the Eastern Labrador Margin.

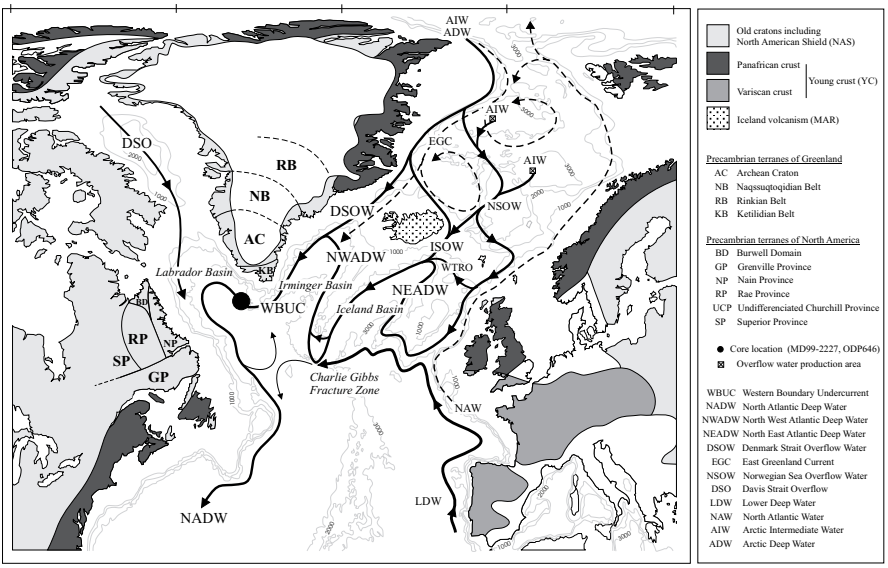

Fig. 2. Studied area: Core location, ocean circulation and geology. Location of cores MD99-2227 and ODP646 in the Labrador Sea, northern North Atlantic. The plain arrows indicate the pathways of deep or intermediate currents (modified from McCartney 1992; Schmitz and McCartney 1993; Dickinson and Brown 1994; Lucotte and Hillaire-Marcel 1994 and from Hansen and Osterhus 2000). The broken arrows indicate surface circulation adapted from Hansen and Osterhus (2000). The structural terranes of the continental crusts adjacent to the northern North Atlantic are indicated by different colors (North American and Greenland Shield, Panafrican and Variscan crusts) and by dots for mantle-derived material (Iceland volcanism).

Calibration of proxies on surface sediments from northern North Atlantic

The clay mineralogical tool

In marine sediments detrital clays reflect the weathering conditions within the watershed (e.g., Chamley 1989). In surface and late Quaternary sediments the composition of clay assemblages depicts a peculiar spatial distribution between the Eastern and the Western North Atlantic basins (Fig. 3). In Eastern Irminger

and Iceland sediments more than 50% of the clay fraction consists of smectites (Fagel et al. 1996 and references therein). The relative abundance of this clay species decreases in Western Labrador Sea basin, mainly replaced by illite and

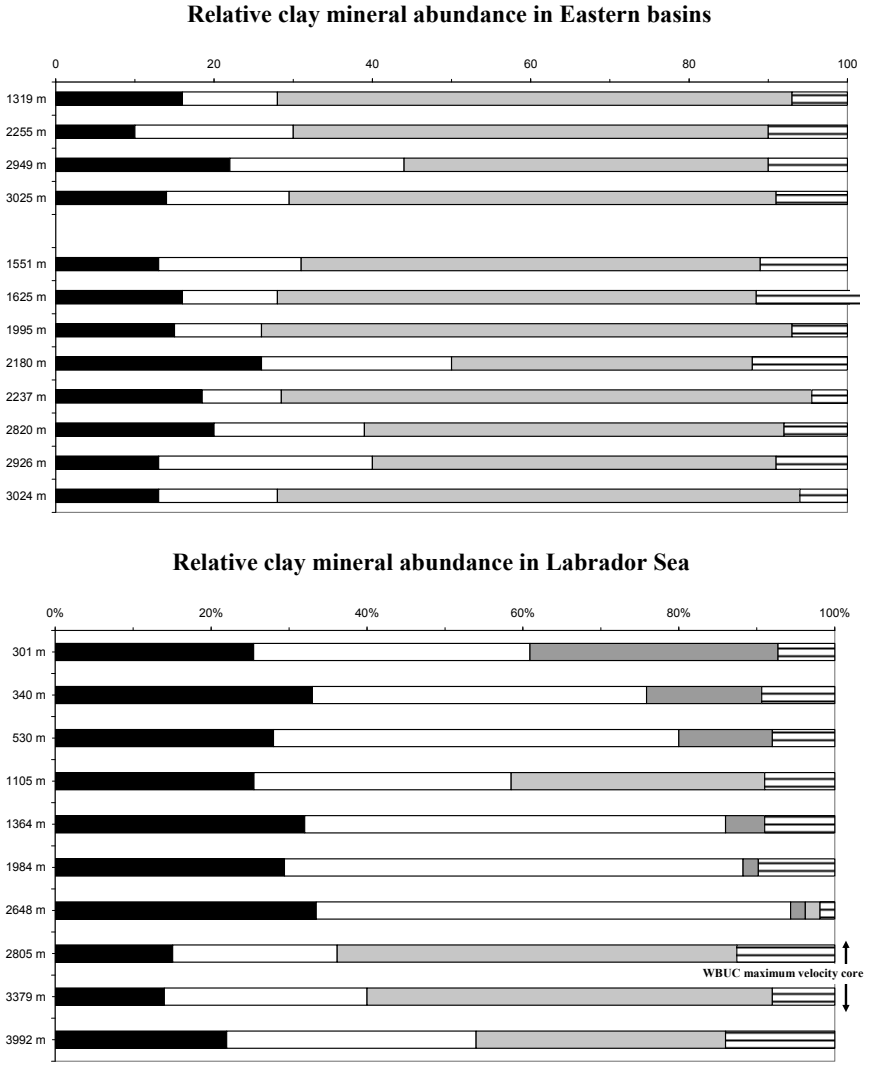

Fig. 3. Spatial and depth distributions of clay minerals in surface sediments from northern North Atlantic. Mean histogram for the western Labrador Sea and for the eastern Irminger and Iceland basins (data from Fagel et al. 1996). On average smectite is the dominant clay mineral in surface sediments from Eastern basins, it is usually replaced by illite and chlorite in western basin. As an exception, note the smectite enrichment in the clay-size fraction of WBUC-influenced Labrador Sea sediments.

chlorite. In Labrador Sea the smectite abundance varies according to sediment depth, supporting for a link between clay assemblages and deep water masses stratification (Fagel et al. 1996). Along both Labrador Sea margins an enrichment in smectites (up to 50% of the clay fraction) is observed in sediments along the high velocity axis of the WBUC, i.e. at water depths of 2,800–3,400 m. In contrast, the clay assemblages of the upper slope and shelf off Greenland and Canada contain primarily illite and chlorite with no or only low amounts of smectites from adjacent continental areas. As smectites dominate the clay assemblages in the Eastern Irminger and Iceland basins, their occurrence in the deep Labrador Sea sediments has been related to distal supplies by deep currents through the WBUC. Based on this specific spatial and vertical mineralogical distribution, the smectite-enrichment will be used to track for WBUC-influenced supplies.

The Nd and Pb isotopical tool

Nd isotopic signature in sediments records the age and the composition of the rock material occurring in the source-area, with no significant change during erosion, transport and deposition (Goldstein and O'Nions 1981). Investigation of Nd isotopes in the clay-size fraction of surface and late Quaternary sediments of the northern North Atlantic allows to identify the main sources (Innocent et al. 1997). Based on characterization of potential geographical sources of particles, three main sources were identified (Fig. 2): an old Precambrian crustal material from Canada, Greenland and/or Scandinavia (North American Shield, NAS), a Paleozoic or younger crustal material from East Greenland, NW Europa, and/or West Scandinavia (Young crust, YC) and, a volcanic source from the mid-Atlantic oceanic volcanism grouping the Iceland, the Faeroe Islands and/or the Reykjanes Ridge (MAR). Eastern basins are characterized by higher Nd isotopic ratios than Western Labrador Sea, reflecting the relative contribution of the local isotopically-different sources (Fig. 4). Beside this spatial distribution the Nd composition of the clay fraction also changes through sediment depth. Like for clay mineralogy a significant shift in the Nd isotope signature is evidenced in sediments that are under the axis of the WBUC velocity core (Innocent et al. 1997) (Fig. 4). The WBUC is thought to be responsible for erosion and transport of clay particles from the western North Atlantic Iceland and Irminger basins, followed by redeposition in the Labrador Sea. Therefore Nd constitutes a suitable tracer of the origin of deep-sea sediments of the North Atlantic. Adding Pb isotopic measurements allows for a better discrimination between the different source-areas of

"young" crustal material (see Fagel et al. 2004). Changes in the Nd and Pb signatures of clay-size fraction of Late Glacial and Holocene sediments provide constraints on the different sources areas that supplied the fine clayey particles into the Labrador Sea.

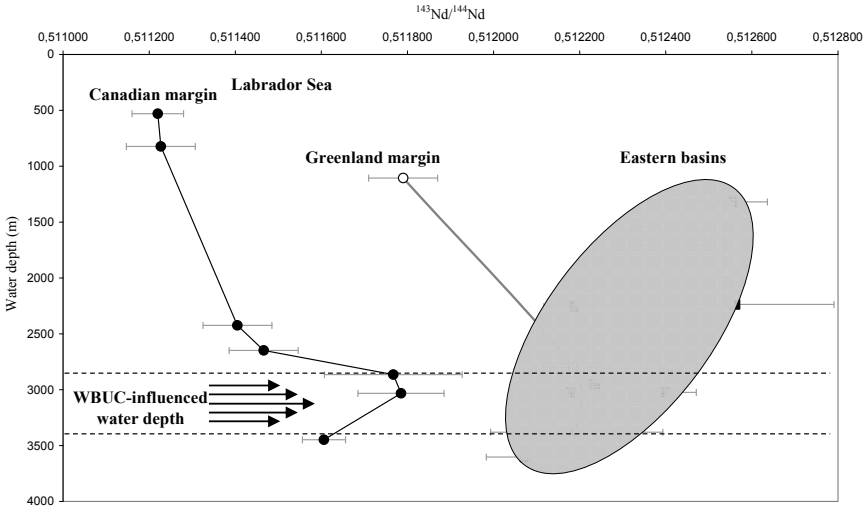

Fig. 4. Spatial and depth distributions of Nd isotope signatures in surface sediments from northern North Atlantic: Labrador Sea margins, circle; Greenland margin, open circle; Canadian margin, closed circle; eastern Iceland and Irminger basins, square (data from Innocent et al. 1997). Along both margins of the Labrador Sea note the significant shift in the Nd isotope signature in the WBUC-influenced sediments.

Results and discussion

Holocene variability of deep current supplies

Nd-Sm concentration and isotopic ratios (Fig. 5) as well as Pb isotopes (Fig. 6) have been measured on the fine fraction of Holocene and deglacial sediments from MD99-2227 core drilled in the Labrador Sea off southern Greenland (Fagel et al. 2004). The clay-size fraction significantly increases through the Holocene, representing up to 70% of the carbonate-free sediment. The smectite/illite ratio increases by a factor of 4 throughout the last 12 kyr. Such mineralogical trend is in agreement with higher smectite-rich Eastern supplies.

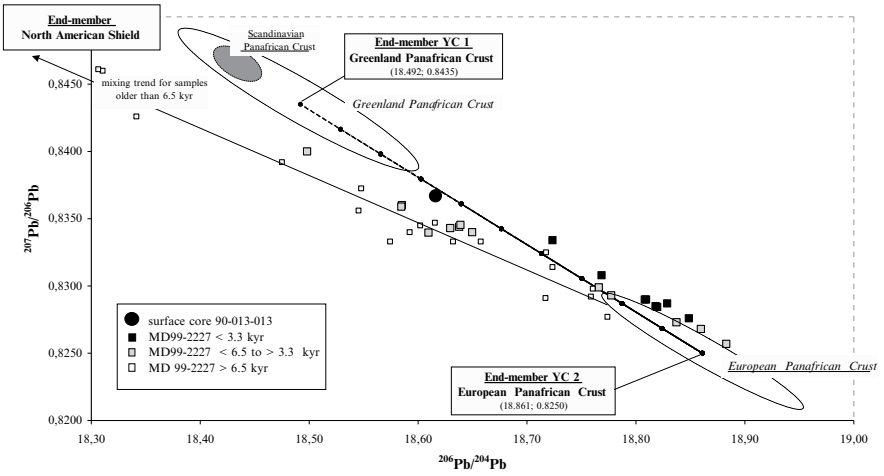

Fig. 5. Nd mixing diagram. Nd isotopic signatures ($^{143}Nd/^{144}Nd$ *vs.* $^{147}Sm/^{144}Nd$) of the clay-size fraction of Holocene and deglacial sediments from core MD99-2227. Data are plotted with regard to the surface sediment sample (filled circle). The linear regression trends (dashed lines) are calculated for two groups of samples, i.e., older than 6.5 kyr (open squares) and younger than 6.5 kyr (plain squares). For the youngest samples, the grey squares characterize the samples between 6.5 and 3.3 kyr and, the black squares the samples <3.3 kyr. The regional continental end-members are defined in Fagel et al. (1999). (Data from Fagel et al. 2004.)

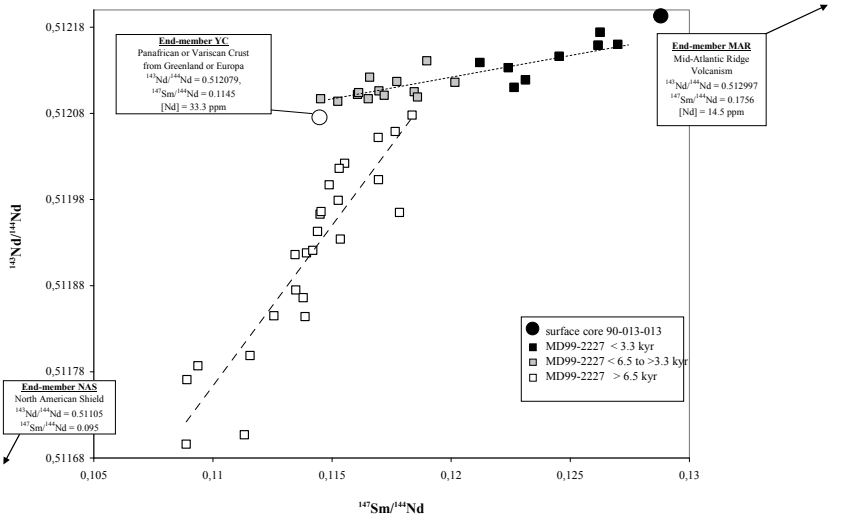

Fig. 6. Pb mixing diagram. Pb isotopic signatures ($^{207}Pb/^{206}Pb$ *vs.* $^{206}Pb/^{204}Pb$) of the clay-size fraction of Holocene and deglacial sediments from core MD99-2227 (modified from Fagel et al. 2004). Data subdivided into the three same groups as for Fig. 5. The arrow indicates the regression trend defined by the samples older than 6.5 kyr. For the samples younger than 6.5 kyr, a calculated mixing-line between two types of young crusts, i.e. the Greenland and European Panafrican crusts, is used. For mixing, we take into account the median value for Greenland Panafrican Crust (GPC) and the mean value for the European Panafrican Crust (EPC). (See Fagel et al. 2004 for more explanation.)

The distribution of the sediment Nd and Pb signatures could be explained by a mixture between three sources (Fig. 2): the North American Shield, the Panafrican and Variscan crusts ("young" crustal source of Europe and Eastern Greenland), and the Mid-Atlantic Ridge (Iceland and Faeroe Islands). Basically we estimate for each sample the relative contribution of fine particle supplies carried by the North Atlantic deep components into the Labrador Sea.

The evolution of the relative contributions of sediment sources suggests major changes in relative contributions of the deep water masses carried by the WBUC over the past 12 kyr (Fig. 7). Clay isotopic signatures indicate two different mixtures of sediment sources succeeding in time. The first mixture is composed of proximal material from Labrador Sea margins and distal deep current-driven crustal source. The mixture is made by material eroded from the North American Shield and from a "young" crustal source. The Nd signatures shift according to the age of the samples (Fig. 5). Such trend reflects a progressive decrease of the proximal supplies during deglaciation. Changes in clay fluxes (Fagel et al. 1997) evidence an increase of distal supplies linked with a progressive intensification of the WBUC.

From 6 kyr onward, a "young" crustal component is still involved but mixed with a mantellic component characteristic of the Mid-Atlantic Ridge. In this interval Pb isotopes allow for a better discrimination between the different source areas of "young" crustal material (i.e., Panafrican crust of Europe and Greenland, Variscan crust of Europe). Sediment Pb isotopic data are plotted along a two end-member mixing, i.e. between the points representative of the Panafrican crust of Europe and of Greenland (Fig. 6). According to the geographical distribution of the identified source areas (reported on Fig. 2) we assume DSOW-like water mass supply the young crustal material from Greenland whereas NEADW brings rather European-like material. From 6 kyr onward the increase of Greenland Panafrican Crust contribution is probably related to the inception of the DSOW.

The establishment of the modern circulation is estimated at ~3 kyr. This last interval is characterized by a decrease of the crustal material. Note the reduced influence of the Denmark Strait Overflow Water is synchronous with the full appearance of the Labrador Sea Water mass (Solignac et al. 2004). We suggest the relative increase in contributions from the Mid-Atlantic Ridge follows the inception of the Iceland-Scotland Ridge Overflow Water mass (ISOW).

Long term stability of deep current supplies (ODSP 646)

Forty Nd isotope signatures were measured on the fine fraction of one sediment core from the Southern Greenland rise (ODP-646) that span the last 360 ka (Fagel and Hillaire-Marcel 2006). These data track changes in the relative supply of fine particles carried into the deep Labrador Sea by the WBUC during the last four glacial-interglacial cycles (G-I).

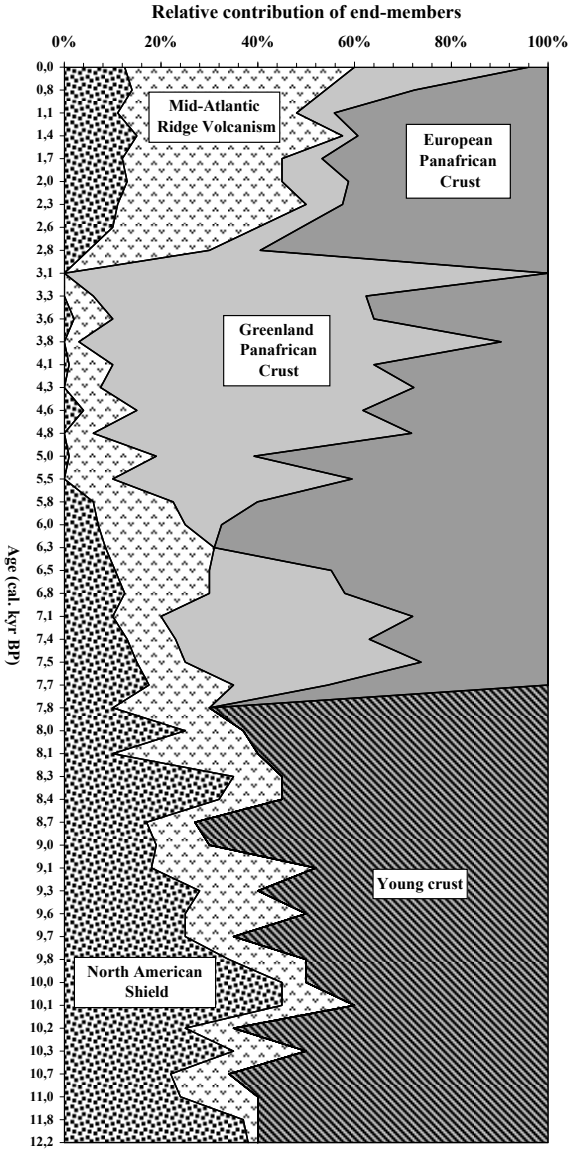

Fig. 7. Estimated relative contributions of sediment supplies over the last 12 kyr at core MD99-2227 location. Mixing takes into account particle supplies from North American Shield (NAS), Mid-Atlantic volcanism (MAR), and young crusts (YC). (Data from Fagel et al. 2004.) During the last 6.5 kyr, Pb data distribution allows to decipher contributions from the Greenland Panafrican crust (GPC) and from the European Panafrican crust (EPC). The maximum contribution from East Greenland observed from 6 to 3 kyr could be related with the inception of DSOW-like driven supplies. (See Fagel et al. 2004 for details.)

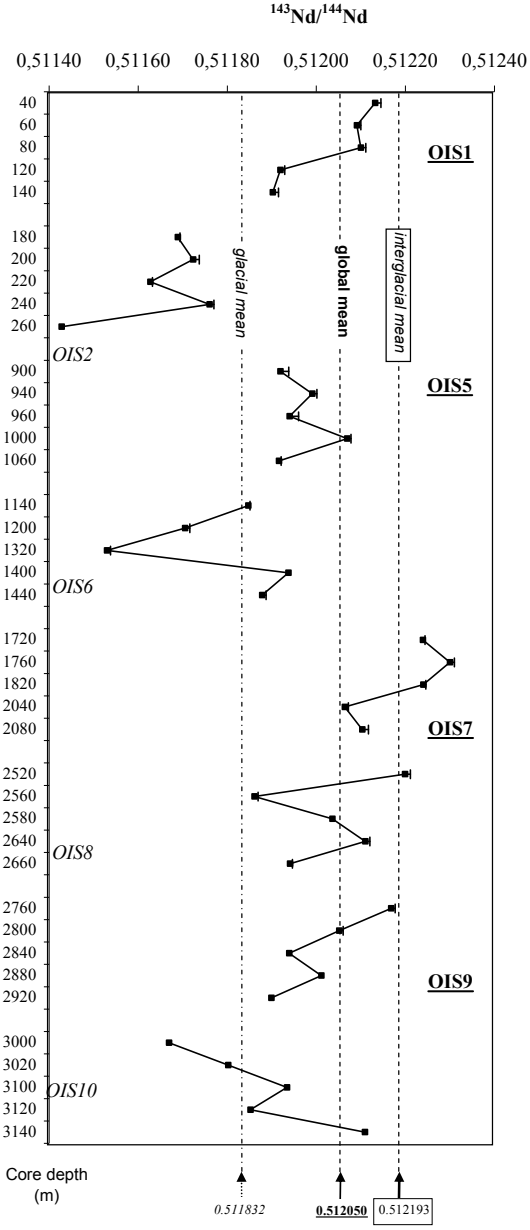

Fig. 8. Nd isotopic signature of the clay-size fraction of last climate cycle sediments from site ODP646 (data from Fagel and Hillaire-Marcel 2006). Stratigraphical Nd distribution according to age model. Note the systematic shift between the Nd signature of glacials and interglacials. Vertical lines represent the averaged signature for glacial samples, interglacial samples or for all the samples (global mean).

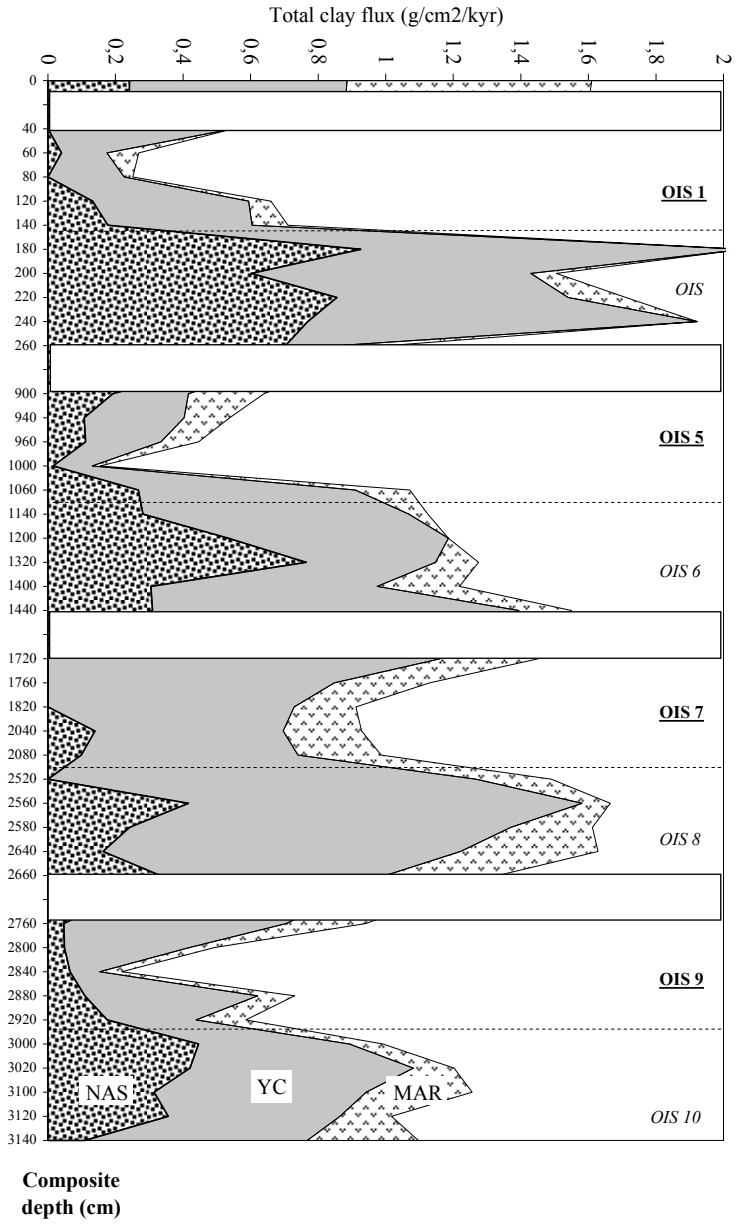

Fig. 9. Estimation of the relative contribution of the three identified end-members (NAS, MAR, YC) within the clayey supplies settled at ODP646 location. Results are expressed as total particle flux taking into account the contribution of each end-member, the clay abundance in the sediment, the sediment density and the sedimentation rate. (See Fagel and Hillaire-Marcel 2006 for calculation.)

Clay mineralogical changes are evidenced between glacials and interglacials. On average glacial clay assemblages display a pronounced drop in smectite (< 40%) balanced by an increase in illite and chlorite. Such mineralogical observation reflects relative changes between proximal (illite-rich) and distal (smectite-rich) supplies. Likely Nd signatures of clay-size fraction also present a systematic shift between glacials and interglacials (Fig. 8). Clay-size fractions from glacial sediments have the lowest Nd isotopic ratios. Like for MD99-2227 Nd data distribution are consistent with a three end-members mixing diagram. The relative contribution of NAS, YC and MAR are reported on Fig. 9. Supplies of young crustal particles were similar during glacial stages of oxygen isotope stages (OIS) 2, 6, and 10, whereas mean volcanic contributions decreased relative to old craton material, from OIS 10 to OIS 6 and from OIS 6 to OIS 2. Compared with other interglacials OIS 7 was marked by a higher contribution from young crustal material but a similar mantellic-derived supply. The old crust contribution (NAS) is twice higher during glacials than interglacials, replaced by MAR contribution during interglacials. Estimated sedimentary fluxes suggest rather higher proximal supplies related to glacial erosion than any dilution process (Fig. 9).

Over the studied interval fine particle supplies to the Labrador Sea were strongly controlled by proximal ice-margin erosion and thus responded to glacial stage intensity. In contrast, the WBUC-carried mantellic-derived supplies (MAR) from the Eastern basins did not change significantly throughout the last 360 kyr, except for a pronounced increase in surface-sediments that suggests unique modern conditions. Over glacial/interglacial Nd ratios in clay-size fraction provide useful information on relative sedimentary supplies from proximal sources, thus on glacial erosion rates. However distal WBUC-controlled inputs from the northern and eastern North Atlantic seem to have been less variable.

Conclusion and perspectives

We analyse the mineralogy and isotope (Nd, Pb) signatures of two sediments cores collected in Labrador Sea (MD99-2227, ODP646). Clay composition and their isotopic ratios bring information on the origin of particles driven by deep currents. Our aim is to monitor deep current variability over the last 10–100 kyr. We emphasize that sedimentary supply variations allow for reconstruct of deep circulation patterns in the North Atlantic. Such indirect approach is promising to indirectly follow past circulation. As the Arctic Ocean also plays a role in the global thermohaline circulation (see Fig. 1) it could be interesting to adapt such approach to characterise the Arctic sedimentary supplies and further precise main Arctic circulation pathways. Previous investigations (Haley et al. 2007) on authigenic fraction of sediments (i.e., Fe-Mn nodules) already evidence some variability in Arctic circulation over the last 15 Myr. However the low rate of nodule formation limits the temporal resolution. Therefore detrital sedimentary

fraction could be an alternative material to track for circulation changes in the Arctic basins over the Holocene.

Acknowledgments

This manuscript summarizes more than 10 years of research made in close collaboration with the team of GEOTOP (C. Hillaire-Marcel, R. Stevenson, C. Hillaire-Marcel, M. Preda – UQAM, Canada) as well as with the support of DSTE (N. Mattielli). Interpretations have been improved by fruitful discussion with C. Innocent (presently at BRGM, France). Part of this work has been done within the framework of master thesis in Oceanology at the University of Liege (R. Brasseur, M. Humblet). On the Belgian side the research was partly funded by FNRS.

References

Biscaye PE (1965) Mineralogy and sedimentation of recent deep-sea clay in the Atlantic Ocean and adjacent seas and oceans. Geol Soc Am Bull, 76, 803–832

Boyle E (1995) Last-glacial-maximum North Atlantic deep water: on, off or somewhere in-between? Philos Trans Roy Soc Lond, A 348, 243–253

Boyle EA, Keigwin LD (1987) North Atlantic thermohaline circulation during the past 20,000 years linked to high-latitude surface temperature. Nature, 330, 35–40

Broecker WS, Denton GH (1989) The role of ocean-atmosphere reorganization in glacial cycles. Geochim Cosmochim Acta, 53, 2465–2501

Chamley H (1989) Clay sedimentology, Springer, Berlin

Dickson RR, Brown J (1994) The production of North Atlantic Deep Water: sources, rates, and pathways. J Geophys Res, 99, 12319–12341

Fagel N (2007) Marine clay minerals, deep circulation and climate. In: Hillaire-Marcel C, de Vernal A (eds.) Paleoceanography of the Late Cenozoic, Volume 1: Methods, pp 139–184. Elservier, Amsterdam

Fagel N, Hillaire-Marcel C (2006) Glacial/interglacial instabilities of the Western Boundary UnderCurrent during the last 360 kyr from Sm/Nd signatures of sedimentary clay fractions at ODP-Site 646 (Labrador Sea). Mar Geol, 232, 87–99

Fagel N, Robert C, Hillaire-Marcel C (1996) Clay mineral signature of the North Atlantic Boundary undercurrent. Mar Geol, 130, 19–28

Fagel N, Hillaire-Marcel C, Robert C (1997) Changes in the Western Boundary Undercurrent outflow since the Last Glacial Maximum, from smectite/illite ratios in deep Labrador Sea sediments. Paleocanography, 12, 79–96

Fagel N, Innocent C, Hillaire-Marcel C, Stevenson R (1999) Nd isotopes as tracers of paleo-currents: a high resolution study of Late Quaternary sediments from the Labrador Sea. Paleoceanography, 14, 777–788

Fagel N, Hillaire-Marcel C, Humblet M, Brasseur R, Weis D, Stevenson R (2004) Nd and Pb isotope signatures of the clay-size fraction of Labrador Sea sediments during the Holocene: implications for the inception of the modern deep circulation pattern. Paleoceanography, 19, doi:10.1029/2003PA000993

Glacial/interglacial instabilities of the Western Boundary UnderCurrent during the last 360 kyr from Sm/Nd signatures of sedimentary clay fractions at ODP-Site 646 (Labrador Sea). Marine Geology 232, 87–99.

Goldstein SL, O'Nions RK (1981) Nd and Sr isotopic relationships in pelagic clays and ferromanganese deposits. Nature, 292, 324–327

Hansen B and Osterhus S (2000) North Atlantic-Nordic Seas exchanges. Prog Oceanogr, 45, 109–208

Hayley BA, Frank M, Spielhagen RF, Eisenhauer A (2007) Influence of brine formation on Arctic Ocean circulation over the past 15 million years. Nature, doi:10.1038/ngeo.2007.5

Hillaire-Marcel C, de Vernal A (2007) Paleoceanography of the Late Cenozoic, Volume 1: Methods. Elservier, Amsterdam

Holloway G (2007) Arctic climatology and meteorology http://nsidc.org/arcticmet/factors/land_sea_distribution.html. Accessed 23 June 2007

Innocent C, Fagel N, Stevenson RK, Hillaire-Marcel C (1997) Sm-Nd signature of modern and late Quaternary sediments from the northwest North Atlantic: implications for deep current changes since the Last Glacial Maximum. Earth Planet Sci Lett, 146, 607–625

Lucotte M, Hillaire-Marcel C (1994) Identification des masses d'eau dans les mers du Labrador et d'Irminger. Can J Earth Sci, 31, 5–13

McCartney MS (1992) Recirculating components to the deep boundary current of the northern North Atlantic. Prog Oceanogr, 29, 283–383

McCave IN, Manighetti B, Beveridge NAS (1995) Circulation in the glacial North Atlantic inferred from grain-size measurements. Nature, 374, 149–151

Moore DM, Reynolds RC (1989) X-Ray diffraction and the identification and analysis of clay minerals. Oxford University Press, Oxford

Raymo ME, Oppo DW, Flower BP, Hodell DA, McManus JF, Venz KA, Kleiven KF, McIntyre K (2004) Stability of North Atlantic water masses in face of pronounced climate variability during the Pleistocene. Paleoceanography, 19, doi:10.1029/2003PA000921

Schmitz WJ, McCartney MS (1993) On the North Atlantic circulation. Rev Geophys, 31, 29–49

Solignac S, de Vernal A, Hillaire-Marcel C (2004) Holocene sea-surface conditions in the North Atlantic – Contrasted trends and regimes between the eastern and western sectors (Labrador Sea vs. Iceland Basin). Quaternary Sci Rev, 23, 319–334

Observing and interpreting the seasonal variability of the oceanographic fluxes passing through Lancaster Sound of the Canadian Arctic Archipelago

Simon Prinsenberg, Jim Hamilton, Ingrid Peterson and Roger Pettipas

Ocean Sciences Division, Bedford Institute of Oceanography, Fisheries and Ocean Canada, 1 Challenger Drive, P.O. Box 1006, Dartmouth, Nova Scotia, Canada, B2Y 4A2, prinsenbergs@mar.dfo-mpo.gc.ca, hamiltonj@mar.dfo-mpo.gc.ca, PetersonI@mar.dfo-mpo.gc.ca, pettipasr@mar.dfo-mpo.gc.ca

Abstract

As part of the Arctic/Sub-Arctic Ocean Flux (ASOF) and the International Polar Year (IPY) programs, a research project consisting of mooring and analysis work has studied the ocean and ice fluxes passing through Lancaster Sound, one of the three main pathways through the Canadian Arctic Archipelago (CAA) since 1998. The aim is to understand the variability in ocean and sea ice volume, heat and freshwater fluxes passing through the CAA and to determine their relationship to the ocean and ice budgets of the Arctic Ocean itself and to the circulation and vertical ventilation of the North Atlantic Ocean. Eight years of mooring data have now been processed and analyzed. The volume, freshwater and heat fluxes exhibit large seasonal and interannual variabilities with small fluxes in the fall and early winter and large fluxes in the summer. The seasonal mean volume flux estimates range from a low of 0.0 Sv in the fall of 1998 to a maximum of 1.3 Sv in the summer of 2000 (1Sverdrup = 1.0×10^6 m^3 s^{-1}). It has an 8 year annual mean of 0.7 Sv and varies interannually by ±0.3 Sv. Model simulations indicate that fluxes through Lancaster Sound make up 40–50% of the fluxes through the entire Canadian Arctic Archipelago, and that they are dependent on the sea level difference between the Beaufort Sea and Baffin Bay and on the horizontal density gradients across the CAA, observations of which are scarce or non-existent. Regression analysis with the Arctic Ocean wind field shows that the fluxes through the NW Passage measured in Lancaster Sound are significantly correlated with the far field wind forcing in the Beaufort Sea. The northeastward winds in the Beaufort Sea, parallel to the western side of the Canadian Arctic Archipelago, show the highest correlation on monthly to interannual time scales. This result is consistent with the transport being driven by a sea level difference between opposite ends of the NW Passage, and the difference being determined by setup caused by alongshore winds in the Beaufort Sea.

J.C.J. Nihoul and A.G. Kostianoy (eds.), *Influence of Climate Change on the Changing Arctic and Sub-Arctic Conditions*,

Introduction

It is generally accepted now that due to climate change, the polar ice caps are melting (ACIA 2004, 2005; IPCC 2007) and indeed, the Arctic Ocean ice extent of September 2007 was the smallest observed over the past 30 years, when satellite imagery was available to document accurately its extent (National Snow and Ice Data Centre, www://nsidc.org.). In addition, all three NW Passage routes through the Canadian Arctic Archipelago (CAA) were ice free for the first time over the 30 year satellite observation period. Changes in the oceanographic and ice fluxes due to natural variability and due to climate change within the CAA have been monitored since August 1998 in Lancaster Sound as part of the international Arctic/Subarctic Ocean Flux (ASOF) program (ASOF 2004), and are being continued under the International Polar Year. The moorings have been monitoring the volume, heat and freshwater fluxes passing through Barrow Strait, the southern-most passage of three within the CAA connecting the Atlantic with the Arctic Ocean. The aim of the program is to better understand the oceanographic and pack ice fluxes passing through the Archipelago, their interannual variability and their relationship to the heat and freshwater budgets of the Arctic Ocean and the CAA, and to the circulation and vertical ventilation of the North Atlantic Ocean.

The first 3 years of processed data from the Lancaster Sound mooring project were reported in Prinsenberg and Hamilton (2005), which described the instrumentation and high frequency variability in ocean parameters. Annual mean transport in Lancaster Sound over 3 years (1998–2001) was found to vary by ±0.25 Sv about a mean of 0.75 Sv, with seasonal fluxes being lowest in the fall and highest in the summer. Further results were published in Melling et al. (2008), describing the long-term variability seen in 6 years of processed data. Now 8 years of data are available to investigate the factors controlling the transport variability that up to now were not well understood. Past analysis of the 1981–82 data from Barrow Strait had shown that seasonal variations in sea level differences along the Northwest Passage are correlated with seasonal variations in transport (Prinsenberg and Bennett 1987); but these results were not connected to the atmospheric forcing. Analyses now indicate that sea level along the coasts of the Arctic Ocean is lower in winter (December–May) than in summer (June–November) because of Ekman transport away from the coasts associated with winter anticyclonic atmospheric circulation (Proshutinsky and Johnson 1997). The present analysis will be show the relationship between winds on monthly to interannual time scales and the flow through Lancaster Sound, using transport estimates from 8 years of mooring data (1998–2006).

Mooring instrumentation

Lancaster Sound is 65 km wide at the mooring site and reaches depths of 285 m (Fig. 1). Annually the mooring array has been recovered and re-deployed in late summer using Canadian Coast Guard icebreakers, at which time CTD profiles and water samples for chemical tracer analysis have been collected. Instrumentation of the array has increased through the years as additional instrumentation became available (Prinsenberg and Hamilton 2005). Mobile and land-fast pack ice conditions are found normally for 10 months of the year. Ice ridge keels within the pack ice are a threat to moorings which, for this reason, were designed not to extend into the top 25 m of the water column. Instrumentation includes Acoustic Doppler Current Profilers (ADCPs) to monitor ocean and ice velocities, Upward Looking Sonars (ULSs) to monitor ice drafts, and CTD units (MicroCats) to monitor water column properties at various depths. Figure 2 shows the array used for the 2003–04 deployment, which also included Tide Gauges and a CTD profiler called ICYCLER. Further descriptions of the instrumentation, data analysis and high frequency ocean variability can be found in Prinsenberg and Hamilton (2005).

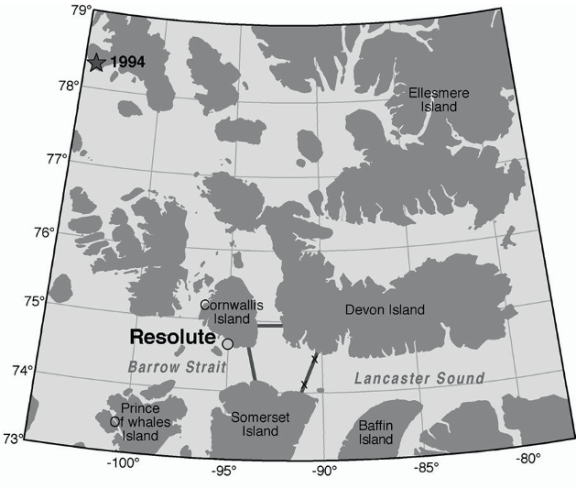

Fig. 1. Map of the eastern Canadian Arctic Archipelago (CAA) section of the NW Passage showing the CTD transects as solid lines, main mooring sites (crosses) in the Barrow Strait-Lancaster Sound region and the north magnetic pole location (Star-1994) which is moving northwards.

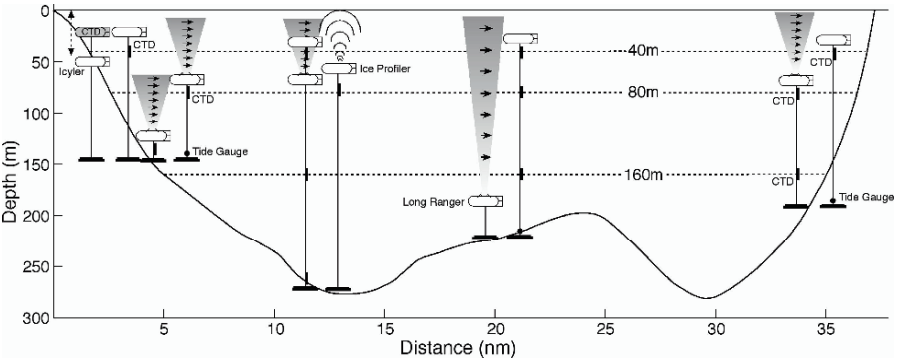

Fig. 2. Lancaster Sound mooring array for 2003–04 looking upstream to the Arctic Ocean with the south shore on the left of the figure and north on the right (37 nm equals 65 km).

Ocean parameters

Salinity and temperature profiles, collected during the summer mooring surveys show that the coldest water (−1.7°C) in summer is found at mid-depth. It has a salinity of 32.8–33.0 and represents water mass remnants of the winter surface mixed layer (Prinsenberg and Hamilton 2005). Above this water mass lies a very stable surface layer formed by dilution by ice melt and local runoff and warming by the atmospheric heat flux. The warmest and freshest water is organized into buoyancy boundary currents that flow in opposite directions along the northern and southern shores. Below the cold mid-depth water mass, the water temperature and salinity increases with depth. This warmer deep water enters the area from northern Baffin Bay. Geostrophic current fields derived from density distributions shows an eastward flowing current that decreases with depth and extends from the southern shore of Lancaster Sound to 2/3 of the way across the Sound. A depth-varying current along the northern shore appears to be restricted to 1/3 of the northern part of the Sound and does not appear to contribute to the total flux through the cross-section.

Figure 3 shows a 2-month example of the current variability seen in Lancaster Sound. The 2-month data sections are bi-hourly along-shore currents at 10 m depth from the southern and northern sites. These small sections of the total 8 year record show the temporal variability that exists throughout the 8 year time series. Ocean currents vary hourly due to tidal components, vary daily due to atmospheric forcing and vary seasonally due to long-term variability in sea level pressure gradients. In addition to these temporal variabilities at each location, there exist large horizontal and vertical spatial variabilities. Tidal currents vary on a 12 h cycle by up to 35 cm/s when the sun and moon tidal constituents generated in the

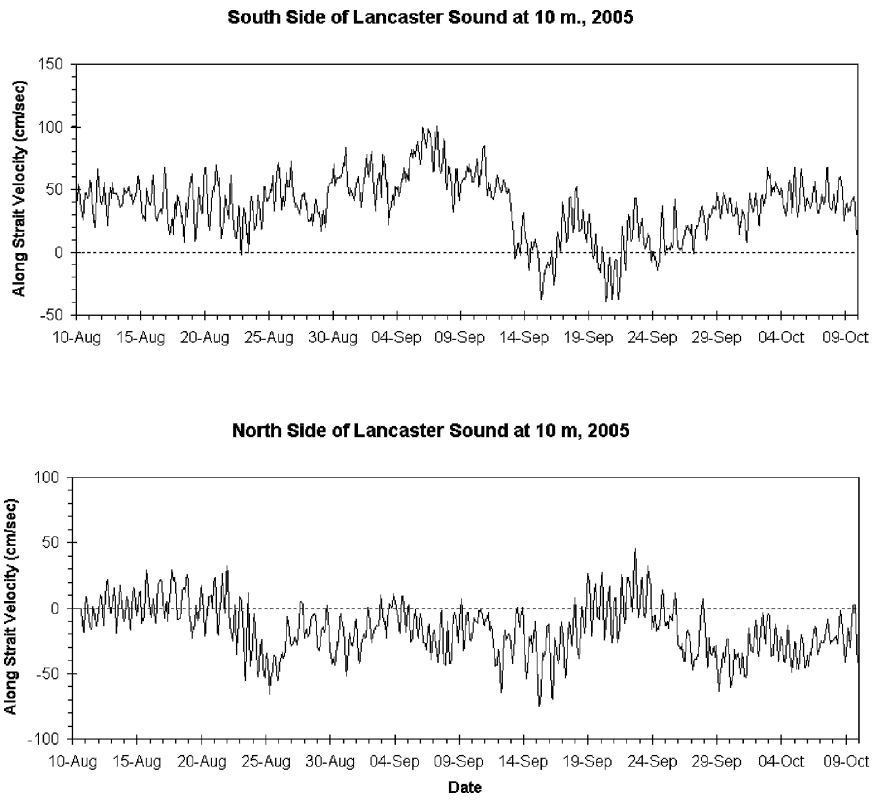

Fig. 3. Along-shore ocean surface velocities (10 m depth) from the southern and northern mooring sites in Lancaster Sound. Bi-hourly data are from August 10 to October 9, 2005.

Atlantic Ocean reinforce or oppose each other. The contribution from the Arctic Ocean tide is weaker as the Arctic tides are smaller and reflected back to the Arctic from the sill and island arch located in western Barrow Strait at 96° W longitude.

The largest long-term mean velocity components, driven by atmospheric and sea level pressure gradients along the NW Passage, are found along the southern shore where daily mean values of the exiting Arctic surface waters reach 50 cm/s and set towards Baffin Bay. Along the northern shore, the long-term currents are smaller and do not have a persistent preferred direction (Fig. 4). In the summer they generally are directed towards the west (Arctic Ocean) and in the winter towards the east (Baffin Bay). Currents normally decrease with depth in response to surface atmospheric forcing and bottom friction. The exception being that during land-fast ice conditions, the ice isolates the ocean surface from wind

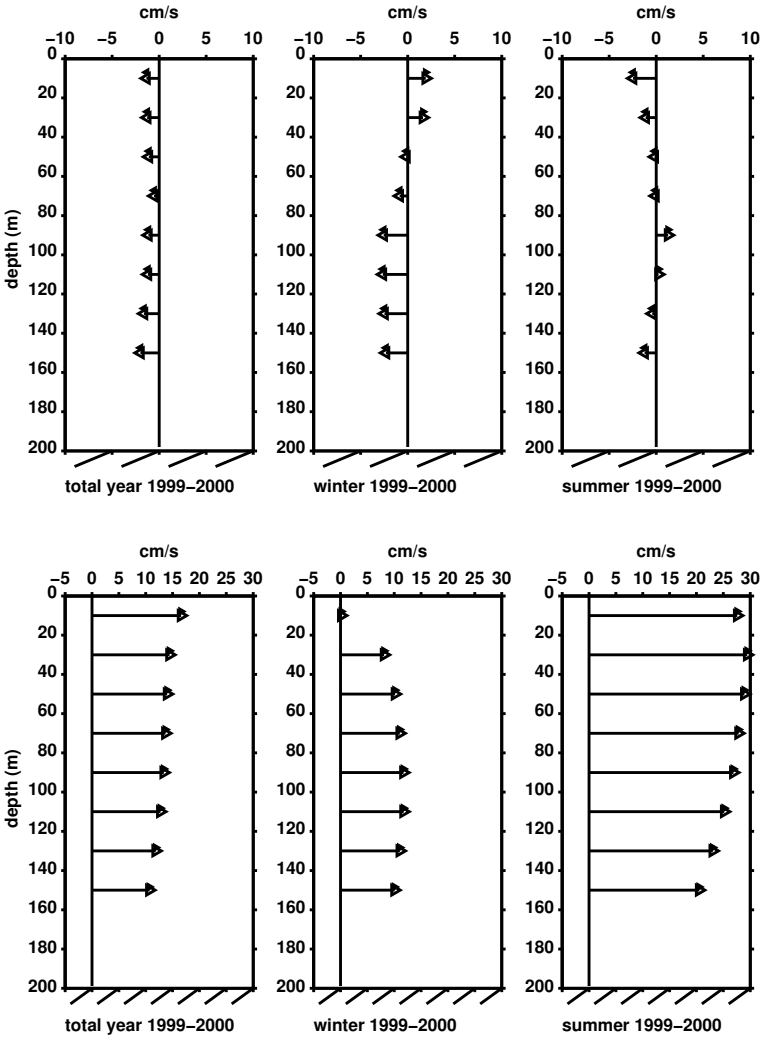

Fig. 4. Along-shore current profiles for the northern (*top*) and southern (*bottom*) sites in Lancaster Sound. Profiles are for year-long deployment of August 1999 to August 2000, the winter 2000 (January to April) and the summer 2000 (June to mid August).

forcing and acts as a friction boundary thereby reducing the surface currents in winter relative to mid-depth values (Fig. 4). The seasonal and yearly mean currents vary interannually in response to large scale atmospheric forcing and as seen later to the sea surface level set-up due to surface winds at the western entrance of the NW Passage section in the CAA (Peterson 2008).

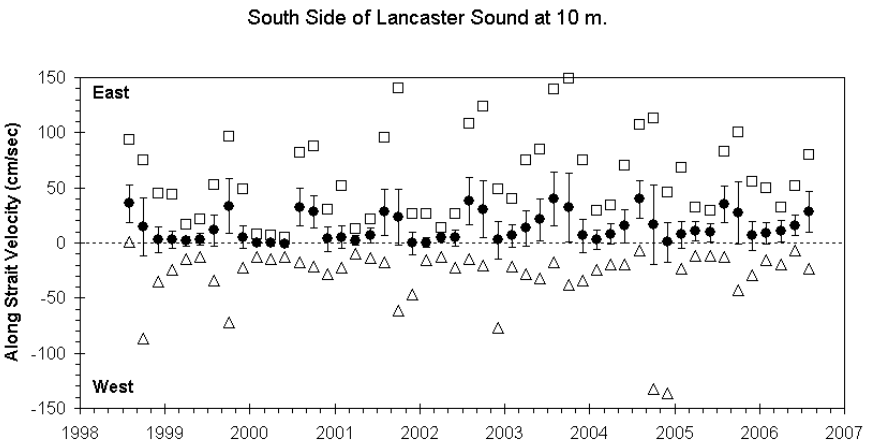

Fig. 5. Eight years of bi-monthly ocean velocity data observed at 10 m depth at the southern site in Lancaster Sound. Shown are bi-monthly vector velocity means (solid circles), standard deviations (bars), and the maximum east (squares) and maximum west (triangles) bi-hourly velocities for each bi-monthly section.

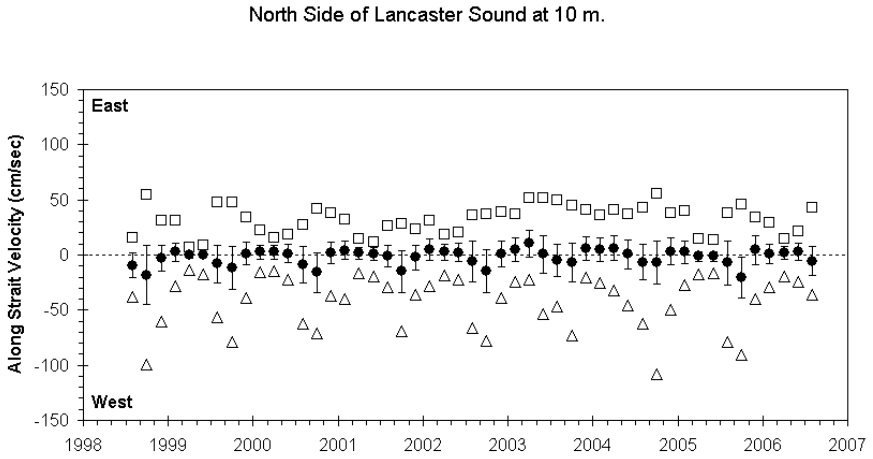

Fig. 6. Same as Fig. 5 but for the northern site in Lancaster Sound.

Figures 5 and 6 show the bi-monthly ocean along-shore current data for the 8 year period. The bi-monthly mean velocities (solid dots) and magnitude of the standard deviation about the mean show that at both sites, the mean currents are lower and are less variable during the winter months than the summer months, when far-field and local wind forcing on the ocean surface can occur. In the summer months the mean currents and variability about the means are larger for

the southern site and are setting eastwards to Baffin Bay. For the northern site, the summer means are small but generally setting to the west. The maximum velocities are similarly largest for the southern site, occur during the open water period and are in the direction of Baffin Bay. The maximum velocities towards the west are less as they oppose the mean currents flowing to Baffin Bay. In contrast, the largest summer maximum velocities along the northern shore are part of the buoyancy coastal currents directed towards the west.

Ice velocities, drafts and fluxes

The ADCPs providing ocean velocities, also provide ice drifts at bi-hourly intervals. To show the total 8 year time series, the bi-hourly ice velocity data were again divided into 2-month sections for which the along-strait ice velocity was used to derive the bi-monthly vector mean velocities and the standard deviations (Std). Since ice is not always present in the summer months, the bi-monthly percent of ice velocity values was also calculated and shown in Figs. 7 and 8 for the southern and northern sites respectively.

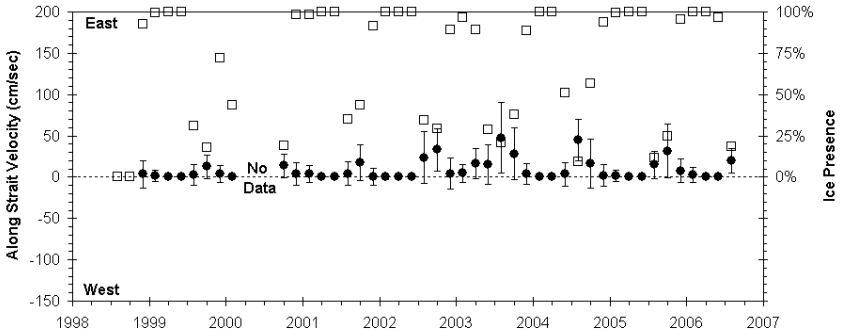

Fig. 7. Eight years of ice velocity data observed in Lancaster Sound located at a site 5 nm from the southern shore (Fig. 2). Bi-monthly means are shown as solid circles, with ±1 standard deviation illustrated with the bars. Percentage of ice presence providing ice velocities are shown by open squares.

Figure 7 shows the results from the southern site of Lancaster Sound where most of the eastwards flowing Arctic surface waters occur (Prinsenberg and Hamilton 2005). Land-fast ice conditions occur normally in March and April and in some severe winters during the months of May and June. In 2003, the ice was mobile for at least part of each 2 month period and land-fast ice conditions did not occur for the total 2 month period (March–April). During mobile ice conditions, the bi-monthly mean velocities are up to 50 cm/s but are generally around 10

cm/s. In these periods, the percentage of ice present is low, allowing the ice to move freely under ocean and wind forcing. Ice velocities towards Baffin Bay are generally larger than those towards the Arctic, as they move along with the eastward bi-monthly mean ocean currents.

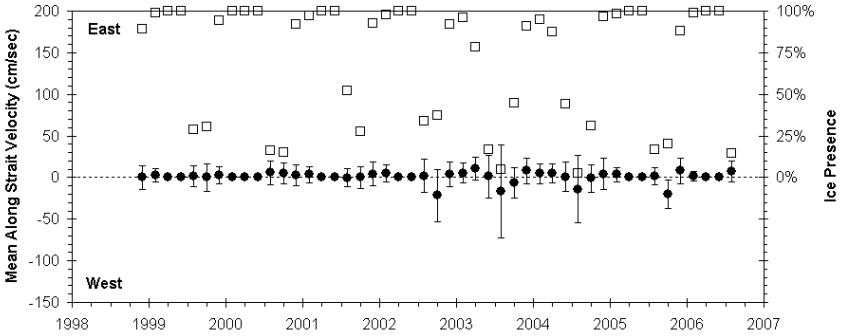

Fig. 8. Same as Fig. 7 but for site 3 nm from the northern shore in Lancaster Sound (Fig. 7).

At the northern site, land-fast ice conditions persisted for the months of March and April for all years except 2003 and 2004 (Fig. 8). Bi-monthly vector mean ice velocities are smaller along the northern shore, and unlike at the southern site, have no preferred direction. In summer months the percentage of ice present drops below 25%, as was the case for the southern site.

Figure 9 shows 2 years of ice draft data from the ice season of 2003–04 when the pack ice remained mobile throughout the winter, and from the ice season 2005–06 when land-fast ice conditions occurred and thus reflect a more normal ice season. With global warming however, mobile ice conditions such as those of 2003–04 may become more prevalent. During mobile ice conditions, ice ridges passing the mooring site reach up to 24 m, but were generally up to 16 m for the 2003–04 winter. In 2005–06 the maximum ice draft was 13 m. From ice charts, it can be seen that the ice arch separating land-fast ice from mobile ice occurred in western Barrow Strait in 2003–04 (95° W), 120 km west of the mooring site, while it established itself at the mooring site in the 2005–06 winter (Can. Ice Service, http://ice-glace.ec.ca). Once land-fast ice conditions were established at the mooring site in February 2006, the sonar monitored the same ice that grew slowly thermodynamically. For the 2005–06 winter, the land-fast ice above the sonar was not ridged and thus low monthly maxima were detected. The small variability detected in the monthly mean is probably due to mooring motion that causes the sonar to monitor ice in a small area and not just one specific location of the pack ice.

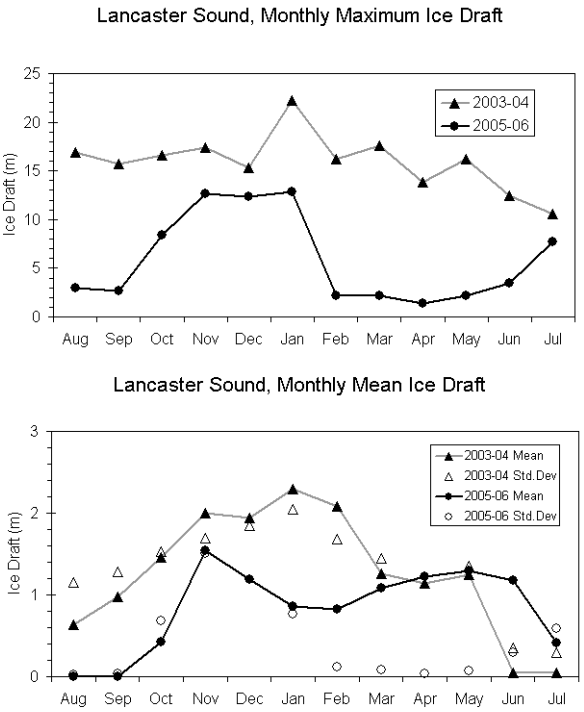

Fig. 9. Two years of ice draft data from the southern site of the Lancaster Sound array. Shown are monthly maxima ice draft (*top panel*) and monthly means and standard deviations in the *bottom panel*.

In the bottom panel of Fig. 9, the monthly mean draft and the standard deviation are shown for the 2003–04 and 2005–06 winters. Relative to the 2003–04 winter, the 2005–06 winter started and ended 2 months later. During mobile ice conditions the monthly Std of ice draft and the monthly mean ice draft vary similarly; meaning that the variability about the mean and the mean itself increase and decrease proportionally. During land-fast ice conditions the Std approaches zero and the mean values vary as expected under thermodynamic ice growth. Once the land-fast ice breaks up in June 2006, ridges start to appear and increase the monthly maximum.

To estimate the freshwater flux associated with the mobile pack ice requires ice drift and ice thickness data such as shown in Figs. 6–8. However, not only are these time series scarce, but also very site-specific, as ice properties are less diffusive than ocean properties.

Although satellite imagery alone cannot provide estimates of ice-volume fluxes, it has provided long time series of ice-area fluxes in the CAA. However, the flux estimates are often hampered by coarse spatial resolution. Kwok (2006) estimated the ice-area transport across the main entrances to the Canadian Archipelago using Radarsat imagery (0.2 km resolution) and found that due to the land-fast ice within the CAA, the western entrances export ice to the Arctic Ocean, and the eastern entrances export ice to Baffin Bay. On average, Nares Strait does export ice from the Arctic to Baffin Bay, but export is prevented when the ice bridge in Smith Sound is present. Agnew et al. (2006) using Advanced Microwave Scanning Radiometer AMSR-E data (6 km resolution) found that transport directions were generally similar. However transport estimates differed in magnitude, perhaps because of different resolutions of the imagery or different time periods. In deriving ice-volume fluxes from ice-area fluxes for freshwater budgets, the uncertainty is further increased by the difficulty of estimating ice thickness. Freshwater fluxes in the form of ice that have been estimated from ADCP ice drift data (Prinsenberg and Hamilton 2005; Melling et al. 2008) are in the range of 1.5–2.5 mSv, and are an order of magnitude smaller than those in the water column.

Ocean fluxes

To estimate fluxes from site-specific time series it is assumed that the mooring data can represent, through weighting, the cross-sectional fluxes. Analysis of data from August 2001 to August 2004 of a modified array provided surface layer (0–60 m) current measurements from ¼ and ½ way across the strait as well as measurements at the southern and northern sites. These data indicate that in winter and spring, the eastwards currents are similar across the southern 2/3 of the strait, while in summer and fall the currents of the southern mooring should be reduced to 55% to represent the mean currents observed over 2/3 of the southern strait. This provides information to better estimate the total fluxes through the cross-section for the sparser arrays prior to 2001. Further details on the estimation of fluxes can be found in Prinsenberg and Hamilton (2005) and Melling et al. (2008).

Fluxes are calculated relative to a salinity of 34.8 and a temperature of –0.1°C, which represents the salinity and temperature of Atlantic Water in the Arctic Ocean (Aagaard and Carmack 1989). Fluxes clearly show the strong seasonal as well as the interannual variability (Fig. 10). Volume and fresh water fluxes exhibit the same variability driven by the currents, while the heat flux mirrors their variability. All three show maximum magnitudes in the summer and minimum magnitudes in the fall. Volume and freshwater fluxes are positive indicating net

transport of Arctic surface waters to the Atlantic Ocean. Heat flux is predominantly negative, indicating that Arctic surface water is colder than Atlantic Water in the Arctic Ocean, and will thus cool the Atlantic Ocean. It has an 8-year mean of –4.1 × 105 W and varies interannually by ±2.0 × 105 W. Seasonal (3-month averages) volume fluxes vary from low values in fall (0.0 Sv in 1998) to high values in summer (1.3 Sv in 2000). Annual means of the volume fluxes vary from 0.4 to 1.0 Sv, and have an 8-year mean of 0.7 Sv. In general, the freshwater flux is 1/15 of the volume flux and follows the volume seasonal variability. It has an 8-year mean of 0.048 Sv and varies interannually by ±0.015 Sv. The 8-year flux data was used to derive the annual cycle, consisting of mean monthly values (Fig. 11). It has a maximum in June of 1.15 Sv and a minimum in December of 0.25 Sv.

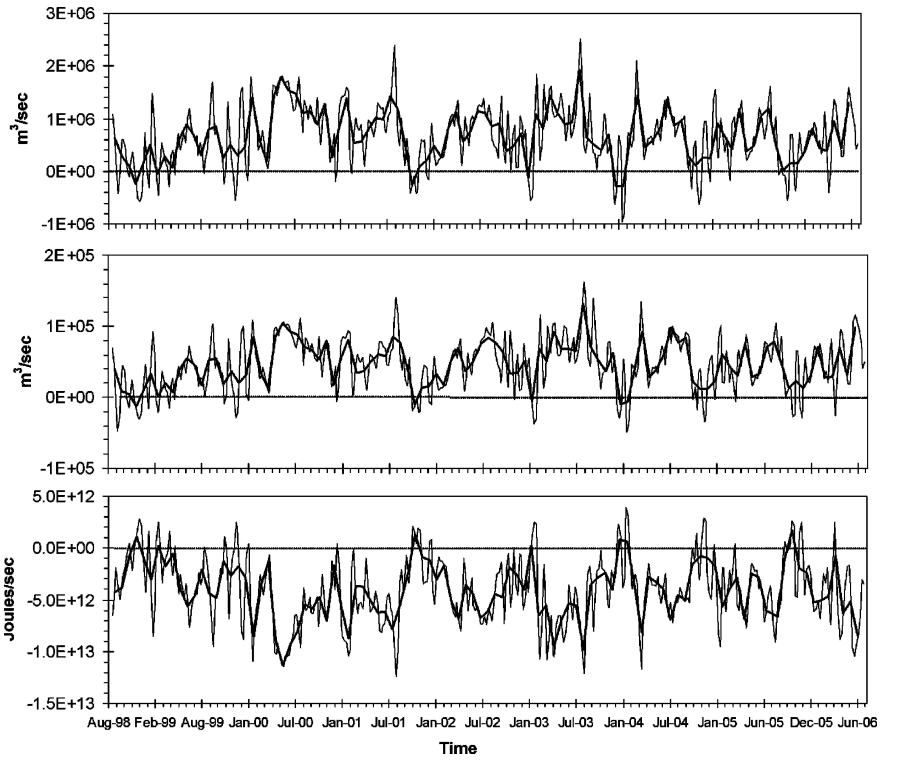

Fig. 10. Weekly (thin line) and monthly (thick line) estimated volume (*top*), freshwater (*middle*) and heat (*bottom panel*) transports through Lancaster Sound from August 1998 to August 2006.

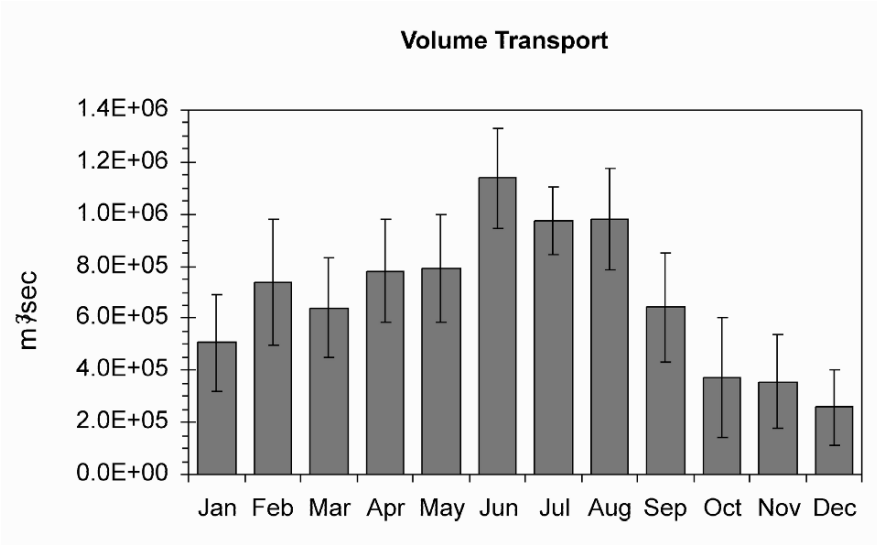

Fig. 11. Mean monthly volume flux through western Lancaster Sound derived from 8 years of mooring data (Aug 1998–Aug 2006).

Wind forcing

The volume transport data were compared with NCEP (National Centre for Atmospheric Prediction) monthly surface wind data (sigma level = 0.995), which has a grid spacing of 2.5˚ latitude by 2.5˚ longitude (Peterson 2008). Multiple correlation coefficients with the observed transports were computed using monthly mean wind data at each grid point (i,j) north of 55˚ N, and a regression model of the form

$$M = a_{ij}U_{ij} + b_{ij}V_{ij} + c_{ij} + \varepsilon \quad (1)$$

where M is volume transport, U_{ij} is the zonal wind component, V_{ij} is the meridional wind component at grid point (i,j), a_{ij}, b_{ij}, and c_{ij} are the regression coefficients, and ε is the residual.

The maximum correlation coefficient (R = 0.68) is found in the Beaufort Sea west of M'Clure Strait at 75° N, 132.5° W, the western entrance of the NW Passage of the CAA. It is over 1,000 km from the mooring array in Lancaster

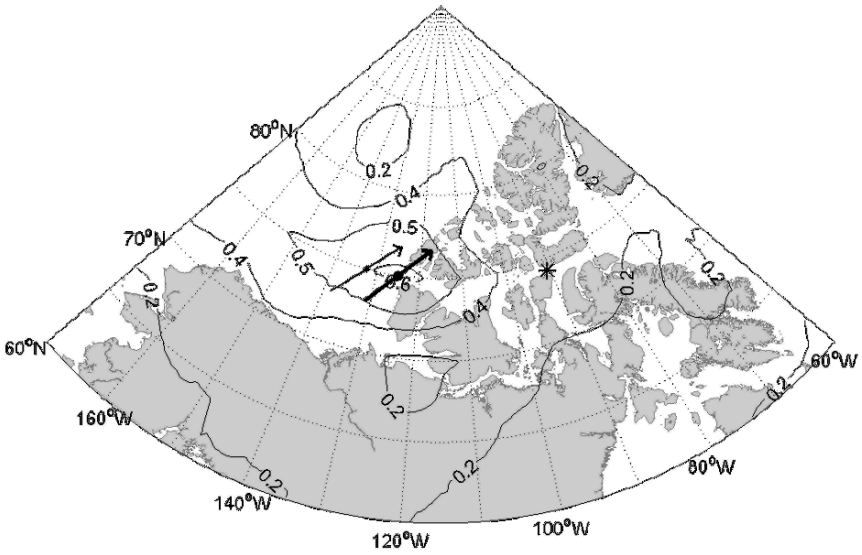

Fig. 12. Map showing correlation coefficients between monthly anomalies of NCEP surface wind and volume transport (contour lines), and the optimum wind location and direction (thick black arrow). The position of the Lancaster Sound mooring line is marked by the asterisk. The thin black arrow shows the optimum wind location and direction using monthly total wind and volume transport.

Sound and its correlation coefficient is double that of the local wind forcing. The optimum wind direction at the western entrance to the NW Passage (thin arrow, Fig. 12) is to the northeast (43˚T), which is parallel to the coastline. Similarly, an optimum wind direction parallel to the western Newfoundland coastline was reported for flow in the Strait of Belle Isle (Garrett and Toulany 1981), and was explained by the winds causing sea level setup or setdown at the ends of the strait, producing a sea level difference from one end to the other.

However, the location of the maximum correlation is not well defined. Since some portion of the correlation may be simply due to the wind and transport having similar annual cycles, the analysis was repeated using monthly anomalies of transport and wind components, computed by subtracting the 8-year mean values for each month. For this second case, the correlation coefficient reduced slightly from 0.68 to 0.62 and remained off the western entrance of the Northwest Passage (thick arrow in Fig. 12). The optimum direction is toward 44˚T, and the time series for the wind anomaly component along this direction is plotted in Fig. 13. The gains, monthly wind anomalies, and the mean annual cycle of transport were used to produce estimates of transport (Fig. 13). The annual cycle of

transport represents 34% of the variance of total transport, and the wind anomalies combined with the annual cycle account for 59% of the variance of monthly transport.

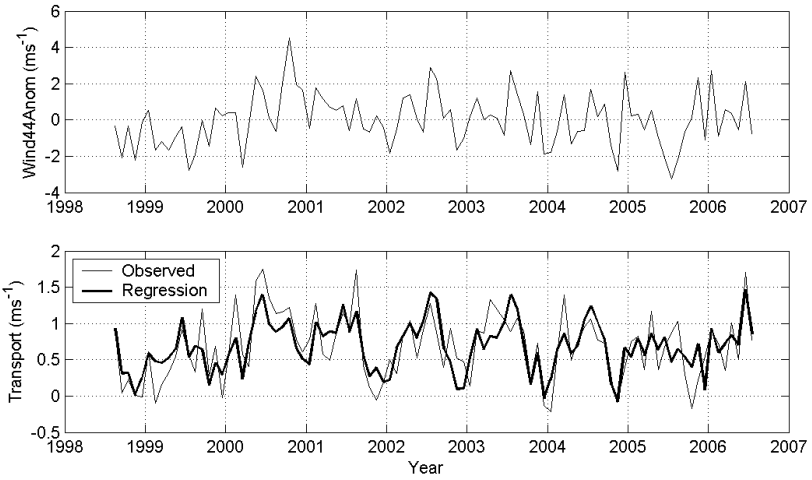

Fig. 13. Alongshore component of monthly wind anomalies at 75° N, 125.0° W (relative to 44°T) and annual cycle plus the wind anomaly effect (bold line), and the observed volume transport (thin line).

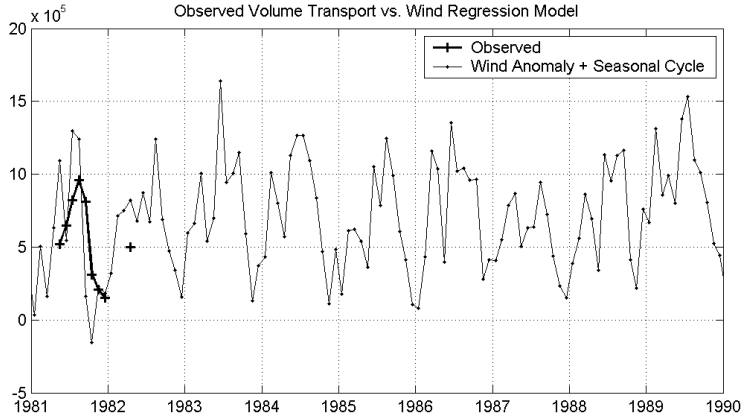

Fig. 14. Monthly transport estimates for the 1980s including the Barrow Strait observations (bold line) derived from the NCEP winds.

The regression coefficients can be used to simulate the transport through Lancaster Sound for other years prior to 1998. Figure 14 shows the monthly simulated transports back to 1980 when the first transport observations were available from Barrow Strait just west of the present mooring array site (Prinsenberg and Bennett, 1987).

The observations compare well with the wind estimates; they are smaller at this site because some of the transport flux coming out of the Sverdrup Basin east of Cornwallis Island (Fig. 1) is not included, as it is in the present mooring observations. Assuming that Barrow Strait contributes three-quarters of the transport of Lancaster Sound (Prinsenberg and Bennett 1987), the 1981–82 observations should be increased by one third.

The annual mean transport (August to July) from 1999 to 2006 (Fig. 15) is also significantly correlated with the alongshore wind (r = 0.88) based on eight points (years). The gain is 0.24×10^6 m^2, and using the relationship between annual mean transport and wind (1999–2006), transport was estimated for the full extent of the NCEP dataset (Fig. 15). The lowest estimated transport value over the entire 58-year record corresponded to the year 1999, while 2001 had the fourth highest value. The extreme low was captured in our mooring observation period. Estimated transport was particularly high from 1989 to 1997, and may have contributed to the freshwater gain observed in the Labrador Sea during this period (Yashayaev 2007).

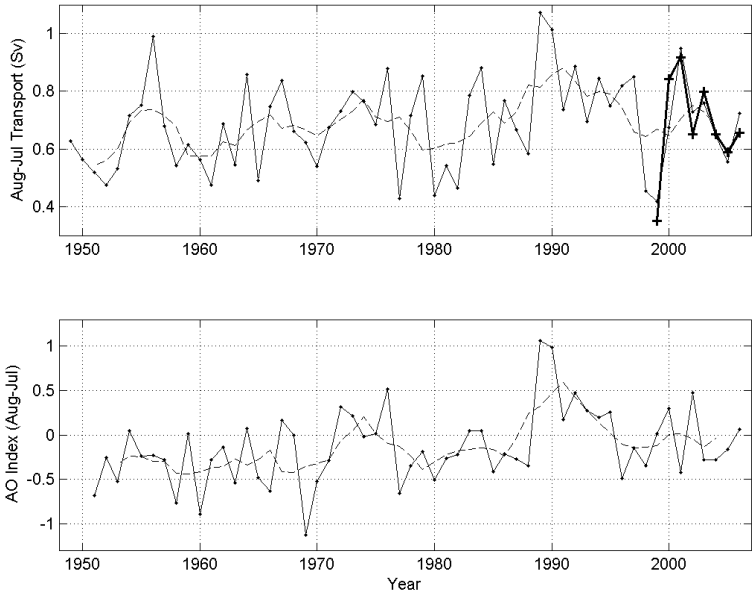

Fig. 15. Top panel shows annual mean transport (August–September) estimated from alongshore winds (thin solid line) and observed transport (bold line). Bottom panel shows the Arctic Oscillation (solid line). The 5-year running means are shown by the dashed lines in both panels.

The Arctic Oscillation index, defined as the leading principal component of Northern Hemisphere SLP, is plotted in Fig. 15, and is averaged between August and July as for the transport estimates based on the alongshore wind. At any given

point, the correlation between the along-shore wind component and the AO index is expected to depend on the loading pattern of the AO index. The correlation of alongshore wind at 75° N, 125° W with the AO index is 0.60. Not surprisingly, the AO and the alongshore wind show similar trends and inter-decadal variability, with high values seen in the early 1990s. However the AO does not capture the interannual variability of the observed transport over the 8-year mooring deployment ($r = 0.21$).

Conclusion

Due to the eastward-setting Arctic surface waters found along the southern shore of Lancaster Sound, the mean currents there are large (15.3 cm/s) as compared to smaller westward-setting mean currents of 2.2 cm/s along the northern shore. Standard deviations about the 8 year mean are 21.5 and 15.0 cm/s respectively for the southern and northern shore sites, while maximum values can reach up to 150 cm/s. Bi-monthly mean velocities reach up to 50 cm/s in summer months along the southern shore, while they only reach 10 cm/s along the northern shore.

Bi-monthly mean ice drifts are smaller because of the long period of land-fast ice conditions, but can similarly reach maximum speeds of 150 cm/s. Ice draft measurements were available for only 2 years and show that the mean, standard deviation and maximum keel depth depend on whether landfast ice occurs at the mooring site. Ice volume fluxes and derived freshwater fluxes in the form as ice are difficult to estimate but appear to be an order of magnitude less than the freshwater fluxes in the water column.

Volume, freshwater and heat transports estimated from the mooring data clearly show the strong seasonal as well as the interannual variability. Heat fluxes are predominantly negative indicating that the Arctic surface water is colder and will cool the Atlantic Ocean. Yearly means of the volume fluxes vary from 0.4 to 1.0 Sv, and have an 8-year mean of 0.7 Sv. In general, the freshwater flux is 1/15 of the volume flux and follows the volume seasonal variability. It has an 8-year mean of 0.048 Sv and varies interannually by ±0.015 Sv.

The 8-year mean monthly volume flux has a summer maximum (1.15 Sv) and a late-fall minimum (0.25 Sv). Seasonal mean values are as low as −0.01 Sv for fall and as high as 1.32 Sv for summer.

Volume transport in Lancaster Sound is significantly correlated with northeastward winds in the Beaufort Sea, parallel to the western side of the CAA, at monthly to interannual time scales. The optimum location and wind direction are consistent with the flow being driven by a sea level difference along the Northwest Passage, and the difference being determined by setup caused by alongshore winds in the Beaufort Sea.

Freshwater and heat transport are highly correlated with volume transport. The correlation coefficients between volume transport and freshwater and heat transport are greater than 0.96 for both total transport and transport anomalies. Thus based on the transport estimates, the results for volume transport generally apply for freshwater and heat transport as well. However, freshwater transport is likely underestimated since it is based on measurements from Conductivity-Temperature-Depth (CTD) sensors at depths greater than 25–30 m (Prinsenberg and Hamilton 2005).

Wind forcing is also important in determining transport in Bering Strait at both weekly to monthly time scales and interannual time scales (Woodgate et al. 2006). However, the transport is primarily affected by local winds parallel to the strait. The mean transport is northward, and is weakest in winter because of strong northerly winds, and strongest in summer.

In contrast, in Lancaster Sound, transport variability is largely determined by winds 1,000 km away at the western end of the Northwest Passage parallel to the adjoining coasts. The mean transport is eastward, and transport is lowest in the fall because of strong northeasterly winds. Transport increases in January–February because of a high pressure ridge over the area producing a weaker northeasterly wind component. Highest transport is observed in the summer because of moderate westerly winds. The correlation of alongshore wind at 75° N, 125° W with the AO index is 0.60 as the alongshore wind show similar trends and inter-decadal variability. However the annual AO index does not capture the interannual variability of the observed transport over the 8-year mooring deployment ($r = 0.21$).

Acknowledgments

The authors would like to thank Murray Scotney for managing the instrumentation for the collection of all the mooring data. Internal and external reviewers are thanked for their helpful comments on the various drafts of the manuscript. Personnel of Canadian Coast Guard icebreakers are thanked for their continued support during field operations. This work was supported by the Canadian Program of Energy Research Development (PERD) and the Department of Fisheries and Oceans' High Priority Program.

References

Aagaard K, Carmack EC (1989) On the role of sea ice and freshwater in the arctic circulation. J Geophys Res, 94: 14485–14498

ACIA (2004) Impacts of a warming arctic: arctic climate impact assessment. Cambridge University Press, Cambridge

ACIA (2005) Arctic climate impact assessment. Cambridge University Press, Cambridge

Agnew TA, Vandewedge J, Lambe A (2006) Estimating the sea ice area flux across the Canadian Arctic Archipelago using the Advanced Microwave Scanning Radiometer (AMSR-E). Unpublished report

ASOF (2004) Arctic/Subarctic Ocean fluxes. Newsletter No. 2, March 2004; http:asof.npolar.no
Garrett CJR, Toulany B (1981) Variability of the flow through the Strait of Belle Isle. J Mar Res, 39: 163–189
IPCC (2007) IPCC fourth Assessment Report (AR-4). Twenty-Seventh Session of the International Panel on Climate Change, Valencia, Spain, November 12–17, 2007
Kwok R (2006) Exchange of sea ice between the Arctic Ocean and the Canadian Arctic Archipelago. Geophys Res Lett, 33: L16501, doi:101029/2006GL027094. l
Melling M, Agnew TA, Falkner KE, Greenberg DA, Lee CM, Munchow A, Petrie B, Prinsenberg SJ, Samelson RM, Woodgate RA (2008) Fresh-water fluxes via Pacific and Arctic outflows across Canadian Polar Shelf. In: Dickson RR, Meinke J and Rhines P (eds) Arctic-Subarctic Ocean fluxes, defining the role of the northern seas in climate. Springer Science and Business Media BV, P.O. Box 17, 3300 AA Dordrecht, The Netherlands, pp. 193–247
Peterson IK (2008) Beaufort Sea wind forcing of the flow through the Northwest Passage. Geophys Res Lett, submitted
Prinsenberg SJ, Bennett EB (1987) Mixing and transports in Barrow Strait, the central part of the Northwest Passage. Cont Shelf Res, 7(8): 913–935
Prinsenberg SJ, Hamilton J (2005) Monitoring the volume, freshwater and heat fluxes passing through Lancaster Sound in the Canadian Arctic Archipelago. Atmos Ocean, 43(1): 1–23
Proshutinsky AY, Johnson MA (1997) Two circulation regimes of the wind driven Arctic Ocean. J Geophys Res, 102: 12493–12514
Woodgate RA, Aagaard K, Weingartner TJ (2006) Interannual changes in the Bering Strait fluxes of volume, heat and freshwater between 1991 and 2004. Geophys Res Lett, 33: L15609, doi:10.1029/2006GL026931
Yashayaev I (2007) Hydrographic changes in the Labrador Sea, 1960–2005. Prog Oceanogr, 73: 242–276

River flux of dissolved organic carbon (DOC) and particulate organic carbon (POC) to the Arctic Ocean: what are the consequences of the global changes?

Viacheslav V. Gordeev and Marina D. Kravchishina

P.P. Shirshov Institute of Oceanology, Russian Academy of Sciences, Moscow, RF, gordeev@ocean.ru, kravchishina@ocean.ru

Abstract

An attempt was made to estimate an increase of particulate organic carbon (POC), dissolved organic carbon (DOC) and total organic carbon (TOC) delivery by the Russian Arctic rivers to the Arctic Ocean by 2100. The calculations are based on the previously published estimations of an increase of river water discharge (Peterson et al. 2002) and of suspended matter discharge (Gordeev 2006) to the end of 21st century. The Intergovernmental Panel on Climate Change (IPCC 2007) predicts the global surface air temperature increase in a range between 1.4° and 5.8°C by 2100. The climate warming will result in the thawing of the multi-annual permafrost in Siberia. The enriched by organic carbon frozen peatlands will be the very effective source of organics to the rivers and streams. Frey and Smith (2005) predict an increase of DOC concentration in the rivers of West Siberia up to 400% due to this process.

Introduction

The problem of the global climate warming excites the apprehensions of mankind in view of the probable significant consequences for the ecosystems, especially in high latitudes. The expected warming may affect a whole spectrum of natural and human systems in the Arctic region (Serreze et al. 2000; McGuire et al. 2006 and other).

A comprehensive study of this problem is carrying out by the Intergovernmental Panel on Climate Change from the beginning of 90th. The IPCC Fourth Assessment Report was published recently (IPCC 2007). The Report includes the analysis of recent climatic variability based on the data of observations, paleoclimatic reconstructions and the results of modeling of present and future changes of climate.

J.C.J. Nihoul and A.G. Kostianoy (eds.), *Influence of Climate Change on the Changing Arctic and Sub-Arctic Conditions*,

Significant increase of average global air temperature was recorded for the last century (Fig. 1a). The 100-year linear trend (1906–2005) of 0.74°C is larger than the corresponding trend of 0.6°C (1901–2000). Eleven of the last 12 years (1995–2006) rank among the 12 warmest years in the instrumental record of global surface temperature (since 1850).

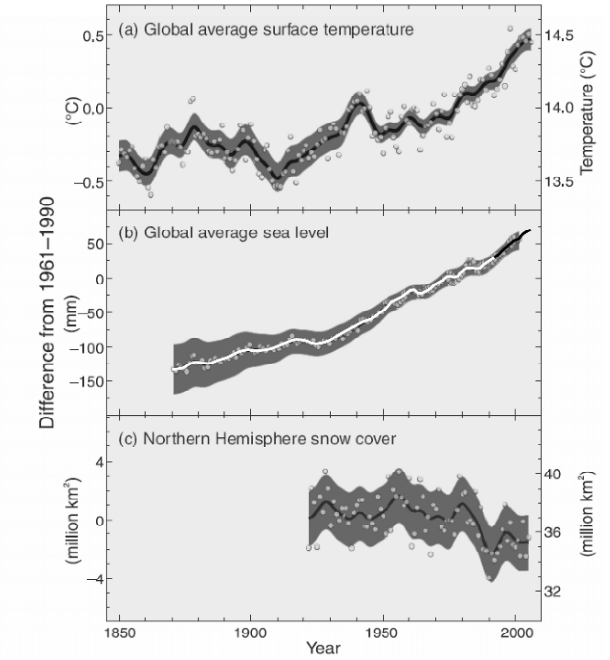

Fig. 1. Observed changes in (**a**) global average surface temperature; (**b**) global average sea level from tide gauge (white) and satellite (black) data; and (**c**) Northern Hemisphere snow cover for March–April (relative to corresponding averages for the period 1961–1990). Smoothed curves – decadal averaged values, circles – yearly values, shaded areas – uncertainty intervals (IPCC 2007).

Satellite data show that annual average Arctic sea ice extent has shrunk by 2.7% per decade since 1978, with larger decreases in summer of 7.4% per decade. Very important information concerns the frozen ground in the Northern Hemisphere. The maximum area extent of seasonally frozen ground has decreased by about 7% since 1900, with decreases in spring up to 15%. Active layer thickness over permafrost in the Russian Arctic has increased from 1956 to 1990 by about 20 cm (31 stations of observation) while seasonal freeze depth has decreased by about 34 cm (211 stations of observation) (Frauenfeld et al. 2004) (Fig. 2).

The atmospheric concentrations of the most important anthropogenic greenhouse gases (GHGs) CO_2 and CH_4 in 2005 exceed by far the natural range over the last 650,000 years. The global atmospheric concentration of CO_2 increased up to 379 ppm in 2005 (a pre-industrial level – 280 ppm), CH_4 up to 1,732 ppb (from 715 ppb) and N_2O up to 319 ppb (from 270 ppb).

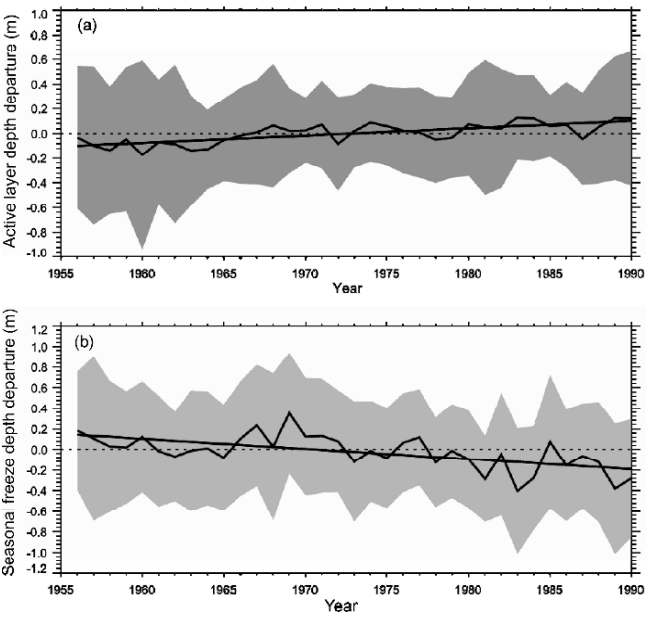

Fig. 2. Variations in the thickness of the active layer over permafrost (**a**) and maximum soil freeze depth in non-permafrost area (**b**) in Russia from 1956 to 1990. The shaded area presents the 5–95% confidence interval from the mean for each year, and the dashed line is the zero reference (Frauenfeld et al. 2004).

All these findings look like the very conclusive proofs of the going climate warming. The multi-model global averages of surface air temperatures were evaluated for the different scenarios of anthropogenic impacts to the end of 21st century (relative to 1980–1999) (Fig. 3). Expected warming will be in a range between 1.8°C and 4.6°C. Decreasing of CO_2 assimilation by the ocean and the land at climate warming may lead to additional increase of temperature on 1°C.

However, not all published data support the given point of view. Polaykov et al. (2002) consider that Arctic variability is dominated by multi-decadal fluctuations. The authors show that over 125-year record the periods were identified when arctic surface air temperature (SAT) trends were smaller or of opposite sign than Northern-Hemispheric trends. Their main conclusion is: "The data do not support the hypothesized polar amplification of global warming". At the same time, evidences of increasing runoff in the Arctic have been reported recently (Shiklomanov et al. 2000; Semiletov et al. 2000; Peterson et al. 2002). The analysis of the Roskomgidromet data shows (Peterson et al. 2002) that aggregate annual discharge of the six largest Eurasian rivers (Northern Dvina, Pechora, Ob, Yenisei, Lena and Kolyma) over the period of observations from 1936 to 1999 has increased at a mean annual rate of 2.0 ± 0.7 km^3/year, so that mean annual discharge is now 128 km^3/year greater than in the 1930s. This amounts to an increase of about 7%. The authors (Peterson et al. 2002) consider that the main

mechanism is most likely due to increased precipitation as forecast by global climate models.

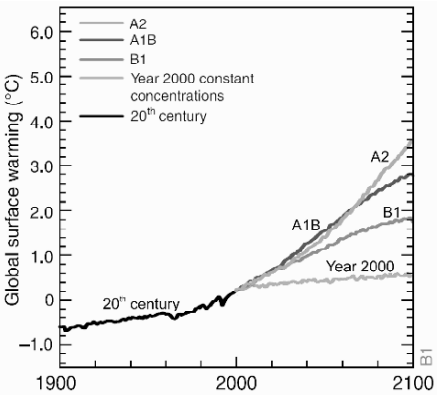

Fig. 3. Increase of global air surface temperature in 21st century. Solid are multi-model global averages of surface warming (relative to 1980–1999) for different scenarios shown as continuation of the 20th century simulations (IPCC 2007).

Durgerov and Carter (2004) confirm that an increase in freshwater inflow to the Arctic Ocean is evident. But they conclude that the arctic mountain and subpolar glaciers are the main source of increased freshwater inflow to the Arctic Ocean over the 1961–1998 and the glacier input will continue to rise.

Wu et al. (2005) report that their climate model predicts an increase of total river discharge into the Arctic Ocean by an annual rate of 8.73 km^3 since the 1960s. Similar results were obtained by Manabe et al. (2004). Their coupled ocean-atmosphere-land model predicts an increase of the Ob and Mackenzie water discharge on 20% to 2050 relative to pre-industrial period level and more than 40% in a few next centuries.

There are the predictions of an increase of delivery into the Kara Sea and the Arctic Ocean of inorganic dissolved salts up to 60% when all permafrost will be degradated (Frey et al. 2007a), and also increase of organic nutrients (on 30–50% of DON, TDN and TDP) by 2100 to the Kara Sea (McClelland et al. 2006; Frey et al., 2007b) and to global ocean (Beusen et al. 2005; Harrison et al. 2005).

A critical issue is the carbon cycling and storage in the Arctic region. Organic carbon in high-latitude soils and peatlands account for up to 50% of global soil carbon (Dixon et al. 1994). Climate warming could mobilize a substantial fraction of this carbon to rivers and streams creating a positive feedback on global warming (Freeman et al. 2004).

A fate of organic carbon in the Arctic rivers and ocean was investigated in several works (Benner et al. 2004; Frey and Smith 2005; Cooper et al. 2005; Neff et al. 2006; Raymond et al. 2007). Frey and Smith (2005) show on a base of measurements of stream and river DOC concentration from 96 watersheds distributed throughout West Siberia that cold, permafrost influenced watersheds

release little DOC to streams, regardless of the extend of peat lands cover, and much higher concentrations in warm, permafrost–free watersheds, rising sharply as a function of peat land cover (Fig. 4). The author's climate model predicts a northward advance of the –2°C mean annual air temperature isotherm by 2100 nearly doubling the land surface with air temperature exceeding this threshold. This will lead to up to about 700% increases in stream DOC concentrations and 29–46% increases in DOC flux to the Arctic Ocean.

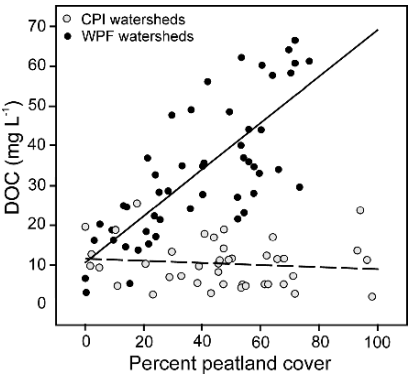

Fig. 4. Dependence of DOC concentration on the present peatland cover (P%) with the sampled watershed. Concentrations in cold permafrost influenced (CPI) watersheds are uniformly low, with a mean value of 10.29 $mg \cdot l^{-1}$ and no statistically significant correlation. Concentrations in warm permafrost-free (WPF) watersheds rise significantly with P% (Frey and Smith 2005).

These predictions were obtained at assuming that no changes in either river water discharge, or in-channel processes. They are in fact conservative. But, as we have seen above, Siberian precipitation and river discharge continue to increase (Frey and Smith 2003; Peterson et al. 2002), so even larger increases are likely. And again, there are the works the conclusions of which are contradicted to these results. Striegel et al. (2005) indicate that in the Yukon River basin water discharge corrected DOC export significantly decreased during the growing season from 1978–1980 to 2001–2003. Counter to current predictions, the authors argue that continued warming could result in decreased DOC export to the Bering Sea and the Arctic Ocean by the rivers, due to increased respiration of organic carbon on land.

The Arctic is a particularly sensitive area in relation to river sediment discharge (Syvitski 2003). An analysis of the sediment loads of 145 rivers in the world with records of more than 25 years including the Siberian rivers with records of up to 62 years (Bobrovitskaya et al. 2003) indicates that 70 rivers show a decrease, due to mainly to dams, and only 7 rivers show evidence of an increase in sediment load (Walling and Fang 2003).

A new stochastic sediment transport model by Morehead et al. (2003) was applied to the Arctic rivers to estimate the sediment load increase as a result of climate warming. In the paper (Gordeev 2006) the data by Peterson et al. (2002)

on six Siberian rivers water discharge and this model were used to estimate the sediment load increase of the same Arctic rivers by 2100. The assessments show that probable increase of the sediment flux of six rivers will be in a range from 30% to 122%.

The aim of this work is an attempt to predict an increase of river DOC and POC input to the Arctic Ocean due to global climate change to the end of this century. These predictions are based on our data on the current Arctic river sediment discharge and DOC, POC and TOC concentrations and fluxes in the Siberian rivers and also on the IPCC predictions of global air temperature increase in 21st century, measured increase of water discharge in the Siberian rivers (Peterson et al. 2002) and model simulation of sediment load due to warming (Morehead et al. 2003).

River water and sediment discharges

Mean multi-annual river water and suspended matter discharges for the main six Arctic rivers are shown in Table. Data are from the Roskomgidromet database for the period 1970–1995. Total discharge from the Eurasian territory into the

Table. River water, suspended particulate matter and organic carbon fluxes to the Arctic Ocean (Gordeev et al. 1996; Gordeev 2000; Gordeev and Rachold 2003)

River	Area	Water discharge	Total suspended matter		Content			Flux			POC in dry SPM	TOC
					DOC	POC	TOC	DOC	POC	TOC		
	(10^3 km^2)	(km^3 year^{-1})	(g m^{-3})	(10^6 t/year^{-1})	(mg l^{-1})			(10^6 t/year^{-1})			(wt %)	(t km^{-2} year^{-1})
Northern Dvina	357	110	37	4.1	11.6	2.6	15.3	1.28	0.28	1.68	6.8	4.7
Pechora	324	131	72	9.4	12.3	0.3	13.0	1.66	0.04	1.70	0.43	5.2
Ob	2,545	404	37	15.5	9.1	0.9	7.1	3.68	0.36	2.87	2.3	1.1
Yenisei	2,595	620	8	4.7	8.5	0.3	7.4	4.86	0.17	4.59	3.6	1.8
Lena	2,448	523	39	20.7	6.6	1.1	7.7	3.6	1.2	4.8	5.8	1.9
Kolyma	647	122	83	10.1	6.1	3.1	8.1	0.74	0.38	0.99	3.0	1.5
Total for six rivers	8915	1910	34	64.5	8.3	1.0	8.3	15.82	2.43	19.06	3.8	2.1
Total Eurasian Arctic	12,987	2,932	36	102.2	6.7	1.3	8.8	19.7	3.81	25.7	3.7	2.0

Arctic Ocean is 2,932 $km^3 \cdot year^{-1}$ and mean specific discharge is 7.3 $l \cdot s^{-1}$ km^{-2} that is lower of the global mean of 11 $l \cdot s^{-1}$ km^{-2} (Milliman 1991). The seasonal variations in water discharge are shown in Fig. 5.

The concentration of suspended particulate matter (SPM) ranges in the Russian Arctic rivers from 6 to 207 mg/l with a mean of 36 mg/l (Table), that is much lower than the global average (460 mg/l, Gordeev 1983). SPM seasonal variations are very similar to water discharge.

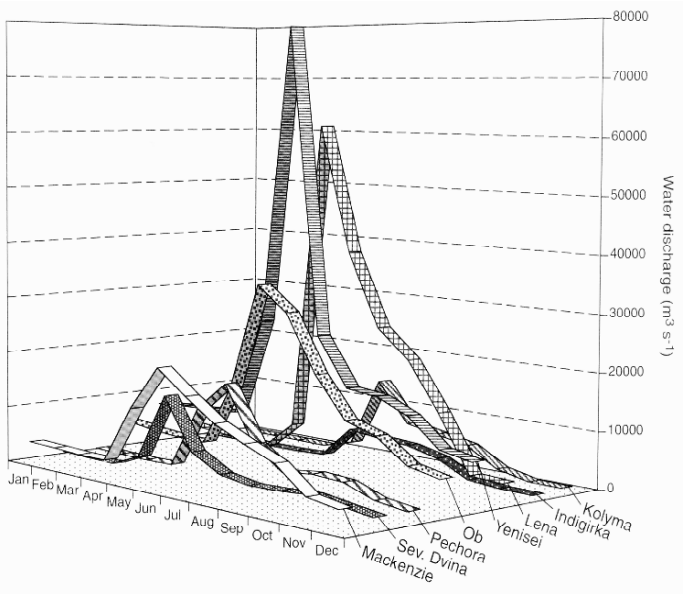

Fig. 5. Seasonal variations in water discharge of the largest arctic rivers. The monthly discharge data are taken from the Regional, Electronic, Hydrographic Data Network for the arctic region (http://www.R-ArcticNET.sr.unh.edu) and represent the average discharges for the years 1980–1993 (Gordeev and Rachold 2003).

Probable increase of DOC concentration and flux by 2100

At the starting point of near 2000 we have the multi-annual assessments of mean concentrations of DOC, POC and TOC and water, SPM and carbon fluxes of the six main arctic rivers into the Arctic Ocean (Table).

There are few data available on seasonal variations of DOC, POC and TOC concentrations and fluxes. Maltseva et al. (1987) indicated that 58–78% of TOC was discharged during freshet and that the portion of TOC transported to the Arctic seas during this period increased from west to east.

Seasonal variations in TOC concentration and fluxes in the lower reaches of the Lena River are given in Fig. 6a. Minimum TOC concentrations are observed in

winter (3.1–4.8 mg C/l) while maximum concentrations occur during freshet in June–July (9.6–14.4 mg C/l).

This pattern is even more pronounced for the TOC fluxes to the Laptev Sea (freshet accounts for more than 50% of the annual TOC discharge).

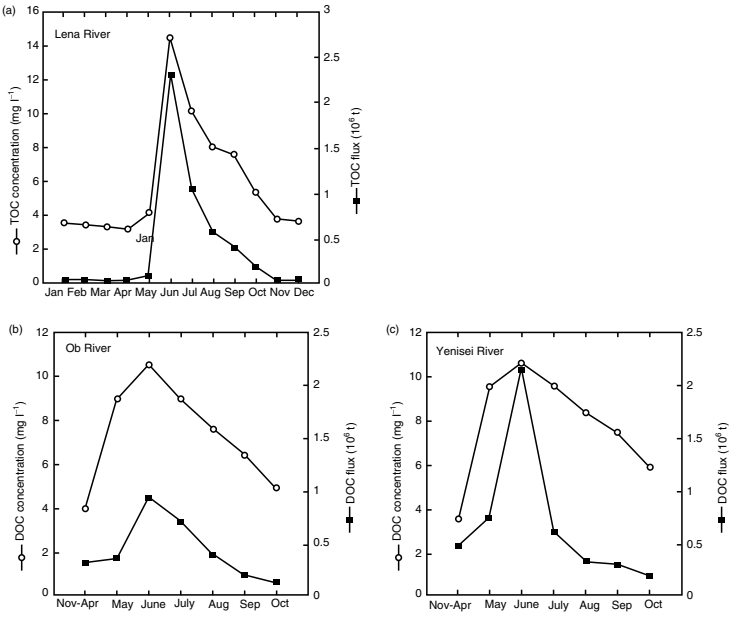

Fig. 6. Seasonal variations of TOC concentrations (Cauwet and Sidorov 1996) and TOC fluxes in the lower reach of the Lena River (**a**), and seasonal variations of DOC concentrations of and fluxes of the Ob and Yenisei Rivers (**b**, **c**) (Kohler et al. 2003).

A similar pattern has been observed for the DOC transport of the Ob and Yenisey rivers (Fig. 6b, c).

Let us estimate a probable increase of DOC river fluxes to the Arctic Ocean by 2100.

If to assume the correctness of the long-term trends in water discharge of the six largest Eurasian rivers that an increase will be at a mean annual rate of 2.0 $\pm$ 0.7 km^3/year up to 2100 and the conservativity of the present mean concentrations of DOC, than it is easy to calculate a probable increase of DOC flux by 2100.

2000: concentration of DOC = 8.3 mg/l, Q (water discharge) = 1,910 km^3/year, DOC flux = 15.82 × 10^6 km^3/year;

2100: concentration of DOC = 8.3 mg/l, Q = 2,110 km^3/year, DOC flux = 17.5 × 10^6 km^3/year, or 10.7% increase.

Wu et al. (2005) predict an increase of total river discharge into the Arctic Ocean by an annual rate of 8.73 km^3/year (since the 1960th). In this case an increase of six rivers discharge by 2100 would be about 2,780 km^3/year and DOC flux about 23.07×10^6 t/year, or 46% increase.

The IPCC projects a global surface air temperature increase of between 1.4 and 5.8°C by 2100. Peterson et al. (2002) consider that on this basis the discharge of the six Arctic rivers would increase by 18–70% or 315–1,260 km^3/year by 2100.

2000: concentration of DOC = 8.3 mg/l, Q = 1,910 km^3/year, DOC flux = 15.82×10^6 t/year.

2100: concentration of DOC = 8.3 mg/l, Q = 2,225–3,170 km^3/year, DOC flux = $(18.5–26.3) \times 10^6$ t/year, or 17–66% increase.

These estimates are in fact conservative.

Several works show that the release of DOC from peatlands and permafrost into rivers will occur under a warming climate in the Arctic (Freeman et al. 2001; Frey and Smith 2005; Guo et al. 2007).

Frey and Smith (2005) have studied 96 cold permafrost influenced (CPI) and warm permafrost-free (WPF) catchments throughout West Siberia in 1999–2001. Measured DOC concentrations in streams and rivers revealed a remarkable contrast between CPI and WPF watersheds (Fig. 5): (1) low DOC concentrations in CPI watersheds; (2) a positive correlation between DOC and peatland cover in WPF watersheds.

The authors find a sharp rise in DOC release to streams where mean annual air temperature (MAAT) exceeds –2°C. Climate model simulations, as we mentioned above, predict a doubling the West Siberian land surface with MAAT exceeding –2°C isoterm by 2100. Based on these empirical relationships and modelled land surface areas the averaged stream DOC concentration will rise from its current value of 29–46%. For CPI watersheds containing extensive peatland cover, the predicted DOC increase is expected to produce up to a 670% for watersheds with 100% peat cover.

The Nadym and Pur rivers with 50% covered by peatlands will show a ~ 400% increase in DOC concentration (from ~10 to ~40 mg/l) in the next century.

It is understandable that this DOC concentration will be rising with time.

If we assume on a base of these findings than the DOC concentration in the six Arctic rivers, which include the Ob and Yenisey, the rivers with the most extensive peatlands in the World, will increase up to 25 mg/l (this is a half of increase for the Pur and Taz, the peatland cover of which among the highest), than DOC flux will rise by 2100 due to this reason on $(5.3–21.4) \times 10^6$ t/year, or 33–135%.

2000: DOC = 8.3 mg/l, Q = 1,910 km^3/year, DOC flux = 15.8×10^6 t/year.

2100: DOC = 25 mg/l, Q = 2,225–3,170 km^3/year, DOC flux = (55.6–79.2) × 10^6 t/year.

Total DOC flux increase due to both of water discharge increase (Peterson et al. 2002) and DOC concentration increase as a result of DOC release from peatlands during climate warming would be estimated as 350–500% by 2100.

Probable increase of POC and TOC fluxes by 2100

An attempt to predict the changes due to climate warming in the fluvial suspended sediment flux to the Arctic Ocean was made in (Gordeev 2006). To do it a stochastic sediment transport model by Morehead et al. (2003) was applied to the Arctic rivers to estimate the sediment load increase. In this model, the long-term mean of the daily sediment discharge Q_s is defined as:

$$Qs = \alpha H^{3/2} A^{1/2} l^{kT},$$

whereby H – river basin relief (m), A – river basin area (km^2), T – mean surface temperature of basin (°C), α and k – dimensionless constants.

This model is accepted because it accounts for the inter- and intra-annual variability of the suspended loads of rivers and is sensitive to drainage basin temperature and can be used to examine the impact of a climate warming scenario on the loads of the Arctic rivers. The model predicts that there will be a 30% increase in sediment load for every 2°C of warming in the drainage basin and a 20% increase in discharge will result in a 10% increase in sediment transport. A global rise in SAT of from 1.4°C to 5.8°C by 2100 coupled with an increase of water discharge from 18% to 70% over present conditions give the estimates that the sediment flux of six Arctic rivers will increase in a range from 30% to 122%, or from 17.8 × 10^6 t/year to 72.6 × 10^6 t/year (Gordeev 2006). The current POC concentration and content in dry SPM in six rivers are 1.0 mg/l and 3.8%, and the flux of POC is about 2.4 × 10^6 t/year (Table). Simple calculations show that by 2100 the POC flux will be in a range from 3.1 to 5.2 × 10^6 t C/year.

2000: POC = 1.0 mg/l, or 3.8% dry wt.; Q_{SPM} = 64.5 × 10^6 t/year;

POC flux = 2.43 × 10^6 t/year.

2100: POC = 1.0 mg/l, or 3.8% dry wt; Q_{SPM} = (82.3–137.1) × 10^6 t/year;

POC flux = (3.1–5.2) × 10^6 t/year.

In these conditions, the flux of TOC is expected to be in a range from 58.9 × 10^6 t/year to 84.4 × 10^6 t/year, or from 310% to 440%.

The six rivers cover 65% of total water discharge and about 63% of total SPM discharge to the Arctic Ocean. Distribution of the six rivers trend to the whole Eurasian Arctic results in the estimates of the TOC fluvial flux to the Arctic Ocean to be in a range – (90.4–130.0) × 10^6 t/year.

Discussion

How to regard to these estimations of DOC, POC and TOC fluxes to the Arctic Ocean over next almost 100 year? It's clear that the most important forcing is an increase of global air temperature. "Warming of the climate system is in equivocal, as is now evident from observations of increases in global average air and ocean temperatures, widespread melting of snow and ice and rising global average sea level" (IPCC 2007, WGI 3.9). We feel an absence of any doubts in this position. However, there is an opposite view on the problem. Sorokhtin (2007)] and Sorokhtin et al. (2007) present the theory of the Earth's climate evolution based on universal chemical – physical laws of matter-energy transformation. They investigate the global forces of nature driving the Earth's climate.

The authors consider that the IPCC conclusions are erroneous. The main climate forcing, to their opinion, is the Sun activity. There is very good correlation between the temperature variations in the Northern Hemisphere and magnetic activity of the Sun (Fig. 7). The arising CO_2 concentration in atmosphere is a result of climate warming but not vice versa. And at the highest CO_2 concentration the climate will be cooler.

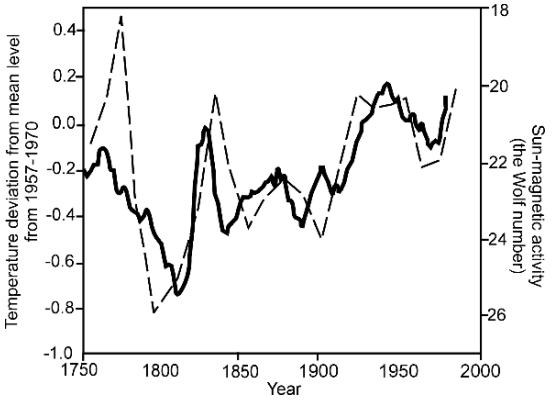

Fig. 7. Positive correlation between temperature variations in the Northern Hemisphere and magnetic activity of the Sun (the Wolf numbers). Left scale and the thick line – deviation of average surface temperature at the current 11-years smoothing, °C. Right scale and dotted line – averaged the sun-magnetic activity (Sorokhtin 2007).

We are not able to prove the truth of one or another position. In this work we formally accept the IPCC position and assume the approach: If the global climate warming will be in reality, than the organic carbon fluxes to the Arctic Ocean will be increased with an acceptable level of probability.

Let us consider shortly the most weak points in our calculations.

The attempts to estimate the possible changes in the river DOC, POC and TOC fluxes to the Arctic Ocean face with a lot of influenced factors and we need to use the model simulations which it is not possible to verify at present time. Very important and poor investigated question is the feedback impact on temperature's increase the variations of atmospheric precipitations, river discharge and so on. Cox et al. (2000) write that the general circulation models have generally exclude the feedback between climate and the biosphere. Their fully coupled, three-dimensional carbon-climate model predicts that carbon-cycle feedbacks could significantly accelerate climate change in the 21st. By 2100, atmospheric CO_2 concentrations on 250 ppm higher in their model than in uncoupled carbon models will result in a global-mean warming of 5.5 K, as compared to 4 K without the carbon-cycle feedback.

There are many uncertainties in the regularities of the delivery of organic carbon from the soils, especially such as the peatlands. The recent works demonstrate (Finlay et al. 2006; Frey et al. 2007a; McClelland et al. 2007; Holmes et al. 2008) that even the present-day assessments of the river DOC fluxes, which not always take into account the seasonal variations, appear to be not reliable. For example, Finley et al. (2006) show that the Kolyma River delivers DOC to the Arctic Ocean on 30% higher than it was accepted earlier.

The −2°C MAAT isotherm represents a critical temperature threshold, above which watersheds produce increasing DOC as a function of peatland abundance (Frey and Smith 2005). At present the MAAT's are ranging from −10°C to +2°C and permafrost is influencing ~55% of its area (northward of 60° N).

A warming Arctic climate may lead to increased release of currently sequestered peat carbon through permafrost degradation process. But this process in highly non-linear and we are not able to understand it in details. This makes our estimates to be quite rough.

Radiocarbon composition was measured for DOC, POC and soil organic carbon (SOC) from the Mackenzie, Yukon and Sagavanirktok River basins (Guo et al. 2007). The authors show that POC in these rivers is dominated by old SOC derived from permafrost thawing and riverbank erosion in contrast to DOC, which is more readily influenced by modern terrestrial biomass. So, melting will be manifest in the age and amount of POC in Arctic rivers. But we do not know if the POC content would be changed in this process or not.

Thawing will magnify the erosion process also. The importance of the different sources of terrigenous organic carbon in the Arctic Ocean was evaluated in (Grigoriev et al. 2004; Rachold et al. 2007). The evaluation shows that about 80% of the total terrigenous TOC flux (40.8×10^6 t/year) is attributed to river discharge

(30×10^6 t/year). Coastal erosion is at present on the second place (6.7×10^6 t/year, or 15%). Sea ice input contributed about 2% only.

We didn't find any estimations of DOC, POC and TOC coastal erosion flux changes due to climate warming in literature. Their increase may be expected in 21st century.

So, we cannot even evaluate the reliability of our calculations of river organic carbon fluxes to the Arctic Ocean due to many factors of influence, which are not known enough at present.

Conclusion

An attempt was made to predict the river fluxes of DOC, POC and TOC to the Arctic Ocean by 2100 due to climate warming. The estimates are based on the following materials:

- The IPCC predictions of global air temperature increase on 1.4–5.8°C to the end of this century
- The Arctic rivers discharge increase over the period from 1936 to 1999 and probable increase due to global warming on 18–70% by 2100 (Peterson et al. 2002).
- Predicted increase of DOC concentrations in Siberian streams and rivers on ≈400% due to release of DOC from peatlands and permafrost under a warming climate in Arctic (Fray and Smith 2005)
- Predicted increase of total suspended particulate matter fluxes to the Arctic Ocean on 30–122% by 2100 (Gordeev 2006)

Our assessments show that probable increase of river organic carbon input to the Arctic Ocean by 2100 may be in a range:

DOC – 350–500%,

POC – 130–215%,

TOC = DOC + POC – 310–440%.

Our short discussion on the results obtained concentrates on the weakest points in these calculations. They consist of:

- Existence of serious arguments against the IPCC predictions of global warming in 21st century. For example, Sorokhtin et al. (2007) consider that the main climate forcing is the Sun activity and arising greenhouse gases concentrations in atmosphere is a result, but not a reason, of climate warming. At the highest CO_2 concentration the climate will be cooler.

- The feedback impact on the temperature increasing, the variations of atmospheric precipitations, river discharge and so on is poor investigated and understood.
- Even the present day assessments of the Arctic river DOC fluxes are not very reliable because of not taking into account the significant seasonal variations (Finley et al. 2006, for example).
- Highly non-linear process of permafrost degradation with warming makes the predicted DOC concentrations and fluxes due to release of currently sequestered peat carbon to be quit rough.
- No estimations of DOC, POC, and TOC flux variations under coastal erosion due to climate warming.

So, a lot of influenced on the assessment factors, which are not adequately investigated and understood, do not allow us to evaluate the real reliability of the calculation's results presented.

Acknowledgments

The authors are very appreciated to the co-leaders of the 40th International Colloquium and the NATO-Russia APW Professor J. Nihoul and Professor A. Kostyanoi for their kind invitation and possibility to participate in these measures. A participation of one of two co-authors (GVV) was supported by the INTAS project "MERIS-Based Assessment of Carbon Supply into the Arctic by River Runoff (MACRO)", INTAS Ref. No.: 06-1000025-9142.

References

Benner R, Benitez-Nelson B, Kaiser K, Amon RMW (2004) Export of young terrigenous dissolved organic carbon from rivers to the Arctic Oceans. Geophys Res Lett doi:10.1029/2003 GL019251

Beusen AHW, Dekkers ALM, Bouwman AF, et al. (2005) Estimation of global river transport of sediments and associated particulate C, N and P. Global Biogeochem Cycles, 19 doi:10.1029/ 2005 GB 002453

Bobrovitskaya NN, Kokorev AV, Lemeshko NA (2003) Regional patterns in recent trends in sediment yields of Eurasian and Siberian rivers. Global Planet Change, 39:127–146

Cauwet G, Sidorov I (1996) The biogeochemistry of Lena River: organic carbon and nutrient distribution. Marine Chem, 53:211–228

Cooper LW, Benner R, McClellend J, et al. (2005) Linkages among runoff, dissolved organic carbon, and the stable oxygen isotope composition of seawater and other water mass indicators in the Arctic Ocean. J Geophys Res doi:10.1029/2005 JG000031

Cox PM, Betts RA, Yones CD et al (2000) Acceleration of global warming due to carbon-cycle feedbacks in a coupled climate model. Nature, 408:184–187

Dixon RK et al. (1994) Carbon pools and flux of global forest ecosystems. Science, 263:185–190

Durgerov MB, Carter CL (2004) Observational evidence of increases in freshwater inflow to the Arctic Ocean. Arctic, Antarctic, Alpine Res, 36:117–122

Finlay YC, Neff Y, Zimov S, et al. (2006) Snowmelt dominance of DOC in high-latitude watersheds: implications for characterization and flux of river DOC. Geophys Res Lett, 33 art no 110401

Frauenfeld OW, Zhang T, Barry RC, Gilichinsky D (2004) Interdecadal changes in seasonal freeze and thaw depth in Russia. J Geophys Res Lett doi:10.1029/2003 JD004448

Freeman C et al. (2001) Export of organic carbon from peat soils. Nature, 412 (6849):758–785
Freeman C et al. (2004) Export of dissolved organic carbon from peatlands under elevated carbon dioxide levels. Nature, 430:195–198
Frey KE, Smith LC (2003) Recent temperature and precipitation increases in west Siberia and their association with the Arctic Oscillation. Polar Res, 22:287–300
Frey K, Smith LC (2005) Amplified carbon release from vast West Siberian peatlands by 2100. J Geophys Res Lett, 32 doi:1029/2004 GL0225
Frey K, Siegel DI, Smith LC (2007a) Geochemistry of West Siberian streams and their potential response to permafrost degradation. Water Res, 43 doi:10.1029/2006 WR004902
Frey K, McClelland JW, Holmes RM, Smith LC (2007b) Impact of climate warming and permafrost thaw on the riverine transport of nitrogen and phosphorus to the Kara Sea. J Geophys Res, 112 doi:10.1029/2006 JG 000369
Gordeev VV (1983) River Runoff to the Ocean and the Features of Its Geochemistry. Nauka, Moscow (in Russian)
Gordeev VV (2000) River input of water, sediment, major ions, nutrients and trace metals from Russian territory to the Arctic Ocean. In: Lewis EL (ed) The Freshwater Budget of the Arctic Ocean. Kluwer, Dordrecht
Gordeev VV (2006) Fluvial sediment flux to the Arctic Ocean. Geomorphology, 80:94–104
Gordeev VV, Rachold V (2003) River input. Ch.2. Modern terrigenous organic carbon input to the Arctic Ocean. In: Stein R, MacdonaldRW (eds) The Organic Carbon Cycle in the Arctic Ocean. Springer, Berlin/Heidelberg/New York
Gordeev VV, Martin J-M, Sidorov IS, Sidorova MN (1996) A reassessment of the Eurasian water, sediment, major ions, and nutrients to the Arctic Ocean. Am J Sci, 296:664–691
Grigoriev MN, Rachold V, Hubberten H-W, Schrmeister L (2004) Organic carbon input to the Arctic Seas through coastal erosion. Ch.2. Modern terrigenous organic carbon input to the Arctic Ocean. In: Stein R, Macdonald RW (eds) The Organic Carbon Cycle in the Arctic Ocean. Springer, Berlin/Heidelberg/New York
Guo L, Ping C-L, Macdonald RW (2007) Mobilization pathways of arctic rivers in a changing climate. Geophys Res Lett doi:10.1029/2007 GL030689
Harrison JA, Caraco N, Seitzinger SP (2005) Global pattern and sources of dissolved organic matter export to the coastal zone: results from a spatially explicit, global model. Global Biogeochem Cycles doi:10.1029/2005 GB002480
Holmes RM, McClelland JW, Raymond PA, et al. (2008) Lability of DOC transported by Alaskan rivers to the Arctic Ocean. Geophys Res Lett doi:10.1029/2007 GL 032837
IPCC Fourth Assessment Report. Climate Change (2007) In: Solomon S, Qin D, Manning M, et al. (eds) The Physical Science Basis. Cambridge University Press, UK/New York
Kohler H, Meon B, Gordeev V, et al. (2003) Dissolved organic matter (DOM) in the estuaries of Ob and Yenisei and the adjacent Kara Sea, Russia. In: Stein R, Fahl K, Futterer DK, et al. (eds) Siberian river run-off in the Kara Sea: Characterisation, quantification, variability and environmental significance. Elsevier, Amsterdam
Maltseva AV, Tarasov MN, Smirnov MP (1987) Organic matter discharge from the USSR territory. Hydrochem Materials 102. Gidrometeoizdat, Leningrad, 130–150 (in Russian)
Manabe S, Milly PCD, Wetherald RT (2004) Simulated long-term changes in river discharge and soil moisture due to global warming. Hydrol Sci, 49:625–642
McGuire AD, Chapin FS, III, Walsh JE, Wirth C (2006) Integrated regional changes in arctic climate deedbacks: implications for the Global Climate System. Annu Rev Environ Resour, 31:61–91
McClelland JW, Dery SJ, Peterson BJ, Holmes RM, Wood EF (2006) A pan-arctic evaluation of changes in river discharge during the latter half of the 20-th century. Geophys Res Lett doi:10.1029/2006 GL025753
Milliman JD (1991) Flux and fate of fluvial sediment and water in coastal seas. In: Mantoura RFC, Martin J-M, Wollast R (eds) Ocean Margin Processes in Global Change. Wiley, Chichester

Morehead MD, JP Syvitski, EW Hutton, SD Peckham (2003) Modeling the temporal variability in the flux of sediment from ungauged river basins. Global Planet Change, 39:95–110

Neff JC, Finlay JC, Zimov SA, et al. (2006) Seasonal changes in the age and structure of dissolved organic carbon in Siberian rivers and streams. Geophys Res Lett, 33 doi:10.1029/2006 GL028222

Peterson BJ, Holmes RM, McClelland JW, et al. (2002) Increasing river discharge to the Arctic. Ocean Sci, 298:2171–2173

Polaykov IV, Alekseev GV, Bekryaev RV, et al. (2002) Observationally based assessment of polar amplification of global warming. Geophys Res Lett, 29 doi:10.1029/2001 GL011111

Rachold V, Bolshiyanov DY, Grigoriev MN, et al. (2007) Nearshore arctic subsea permafrost in transition. EOS, Transactions. Am Geophys Union, 88:149–156

Raymond PA, McClelland JW, Holmes RM, et al. (2007) Flux and age of dissolved organic carbon exported to the Arctic Ocean: a carbon isotopic study of the five largest arctic rivers. Global Biogeochem Cycles doi:10.1029/2007 GB002934

Semiletov IP, Savelieva NI, Weller GE, et al. (2000) The dispersion of Siberian river flows into coastal water: meteorological, hydrological and hydrochemical aspects. In: Lewis EL (ed) The Freshwater Budget of the Arctic Ocean. Kluwer, Dordrecht

Shiklomanov IA, Shiklomanov AI, Lammers RB, et al. (2000) The dynamics of river water inflow to the Arctic Ocean. In: Lewis EL (ed) The Freshwater Budget of the Arctic Ocean. Kluwer, Dordrecht

Sorokhtin OG (2007) Life of the Earth. Institute of Computer Investigations, Moscow-Ijevsk (in Russian)

Sorokhtin OG, Khilyuk LF, Chilingarian GV (2007) Global Warming and Global Cooling. Elsevier Science & Technology, The Netherlands

Serezze MC, Walsh JE, Chapin FS, III, et al. (2000) Observational evidence of recent change in the northern high-latitude environment. Climatic Change, 46:159–207

Striegl RG, Aiken GR, Dornblaser MM, et al. (2005) A decrease in discharge-normalized DOC export by the Yukon River during summer through autumn. Geophys Res Lett doi:10.1029/ 2005 GL024413

Syvitski JP (2003) Supply and flux of sediment along hydrological pathways: research for the 21 century. Globa Planet Change, 39:1–11

Walling DE, Fang D (2003) Recent trends in the suspended sediment loads of the world's rivers. Global Planet Change, 39:111–126

Wu P, Wood R, Stott P (2005) Human influence on increasing arctic river discharge. Geophys Res Lett doi:10.1029/2004GL021570

Mechanisms of the recent sea ice decay in the Arctic Ocean related to the Pacific-to-Atlantic pathway

Motoyoshi Ikeda

Graduate School of Environmental Science, Hokkaido University Sapporo, Japan, mikeda@ees.hokudai.ac.jp

Abstract

The **sea** ice cover in the Arctic Ocean has been reducing and hit the low record in the summer of 2007. The anomaly was extremely large in the Pacific sector. The sea level height in the Bering Sea vs. the Greenland Sea has been analyzed and compared with the current meter data through the Bering Strait. A recent peak existed as a consequence of atmospheric circulation and is considered to contribute to inflow of the Pacific Water into the Arctic Basin. The timing of the Pacific Water inflow matched with the sea ice reduction in the Pacific sector and suggests a significant increase in heat flux. The other component is the Arctic Dipole Mode (ADM) as the second EOF of sea level pressure with dipoles over Siberia and Canada at opposite signs. In last 50 years, the Pacific sector had low ice cover at a 1–2 year lag from the ADM with a low pressure over Siberia. Since this mode was extremely intense in 2007 summer, the sea ice is predicted to be low in 2008. It has been claimed that most projections underestimate sea ice reduction in the Arctic during this century. Our tasks include removal of possible biases due to different sensors and accurate estimates of the important feedbacks contained in the atmosphere-ice-ocean system. Then, an answer will be found for the questions when the Arctic sea ice becomes a seasonal ice cover.

Introduction

The sea ice cover in the Arctic Ocean has declined in the last 40 years and reaches the extreme condition as shown in Figs. 1 and 2, while its decadal variability has increased (e.g., Wang and Ikeda 2000). This fact makes us imagine that the ice cover will change into a seasonal one in near future. Actually, the observed ice decrease seems faster than that in the IPCC Report prediction, in which the ice cover in summer is predicted to become minimal near the end of the 21st century (Stroeve et al. 2007). In particular, the summer ice cover hit a record low in 2007 so that some specialists may believe disappearance by 2020. On the basis of

J.C.J. Nihoul and A.G. Kostianoy (eds.), *Influence of Climate Change on the Changing Arctic and Sub-Arctic Conditions*,

significant year-to-year variability, however, such an early disappearance might be exaggeration. Therefore, we really need to examine the mechanisms crucial for the rapid ice decrease.

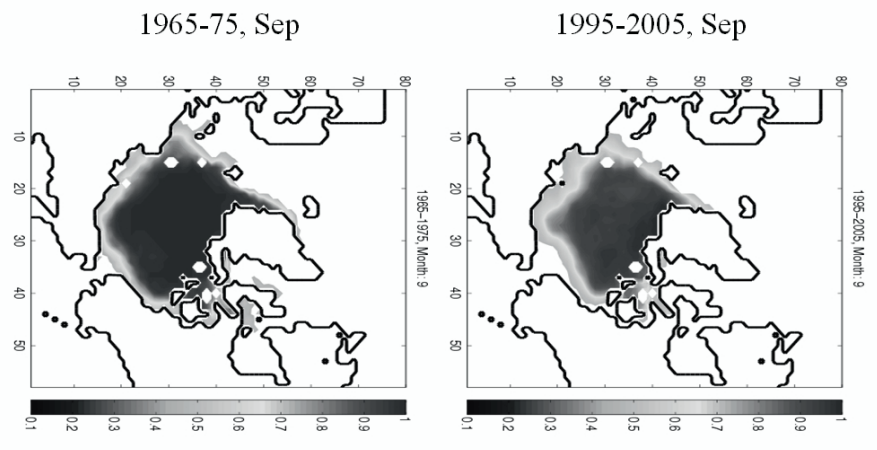

Fig. 1. Observed ice cover concentration in the arctic basin. Ice reduction is significant in last 30 years.

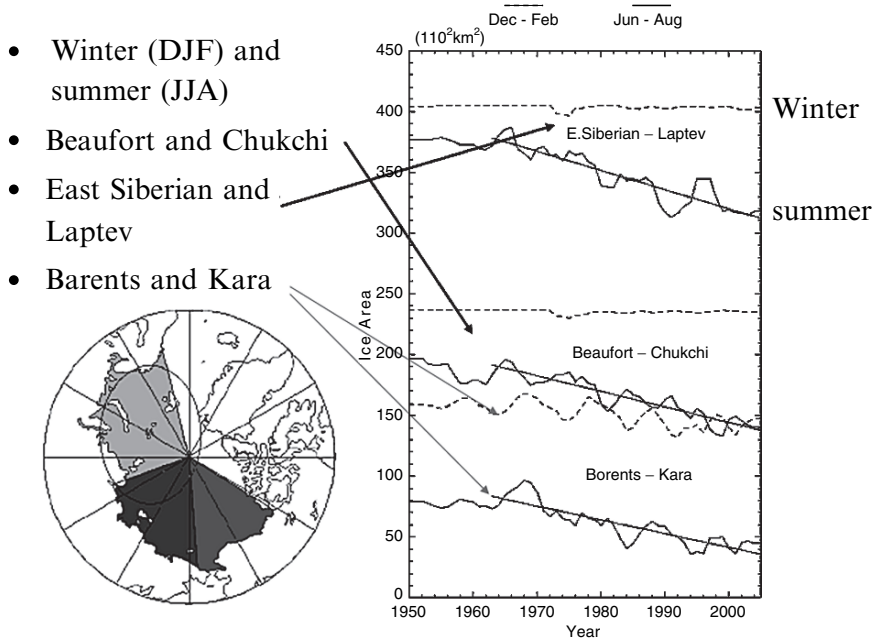

Fig. 2. Ice cover trends and decadal variability in three regions, the Beaufort-Chukchi Sea, the East Siberian-Laptev Sea and the Barents-Kara Sea. A 3-year Fanning file is applied to the ice cover time series.

The Polar Vortex is a major cyclonic circulation in the Arctic atmosphere and has more significant decadal oscillations than the trend. The recently archived data extending from clouds, the atmospheric boundary layer to biogeochemical components in the Arctic Ocean have been analyzed for providing a close insight into Arctic environmental change, which may occur in response to global warming or as part of natural variability. The achieved results include the following signals: the cloud cover has increased and is estimated to contribute to the ice reduction through the radiation balance at the magnitude similar to the ice-albedo feedback (Ikeda et al. 2003). The atmospheric boundary layer thickness has reduced, and the stratosphere is cooling as a result of global warming. The biogeochemical data indicate vertical motion in the ocean interior responding to the variable Polar Vortex (Ikeda et al. 2005)

In the Arctic, the most pronounced atmospheric pattern is the Northern Annular Mode (NAM), which was first reported as the Arctic Oscillation by Thompson and Wallace (1998). A difference between this mode and the North Atlantic Oscillation (NAO) has been discussed from the viewpoints of statistics and dynamics: which mode is dynamically meaningful. The horizontal pattern is the intensified/weakened Polar Vortex with a significant vertical coherence from the surface to the stratosphere. The decadal signal had a clear peak around 1990 with strong Polar Vortex in Fig. 3. The less ice anomalies occurred around this peak,

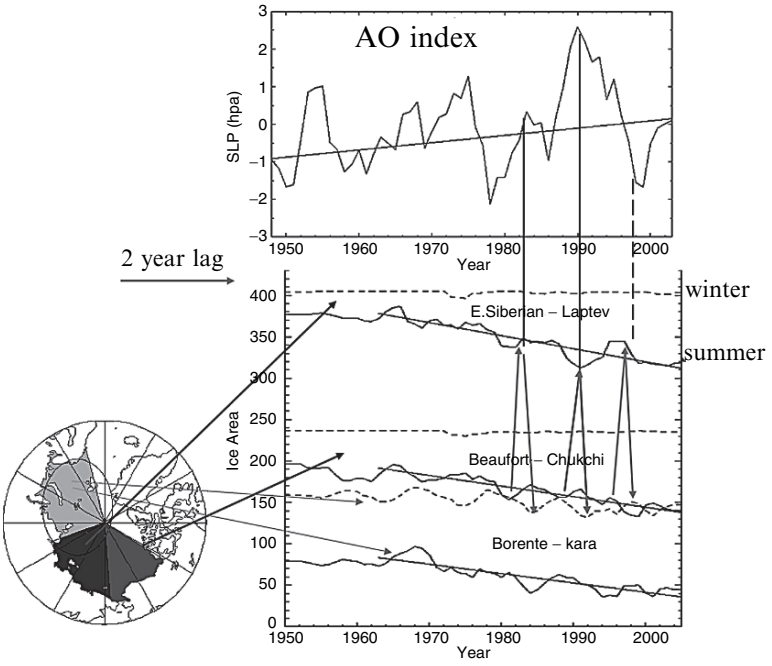

Fig. 3. Decadal variability in the arctic oscillation and sea ice cover produced by the AO. The AO is defined by a difference in the zonal mean sea level pressure between 70° N and 85° N.

propagating from the Beaufort-Chukchi Sea, the East Siberian-Laptev Sea to the Barents-Kara Sea in several years. In contrary, a less ice anomaly occurred around 1998 in the Beaufort-Chukchi Sea but did not correlate with a positive AO. We attempt to explore the cause of this finding and expect to give insight into possible mechanisms responsible for the rapid ice decrease in last 10 years.

The decrease is enhanced in the Beaufort-Chukchi Sea, which leads us to examine inflow of the warmer Pacific Water through the Bering Strait. In section "Arctic pathway", sea surface height is examined to see if the higher sea level in the Bering Sea contributed to ice reduction. Then, the Arctic atmospheric circulation is further analyzed in section "Wind-induced ice cover variability" to find correlation with ice anomalies in the Pacific sector. In section "Discussion", these results are discussed.

Arctic pathway

Aagaard and Carmack (1989) reported that the Pacific Water is an important source of fresh water in the Arctic Ocean. The Pacific Water is also a heat source. An analysis is now extended to the sea level in the Bering Sea vs. the Greenland Sea and compared with the current meter data through the Bering Strait. The interannual variability is examined to show whether a peak was induced as a consequence of atmospheric circulation and contributed to inflow of the Pacific Water into the Arctic Basin. This idea will be verified with the timing of a sea ice

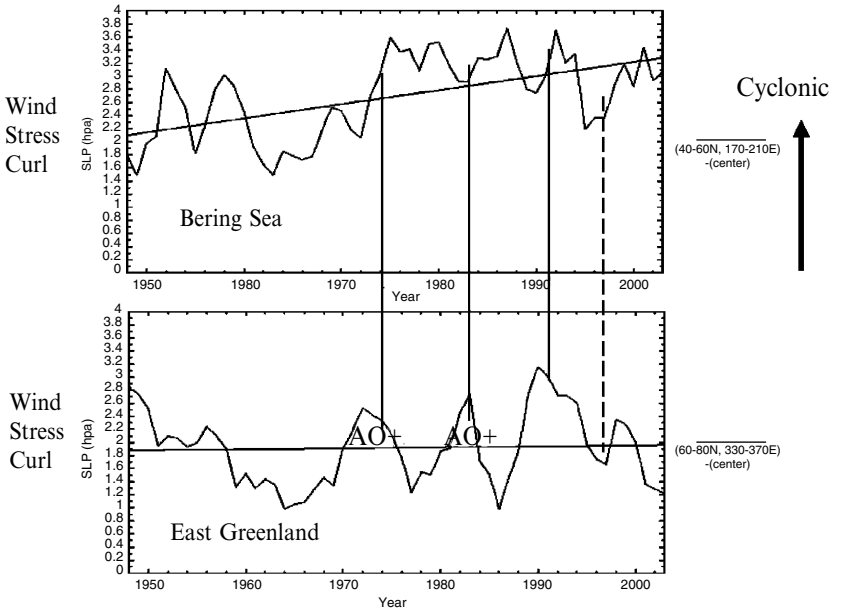

Fig. 4. Wind stress curl over the Bering Sea and the East Greenland Sea.

reduction in the Pacific sector. Since a significant increase in heat flux may be associated with the inflow, this component should be included in the model prediction for answering the question when the Arctic sea ice becomes a seasonal ice cover.

It is well accepted that a basin-scale sea level varies responding to wind-driven circulation. As cyclonic (anticyclonic) wind stress curl drives the ocean, the first baroclinic mode develops in time associated with surface Ekman divergence (convergence) and propagates westward, and the sea level descends (rises) in the central part of the basin. Following this simple concept, the NCEP/NCAR data were processed over the Bering Sea and also the East Greenland Sea for 50 years. Both analysis domains have zonal lengths of 40° and meridional lengths of 20°: i.e., the Bering Sea domain covers (170° E–150° W, 40° N–60° N), and the East Greenland Sea domain covers (30° W–10° E, 60° N–80° N). As shown in Fig. 4, a multi-decadal variability is evident over the Bering Sea, while it is mainly decadal over the East Greenland Sea.

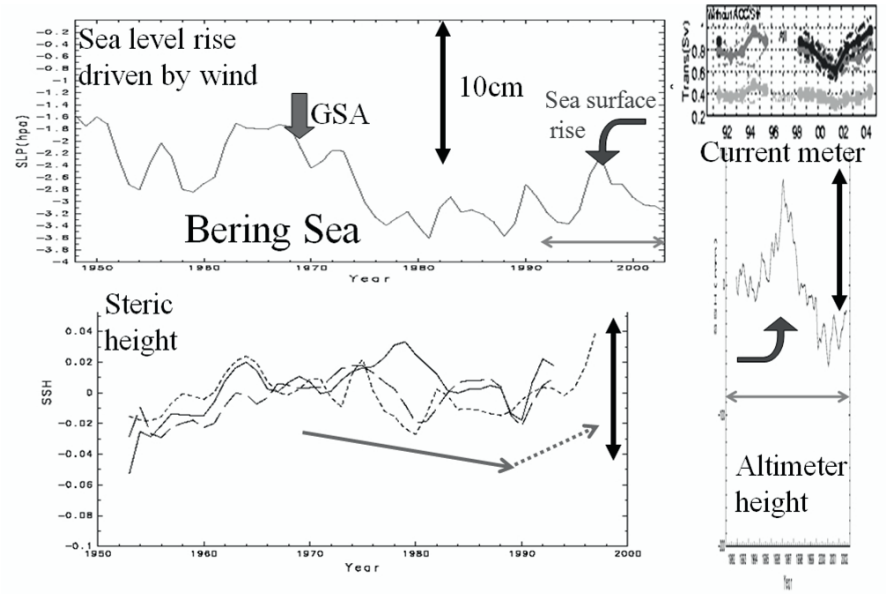

Fig. 5. Sea level in the central part of the Bering Sea estimated from the wind stress curl over the Bering Sea. It is compared with the steric heights in three zonal sections of the Bering Sea produced from World Ocean Atlas, the TOPEX/POSEIDON altimeter height in the Bering Sea during the ice-free season and the current meter data in the Bering Strait (Woodgate et al. 2006).

The wind-driven general circulation is established as a non-dispersive, first baroclinic Rossby wave, whose phase speed is determined to be about 0.01 m s^{-1} from the stratification in the Bering Sea. Within the analysis domain with a 2,500-km zonal length, the sea level is essentially similar to the reversed wind stress curl smoothed in time and lagged by 2–3 years. Figure 5 shows the sea level in the Bering Sea with a distinct peak around 1998, following a generally low sea level

for the period of 1975 through 1995. This peak is also shown in the altimeter data in the Bering Sea so that the wind-driven sea level may be meaningful and interpreted to cause the low ice anomaly in the Pacific sector. The hydrographic data in World Ocean Atlas were analyzed for the layer above 1,000-m depth and indicate a growing trend in the Bering Sea, whereas the recent data are still sparse. The current meter data are unfortunately missing for the peak, although the trough around 2002 is consistent with the trough in the altimeter data (Woodgate et al. 2006).

An additional interesting feature is an earlier high sea level all way through 1960s in a consistent manner with the steric height. This anomaly could be related to the Great Salinity Anomaly (GSA), during which freshwater was exhausted toward the Greenland Sea and the entire northern North Atlantic in late 1960s to early 1970s (Dickson et al. 1988). Although its sign has been well recognized, it is debatable whether the source existed in the Pacific.

The thermodynamic effect is estimated for the pathway transport. Once it increases the transport by 10% (10^5 m^3 s^{-1}) of the Pacific Water at 3°C, extra heat flux melts 2-m thick sea ice over 10^5 km^2 in a year. In winter, sea ice decays from its bottom but does not enhance air-sea heat flux so much, and then, the albedo-ice feedback works in summer and melts more ice.

In this paper, a higher sea level in the Bering Sea was suggested to be one of the causes of a less ice anomaly in the Pacific sector. A wind-driven general circulation was shown to be related to the sea level variability. It is noted that this view is based on the assumption that pressure field is horizontally uniform in the lower ocean. However, there is a topographic barrier between the Bering Sea and the Arctic Ocean. A further study is needed for clarifying validity of the steric height concept. One of the possible methods is to use a global ocean model to simulate the sea surface heights in the Bering Sea and the Arctic Ocean, which are connected all way across the Pacific and Atlantic equatorial regions and the Antarctic Circumpolar Current region. Various processes in these regions are well imagined to produce a pressure difference in the lower parts of the Bering Sea and the Arctic Ocean.

In addition to sea level variability in the Bering Sea, a wind stress along the Bering Strait must play some roles on the pathway, as suggested by Woodgate et al. (2005). Actually, the pathway transport increased from 2002 to 2004 (Woodgate et al. 2006). It is an urgent task to evaluate which is dominant for the pathway transport, sea level in the Bering Sea or wind stress along the Bering Strait.

Wind-induced ice cover variability

A more fundamental question is how crucial wind-driven ice motion is for a less ice anomaly in the Pacific sector of the Arctic Basin. Once a southerly wind pushes sea ice away from the coastal region in summer, solar radiation effectively heats the ocean and accelerates ice melting. This effect is considered to be a major one for the record low in summer of 2007 (J. Wang, personal communication 2008).

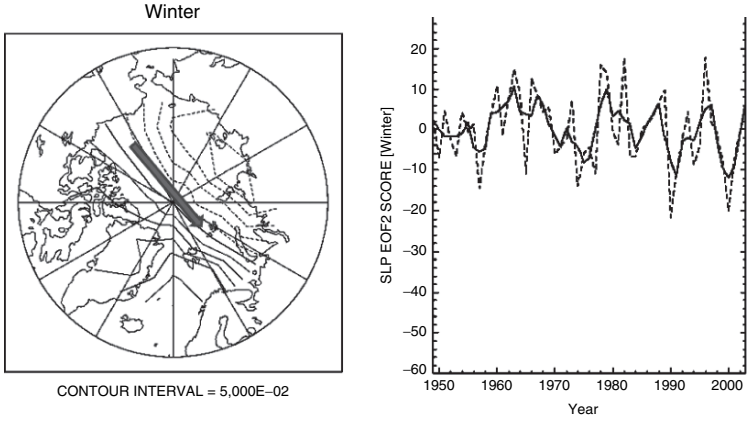

Fig. 6. The second EOF of sea level pressure in winter north to 70° N.

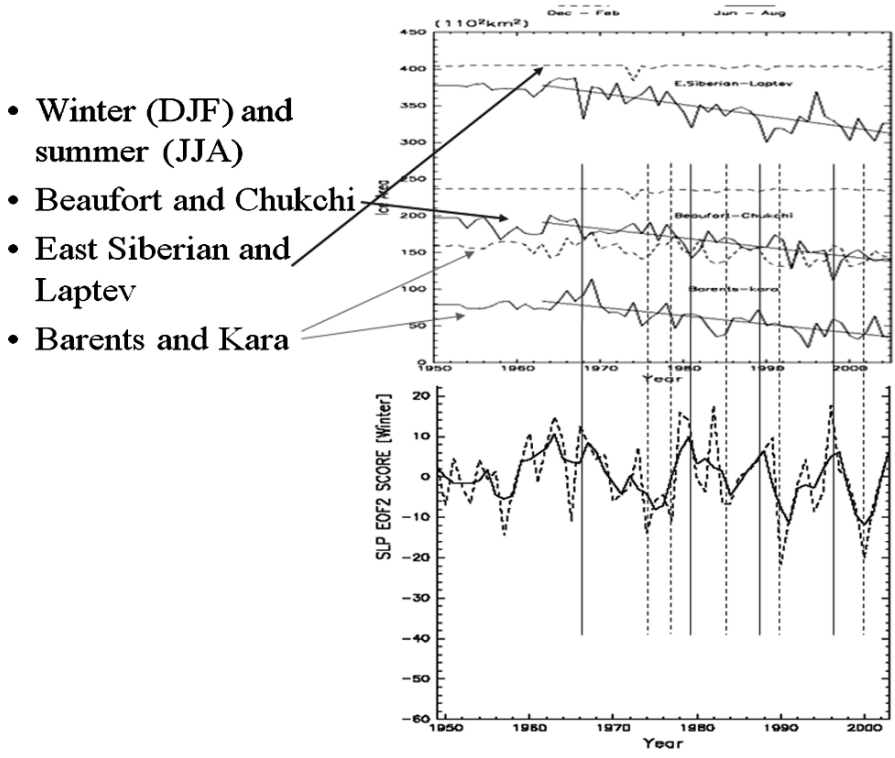

Fig. 7. Sea ice anomalies in three regions without 3-year smoothing. Positive ADMs are correlated with low ice in the Beaufort & Chukchi Sea with a 1–2 year lag.

Once the atmospheric circulation is analyzed, we usually rely on the first EOF. This mode basically corresponds to fluctuation between intense and weaker phases of the Polar Vortex and called NAM/AO. Although it has effects on the ice cover in the Pacific sector (section "Introduction"), the direct wind effects work on zonal ice motion. Then, we extended analyses to the second EOF, as done by Wu et al. (2006), and found a horizontal feature with two poles shown in Fig. 6, where the domain was restricted to north of 70°N. This mode is called the Arctic Dipole Mode (ADM) in this paper and much stronger in winter (Dec.–Feb.) than the other seasons. During the positive phase, meridional winds effectively push sea ice seaward in the Pacific sector. The opposite tendency appears in the Barents-Kara Sea. The time series presents decadal and year-to-year variability with a slow negative trend.

A correlation is inspected visually between the sea ice cover and the ADM in Fig. 7, in which the ice cover time series is lagged or shifted leftward by 1.5 years. Here, the Fanning filter is not applied so that the year-to-year variability is clearly shown. A negative correlation is found between the ADM and the Beaufort-Chukchi Sea ice cover in summer with 1 year or 2 year lags: i.e., the ice cover decrease appears in summer 1.5 or 2.5 years after the positive winter ADM. This correlation became significant after 1970 particularly. The ice cover in the Barents-Kara Sea shows a positive correlation.

Discussion

In this paper, both Pacific Water inflow and wind-induced ice motion have been examined how effective they are on ice cover anomalies in the Pacific sector. By separating them by time scales, the Pacific Water inflow gives effects at decadal to multi-decadal scales, while wind effects within the Arctic Basin are responsible for year-to-year anomalies.

In 2007 summer, the ADM was very intense. If the past statistics hold, the ice cover will be less than normal in the summers of 2008 and 2009. However, solar radiation, which is not examined in this paper, may be also effective and could yield a different result. From the past statistics on the ADM trend, we can provide another prediction that the ADM will not keep its effects on less ice cover in the Pacific sector for a longer term. In the other words, the anomalous condition in these few years is not a direct trigger for the change in the summer ice cover into a seasonal one.

Coupled ice-ocean models have been used for simulating the signals in the Arctic seas, and in turn verified in comparison with the data. The models well duplicate the ice cover variability in the Arctic Ocean, the Labrador Sea and the Okhotsk Sea for seasonal cycle and decadal variability. Both modeling and observational approaches should be coordinated so that more reliable tools may be provided for predicting future change in the Arctic seas. An ultimate attempt is to use a coupled ice-ocean-atmosphere model, in which crucial mechanisms should

be tackled and enables us to find answers for the questions when the Arctic sea ice becomes a seasonal ice cover.

Acknowledgments

The financial support by Japanese Ministry of Education, Culture, Sport, Science and Technology was fundamental to this work. Appreciation is extended to fruitful discussion with Drs. J. Overland, S. Prinsenberg, J. Wang, G. Panteleev, J. Zhang and K. Mizobata.

References

Aagaard K, EC Carmack (1989) The role of sea ice and other fresh water in the arctic circulation. J Geophys Res, 94, 14485–14498

Dickson RR, Meincke J, Malmberg SA, Lee AJ (1988) The great salinity anomaly in the northern North Atlantic 1968–1982. Prog Oceanogr, 20, 103–151

Ikeda M, Wang J, Makshtas A (2003) Importance of clouds to the decaying trend in the arctic ice cover. J Meteorol Soc Jpn, 81, 179–189

Ikeda M, Colony R, Yamaguchi H, Ikeda T (2005) Decadal variability in the Arctic Ocean shown in hydrochemical data. Geophys Res Lett, 32, L21605, doi:10.1029/2005GL023908

Stroeve J, Holland MM, Meier W, Scambos T, Serreze M (2007) Arctic Sea ice decline: Faster than forecast. Geophys Res Lett, 34, L09501, doi:10.1029/2007GL029703

Thompson DWJ, Wallace JM (1998) The arctic oscillation signature in the wintertime geopotential height and temperature fields. Geophys Res Lett, 25, 1297–1300

Wang J, Ikeda M (2000) Arctic oscillation and Arctic Sea ice oscillation. Geophys Res Lett, 27, 1287–1290

Woodgate RA, Aagaard K, Weingartner T (2005) A year in the physical oceanography of the Chukchi Sea: Moored measurements from fall 1990–1991. Deep Sea Res, 11, 52, 3116–3149

Woodgate RA, Aagaard K, Weingartner TJ (2006) Interannual changes in the Bering Strait fluxes of volume, heat and freshwater between 1991 and 2004. Geophys Res Lett, L15609, doi:10.129/2006GL026931

Wu B, Wang J, Walsh JE (2006) Dipole anomaly in the winter arctic atmosphere and its association with sea ice motion. J Climate, 19, 210–225

Frontal Zones in the Norwegian, Greenland, Barents and Bering Seas

Andrey G. Kostianoy[1] and Jacques C.J. Nihoul[2]

[1] P.P. Shirshov Institute of Oceanology, Russian Academy of Sciences, 36 Nakhimovsky Pr., Moscow, 117997, Russia, kostianoy@online.ru

[2] Modelenvironment, University of Liège, Sart Tilman, B-4000 Liege, Belgium, J.Nihoul@ulg.ac.be

Abstract

The Arctic Ocean and Subarctic seas are important components of the global climate system and are the most sensitive regions to climate change. Physical processes occurring in these regions influence regional and global circulation, heat and mass transfer through water exchange with the Atlantic and Pacific Oceans. One of the overall objectives of Arctic and Subarctic oceanographic research is to gain a better understanding of the mesoscale physical and biological processes in the seas. This review is based on the book "Physical Oceanography of Frontal Zones in the Subarctic Seas" by A.G. Kostianoy, J.C.J. Nihoul and V.B. Rodionov published in Elsevier in October 2004. The book presents the systematization and description of accumulated knowledge on oceanic fronts in the Norwegian, Greenland, Barents, and Bering seas. The work was based on numerous observational data, collected by the authors during special sea experiments directed to the investigation of physical processes and phenomena in areas of the North Polar Frontal Zone (NPFZ) and in the northern part of the Bering Sea, on archive data of the USSR Hydrometeocenter and other research institutions, as well as on a wide Russian and Western literature. The book contains general information on the oceanic fronts in the Subarctic seas, brief history of their investigation, state of the current knowledge, as well as detailed description of the thermohaline structure of all frontal zones in the Norwegian, Greenland, Barents, and Bering seas and of neighboring fronts of Arctic and coastal origins.

Introduction

Frontal zones and fronts are natural boundaries in the ocean. Drastic changes in the properties of oceanic waters – evidently of frontal origin – like sharp interfaces between warm and cold water masses or changes of current direction, were known to seamen since at least the 15th century. Phenomenological studies of surface effects of oceanic fronts relate to the middle of the 19th century. A great

J.C.J. Nihoul and A.G. Kostianoy (eds.), *Influence of Climate Change on the Changing Arctic and Sub-Arctic Conditions*,

contribution to the understanding of the physical nature of fronts was made by the pioneer studies of the Japanese oceanographer Michitaka Uda in 1938 (Uda 1938). However the intense investigation of fronts only began in the 1970s as a consequence of the accumulation of numerous observations in the ocean, their analysis, the development of theoretical hydrodynamic concepts and the wide use of new oceanographic equipment and methods (especially remote sensing) which made it possible to measure oceanic properties with high space and time resolution. There was a gradual reconsideration of the views of fronts as rather static and almost impenetrable boundaries separating water masses, widely accepted by the traditional descriptive oceanography before the 1970s. An approach viewing the fronts as a physical phenomenon with a complex inner dynamics possessing self-supporting characteristics received more and more recognition among scientists. The fronts were then regarded as one important unit in the chain of the energy transfer from scale to scale (the "energy cascade") from the elements of the global oceanic circulation down to small-scale phenomena. Besides permanent frontal zones of a climatic nature, including large oceanic currents of the Gulf Stream type, a variety of fronts exists in the ocean associated with coastal currents, gyres, eddies, upwellings, intrusions in the intermediate waters, river discharges into coastal zones, etc. Frontal instabilities, in their turn, give rise to the formation of eddies and jets with their own frontogenetic mechanisms and lifetime from a day to 2 or 3 years which produce cross-frontal water exchange and horizontal mixing in the neighbouring waters (Zatsepin and Kostianoy 1994; Ginzburg and Kostianoy 2002). So, oceanic fronts are multiscale in both space and time. Besides, various phenomena and processes are associated with fronts, such as high biological productivity and abundant fishing, anomalies in conditions of sound propagation, anomalies of wind waves, high velocity of jet currents, sharp changes of sea color, intense vertical movements, local weather conditions, etc. Large-scale fronts have important effects on the weather and also on the climate.

An important contribution to the study of oceanic fronts was made by Professor Konstantin N. Fedorov (corresponding member of the USSR Academy of Sciences). His fundamental work "The Physical Nature and Structure of Oceanic Fronts" published in its Russian edition in 1983 and by Springer-Verlag in 1986 remains a basic reference for all oceanographers involved in the study of fronts, it contains a summary of all the data collected in the beginning of the 1980s (Fedorov 1983, 1986).

The possibilities of the traditional descriptive approach to the problem of the frontal zones are not exhausted yet. Many regions of the World Ocean have not been actually explored, even within the limits of this approach, or the information about them remains fragmentary and not systematized. The investigation of the Norwegian, Greenland, Barents, and Bering seas (Fig. 1) has been going on since the end of 19th century. A great amount of field observations has been collected (the Subarctic seas are among the best explored regions of the World Ocean).

Fig. 1. The Arctic Ocean and Subarctic Seas (http://www.lib.utexas.edu/maps/islands_oceans_poles/arctic_region_2000.jpg).

Many descriptions of their background hydrology are available but, unfortunately, the information about the characteristics of the fronts remains very fragmentary. Still, the existing observations constitute a rich data base to construct a useful depiction of these fronts – which, within the water area of the Norwegian, Greenland and Barents seas are part of the climatic North Polar Frontal Zone (denoted NPFZ in the following) – even within the limits of the traditional hydrological approach.

This review presents the systematization and brief description of accumulated knowledge on oceanic fronts in the Norwegian, Greenland, Barents, and Bering seas, and it is partly based on the book by V.B. Rodionov and A.G. Kostianoy "Oceanic Fronts of the North-European Basin Seas" published in Russian edition in 1998 (Rodionov and Kostianoy 1998) and "Physical Oceanography of Frontal Zones in the Subarctic Seas" by A.G. Kostianoy, J.C.J. Nihoul and V.B. Rodionov published in Elsevier in 2004 (Kostianoy et al. 2004). This work was based on the numerous observational data, collected by the authors during special sea experiments directed to the investigation of physical processes and phenomena inside certain parts of the NPFZ and in the northern part of the Bering Sea, on archive data of the USSR Hydrometeocenter and other research institutions, as well as on a wide scientific literature published in Russian and Western editions. The books contain general information on the oceanic fronts of the Subarctic seas, brief history of their investigation, state of the knowledge, as well as detailed description of the thermohaline structure of all frontal zones in the Norwegian, Greenland, Barents, and Bering seas and of neighbouring fronts of Arctic and coastal origins. Special attention was given to the study of the multifrontal character of the NPFZ and of peculiarities of its internal structure at different sections, to the description of diverse oceanic features observed in the NPFZ, as well as to some characteristics of the horizontal and vertical fine structure of hydrophysical fields in the NPFZ. Observations were completed by the results of the numerical modeling of the northern Bering Sea where an extensive survey was carried out for 5 years in the scope of the NSF ISHTAR Program (Walsh et al. 1989). The main features of the northern Bering Sea's summer ecohydrodynamics were investigated with the help of three-dimensional direct and inverse models developed at the GeoHydrodynamics and Environment Research Laboratory (GHER) of the University of Liege, Belgium (Nihoul 1986, 1993).

Definitions

In published works on fronts the authors, as a rule, use various definitions of the terms "frontal zone", "frontal interface", "front", "frontal line". The differences in definitions are related to the concepts of frontal zones accepted by the different authors. Each definition is acceptable and generally applicable to resolve specific problems and describe certain aspects of the investigated phenomenon. Stepanov (1960) noted a connection of the frontal phenomena with convergences in the ocean. Studying the fronts of the Gulf Stream system Baranov (1966, 1972) defined frontal zones on the basis of the concepts of "water masses" as a broad transitional zone between various water masses, which is rather stationary in time and space. Describing the main climatic frontal zones of the World Ocean, Gruzinov (1986) defined them as "quasistationary zones of interaction between waters of various hydrological characteristics having individual ecosystems, which reveal

themselves all over the thermocline by maximum horizontal gradients of hydrological characteristics and vertical currents". Gruzinov specifies that his work is concerned with "main" or climatic fronts. At the same time Baranov and Gruzinov added that from a climatic point of view, the frontal zone may be considered, as well, as a region of the ocean in which seasonal and interannual transitions of a given front occur. There are also a number of other definitions summarized by Fedorov (1983, 1986). These definitions, which are quite adequate to the problem of the physico-geographical description of the climatic frontal zones, however, do not single out features of their dynamics which produce a significant sharpening of contrasts of the main parameters, and cause the appearance of fronts of various scales (not only climatic) in this zone. These features are taken into account by the definition given by Fedorov (1983, 1986), according to which the frontal zone in the ocean is a zone "in which the spatial gradients of the main thermodynamic characteristics are very high in comparison with the average". This definition is not based on climatology concepts such as "water masses", "thermocline" etc., which require definitions by themselves, and implies the application of some appropriate numerical criterion selected by each investigator. Following Fedorov, the frontal interface will be defined as "a surface within the frontal zone, which coincides with the surface of the maximum gradient of one or several characteristics (temperature, salinity, density, velocity, etc.)". Then, strictly a "front" can be regarded as the result of the intersection of the frontal interface with any given surface, particularly with the free surface of the ocean or with an isopycnal surface (Fedorov 1986).

The North Polar Frontal Zone (NPFZ) in the Norwegian, Greenland and Barents Seas is a complicated oceanic feature, in which processes of all scales are represented. As a whole, NPFZ represents a climatic frontal zone generated by the interaction of two elements of the planetary circulation: relatively warm and salty waters of the Atlantic Ocean, which extend from the South to the North, and colder and fresher waters, which penetrate from Polar areas to the South, formed during general cooling, ice thawing and mixing thawing products with enclosing waters. A rather complicated bottom topography and the coastal line topography of the investigated region result in the division of main streams of waters into separate branches and, therefore, in the existence of the branchy system of permanent currents. The convergence of the currents and their interaction with elements of the topography and the coast line result in the NPFZ to be divided into several frontal zones of smaller scales (100 km). Besides the interaction of sea water with continental drainage waters transported by secondary branches of the general circulation leads to the formation of frontal zones also. Thus the climatic NPFZ is a system of frontal zones with various characteristics. However it is necessary to remember that these frontal zones are "only separate parts of the NPFZ, and, therefore, they must be regarded as climatic".

According to the definition, the gradients of temperature and salinity across the frontal zones should considerably exceed the average climatological gradient. For the region being studied the average climatic values of the horizontal gradients of

temperature and salinity are not higher than respectively 0.01°C/km and 0.001‰/km.

A characteristic feature of the majority of frontal zones of this water area is a multifrontal internal structure, i.e. the presence of several fronts (very often of different types). Permanent fronts related to persisting climatic causes, fronts of synoptic or seasonal nature, and also small-scale fronts of local origin are present, justifying the separation made by Fedorov between "frontal zone" and "front".

Frontal zones in the Norwegian and Greenland seas

The description of the characteristics of frontal zones in the Norwegian and Greenland seas was based on the analysis of hydrological data received by the USSR Hydrometeocenter in 1984–1987. The information came from about 10,000 stations. The measurements of vertical profiles of temperature and salinity were made at approximately 30% of stations, only measurements of temperature profiles were made at the others. The resolution of the stations was 10–30 miles.

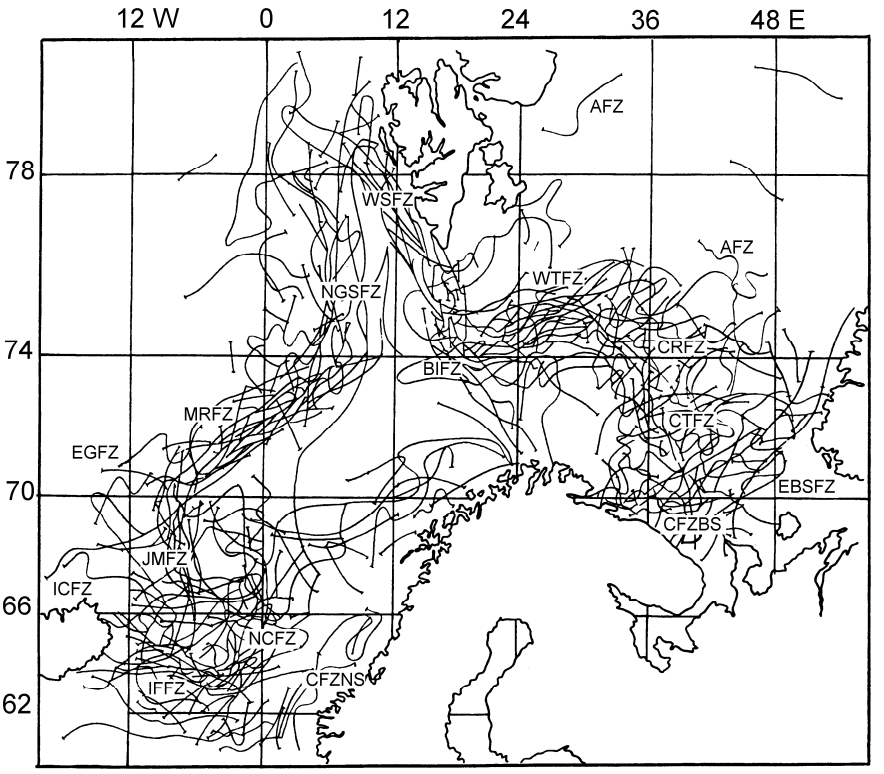

Fig. 2. The position of high gradient zones in temperature field (all observations for 48 months of 1984–1987).

The technique for the determination of the fronts' characteristics was the following: the data for every year were classified according to months, and the position of stations for each month was marked on a map. The vertical profiles of temperature and salinity were analyzed to distinguish pairs or groups of stations on sections, between which high-gradient areas with changes of temperature and/or salinity, considerably exceeding mean climatic ones, were observed. Then it was possible to state that one or more fronts are located between adjacent stations, and that the stations are situated inside or on the rim of the frontal zone. The analysis of the totality of the sections for each month allowed to plot the location of the high-gradient areas on the map as lines dividing waters with different characteristics. In Figs. 2 and 3 one can see the combined maps of the high-gradient zones in temperature and salinity fields at the sea surface for all hydrological seasons altogether made by the superposition of 48 monthly maps. Thus these maps represent a high resolution snapshot of a complete frontal system in the Norwegian, Greenland and Barents seas simultaneously, that is unreachable by satellite monitoring due to cloudiness.

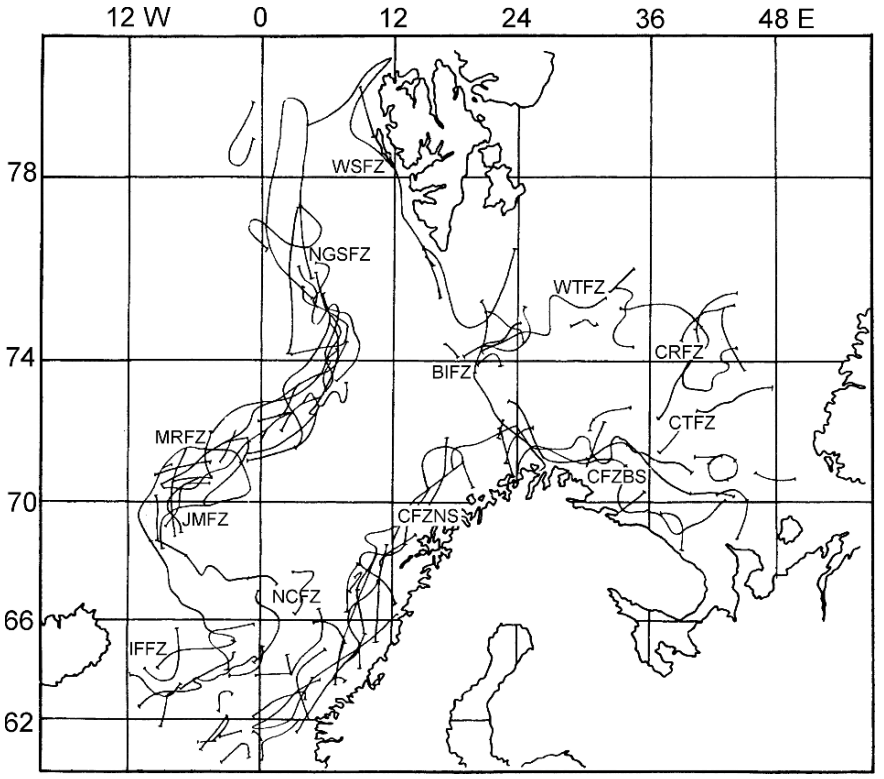

Fig. 3. The position of high gradient zones in salinity field (all observations for 48 months of 1984–1987).

It follows from them that the location of the high-gradient zones has a large space and time variability, generally related to the existence inside the frontal zones of several local fronts and/or a significant intra-seasonal variability of their position. The simultaneously observed high-gradient sites do not provide a narrow and continuous picture. It is possible to distinguish only rather broad areas (the frontal zones), in which the main changes of properties (i.e. sharpening of horizontal gradients) between water masses take place.

Various parts of the NPFZ considerably differ by their characteristics. So it is expedient to distinguish its individual parts (or frontal zones of smaller scale) due to different types of water interactions, bottom and coastal topography, features of quasi-permanent currents, etc. Based on the analysis of wide scientific publications, satellite and *in-situ* data in the Norwegian and Greenland seas it was possible to distinguish the following nine parts of the climatic NPFZ and adjacent frontal zones differing from each other in main characteristics, and to describe them in detail in (Kostianoy et al. 2004):

1. The Norwegian Current Frontal Zone (NCFZ) is conditioned by the interaction of the Norwegian Current with the East Icelandic Current in the Norwegian and Lofoten Basins, and the Norwegian Plateau. There is a great amount of work devoted to the general hydrology of the Norwegian Sea, however there is very little information published on the local fronts relating to the NCFZ.
2. The Coastal Frontal Zone of the Norwegian Sea (CFZNS) is formed by the interaction between water of the Norwegian Coastal Current (to the south of 65° N it is called the Baltic Current) with water of the western branch of the Norwegian Current and the eastern branch of the North Atlantic Current (to the south of the Faeroe–Shetland Strait).
3. The Iceland-Faeroe Frontal Zone (IFFZ) is formed by the interaction of the North Atlantic Current water and the East Icelandic Current water, stretching from the Iceland coast along the Iceland-Faeroe Ridge approximately up to 62–64° N, 3–5° W. The IFFZ was repeatedly investigated from the beginning of the 1960s.
4. The East Greenland Frontal Zone (EGFZ) is the zone of interaction of the East Greenland Current and Irminger Current, stretching along the continental slope of Greenland.
5. The Iceland Coastal Frontal Zone (ICFZ) is the zone of interaction of the Coastal Iceland branch of the Irminger Current with waters of the East Greenland and East Icelandic Currents, located in the region of the northern and eastern shelf break of Iceland. Research on this zone have been carried out very intensively in the 1950s and 1960s in the support of fishing.
6. The Jan Mayen Frontal Zone (JMFZ) is the zone of interaction of the East Icelandic Current with the East Greenland Current, passing almost meridionally between 6° and 9° W from the Iceland–Faroe Ridge along the Jan Mayen Ridge approximately up to 70° N.

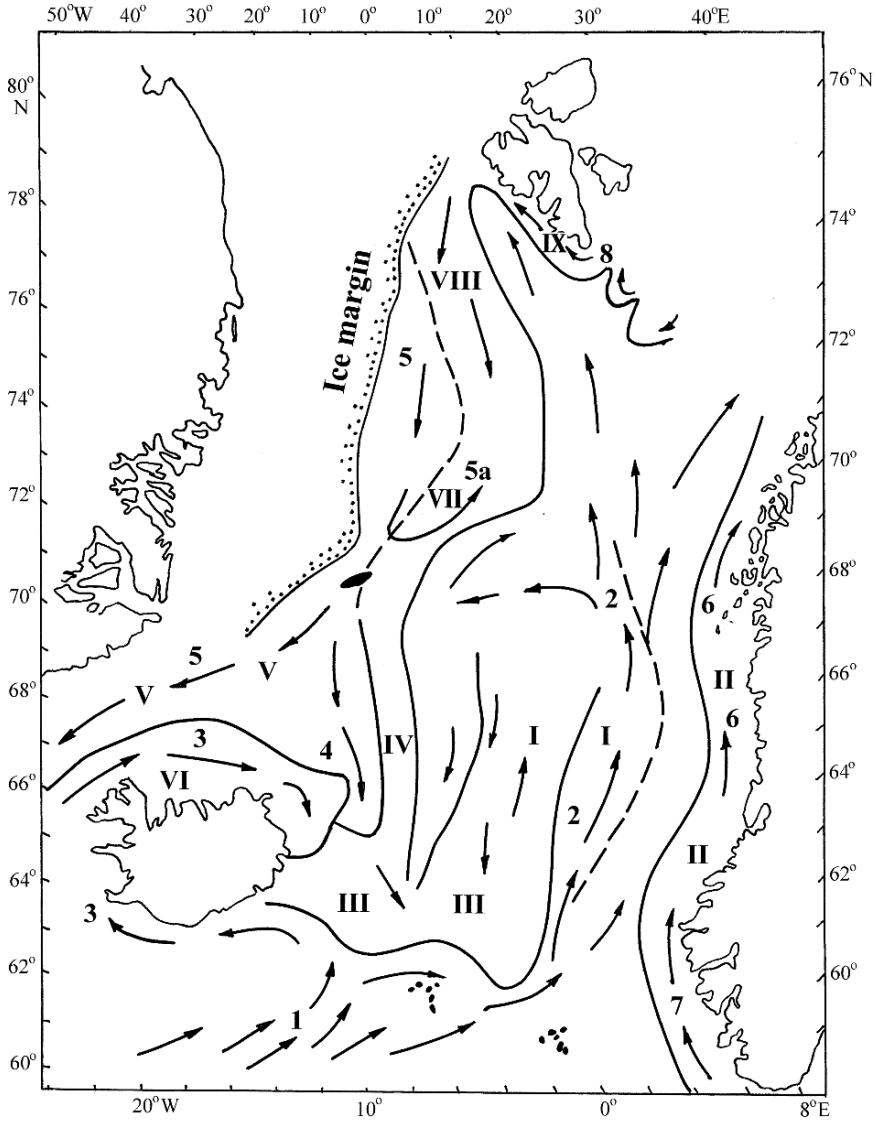

Fig. 4. The pattern of the main currents and frontal zones (FZ) in the Norwegian and Greenland seas. The Roman numerals designate the frontal zones and the Arabic – the currents:

- I – Norwegian Current FZ, II – Coastal FZ of the Norwegian Sea, III – Iceland–Faeroe FZ, IV – Jan Mayen FZ, V – East Greenland FZ, VI – Iceland Coastal FZ, VII – Mohn Ridge FZ, VIII – Northern Greenland Sea FZ, IX – West Spitsbergen FZ.
- 1 – North Atlantic Current, 2 – Norwegian Current, 3 – Irminger Current, 4 – East Icelandic Current, 5 – East Greenland Current (5a – Jan Mayen branch), 6 – Norwegian Coastal Current, 7 – Baltic Current, 8 – West Spitsbergen Current.

7. The Mohn Ridge Frontal Zone (MRFZ) is located in the region of the Mohn Ridge, and is a zone of interaction of waters of the Jan Mayen branch of the East Greenland Current with waters of the western branch of the Norwegian Current limited in the south by 70° N, and in the north by 73–74° N.
8. The Northern Greenland Sea Frontal Zone (NGSFZ) is formed as a result of the interaction of water of Atlantic origin, penetrating through the Greenland basin, with Arctic water. It is located in the area of the Greenland basin, to the north of the Mohn Ridge. This region has been rather well investigated due to the MIZEX experiments and other programs.
9. The West Spitsbergen Frontal Zone (WSFZ) is located along the western edge of the Spitsbergen shelf and is caused by the interaction of water of Atlantic origin with water penetrating from the Barents Sea shelf off the Spitsbergen Archipelago.

The pattern of the main currents and the location of the main frontal zones in the Norwegian and Greenland Seas are presented in Fig. 4.

Earlier there were few attempts to distinguish different parts of the NPFZ in the Norwegian, Greenland and Barents seas. However such systematization was made either not on the whole water area or in a very detailed way, or only on the temperature field.

First of all, one shall consider V.K. Agenorov's work (Agenorov 1947). For the first time, a new method of selection of water masses and detection of the position of the frontal zones based on the analysis of fields of gradients of a number of hydrological characteristics and of vorticity developed by V.K. Agenorov (1944) was used. Based on the data of the temperature field in the Barents Sea in summer months, maps of main water masses with distinctly marked frontal zones and front positions at 25, 50, 100 and 200 m depth for July–September were drawn.

Kolesnikov (1962, 1967) was the first to systematize frontal zones in the Norwegian Sea. He revealed and studied separately the frontal zones of the Mohn Ridge, the Jan Mayen, the Iceland-Faeroe and the frontal zone of the Norwegian Current (Helholand frontal zone as called by Kolesnikov [1967]). The analysis was made basing on the materials of monthly micro surveys, which were carried out by the BaltNIRO and PINRO, and also by other Soviet and foreign expeditions from 1951 to 1960. The position of frontal zones was determined according to V.K. Agenorov's method. It was showed that the system of the fronts in the Norwegian Sea is connected with specific rises of bottom topography – the Mohn Ridge, Jan Mayen Ridge, Iceland-Faeroe Ridge, Thomson Ridge, and the eastern slope of the Norwegian Basin.

On the basis of the 2,300 AXBT surveys of the temperature field in the Norwegian Sea, Smart (1984) identified the Iceland-Faeroe, Jan Mayen, Iceland Coastal and Norwegian Current frontal zones. Johannessen (1986) mentioned the Iceland-Faeroe, East Greenland, Norwegian Coastal, Polar Oceanic and Barents Sea Polar fronts. Kuznetsov et al. (1986) identified frontal zones corresponding to the Jan Mayen, Iceland-Faeroe, Norwegian Coastal Currents and the frontal zone

of the Norwegian Current. Korablev (1987) processed the hydrological information with the resolution of 60 miles over the main part of the Norwegian and Greenland seas and identified the Iceland-Faeroe, Jan Mayen, Norwegian Current, Mohn Ridge and Northern Greenland frontal zones. This work was generalized in (Alekseev and Nikolaev 1987; Nikolaev and Alekseev 1989; Alekseev and Bogorodskiy 1994). A more complete history of the research of oceanic fronts in the Subarctic seas can be found in (Kostianoy et al. 2004).

Unfortunately, all the classifications of the frontal zones were made only on the basis of the temperature field. Apparently, this did not allow to identify precisely the frontal zones, strongly and steadily expressed in the salinity field and weakly or unstably in the temperature field (with modification of a magnitude and alternation of a sign of cross-frontal drop of thermohaline characteristics in different seasons). Besides insufficient time and space resolution of the collected data did not allow to describe seasonal variability of the spatial and thermohaline characteristics of the frontal zones and the structure of fronts inside them.

Rodionov and Kostianoy (1998) and Kostianoy et al. (2004), on the basis of the joint analysis of data from the Russian Hydrometeocenter archive for 1984–1987 and other published information made a systematization of frontal zones in the Norwegian, Greenland and Barents seas and described their characteristics for all seasons. The main characteristics were determined on the basis of the temperature and salinity vertical profiles at both sides of each frontal zone. The width of the frontal zones, the characteristic drop in temperature, salinity, and relative density across the frontal zones, as well as a set of other supplementary parameters for the near-surface and deep layers were calculated. Besides, on the basis of the hydrological data published in 1900–1992, the characteristics of the local fronts inside the frontal zones were evaluated by graphic analysis of the hydrological sections shown in historical publications. For this special analysis, the sections with a resolution between stations of no more than 20 km were used (Rodionov and Kostianoy 1998; Kostianoy et al. 2004).

Frontal zones in the Barents Sea

The structure and characteristics of the North Polar Frontal Zone in different regions of the Barents Sea differ rather strongly. There was very little information on the frontal zones in the Barents Sea in the literature. Detailed definitions of these zones are either absent in the literature or have a local and incidental character. An attempt to distinguish and describe the system of frontal zones of the Barents Sea based on a number of large-scale surveys was undertaken by Chvilev (1990, 1991).

According to the joint analysis of the USSR Hydrometeocenter's archive data of 1984–1987 (approximately 10,000 stations) and published information, the

following main frontal zones or groups of frontal zones, included in the climatic NPFZ system, can be revealed in the Barents Sea (Rodionov and Kostianoy 1998):

1. The Bear Island Frontal Zone (BIFZ) is a zone of interaction of the Bear Current water with the North Cape Current water. It is located along the edge of the Bear Island shelf. The Spitsbergen Frontal Zone is a zone of interaction of the East Spitsbergen Current with enclosing water masses located along the southern and eastern edges of the Spitsbergen Archipelago shelf.
2. The Western Trough Frontal Zone (WTFZ) is located along the periphery of the western trough of the Barents Sea, and is caused by the interaction of the northern branch of the North Cape Current with enclosing waters.
3. The Central Rise Frontal Zone (CRFZ) is formed by the interaction of water of the central branch of the North Cape Current with the Barents Sea water formed above the Central Rise.
4. The Central Trough Frontal Zones (CTFZ) are located at the periphery of the Central Trough, and are formed by the interaction of the Barents Sea water, flowing down to the Central Trough, with waters of Atlantic and coastal origin.
5. The Marginal Ice or Arctic Frontal Zones (AFZ) are formed on the periphery of a lens of cold freshened waters, formed by ice melting.
6. The Eastern Barents Sea Frontal Zones (EBSFZ) are caused by the interaction of the waters of the Murmansk and Novaya Zemlya Currents with waters of the Novaya Zemlya shelf, and waters of the area between Kanin Nos Peninsula and Novaya Zemlya.
7. The Coastal Frontal Zones of the Barents Sea (CFZBS) are formed by the interaction of the Barents Sea water, waters of the coastal branch of the North Cape Current, waters of the Murmansk Current, and waters of the river discharge.

The pattern of the main currents and the location of the main frontal zones of the Barents Sea are presented in Fig. 5. The main parameters of the frontal zones of the Barents Sea were determined using a technique similar to that used for the frontal zones of the Norwegian and Greenland seas, and can be found in (Rodionov and Kostianoy 1998; Kostianoy et al. 2004).

Considerably fewer hydrological surveys and sections with a spatial resolution permitting to determine the characteristics of fronts were conducted in the Barents Sea than in the Norwegian and Greenland Seas.

It is worth to note that analyzing the data for every April of 1984–1987 in the area of the boundary of the Norwegian and the Barents seas, Rodionov and Kostianoy (1998) detected an extended thermohaline frontal zone stretching from the area of the Bear Island shelf up to the North Cape, which they named as the North Cape frontal zone (Fig. 6). To the west are the waters with $T \approx 5–6°C$, $S \approx 35.1–35.2$ psu, corresponding to the Atlantic waters, to the east waters with $T \approx 2–3ºC$, $S \approx 34.8–34.9$ psu, very close to the coastal waters of the Kola Peninsula, according to their characteristics. Despite of a great amount of observations in the given region all the year round, this zone was never surveyed in other months. The

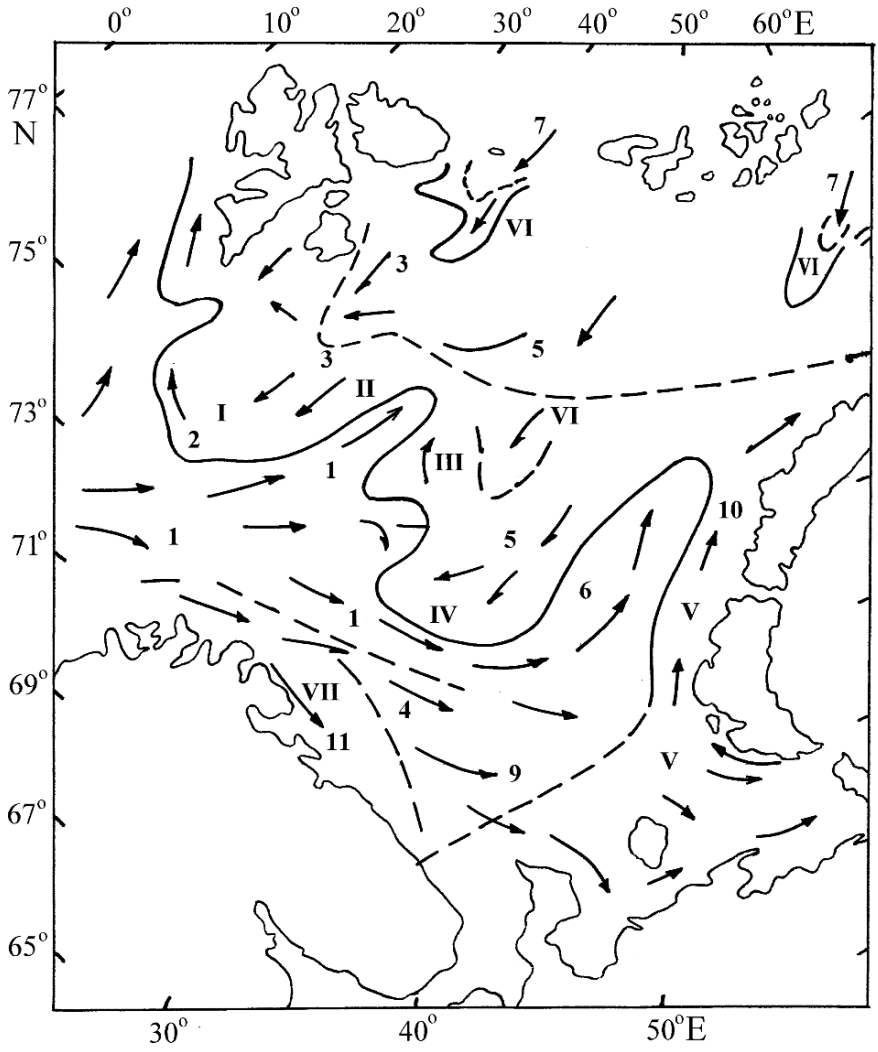

Fig. 5. The main current pattern and the frontal zones of the Barents Sea. The Roman numerals indicate the following frontal zones:

- I – Bear Island Frontal Zone, II – Western Trough Frontal Zone, III – Central Rise Frontal Zone, IV – Central Trough Frontal Zone, V – Eastern Barents Sea Frontal Zones, VI – Marginal Ice (Arctic) and Deep Frontal Zones, VII – Coastal Frontal Zones.
- The Arabic numerals indicate the currents: 1 – North Cape Current, 2 – Bear Current, 3 – East Spitsbergen Current, 4 – Murmansk Current, 5 – Central Current, 6 – Novaya Zemlya Current, 7 – Deep Current, 8 – Kolguev-Pechora Current, 9 – Kanin Current, 10 – Litke Current, 11 – Murmansk Coastal Current.

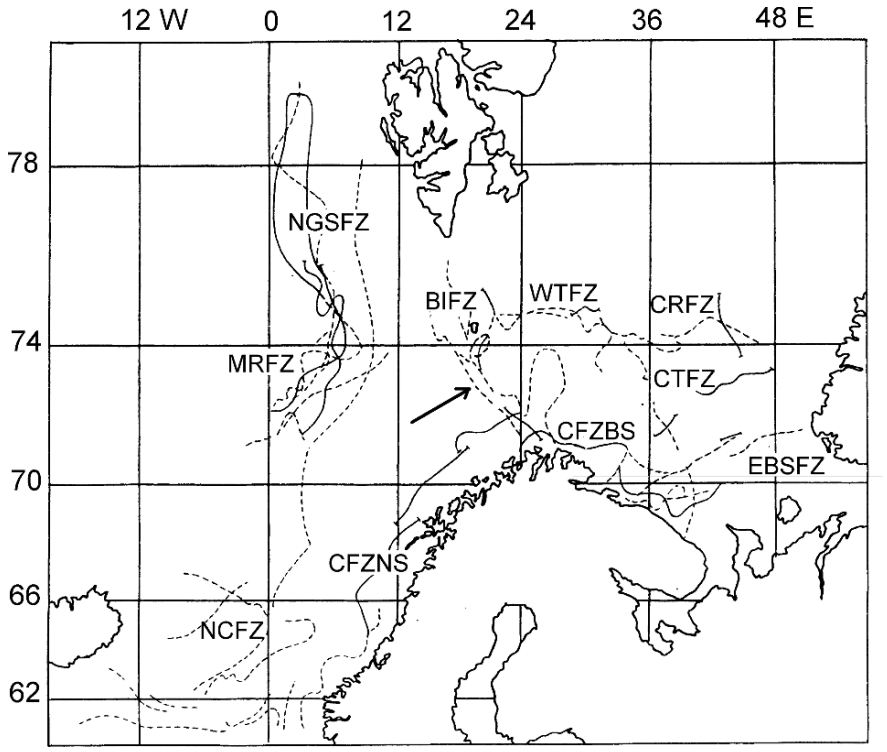

Fig. 6. Position of the high-gradient zones in the field of temperature (dotted line) and salinity (solid line) in April (total sum of observations for 1984–1987). Arrow shows the North Cape frontal zone.

existence of this zone was not mentioned in any literature known to the authors. This could be explained by the fact that many hydrological sections (even standard ones) have been made essentially along the line joining the North Cape and Bear Island, i.e. along this frontal zone and not across it. That is why, probably, the North Cape frontal zone was not observed earlier. The question of the origin of this frontal zone requires an additional and detailed research, however its presence only in April implies a relation with a synchronous uppermost southwestern position of the ice margin in the Barents Sea, at least in 1984–1987.

Frontal zones in the Bering Sea

The Bering Sea is a northward extension of the Pacific Ocean between Siberia and Alaska. Separated from the Pacific Ocean by the Aleutian Islands, it is connected with the Arctic Ocean via the Bering Strait. The general circulation in the Bering

Sea is complicated and variable due to the interaction of wind, water inflow through the Aleutian Islands, tides, bottom relief and other factors (Fig. 7). The main feature of the circulation is a general cyclonic motion in the deep basin, the so-called Bering Sea Gyre. It is composed by the North Aleutian Slope Flow (the eastward motion of water incoming through the Aleutian Islands via Near Strait, Amchitka, Buldir and Amukta Passes), the Bering Slope Current flowing northwestwards and the Kamchatka Current flowing southwards.

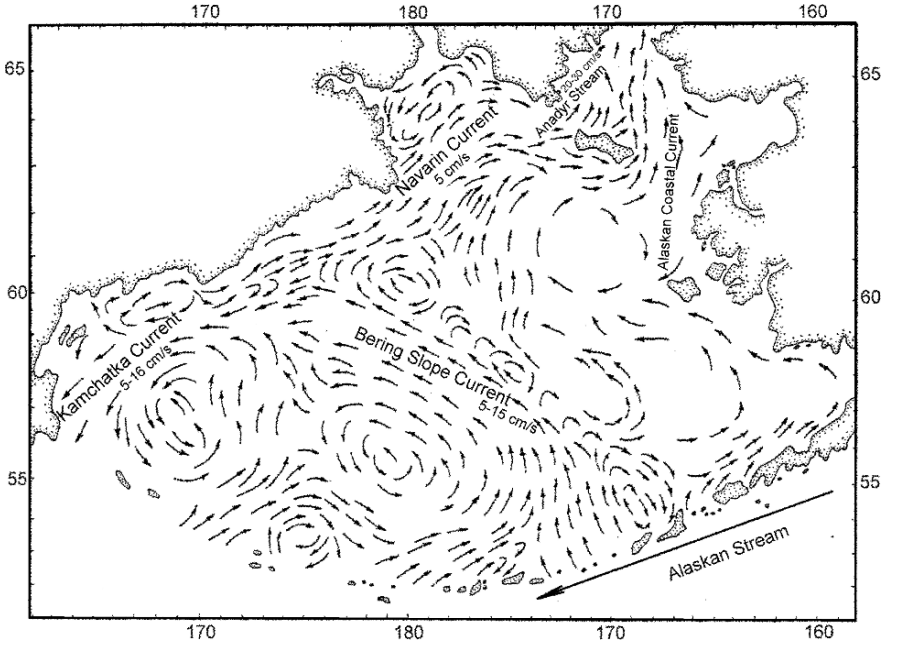

Fig. 7. Composite surface circulation in the Bering Sea derived from diagnostic calculations. (Adapted from Terziev 1999.)

Dodimead et al. (1963) were probably the first to indicate the internal front which separates coastal and middle shelf water masses in Bristol Bay, and the front along the shelf break. Major oceanographic studies in the Bering Sea by PROBES (Processes and Resources of the Bering Sea Shelf), OCSEAP (Outer Continental Environmental Shelf Assessment Program) and other programs focused on the southeastern shelf area, this is why this region is the best documented (see list of references in Kostianoy et al. [2004]). Kinder and Coachman (1978), Schumacher et al. (1979), Coachman et al. (1980), Kinder and Schumacher (1981) described frontal systems in the eastern Bering Sea. Iverson et al. (1979) gave a description of fronts in this region based on results of PROBES, which became a classical one for the southeastern Bering Sea. Information about the fronts in other parts of the sea can be found in several publications, but a synoptic view of the

whole frontal system of the Bering Sea based on CTD observations and/or satellite imagery, and its variability is absent (see also Belkin and Cornillon [2003]).

A systematization of the frontal zones and fronts in the Bering Sea is given below based on information accumulated from publications, satellite imagery and SST data, as well as from CTD observations and numerical modeling performed during the ISHTAR Program.

1. The Bering Slope Front is a basic frontal feature extending some 1,000 km along the continental slope of the Bering Sea year-round. The highest contrasts across the front are observed from January to June. It is associated with the Bering Slope Current, concentrated in the upper 300 m, which has velocities of 5–15 cm/s and a transport of 3–5 Sv. It is more correct to call this front a frontal zone, because of its spatial structure, comprising meanders and eddies, and permitting intense cross-shelf water exchange. The Bering Slope Frontal Zone is responsible for the "Green Belt" associated to it. The concept of the Bering Sea Green Belt (a highly productive habitat along the edge of the continental shelf) is based upon compelling observations of a variety of physical and biological features acquired from many sources over many years (Springer et al. 1996).
2. The Inner, Middle and Shelf Break Fronts in the eastern Bering Sea. The balance between tidal and wind mixing and buoyancy flux (freshwater discharge, ice melting, insolation) results in three distinct hydrographic and biological domains. In the coastal domain ($z < 50$ m, 200 km large) tidal and wind mixing usually overlap, resulting in a weakly stratified or mixed water column. In the middle shelf domain ($50 < z < 100$ m, 150 km large) the overlap between the near surface and bottom mixed layers is limited, and during weak wind mixing in summer, a two-layered vertical structure is formed. The outer shelf domain ($100 < z < 180$ m, 120 km large) has separate mixed upper and bottom layers. The domains are delimited by the Inner (10 km wide), Middle (50–75 km wide), and Shelf Break (50 km wide) Fronts, which follow the 50, 100, and 200 m isobaths, respectively.
3. Coastal fronts. A system of three hydrological zones exists over the western shelf, which is much narrower than the eastern one. These hydrological zones, coastal, transitional and oceanic, are easily distinguished by thermohaline characteristics. The coastal zone has low-salinity (<31.0 psu) surface water and a strong pycnocline. The transitional zone is characterized by a weak two-layered structure. The oceanic zone is identified by a three-layered vertical structure with relatively warm bottom temperatures, indicating the presence of slope waters. The location of these zones, and the coastal fronts separating them, are not as stationary as at the eastern shelf, because of the Kamchatka Current, a strong boundary current which determines the water dynamics at the western shelf and slope. The Kamchatka Current itself has a front on its eastern periphery, which is more pronounced southward of the Kamchatka Strait.

4. Freshwater fronts, originating from river discharges into coastal areas of the ocean, are divided in two types. According to Fedorov (1986), if the river has an estuary, the latter can have its own estuarine front independently of the front which encloses the lens of freshened waters in the open sea, and which he referred to as the river discharge front. In large estuaries, tidal mixing can be so intensive that river discharge fronts may not be present at all beyond the estuary. In the Bering Sea, July is a month of maximum freshening of the surface layer in the bays and sounds, caused by maximal river discharges in June–July. Main river runoffs in the Bering Sea are from the Yukon (45% of the total discharge), Anadyr (20%), Kuskokwim (12%), Nushagak (3%) and Kvichak Rivers. Freshwater plumes and related coastal fronts (river discharge fronts of the Anadyr and Yukon Rivers) are perfectly visible on the IR satellite images due to a strong SST contrast. Estuarine fronts are perfectly identified by sharp salinity and thermal contrasts related to general freshening in the Gulf of Anadyr, Norton Sound, Bristol and Karaginskiy Bays.

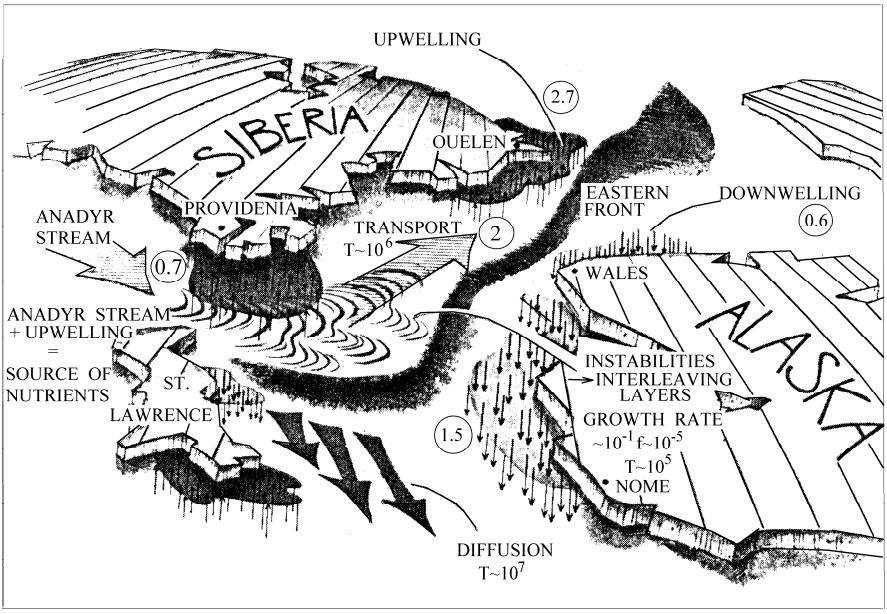

Fig. 8. Cartoon of the ecohydrodynamics of the Bering Sea. The figures in the circles are the total (ammonium, urea and nitrate) integrated nitrogen uptake rates (mg-at N m^{-2} h^{-1}) during the summer 1987.

5. The Date Line Front. The thermohaline characteristics of the Anadyr Stream (33 psu) contrast with the Alaskan Coastal Current transporting low-salinity (<32.1 psu), seasonally warm coastal water northwards along the western coast of Alaska and through the eastern channel of the Bering Strait. These waters

are separated by the Date Line Front passing from St. Lawrence Island to the Bering Strait, and farther northward (Fig. 8). Experimental evidence of the Date Line Front is found in the remote sensing images of the northern Bering Sea (Nihoul 1986) and in several field surveys (Coachman et al. 1975).

6. Upwelling fronts. The strongest upwellings/upsloping areas are located along the Siberian coast (around Capes Chukotskiy and Dezhnev) and the eastern coast of St. Lawrence Island, where vertical velocities as high as 4 m day^{-1} can be found. CTD casts in the Anadyr Strait made during the Akademik Korolev cruise (ISHTAR Programme) in August 1988 demonstrated coastal upwelling with a front located in the middle of the strait (Nihoul et al. 1993). SST contrasts across the surface front reached 4°C. The depth of the front was 30 m. This upwelling is maintained by the Anadyr Stream together with favorable winds, and seems to disappear very rarely, for short period of time, presumably when it is blocked by strong southward blowing winds and/or reversal currents in the Bering Strait. Upwellings in the centers of bays due to a cyclonic circulation is a most common feature of the Bering Sea coastal dynamics (Terziev 1999). Such an upwelling in the Bristol Bay was reported by Kinder and Schumacher (1981). It is attributed to a cyclonic flow that approximately follows the 50 m isobath and lift the isopycnals and isotherms. The same feature at the entrance of Norton Sound was reported by Nihoul et al. (1993).

Conclusions

The Arctic Ocean and Subarctic seas, namely, the Norwegian, Greenland, Barents, and Bering seas, are important components of the global climate system and are the most sensitive regions to climate change. Physical processes occurring in these regions influence regional and global circulation, heat and mass transfer through water exchange with the Atlantic and Pacific Oceans. One of the overall objective of the Arctic and Subarctic oceanographic research is to gain a better understanding of the mesoscale physical and biological processes in the seas. Inclusion of more accurate parameterizations of mesoscale physical processes in large-scale models of interaction between atmosphere, ice, and ocean would result in a major improvement in climatological studies. Unfortunately, most global climate models are not capable of sufficiently reproducing the climatological state of the Arctic Ocean, sea ice, and atmosphere.

Obviously, numerous global climate models and regional Arctic Ocean models depend heavily on the “ground truth” data for their correct realization, validation, and interpretation of the simulation results. Such data, besides salinity and temperature distributions, density stratification, etc., should include data on the mesoscale structure and dynamics of the oceanic frontal zones and fronts. Such information has been, until recently, sparse in temporal and spatial coverage. Improved modeling and better prediction of frontal zones and ice-edge position, ice type,

concentration, and thickness in these regions would be an important step toward expanding human activities, such as, naval transport and operations, oil and gas exploration and production, fishing, and coastal zones management.

References

Agenorov VK (1944) On basic water masses in the hydrosphere. Trudy NIU GUGMS SSSR, Gidrometeoizdat, Moscow

Agenorov VK (1947) On water masses of the Barents Sea in summer. Trudy GOIN, 1(13): 83–94 (in Russian)

Alekseev GV, Bogorodskiy PV (Eds) (1994) Regularities of Large-Scale Processes in the Norwegian Energy-Active Zone and Surrounding Regions. Gidrometeoizdat, St. Petersburg (in Russian)

Alekseev GV, Nikolaev YuV (1987) Field investigations in the Norwegian Energy-Active Zone of the ocean in 1981–1985. In: Results of Science and Techniques. Atmosphere, Ocean, Space - Program "Sections", VINITI, Moscow, Vol 8, 233–240 (in Russian)

Baranov YeI (1966) Short-period fluctuations of the Gulf Stream front in winter-spring season 1963. Okeanologiya, 6(2): 228–233 (in Russian)

Baranov YeI (1972) Monthly mean position of hydrological fronts in the North Atlantic Ocean. Okeanologiya, 12(2): 217–224 (in Russian)

Belkin I, Cornillon P (2003) SST fronts of the Pacific coastal and marginal seas. Pacific Oceanography, 1(2): 90–113

Chvilev SV (1990) Hydrological fronts of the southwestern part of the Barents Sea and their seasonal variability. In: Hydrology of the Southern Ocean and North Atlantic Ocean, LGMI, Leningrad (in Russian)

Chvilev SV (1991) Frontal zones of the Barents Sea. Meteorologiya i Gidrologiya, 11: 103–108 (in Russian)

Coachman LK, Aagaard K, Tripp RB (1975) Bering Strait: The Regional Physical Oceanography, University of Washington Press, Seattle, WA

Coachman LK et al. (1980) Frontal Systems of the South-Eastern Bering Sea shelf, 2-nd IANN Symposium on Stratified Flows, June 1980, Trondheim, 917–933

Dodimead AJ, Favorite F, Hirano T (1963) Salmon of the North Pacific Ocean. Part 2. Review of oceanography of the Subarctic Pacific region. Bull N Pac Fish Comm, 13: 195

Fedorov KN (1983) Physical Nature and Structure of Oceanic Fronts, Gidrometeoizdat, Leningrad (in Russian)

Fedorov KN (1986) The Physical Nature and Structure of Oceanic Fronts, Springer, Berlin/Heidelberg/New York/London/Paris/Tokyo

Ginzburg AI, Kostianoy AG (2002) Fronts and mixing processes. In: Nihoul JCJ and Chen C-TA (Eds) Oceanography, Encyclopedia of Life Support Systems (EOLSS), UNESCO/EOLSS Publishers, Oxford, UK [http://www.eolss.net]

Gruzinov VM (1986) Hydrology of Frontal Zones of the World Ocean. Gidrometeoizdat, Leningrad (in Russian)

Iverson RL, Coachman LK, Cooney RT, English TS, Goering JJ, Hunt GL, Jr., Macauley MC, McRoy CP, Reeburg WS, Whitledge TE (1979) Ecological significance of fronts in the southeastern Bering Sea. In: Livingston RJ (Ed) Ecological Processes in Coastal and Marine Systems, Plenum Press, New York/London, 437–466

Johannessen OM (1986) Brief overview of the physical oceanography. In: Hurdle BG (Ed) The Nordic Seas, Springer, New York, 103–127

Kinder TH, Coachman LK (1978) The front overlying the continental slope in the Eastern Bering Sea. J Geophys Res, 83(9): 4551–4559

Kinder TH, Schumacher JD (1981) Hydrographic structure over the continental shelf of the southeastern Bering Sea. In: Hood DW and Calder JA (Eds) The Eastern Bering Sea Shelf: Oceanography and Resources, Vol 1, Department of Commerce, USA, 31–52

Kolesnikov VG (1962) Location of frontal zones in the Norwegian Sea and their influence on the distribution of the atlantic-scandinavian herrings. Trudy BaltNIRO, 8 (in Russian)

Kolesnikov VG (1967) Oceanological Bases of Fishery Prognoses in the Norwegian Sea, AtlantNIRO, Kaliningrad (in Russian)

Korablev AA (1987) System of fronts in the Norwegian Energy-Active Zone of the Ocean. In: Results of Science and Techniques. Atmosphere, Ocean, Space – Program "Sections", VINITI, Moscow, Vol 8, 380–386 (in Russian)

Kostianoy AG, Nihoul JCJ, Rodionov VB (2004) Physical Oceanography of Frontal Zones in the Subarctic Seas, Elsevier, Elsevier Oceanography Series, Amsterdam.

Kuznetsov VL, Proshutinskiy AYu, Tarasov AB (1986) On the location and structure of frontal zones in the Norwegian Sea. Trudy AANII, 408: 56–67 (in Russian)

Nihoul JCJ (1986) Aspects of the northern Bering Sea ecohydrodynamics. In: Nihoul JCJ (Ed) Marine Interfaces Ecohydrodynamics, Elsevier, Amsterdam.

Nihoul JCJ (1993) Application of Mathematical Modelling to the Marine Environment, E. Riga Publication, Liege

Nihoul JCJ, Adam P, Brasseur P, Deleersnijder E, Djenidi S, Haus J (1993) Three-dimensional general circulation model of the northern Bering Sea's summer ecohydrodynamics. Cont Shelf Res, 13(5–6): 509–542

Nikolaev YuV, Alekseev GV (1989) Structure and Variability of Large-Scale Oceanographic Processes and Fields in the Norwegian Energy-Active Zone, Gidrometeoizdat, Leningrad (in Russian)

Rodionov VB, Kostianoy AG (1998) Oceanic Fronts of the North-European Basin Seas, GEOS, Moscow (in Russian)

Schumacher JD et al. (1979) A structure of front over the continental shelf of the Eastern Bering Sea. J Phys Oceanogr 9: 79–87

Smart JH (1984) Spatial variability of major frontal systems in the North Atlantic - Norwegian Sea area: 1980–1981. J Phys Oceanogr, 14(1): 185–192

Springer AM, McRoy CP, Flint MV (1996) The Bering Sea Green Belt: shelf-edge processes and ecosystem production. Fish Oceanogr, 5(3–4): 205–223

Stepanov VN (1960) Basic water convergences and divergences in the World Ocean. Bull Oceanogr Commission AN SSSR, 6: 15–22 (in Russian)

Terziev FS (Ed) (1999) The Bering Sea, Hydrometeorological Conditions, Gidrometeoizdat, St. Petersburg (in Russian)

Uda M (1938) Researches on "siome" or current rip in the seas and oceans. Geophys Mag, 11(4): 306–372

Walsh JJ et al. (1989) Carbon and nitrogen cycling within the Bering/Chukchi Sea: source regions for organic matter affecting AOU demands of the Arctic Ocean. Prog Oceanogr, 22: 277–359

Zatsepin AG, Kostianoy AG (1994) Fronts in the Ocean: barriers or mixing zones? Proceedings of the CREAMS'94 International Symposium, Fukuoka, Japan, Jan 24–26

How do the very small-sized aquatic microbes influence the very large-scale biogeochemical cycles?

Louis Legendre and Richard B. Rivkin

UPMC Université Paris 06, UMR 7093, Laboratoire d'Océanographie de Villefranche, 06230 Villefranche-sur-Mer, France; CNRS, UMR 7093, LOV, 06230 Villefranche-sur-Mer, France, legendre@obs-vlfr.fr
Ocean Sciences Centre, Memorial University of Newfoundland, St. John's, Newfoundland A1C 5S7, Canada, rrivkin@mun.ca

Abstract

Pelagic microbes have major roles in marine systems. There, they dominate the production and cycling of organic matter, and they mediate the biogeochemical cycling of biologically relevant chemical elements and climatically active gases. The present review focuses on general mechanisms that allow the very small-sized marine microbes to influence the very large-scale biogeochemical cycles that are crucial for climate processes. We explore the contrasting (or complementary) ideas that microbes are key components of marine pelagic food webs and biogeochemical cycles because of their physiological characteristics (e.g. high specific metabolic rates) coupled with large standing stocks, or (and) because of their unique positions in pelagic food webs, where they concurrently produce, consume and remineralise organic matter. We examine the hypothesis that the combined action of bottom-up (i.e. environmental) and top-down (i.e. food-web) processes channels inorganic and organic compounds toward microbes, which transform and redirect these compounds toward the environment (as inorganic and organic substances) and the remainder of aquatic food webs. Finally, we explore the responses of microbes and metazoans to climate-driven changes in environmental conditions, with particular reference to the Arctic.

Microbes in pelagic systems

Microbes are the smallest components marine pelagic food webs. Marine pelagic microbes are usually defined as cellular organisms <200 μm (e.g. Legendre and Rivkin 2008). Within the context of this definition, viruses, although very small (ca. 20–200 nm), are not typically considered microbes because they are not self-sustaining, cellular organisms. Marine pelagic microbes include heterotrophic

J.C.J. Nihoul and A.G. Kostianoy (eds.), *Influence of Climate Change on the Changing Arctic and Sub-Arctic Conditions*,

Bacteria and *Archaea* (0.2–ca. 1.2 μm), phytoplankton (cells ranging from 0.6 to 2,000 μm; most are ≤200 μm), heterotrophic and mixotrophic flagellates (1.5–15 μm; some heterotrophic dinoflagellates reach 30 μm) and ciliates (7–200 μm, or more). In this chapter as in Legendre and Rivkin (2008), heterotrophic *Bacteria* and *Archaea*, although evolutionarily very distinct, are combined in a functional category called "heterotrophic bacteria" (hereinafter bacteria).

Microbes encompass a wide taxonomic and nutritional diversity. Taxonomically, they include representatives from the three domains of life, i.e. *Archaea*, *Bacteria* and *Eucarya*. For their nutrition, microbes employ a wide array of mechanisms that include photoautotrophy, photolithotrophy, photoheterotrophy, chemolithtrophy, chemoheterotrophy, osmotrophy and phagotropy.

Legendre and Rivkin (2008) proposed an approach where heterotrophic microbes are grouped into a microbial hub, and larger organisms into a metazoan compartment. Using the microbial-hub approach, they concluded that heterotrophic microbes always dominate respiration in the euphotic zone, even when most particulate primary production is grazed by metazoa, and climate warming will increase microbial-hub respiration and channeling of primary production toward heterotrophic community respiration, and decrease the corresponding metazoan flows.

Pelagic microbes also have major roles in marine systems, where they dominate the production and cycling of organic matter, and they mediate the biogeochemical cycling of biologically relevant chemical elements and climatically active gases (e.g. CO_2, N_2O, DMS). The present chapter will focus on some general mechanisms that allow the very small-sized marine microbes to influence the very large-scale biogeochemical cycles.

In the present review, we explore the contrasting (or complementary) ideas that microbes are key components of marine pelagic food webs and biogeochemical cycles because of their physiological characteristics (e.g. high specific metabolic rates) coupled with large standing stocks, or (and) because of their unique positions in pelagic food webs, where they concurrently produce, consume and remineralise organic matter. We examine the *hypothesis* that the combined action of bottom-up (i.e. environmental) and top-down (i.e. food-web) processes channels inorganic and organic compounds toward microbes, which transform and redirect these compounds toward the environment (as inorganic and organic substances) and the remainder of aquatic food webs. References documenting the various processes described here are detailed in Legendre and Rivkin (2002, 2005, 2008).

Physiological characteristics, large standing stocks, and unique positions of microbes in pelagic food webs

The special roles of microbes in food webs and biogeochemical cycles are often explained by some of their *physiological characteristics* coupled with their *large standing stocks*. The physiological characteristics include: high turnover and

growth rates, e.g. up to 5 day^{-1} for phytoplankton), 3 day^{-1} (bacteria) and 1 day^{-1} (protozoplankton) (White et al. 1991; Ducklow and Carlson 1992; Rose and Caron 2007; Bec et al. 2008); a wide range of C:N ratios, e.g. 6.6 to >12 (phytoplankton), 4–4.5 (bacteria), and 4.5–6 (protozooplankton); high nucleic acid content; and rapid adaptation of bacteria via gene transfer agents (Button and Robertson 2001; Canchaya et al. 2003; Casjens 2003; Lang and Beatty 2007). The standing stocks of phytoplankton, bacteria and protozooplankton in the euphotic zone of oceans are: 0.78, 0.35 and 0.16 Pg C (total: 1.3 Pg C), which is one order of magnitude greater than the standing stock of mesozooplankton, i.e. 0.1 Pg C (Le Quéré et al. 2005).

To illustrate the large number of phytoplankton cells in oceans, Andersen (2008) imagined creating (in mind) a long string by placing side by side the 3.6×10^{25} phytoplankters (average diameter: 2 μm) that exist at any one instant in the euphotic zone (average depth: 100 m). Using the Earth and the Moon as reference points, he calculated that the string of phytoplankton cells would extend from the Earth to the Moon and back (i.e. 770,000 km roundtrips) 100 billion times (ten billion times in Andersen 2008)! Doing a similar calculation for the 3.6×10^{28} bacteria (average diameter: 1 μm) that exist at any one instant in the upper 200 m of the ocean (Whitman et al. 1998; about 10% of these are autotrophic cells) gives a string of cells that would extend from Earth to Moon and back 50 trillion times. The corresponding value for the whole ocean from surface to bottom (including the top 10 cm of marine sediments: 11.8×10^{28} bacteria) is 150 trillion times.

The special roles of microbes can be explained not only by their physiological characteristics and large standing stocks, but also (or alternatively) by their *unique positions in pelagic food webs*. To illustrate this point, Legendre and Rivkin (2008) examined the effect on bacterial activity of a progressive increase in the number of food-web links in a model (i.e. connections among compartments: food-web complexity). They found that increasing food-web complexity was accompanied by increase in the food-web channelling of organic carbon to bacteria, which led to increased bacterial respiration. For example, going from a model with 10 flows among trophic compartments to a model with 15 flows tripled bacterial respiration. In other words, while keeping constant the model parameters for bacteria (i.e. their physiological characteristics), the contribution of these organisms to heterotrophic community respiration increased with food-web complexity. Hence, the complexity of pelagic food webs and the accompanying feedbacks can account, at least in part, for the major role of bacteria in carbon cycling.

In order to illustrate *quantitatively* the points in the previous paragraphs, we use here a simple steady-state model that compares the effects of increasing physiological rates *versus* increasing the complexity of the food web, i.e. its internal linkages. Figure 1 shows the parameters (left side) and the modelled flows (right side) of a reference model and three variants. In all models, there is a flow of external resource into compartment A, a loss flow from each compartment, and flows among compartments. The “production” of compartments B, C, … is passed

to the next compartment (e.g. through predation), were it is partly lost; this process is repeated until the food web has used up all the resource supplied. The three modified models illustrate the respective effects of increasing the rate of loss of A (by 50%), adding recycling of resource from B to A, and adding recycling of resource from all compartments to A.

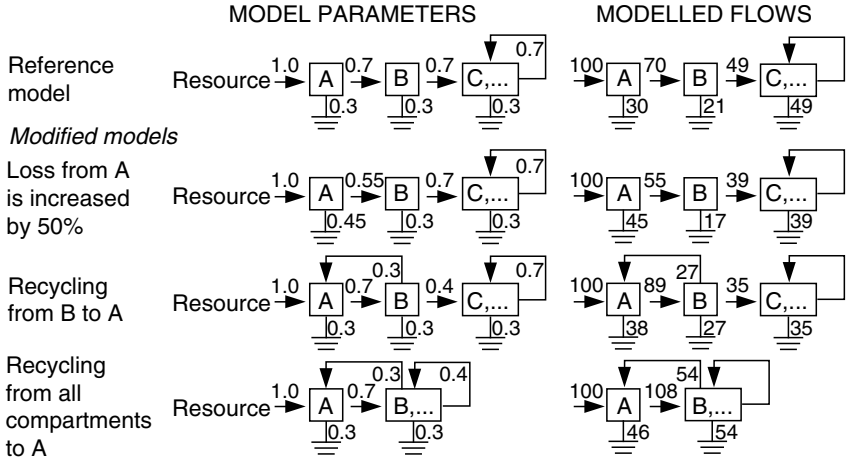

Fig. 1. Steady-state model that compares the effects of increasing physiological rates *versus* increasing the complexity of the food web, i.e. its internal linkages: reference model and three variants. *Left side*: model parameters; *right side*: modelled flows. Details are given in the text.

The left side of Fig. 1 shows the parameters of the reference and the three modified models. Because the models are in steady state, the sum of the output-flow parameters from any compartment is equal to 1.0. The right side of Fig. 1 shows the modelled flows for each model. Because the models are in steady state, the sum of output flows from a compartment is equal to sum of input flows into that compartment.

On the right side of Fig. 1, the external input of resource is the same in all models, i.e. 100 units of resource (in term of the chemical element considered, e.g. C, N, P). Because of recycling, the total input of resource into compartment A increases to 127 when there is recycling from B to A, and to 154 when there is recycling from all compartments to A. The loss from compartment A in the model with full recycling and in the model with increased loss is 46 and 45, respectively, showing that increasing the complexity of the food web (i.e. the number of internal linkages) has the same net effect on the modelled loss from A as increasing the physiological rate of loss by A. To better understand the results of the model, one can imagine that compartment A represents bacteria. In such a case, the loss from A would be bacterial respiration, and increasing the physiological rate of loss by A would be increasing the ratio of respiration to

resource uptake by bacteria. Figure 1 (right side) also shows that the amount of resource transferred by compartment A to the remainder of the food web is much higher in the model with full recycling (i.e. 108) and than in the model with increased loss (i.e. 55), which indicates that increasing the complexity of the food web (i.e. its internal linkages) increases the overall activity of the whole food web.

The *ecological interpretation* of the model is as follows. Compartment A receives input from both outside the food web (external resource) and within (recycling), it loses (i.e. remineralises or excretes) part of the resource it acquires, and it transfers the remainder to the food web. The resource could be an inorganic or an organic nutrient. The chemical element modelled could be C, N, P, etc. Compartment A corresponds to microbial compartments (autotrophic and/or heterotrophic) in real pelagic food webs. The model results have both ecological and biogeochemical significance, as explained in the following paragraphs.

The *food-web resources* can be dissolved or particulate. The threshold between the two size categories depends on the retention characteristics of the filters used to separate the filtrate from the particles, i.e. it is generally 0.7, 0.2 or 0.1 μm. In addition, researchers often distinguish between small and large particles. Here again, the threshold between the two size categories depends on the porosity of the filter used to separate the two types of particles, i.e. it is generally 2 or 5 μm.

The origin of *dissolved resources* is both external and internal to the food web. External resources are both inorganic and organic nutrients, from deep waters (upwelling, deep convection, ventilation) and continents (flowing fresh waters, i.e. rivers and groundwater, and atmosphere). Internal resources are inorganic and organic nutrients produced by autotrophs (phytoplankton exudation) and heterotrophs (recycling). The food-web use of dissolved resources is quite specialised, because specific metabolic rates (i.e. rates per unit biomass or size) are generally a direct function of size and surface to volume ratio. Given that microbes are small and have high turnover and growth rates, they (especially phytoplankton and bacteria) outcompete larger organisms in the uptake of dissolved resources.

In the food web, autotrophs and heterotrophs both contribute to the production of dissolved organic matter (DOM), but with different mechanisms. (1) Phytoplankton release part of their photosynthate as dissolved organic carbon (DOC). This is called exudation. (2) The organic materials consumed by heterotrophs often have a C:N ratio equal to or higher than their own. Hence, in order to maintain their internal stoichiometric balance, heterotrophs can release the excess elements as CO_2, NH_3 and DOM (or take up inorganic nutrients). This is called respiration or excretion, and more generally recycling (physiologists often use the term "excretion" for the release of both CO_2 and organic compounds). (3) The viral lysis of bacteria, phytoplankton and protozoa causes the release of cellular material in the surrounding medium. Respiration, excretion and loss due to viral lysis are called remineralisation.

The origin of *particulate resources* is also both external and internal to the food web. The external resources include organic particles from continents. The internal resources are organic particles produced by the food web, such as phytoplankton

cells, detritus and marine snow (e.g. faecal pellets, and transparent exopolymeric particles, TEP). The food-web use of particulate resources by microbes may include competition with larger organisms. On the one hand, protozoa generally consume small particles that are below the size that can be effectively ingested by metazoa (mostly bacteria and small phytoplankton), i.e. there is no competition between protozoa and metazoa. As an important exception to this, some heterotrophic dinoflagellates readily ingest diatoms and thus effectively compete with larger zooplankton (e.g. reviews of Sherr and Sherr 1994, 2008). In addition, the main grazers of mesozooplankton faecal pellets may be protozoa (Poulsen and Iversen 2008), and not copepods as usually thought (Iversen and Poulsen 2007). Bacteria indirectly compete with metazoa for large particles (phytoplankton, detritus and marine snow) in a unique way. Bacteria break down particles with exoenzymes (hence, making them unavailable to larger organisms), and take up the released DOM. Thus, heterotrophic microbes continually modify their environment to optimize the availability of essential resources while limiting the access of these same resources for other components of the pelagic food web.

Table 1. Relations between the size of food-web resources (origin: external and internal), the source of internal resources within the food web, and the use of resources by microbes *versus* metazoa.

Size of food-web resources	Source within the food web	Microbes versus metazoa
Dissolved (<0.7, <0.2, or <0.1 μm)	Phytoplankton and heterotrophs (i.e. from the bottom and the top of the food web)	Microbes outcompete metazoa in using dissolved resources
Small particles (<2, or <5 μm)	Mostly phytoplankton (i.e. from the bottom of the food web)	Microbes use small particles without competing with metazoa
Large particles (>2, or >5 μm)	Phytoplankton and heterotrophs (i.e. from the bottom and the top of the food web)	Microbes compete with metazoa for large particles

Table 1 summarises the relations between the *size of food-web resources* (their origin is both external and internal), the *source of internal resources* within the food web, and the *use of resources* by microbes *versus* metazoa. Because the internal resources come from the whole food web, it is convenient to divide the sources between the bottom of the food web, i.e. phytoplankton, and the top, i.e. metazoa, the heterotrophic microbes occupying an intermediate position. That unique position provides microbes with access to resources from both the bottom and the top of the food web. As a consequence, microbes use almost all the dissolved resources, and a significant share of the particulate resources, and they monopolise (or dominate the use of) external and internal resources. In other words, microbes not only utilise most of the resources, but they also prevent metazoa from accessing them, i.e. they "corner the market" of resources.

It follows from the previous paragraphs that because they dominate the use of resources, microbes play key roles in food webs. Autotrophic microbes (phytoplankton) used dissolved inorganic resources, i.e. in coastal waters they

compete with benthic autotrophs, and in the coastal and open ocean they compete with heterotrophic bacteria. Heterotrophic microbes use both dissolved and particulate resources. Concerning the inorganic and organic resources, bacteria compete with phytoplankton for inorganic nutrients, and are the dominant users of dissolved organic matter (there are a few reports indicating that some planktonic protozoa can also use DOM, e.g., Laybourn-Parry et al. 1997, but this is not of ecological significance). The small organic particles that are not efficiently grazed by metazoa are consumed by protozoa. The large organic particles are the object of a competition between microbes (bacteria and protozoa) and metazoa.

Food-web functioning

In this section, we examine the general *functioning of the pelagic food web*. In order to do so, we group various key food-web processes under three broad food-web functions: photosynthetic production (net of autotrophic respiration), which is due to phytoplankon (i.e. microbes), microbial heterotrophic activity, which is due to bacteria and protozoa, and metazoan activity, which is due to organisms larger than microbes (i.e. metazoa). The resulting conceptual model is shown in Fig. 2.

Net photosynthetic production (Fig. 2A) refers here to oxygenic photosynthesis, which differs from anoxygenic photosynthesis that also takes place in the water column of oceans (e.g. Lami et al. 2007; the ecological significance of aerobic anoxygenic phototrophic bacteria is presently poorly understood). Oxygenic photosynthesis (e.g. Falkowski and Raven 2007) uses as inputs CO_2, H_2O, inorganic nutrients and the free energy of sunlight (i.e. photons). Its outputs are particulate organic matter (POM; here, phytoplankton biomass), DOM (exudates) and O_2.

Microbial heterotrophic activity (Fig. 2B) refers to the heterotrophic microbial metabolism. The inputs are DOM (mostly used by bacteria), inorganic nutrients (for which there is competition between bacteria and phytoplankton), POM (bacteria and protozoa compete with metazoa) and O_2. The outputs are POM (i.e. microbial biomass), DOM and inorganic nutrients (resulting from excretion, nutrient regeneration and viral lysis) and CO_2.

Metazoan activity (Fig. 2C) refers to the metazoan metabolism. The inputs are POM (for which there is competition with bacteria and protozoa) and O_2. The outputs are POM (i.e. metazoan biomass, faecal material and various biological products, e.g. appendicularian houses), DOM and inorganic nutrients (resulting from excretion) and CO_2.

Figure 2 illustrates the interconnections among the three broad food-web functions. Outputs from one function are inputs into another. In steady state, net phytoplankton production and heterotrophic metabolism balance each other, i.e. A = B + C.

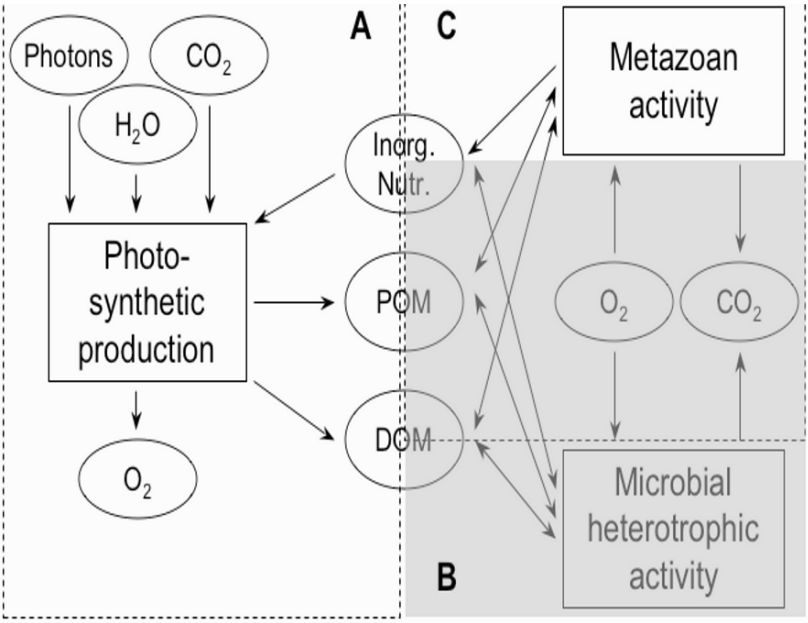

Fig. 2. Conceptual model that groups key food-web processes under three broad food-web functions: (**A**) photosynthetic production, (**B**) microbial heterotrophic activity, and (**C**) metazoan activity. Arrows: inputs and outputs for each function, and interconnections among functions. The three large rectangles specify the domains of the three food-web functions (**A** and **C**: dashed lines; **B**: shaded area).

In the euphotic zone of oceans, nutrients are not only recycled, but they can also be imported and exported. Conversely, organic matter (POM and DOM) can be exported, laterally and downwards. Figure 3 schematises the pelagic food web in the euphotic-zone context. The photosynthetic production (*PP*) that is fuelled by imported nutrients is called "new" (PP_{new}), and the *PP* that is based on recycled nutrients is called "regenerated" (PP_{reg}).

If we consider first Fig. 3A only (i.e. the simplest pelagic "food web"; it is not really a food web as it includes only phytoplankton), we see that the import of new nutrients and the export of organic matter balance each other. If we consider next Fig. 3A and B together (i.e. phytoplankton-microbial food web), we see that the import of new nutrients and the export of organic matter balance each other, and that microbial metabolism and nutrient recycling also balance each other. If we consider finally Fig. 3A–C together (i.e. complete pelagic food web), we see that the import of new nutrients and the export of organic matter balance each other, and that heterotrophic metabolism and nutrient recycling also balance each other. The roles of microbes in the balance between food-web processes (metabolism and nutrient recycling) and biogeochemical processes (import of new nutrients and export of organic matter) will be discussed in Section "Biogeochemical roles of microbes".

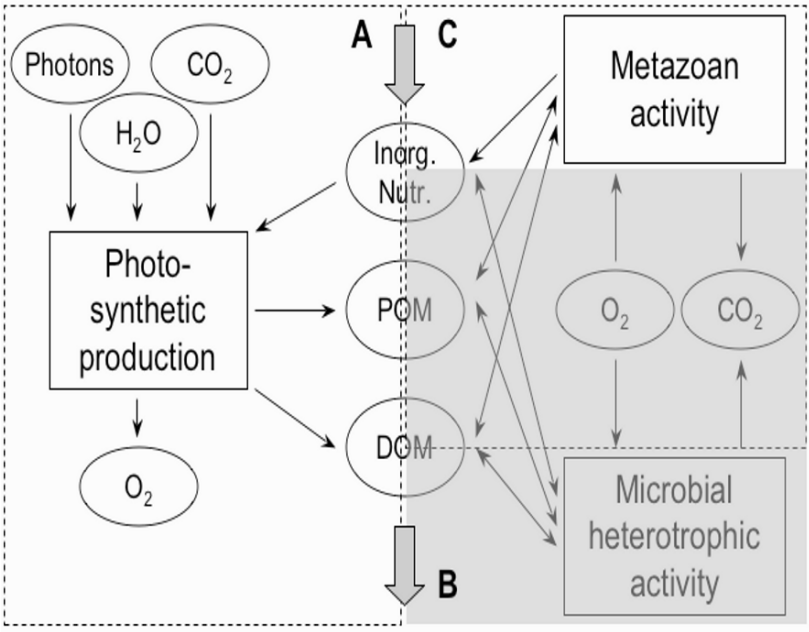

Fig. 3. Conceptual modem of the pelagic food web in the euphotic-zone context. Same as Fig. 2, with two additional, broad arrows representing the input of nutrients into, and the export of organic matter (POM and DOM) from the euphotic zone.

Our conceptual analysis of pelagic food webs has led us, so far, to the following conclusions concerning *food-web functioning*. (1) Microbes are key players in food webs because of both high metabolic rates and unique position in food webs. (2) They use almost all dissolved resources, and they have a significant share of particulate resources. (3) Because they monopolise a high share of resources, microbes are the main producers, remineralisers, and conduits of organic matter toward other food-web compartments.

We now briefly address the food-web roles of microbes with a *quantitative approach*. To do so, we used the food-web model of Legendre and Rivkin (2008) to which we added export flows (Fig. 4, left side). The model is in steady state, meaning that masses of model compartments are constant; its currency is carbon. The food-web model includes seven food-web compartments: particulate and dissolved *PP* (PHYTO-POC and PHYTO-DOC), bacteria (BACT), microzooplankton (μZOO), mesozooplankton (MZOO), larger organisms (LARGE), and faecal pellets (DETR, detritus). The compartments are interlinked by food-web carbon flows, and there are two components of export, i.e. faecal pellets and other organic materials (phytodetritus, etc.) The growth efficiencies of BACT, μZOO and MZOO are temperature-dependent.

Table 2. Respiration (R) in the euphotic zone for three food-web compartments – i.e. BACT (R_b), μZOO ($R_{\mu z}$) and metazoans (MZOO + LARGE, R_{met}) – expressed as a fraction of heterotrophic community respiration (R_c). The model was run for the microbial and the herbivorous food webs, i.e. the fraction of PHYTO-POC grazed by μZOO is larger in the microbial food web (i.e. 0.90) than in the herbivorous food web (i.e. 0.25). Values calculated at 15°C.

Food web (15°C)	R_b/R_c	$R_{\mu z}/R_c$	R_{met}/R_c
Microbial	0.56	0.18	0.27
Herbivorous	0.48	0.07	0.45

Table 2 gives the results of a modelling exercise showing that R of microbes (BACT + μZOO) is larger than R of metazoa (MZOO + LARGE), even when MZOO are the dominant grazers of PHYTO-POC (i.e. herbivorous food web). This result is consistent with the conclusion of our conceptual analysis that microbes are the main remineralisers of organic matter in the euphotic zone.

Biogeochemical roles of microbes

Section "Food-web functioning" was focussed on the *roles of microbes in food-web functioning*. We now examine the *biogeochemical roles of microbes*, i.e. their effects on flows of chemical elements. The present discussion is based on Fig. 3.

We previously concluded from Fig. 3 that heterotrophic metabolism and nutrient recycling are balanced, and we had explained that PP_{reg} is based on recycled nutrients. Hence, the biogeochemical processes of nutrient recycling, respiration and PP_{reg} are controlled by heterotrophs, which are dominated by microbes.

We also concluded from Fig. 3 that the export of organic matter and the import of new nutrients balance each other, and we had explained that PP_{new} is fuelled by imported nutrients. The import of new nutrients into the euphotic zone is determined by circulation and mixing patterns within the ocean and across the air-sea boundary. Hence, the biogeochemical processes of nutrient import, organic matter export and PP_{new} are controlled by the physics of the ocean and atmosphere. Do microbes play any role in these processes? The C:N ratio of heterotrophs is often smaller than the C:N of resources (the average C:N of marine plankton is 6.6; Redfield 1934), and the excess carbon from feeding is often released by heterotrophs as CO_2, DOM and detrital POM with high C:N (see above). As a result, the C:N of the organic matter that is exported from the euphotic zone is generally higher than 6.6 (Williams 1995; Loh and Bauer 2000; Hopkinson and Vallino 2005). It follows that heterotrophs (mostly microbes) influence the chemical composition of the organic matter that is exported downwards.

In Section "Food-web functioning", we identified and explained key roles of microbes *in food web functioning*. In the present section, we briefly identified and explained the roles of microbes *in biogeochemical* cycles. Our conclusions are as

follows. (1) Microbes largely control key biogeochemical processes, i.e. PP_{reg} and heterotrophic respiration. (2) They also influence the chemical composition of the organic matter that is exported out of the euphotic zone.

Environmental effects, including climate change

Until now, we have discussed food-web properties *independently of environmental conditions*. Do these conditions affect the metabolic rates and the food-web position of pelagic microbes? It is well known that the metabolic rates of organisms depend on both their characteristics (e.g. surface/volume ratio) and the environmental conditions (e.g. temperature, nutrients). In addition, because microbes access resources from both the bottom and the top of the food web, their position in the food web depends on food-web structure. The latter is largely controlled by environmental conditions. We have reported above the modelling result of Legendre and Rivkin (2008) that food-web complexity largely determines the role of microbes (see also Fig. 1). It follows that environmental conditions have strong effects on pelagic microbes.

The next point concerns the effects of *environmental changes* on pelagic microbes and biogeochemical fluxes. Such changes can be bottom-up or top-down. Examples of *bottom-up environmental changes* are the increasing ocean temperature and the decreasing nutrient concentrations caused by increased stratification. As a response to increasing water temperature, the metabolic rates of heterotrophic microbes will increase faster than those of both phytoplankton (López-Urrutia et al. 2006) and metazoans (because of higher surface/volume ratio), causing more recycling among microbes and less transfer to other compartments. As a response to decreasing nutrients, bacteria may compete more efficiently for inorganic nutrients than phytoplankton because their affinity for nutrients is generally lower than that of phytoplankton (Kirchman 2000). Examples of *top-down environmental changes* are the drastic reduction in the numbers of top predators by commercial fisheries, and the introduction of invasive species. As a consequence, future marine food webs may be different than presently, e.g. the often dominant crustaceans may be replaced by other organisms, which would cause changes in the chemical composition of export (e.g. the C:N of marine seston is positively related to salp and appendicularian abundance, and negatively to calanoid copepods; Hassett et al. 1997). Also, future marine food webs may be less complex than presently, e.g. by elimination of top predators, causing less nutrient to be recycled toward microbes, and thus lower PP_{reg}.

Table 3. Relative difference (%) between R_x/R_c at 25°C and 15°C for three food-web compartments. Same model as in Table 2.

Food web (25–15°C)	R_b/R_c	$R_{\mu z}/R_c$	R_{met}/R_c
Microbial	+6%	+22%	–27%
Herbivorous	+2%	+2%	–3%

In our conceptual analysis, above, we identified *temperature* as one of the most important bottom-up environmental forcings. Seawater (and air) temperatures are predicted to continue increasing as a result of increases in the concentrations of greenhouse gases in the atmosphere. Increased water temperature would cause the metabolic rates of microbes to increase faster than those of metazoans, causing a shift in recycling from metazoa toward microbes and less transfer of organic matter from microbes toward other compartments. We now examine this conclusion *quantitatively*, using the same food-web model as previously. Table 3 gives the results of a modelling exercise showing that with increasing temperature, R of microbes increases and R of metazoa decreases, even when MZOO are the dominant grazers of PHYTO-POC (herbivorous food web). This result is consistent with the conclusion of our conceptual analysis that with increasing temperature, there will be more recycling among microbes, and thus less transfer to other compartments.

We further explore the potential effects of changes in temperature and pelagic food-web type on food-web functioning and biogeochemical fluxes using the *microbial hub approach* proposed by Legendre and Rivkin (2008), where BACT and μZOO are grouped into the microbial hub, and larger organisms into a metazoan compartment. Because as stressed by Legendre and Rivkin (2008), only community respiration (R_C) is always $\leq PP$, it follows that R is the only additive food-web property, and the fraction of PP that is respired by a heterotrophic compartment is the only metric that can be used for comparing compartments. As a consequence in the microbial-hub approach, we calculate five summary R flows among three broad food-web compartments: phytoplankton, the microbial hub and metazoa. The values of the summary R flows are computed from the modelled flows for the food-web model on left side of Fig. 4 (they could be computed from the flows of any model, or obtained by field observations). The five flows in the microbial-hub version of the model correspond to different components of community respiration (R_C): metazoan R, R_{met}; direct metazoan channelling of PP_T toward R_C, $R_{met}(PP_T)$; microbial hub R, R_{hub}; direct microbial-hub channelling of PP_T toward R_C, R_{hub} (PP_T); and difference between the transfer of carbon from the hub to metazoan R, and from metazoa to the hub R, R_{met}(hub) (this flow can be positive or negative, hence the double arrow in Fig. 4).

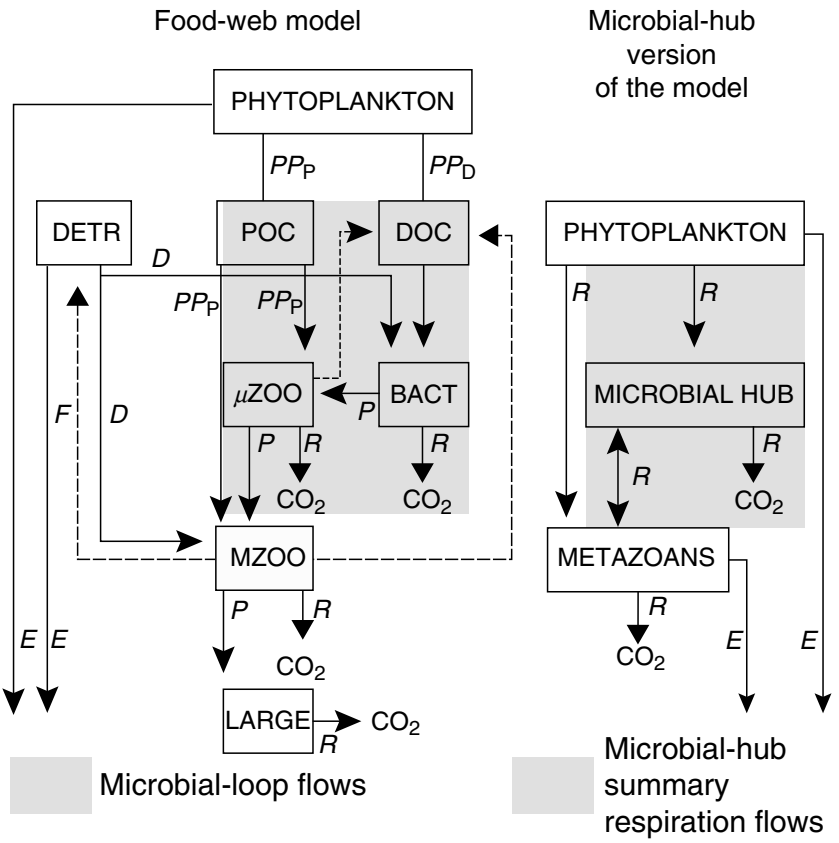

Fig. 4. *Left side*: food-web model of Legendre and Rivkin (2008) with added export flows. The seven food-web compartments are: particulate and dissolved *PP* (PHYTO-POC and PHYTO-DOC), bacteria (BACT), microzooplankton (μZOO, <200 μm), mesozooplankton (MZOO, 0.2–2.0 mm), larger organisms (LARGE, >2 mm), and faecal pellets (DETR, detritus). The two components of export are: faecal pellets, and other organic materials (phytodetritus, etc.) The arrows represent carbon flows into and out of compartments: primary production (*PP*, particulate, PP_P, and dissolved, PP_D); heterotrophic detritus consumption (*D*), excretion (*E*), egestion (*F*), production (*P*) and respiration (*R*). *Right side*: application of the microbial-hub approach to the model: PHYTO-POC and PHYTO-DOC are merged into PHYTO, μZOO and BACT make up the microbial hub (HUB), and MZOO are combined with LARGE into the metazoan compartment (METAZ). The arrows represent summary *R* flows. The HUB consumes PHYTO, receives carbon from METAZ, and redirects the carbon it ingests towards CO_2 (respiration) and METAZ. Solid arrows: forward flows; dashed arrows: backward flows; double-headed arrow: net flow possible in both directions. Shaded rectangles: microbial-loop flows, and summary *R* flows resulting from the microbial-hub approach. Details are given in the text.

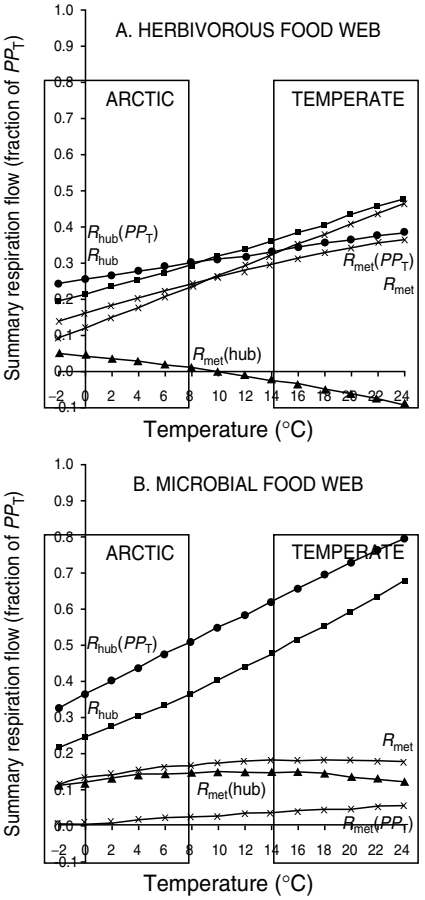

Fig. 5. Responses of the five summary *R* flows (microbial-hub approach, Fig. 4) to temperature for the (**A**) herbivorous and (**B**) microbial pelagic food webs. All values are expressed as a percentage of PP_T (i.e. maximum potential R_C). There are two temperature zones identified: arctic (i.e. –2°C to 8°C) and temperate (i.e. 14–24°C); the minimum temperature for temperate conditions (i.e. 14°C) corresponds to the transition in the climatology of heterotrophic bacteria and the photosynthetic cyanobacterium *Synechococcus* reported by Li (1998; i.e. direct relationship of annual average abundances to annual average temperature below 14°C, and no relationship above).

Figure 5 shows the values of the five summary *R* flows for the microbial and the herbivorous pelagic food webs, under changing temperature in *Arctic and temperate conditions*. All summary flows are expressed as a percentage of PP_T (which provides the value of maximum potential R_C). For the herbivorous food

web (Fig. 5A), the five summary *R* flows show changes with temperature: in both Arctic and temperate conditions, there are slight increases of the four microbial-hub and metazoan *R* flows with temperature. The fifth flow, R_{met}(hub), is positive in Arctic conditions, meaning that the microbial hub channels more carbon towards R_{met} than metazoa channel carbon toward R_{hub}, and the reverse takes place in temperate conditions. For the microbial food web (Fig. 5B), there are strong increases of microbial-hub *R* flows with increasing temperature in both Arctic and temperate conditions, whereas there is little change in the other summary *R* flows. Figure 5 shows that some responses to temperature increase are similar in Arctic and temperate conditions, and others are different. *Similar responses* to temperature increase in the two conditions are: for the herbivorous food web, small increases of metazoan and microbial-hub *R* flows, and for the microbial food web, strong increases of microbial-hub *R* flows. *Different responses* of the herbivorous food web to temperature increase in the two conditions are: in Arctic conditions that the microbial hub channels more carbon towards R_{met} than metazoa channel carbon toward R_{hub} (decreases with increasing temperature), and the reverse occurs in temperate conditions, i.e. the microbial hub channels less carbon towards R_{met}.

We conclude from Fig. 5 that temperature increase in Arctic and temperate waters will have different effects on respiration flows in the euphotic zone depending on the pelagic food web that is present. With the *microbial food web* present (e.g. non-bloom conditions, including under the ice cover), there will be strong increases of microbial-hub *R* flows. With the *herbivorous food web* present (e.g. phytoplankton blooms, in winter-spring in temperate waters and after the melting of the ice-cover in the Arctic), there will be slight increases of the four metazoan and microbial-hub *R* flows, and a decrease in the channelling of carbon by the microbial hub channels towards R_{met}. Concerning the latter, under Arctic conditions, the microbial hub will channel more carbon towards R_{met} than metazoa channel carbon toward R_{hub}, whereas under temperate conditions, the reverse will take place, i.e. the microbial hub will channels less carbon towards R_{met} than metazoa channel carbon toward R_{hub}. *Overall*, increasing temperature will not only increase respiration in the euphotic zone, but it will reinforce the role of microbes in community respiration. This is consistent with the conclusions of both our conceptual analysis above, and our modelling exercise on the effect of temperature on microbial and metazoan *R* (Table 3).

General conclusions

Our *initial hypothesis* was that the combined action of bottom-up (i.e. environmental) and top-down (i.e. food-web) processes channels inorganic and organic compounds toward microbes, which transform and redirect these compounds toward the environment (as inorganic and organic substances) and the remainder of aquatic food webs.

In the present study, we found that: microbes are *key players in food webs* because of both high metabolic rates and unique position (access resources from both the bottom and the top of the food web); microbes also have a major role in regulating *biogeochemical cycles*, because they largely control key biogeochemical processes, and influence the chemical composition of the organic matter that is exported from the euphotic zone; there are strong effects of bottom-up and top-down *environmental changes* on the biogeochemical activity of microbes. We also found that with *increasing temperature*, there will be more recycling among microbes, and thus less transfer to other compartments. Finally, we concluded that temperature increase *in Arctic and temperate conditions* will have different effects on respiration flows in the euphotic zone depending on the pelagic food web that is present. *Overall*, increasing temperature will not only increase respiration in the euphotic zone, but it will reinforce the role of microbes in community respiration.

Acknowledgments

This research was supported by funding from CNRS and the Université Pierre et Marie Curie, France, to the Laboratoire d'Océanographie de Villefranche (LL), and by grants from the Natural Sciences and Engineering Research Council of Canada to RBR.

References

Andersen RA (2008) Moon boards. Limnol Oceanogr Bull, 17, 8–9

Bec B, Yves C, André V, David M, Souchu P (2008) Growth rate peaks at intermediate cell size in marine photosynthetic picoeukaryotes. Limnol Oceanogr, 53, 863–867

Button D, Robertson BR (2001) Determination of DNA content of aquatic bacteria by flow cytometry. Appl Environ Microbiol, 67, 1636 –1645

Canchaya C, Proux C, Fournous G, Bruttin A, Brüssow H (2003) Prophage genomics. Microbiol Mol Biol Rev, 67, 238–276

Casjens S (2003) Prophages and bacterial genomics: what have we learned so far? Mol Microbiol, 49, 277–230

Ducklow HW, Carlson CA (1992) Oceanic bacterial production. Adv Microb Ecol, 12, 113–181

Falkowski PJ, Raven JA (2007) Aquatic Photosynthesis, 2nd Ed. Princeton, NJ: Princeton University Press

Hassett RP, Cardinale B, Stabler LB, Elser JJ (1997) Ecological stoichiometry of N and P in pelagic ecosystems: comparison of lakes and oceans with emphasis on the zooplankton-phytoplankton interaction. Limnol Oceanogr, 42, 648–662

Hopkinson CS, Vallino JJ (2005) Efficient export of carbon to the deep ocean through dissolved organic matter. Nature, 433, 142–145

Iversen MH, Poulsen LK (2007) Coprorhexy, coprophagy, and coprochaly in the copepods Calanus helgolandicus, Pseudocalanus elongatus, and Oithona similis. Mar Ecol Prog Ser, 350, 79–89

Kirchman DL (2000) Uptake and regeneration of inorganic nutrients by marine heterotrophic bacteria. In DL Kirchman (Ed), Microbial Ecology of the Sea (pp 261–288). New York: Wiley Liss

Lami R, Cottrell MT, Ras J, Ulloa O, Obernosterer I, Claustre H, Kirchman DL, Lebaron P (2007) High abundances of aerobic anoxygenic photosynthetic bacteria in the South Pacific Ocean. Appl Environ Microbiol, 73, 4198–4205

Lang AS, Beatty JT (2007) Importance of widespread gene transfer agent genes in alphaproteobacteria. Trends Microbiol, 15, 54–62

Laybourn-Parry J, James MR, McKnight DM, Priscu J, Spaulding SaA, Shiel R (1997) The microbial plankton of Lake Fryxell, southern Victoria Land, Antarctica during the summers of 1992 and 1994. Polar Biol, 17, 54–61

Legendre L, Rivkin RB (2002) Fluxes of carbon in the upper ocean: regulation by food-web control nodes. Mar Ecol Prog Ser, 242, 95–109

Legendre L, Rivkin RB (2005) Integrating functional biodiversity, food-web processes and biogeochemical carbon fluxes into a conceptual approach for modeling the upper ocean in a high-CO_2 world. J Geophys Res, 110, C09S17, doi:10.1029/2004JC002530

Legendre L, Rivkin RB (2008) Planktonic food webs: Microbial hub approach. Mar Ecol Prog Ser, 365, 289–309

Le Quéré C, Harrison SP, Prentice IC, Buitenhuis ET, Aumont O, Bopp L, Claustre H, da Cunha LC, Geider R, Giraud X, Klaas C, Kohfeld KE, Legendre L, Manizza M, Platt T, Rivkin RB, Sathyendranath S, Uitz J, Watson AJ, Wolf-Gladrow D (2005) Ecosystem dynamics based on plankton functional types for global ocean biogeochemistry models. Global Change Biol, 11, 2016–2040

Li WKW (1998) Annual average abundance of heterotrophic bacteria and Synechococcus in surface ocean waters. Limnol Oceanogr, 43, 1746–1753

Loh AN, Bauer J (2000) Distribution, partitioning and fluxes of dissolved and particulate organic C, N, and P in the eastern North Pacific and Southern Oceans. Deep-Sea Res, 47, 2287−2316

López-Urrutia A, San Martin E, Roger P Harris RP, Irigoien X (2006) Scaling the metabolic balance of the oceans. Proc Natl Acad Sci, 103, 8739–8744

Poulsen LK, Iversen MH (2008) Degradation of copepod fecal pellets by the plankton community in a coastal area. Mar Ecol Prog Ser, 367, 1–13

Redfield AC (1934) On the proportions of organic derivations in sea water and their relation to the composition of plankton. In RJ Daniel (Ed), James Johnson Memorial Volume (pp 177–192). Liverpool: University Press of Liverpool

Rose JM, Caron DA (2007) Does low temperature constrain the growth rates of heterotrophic protists? Evidence and implications for algal blooms in cold waters. Limnol Oceanogr, 52, 886–895

Sherr EB, Sherr BF (1994) Bacterivory and herbivory: key roles of phagotrophic protists in pelagic food webs. Microb Ecol, 28, 223–235

Sherr EB, Sherr BF (2008) Heterotrophic dinoflagellates: a significant component of microzooplankton biomass and major grazers of diatoms in the sea. Mar Ecol Prog Ser, 352, 187–197

White PA, Kalff J, Rasmussen JB, Gasol JM (1991) The effect of temperature and algal biomass on bactenal production and specific growth rate in freshwater and marine habitats. Microb Ecol, 21, 99–112

Whitman W, Coleman D, Wiebe W (1998) Prokaryotes: the unseen majority. Proc Natl Acad Sci, 95, 6578–6583

Williams PJ (1995) Evidence for the seasonal accumulation of carbon-rich dissolved organic material, its scale in comparison with changes in particulate material and the consequential effect on net C/N assimilation ratios. Mar Chem, 51, 17−29

Social, economic, legal and political issues of the Russian Arctic

Igor S. Zonn

Engineering Scientific Production Center for Water Economy, Reclamation and Ecology, Moscow, Russia, igorzonn@mtu-net.ru

Abstract

The Arctic zone geopolitically is very important for all Arctic states. And it became such for Russia especially after breakdown of the USSR and reduction of its territory after separation of its southern and western regions because of spatial re-orientation of Russia development and acknowledgement of the role of Arctic in the long-term strategy of economic development. This area gives 95% of gas, 75% of oil, 90% of tin, the greater part of gold and diamond production. Arctic has enormous economic significance for Russia in view of the prospective development of hydrocarbons. Potential geological resources of oil and gas in Arctic and nearby regions are evaluated at over 200 billion tons and 400 trillion cubic meter, respectively. However, development of these resources occurring in extreme natural-climatic conditions will demand scale foreign investments. And we should not forget about the issues of their transportation, storage and processing. In the recent years the Arctic sea region turned into a source of international tension due to rivalry in getting access to its natural resources. This is caused, to some extent, by the fact that the legal regime of Arctic has not been determined in full so far. Installation in late 2007 of the Russian flag on the bottom of the Arctic Sea near the North Pole provoked the beginning of the "Great Northern Game" the stakes in which are extension of a continental shelf for development of natural resources. Already now it can be said with assurance that the 21st century will become the time of struggle for the Arctic expanses and will give rise to ambiguous response from the Arctic countries that is difficult to predict.

The Arctic Zone of Russia (AZR)

It is generally known that the Arctic is an area around the Earth's North Pole including the Arctic Ocean with its seas and islands and also the margins of Eurasia and North America surrounding it. There are many notions of the Arctic and, thus, determination of its borders.

J.C.J. Nihoul and A.G. Kostianoy (eds.), *Influence of Climate Change on the Changing Arctic and Sub-Arctic Conditions*,

The southern border of Arctic coincides with the southern boundary of the tundra zone; its area being 27 million square kilometer. If we limit Arctic in the south by the Northern Polar Circle, then its area will be 21 million square kilometer. The Arctic Zone of Russia (AZR) as it was defined in 1989 by the State Commission at the Council of Ministers for the Arctic includes the territories of the Murmansk and Arkhangelsk regions, the Nenets, Yamalo-Nenets, Taimyr (Dolgano-Nenets) and Chukotka Autonomous Areas, the Republic of Saha (Yakutia) as well as lands and islands mentioned in the Resolution of the USSR Central Executive Committee of April 15, 1926 "On Declaration of the USSR Territory, Lands and Islands Located in the Arctic Ocean", the inland waters and a territorial sea near the northern coast of the Russian Federation.

The marine part of Russian Arctic comprises the water areas in the sectors with the apex in the North Pole and with the base being the Arctic coast. The sides of these sectors are formed by meridians passing through the terminal points on the coasts of the Arctic states.

The area of the Russian sector is approximately 9.46 million square kilometer, including water area – 6.8 million square kilometer and continental shelf – 6.19 million square kilometer. An area of 5.14 million square kilometer (70%) is permanently covered by the Arctic ice, out of which 1.5 million square kilometer – by the pack ice.

The length of the Russian coast is 28,000 km, and together with the islands – some 62,000 km.

At present many researchers both in Russia and abroad acknowledge that the Arctic is the giant potential reserve of natural resources that is capable to meet the needs of the mankind.

For Russia the Arctic zone with the nearby territories of the North is:

- About 30 billion cubic meter of the forest stock, 40% of the freshwater stock, 50% of the sea products, over one million heads of northern reindeers, a unique herd (about 4,000 heads) of the musk ox, a considerable community of walrus, Greenland seals, ringed seal, white whale
- About 50,000 of Ross' gulls, 30,000 of red-breasted geese, 15,000 of Bewick's swans (all included in the Red Book)
- 15,000 km^3 of fresh water reserves in continental ice
- 28,305,374 ha (4.1% of the area) of specially protected natural territories
- Of the world reserves of mineral deposits (in %): 30 – diamonds, 20 – platinum metals and nickel, 15 – copper, 10 – cobalt, 10 – oil (without a shelf area), 30 – natural gas, 50 – apatites, 15 – tin, 6–8 – tungsten and mercury, 35 – niobium
- Of the Russian reserves of mineral deposits (in %): 40 – gold, 60 – oil, 60–90 – gas, coal, nickel, copper, antimony, cobalt, tin, tungsten, mercury, apatite, phlogopite, 90 – chromium and manganese, 97 – platinum metals, 100 – diamond ores and vermiculite
- Of the Russian production level (in %): 100 – diamonds, antimony, apatite concentrate, phlogopite, vermiculite, rare metals and rare earth metals, 98

– platinoids, 95 – gas, 90 – nickel and cobalt, 60 – copper and oil, about 50 – forest and fishery products (Dodin 2005).

In general, AZR provides 1/5 of the national income and about 60% of the total export.

The region is known for its unity, both in terms of natural science and from the socioeconomic viewpoint. This includes:

- Severe climate with a long winter and a short vegetation period
- Similar hydrography (e.g. numerous lakes, waterlogging), covering basins of many rivers flowing into the Arctic Ocean (other than the largest rivers, such as North Dvina, Pechora, Ob, Yenisey, Lena, Kolyma)
- Wide extension (over the greater part of the territory) of permafrost rocks
- Poor flora and fauna, similarity of structure and functioning of ecosystems
- Typological similarity of traditional economic branches (domination of large herds of reindeers, offshore hunting and fishing) over a large territory, poor development of farming (in fact, only urban farm development – vegetable growing, meadow management)
- Similar industrial development – prevailing of spot-like extraction industry
- Similarity of the ethno-demographic structure of the population, a settlement pattern (Russian Arctic 1996)

Some of the mentioned factors are responsible for the well-known high sensitivity of the natural environment and instability of the Arctic landscapes to anthropogenic impacts: even insignificant impacts lead to serious disturbance of the natural environment the consequences of which are felt during a very long time.

The geographical position of Arctic, its sizes and severe climatic conditions are the main factors impeding its development.

The difficulties to be met in Arctic development:

- The need to cope with vast expanses
- The need of adaptation to the most severe natural conditions
- Remoteness from large economic, administrative and political centers of Russia and international markets
- Selection of the developed resources with regard to transport accessibility of a particular region
- Hot spot nature of resources development

The population of Russian Arctic

The population of Russian Arctic is approximately two million people that live in the North (from 1990 to 2000 the population outflow was one million people), 16% of the population lives in the European North; 81% of the population lives in the Asian North. About 80% of the population lives in 40 small towns (with the population over 10,000). Large cities (with the population over 100,000) are

Murmansk, Arkhangelsk, Syktyvkar, Vorkuta, Severodvinsk, Ukhta, Norilsk. The population of the Murmansk Region is 750,000 people (40%), the population density is 7 men/km^2. The population of the Yamalo-Nenets Area is 500,000 people (27%), the population density – 0.7 men/km^2. The population of the Taimyr Area (including Norilsk industrial region) is 327,000 people (18%), the population density – 0.4 men/km^2. The population of the Chukotka Area is 157,000 people (8%), the population density – 0.2 men/km^2. The population of Arctic regions of Yakutia is 82,000 people (4%), the population density – 0.2 men/km^2.

Small native peoples of Arctic are the peoples inhabiting the areas of the North, Siberia and Far East the territories of traditional settlement of their predecessors, maintaining the traditional way of life and trades; they number less than 50,000 people that identify themselves as independent ethnic communities.

In the Russian Arctic there are 27 small peoples numbering approximately 200,000. They are spread over the whole territory. Their average lifespan is 49 years. Only about 50% has the elementary and secondary education. The unemployment level here is four times higher than the average for the northern subjects of Russia. Their traditional occupations are reindeer rearing, hunting, fishing, hunting sea animals, and handicraft. And they contribute only 0.4% of GNP of the northern subjects of Russia.

Specific structure of the population

1. Very low population density.
2. The native population is scattered over the whole territory.
3. The newcoming population concentrates in the industrial development centers.

Causes of disastrous conditions of the northern peoples:

- Extreme natural and climatic conditions for living
- Underpopulation
- Remoteness from economic centers
- Dispersed settlement
- Breakup of traditional economic sectors and their low efficiency
- Archaic way of life
- Sharp life modernization
- Technogenic destruction of the habitat as a result of nuclear tests and intensive management of natural resources, including production of rare-earth elements
- Survival of paternalistic attachments
- Unreadiness for market relations

Oil and gas of Russian Arctic

Russian Arctic is a new fuel base. At present here more than over 100 million tons of oil are produced here. Among the ten major oilfields there are Samotlor, Priobsky, Fedorovsky, Lyantorsky, Mamontovsky and others.

In 1989 in the Pechora Sea shelf (950 km from Murmansk) the Prirazlomnoye oilfield was discovered. Initial geological reserves are evaluated at 230 million tons.

By 2010 it is planned to extract 7.5 million tons of oil a year in the Prirazlomnoye oilfield. Oil delivery by tankers.

In the recent years there were explored:

West-Siberian province

Supergiant gas fields:

- Urengoy 7.29 trillion cubic meter
- Yamburg 4.78 trillion cubic meter
- Bovanenkovskoye 4.92 trillion cubic meter
- Zapolyarny 3.53 trillion cubic meter
- Russian and others

Barents-Kara province

Supergiant gas condensate fields:

- Shtokman 3.2 trillion cubic meter
- Rusanovsky (Kara Sea) 3.0 trillion cubic meter
- Leningradsky (Kara Sea) 3.0 trillion cubic meter
- Ludlovsky – gas field

Seventy percent of the explored natural gas reserves in Russia (47.2 trillion cubic meter) are concentrated in the Yamalo-Nenets Autonomous Area. From this place gas will be supplied to Europe via the Baltic pipeline system.

Table 1 presents evaluation of the recoverable potential of oil and gas resources in the Arctic water area.

Table 1. Oil and gas resources in the arctic water area.

Country, sea, region	Oil (billion tons)	Gas (trillion cubic meter)
Arctic	20.0–46.0 (to 66)	36.5–83.0 (to 100.5)
Russia	11.0–24.0	25.5–57.0
Barents	3.0–8.0	9.0–13.0
Kara	5.0–6.0	10.0–30.0
Laptev	0.5–2.0	1.5–2.0
East Siberian	2.0–6.0	3.5–8.0
Chukchee	0.5–2.0	1.5–4.0
Potential resources	200.0	400.0

Russian Arctic economy

The economic development of Arctic in the Soviet period was characterized by:
- Selective industrial development of natural resources that was dictated either by the current needs of the country, in general, or the needs of the Northern Sea Route development but limited by inadequate prospecting of natural resources.
- Selection of resources for development with regard to transport accessibility of a particular region.
- The result of two above factors is a spot-like development of Arctic with establishment of several localized centers not connected with each other.

The post-Soviet period is characterized by:
- Opening and development of oilfields.
- Development of the infrastructure related to development of oil and gas resources.
- Development of the pipeline transport.
- Gradual transition from a spot-like to frontal pattern.
- Growth of transport tariffs leads to a greater isolation of the Arctic region from the rest of the country.
- Growing cost of power is a hindrance for future industrial and social development.

Among the major industrial centers in Russian Arctic there are the following: Arkhangelsk – Machine-building complexes for forestry and sea industry; Murmansk – Sea industry complex, machine-building, construction industry; Vorkuta – Coal and construction industries; Norilsk – Nonferrous metallurgy; Ukhta – Oil refining, gas processing, chemical industry (The Arctic 2002).

Arctic regional direction

The national marine doctrine in the Arctic region adopted by the Russian government is determined by special importance of ensuring free passage for the Russian fleet to the Atlantic Ocean, abundant natural resources in the exclusive economic zone and continental shelf of Russia, the decisive role of the Northern Fleet for the country defense from the sea and ocean and also a growing significance of the Northern Sea Route for sustainable development of Russia.

In view of the above the following long-term targets were identified:
- Investigation and development of Arctic with a view to develop the export industries, priority coping with social problems
- Protection of the Russian interests in Arctic

- Construction of ice-class ships for sea carriages, specific ships for fish, research and other special-purpose fleet
- Taking into consideration the country's interests in exploration and development of biological and mineral resources in the exclusive economic zone and on the continental shelf of Russia
- Creation of conditions, including with utilization of the region capacities, for basing and use of the elements of marine potential for defense of sovereignty, sovereign and international rights of Russia in the Arctic region
- Restriction of foreign naval activity in the agreed regions and zones on the basis of bilateral and multilateral agreements with the leading sea powers
- Ensuring the national interests of Russia in relation to the North Sea Route, centralized state management of this transport system, provision of ice-breaking services and granting of equal access for the interested carriers, including foreign
- Renovation and safe operation of the nuclear ice-breaker fleet
- Ensuring the interests of Russia at delimitation of the sea space and bottom of the Northern seas among the Arctic littoral states
- Consolidation of efforts and resources of the federal center and subjects of the Russian Federation for development of the arctic shipping, sea and river delta ports and "Northern Delivery" as well as information systems supporting these activities

Legal regional of Arctic

Sectoral principle

The international legal regime of Arctic is of key significance taking into consideration opening here of oil and gas fields, successful prospecting of solid mineral deposits and, as a result, appearance of various territorial claims of the Arctic states.

Official Russian claims to the Arctic sector are presented in the following documents:

Note-Dispatch of the Russian Government of September 20, 1916 informed that the islands Genrietty, Zhanetty, Bennets, of the Solitude, Novosibirsk, Wrangel, New land, Kolguev, Vaigach and others belong to Russia "because their belonging to the territory of the Empire had been generally recognized for many centuries"; Memorandum of the Soviet Government of November 4, 1924 confirmed this Note-Dispatch. In 1926 the Resolution of the Presidium of the USSR Central Executive Committee "On Declaration of the USSR Territories, Lands and Islands in the Arctic Ocean" declared the geographical Arctic space in the form of a sector

between meridians 32°04'35" E.L. and 168°49'30" W.L. (without the eastern islands of the Spitsbergen Archipelago).

The borders of polar sectors are not likened to state borders, while the establishment of a polar sector does not predetermines the legal status of the marine space in this sector (i.e. it does not refer either to the bottom or fish resources). The rights of the USSR in the Arctic regions belonging to its territory were supported by the USSR Law "On the State Border" of 1982, the Decree of the Presidium of the USSR Supreme Council "On the Continental Shelf of the USSR" of 1968. These regulatory-legal acts were included into the Russian legislation.

In 1998 the Draft Federal Law "On the Arctic Zone of the Russian Federation" was submitted for consideration to the RF State Duma (Kovalev 2003).

It should be noted that Canada adheres to the sectoral principle, too. It means that the national legislation prevails over the international one.

The second "Internationalization" principle that was proposed still in the early 1970s is supported by USA, Norway, Denmark

The followers of this principle have certain differences and there is no single approach to this issue.

The universal norms defining the general regime of an open sea shall be applicable in full to the Arctic water space.

Regional approach to addressing the Arctic issues on the basis of wide cooperation of the Arctic countries.

Partial internationalization of Arctic beyond the 200-mile exclusive economic zone.

The USA will benefit more from internationalization of the high-latitude zone of Arctic beyond the 200-mile line from the Canadian and Russian coasts.

In the recent decade the process of Arctic internationalization gains momentum and is entitled to success, which is facilitated by the Arctic Council established in 1996 comprising eight Arctic countries.

Legal hot spots in Arctic

Let us consider briefly the historical steps made for coping with these "hot spots" (Table 2). In 1974 USSR suggested Norway carry out delimitation of the sea space on the basis of the "Soviet polar sector" border. Norway having no Arctic sector of its own insisted on application of the median line concept.

Table 2. Legal hot spots in arctic.

Norway–Russia	Delimitation of 175,000 km^2 of the Russian part of the Barents Sea shelf
Denmark–Canada	Small uninhabited Hansa Island locating between the Greenland and the Buffin Land
USA–Canada	Northwest Passage. Dispute over the marine border in the Man Bay
USSR–Russia–USA	Delimitation of borders of the Bering and Chukotka Seas

Then in 1977 Norway declared the exclusive economic zone near its coast; Norway declared a fish protection zone 200 nautical mile wide around Spitsbergen and Bear Island in violation of the 1920 Paris Treaty about Spitsbergen (the Treaty did not entitle Norway to spread its sovereign rights and exclusive jurisdiction beyond the Spitsbergen Archipelago).

And a year later in 1978 USSR and Norway came to a temporary agreement defining the so-called "gray zone" located between the sector line and the median line. The total fishing quota for the USSR and Norway and also for third states under the Soviet or Norway licenses was identified for this zone. The "Gray zone" is a fishing area that comprises a part of the disputable water area and some parts of the exclusive economic zones of Norway and Russia. The area of the "gray zone" is 67,500 km^2, including:

- 23,000 km^2 – the economic zone of Norway
- 3,000 km^2 – the economic zone of Russia

In 2005 the dispute over the "gray zone" due to the incident with the "Electron" trawler got aggravated. In 2007 the Norway Oil Directorate completed mapping of the sea bottom to the north of Spitsbergen. Norway claims that its water area is sixfold more than its mainland territory. They think in Norway that the shelf they possess runs from the Ekofisc field in the south to the point equidistanced from the North Pole and Spitsbergen in the north. But they should prove that Spitsbergen is an extension of the Norway shelf.

USA unilaterally set the borders of the 200-mile zone making measurements from all points on the coast. This border is fixed in the Treaty on Division of the Economic Zone and Continental Shelf between Russia and USA in the Chukotka and Bering Seas signed by USSR Foreign Minister E. Shevardnadze and US Secretary of State J. Baker in 1990. USA ratified this Agreement, Russia – not.

As a result the shelf of the Bering and Chukotka seas is de facto divided between Russia and USA at a ratio of 30:70, respectively. Here Russia lost

- 46,000 km^2 of the shelf and 7,000 km^2 of the deepwater central part
- 150,000–200,000 tons of Alaska Pollack annually (US$100–120 million)
- Potential oilfields in the seabed

Not easy were the relationships on delimitation of the marine borders between USA and Canada in the Arctic zone. We mean here the dispute over the sea border in the Maine Bay:

1945 – Proclamation of US President H. Truman on the continental shelf that consolidated the US legal claims to the continental shelf in the Maine Bay.
1970 – Canada agreed to establishment of a division line in the Maine Bay area following the principles of the 1958 Geneva Convention on the Continental Shelf.
1977 – Canada set a 200-mile fishing zone and officially declared about its territorial waters in this region.
1984 – The dispute over the Maine Bay was submitted for consideration to the UN International Court. According to the court judgment two thirds of its waters were assigned to the USA and one third – to Canada. In development of the court judgment the USA claiming the whole Georges bank suggested that Canada establishes an annual moratorium on introduction of its fishing regulations in the Maine Bay. Canada turned down this suggestion motivating that the dispute concerned the continental shelf and had no relation to the fishing.

Struggle for the Lomonosov Ridge

The Arctic legal policy of Russia is a matter of the future.

In summer 2007 Russia made an attempt to establish sovereignty over its part of the continental shelf.

Bathyscaphs "Mir-1" and "Mir-2" reached the seabed near the North Pole, took ground samples and installed the state flag of Russia on the seabed.

In 2009 it is planned to submit an application to the Commission on Borders on the Continental Shelf for joining the Lomonosov and Mendeleev ridges to the Russian continental shelf.

Commission will study the natural science parameters of the submitted data. It is not vested any legal or arbitration authorities.

Here are some headings from the Russian mass media concerning Expedition "Arctic-2007": "Researchers are ready to "add" Russia northern possessions", "For the Polar friend", "Over a thin ice", "Pale policy", "Geological exploratory attack", "Ride of sovereignty", "In chase of treasures", "Whose leg on the Pole?", "Political geology", "Lomonosov Ridge is broken for elections".

2000 – The Lomonosov ridge reaches Russia, Greenland and Canada. After the Russian Expedition "Arctic-2000" it was declared that underwater Lomonosov and Mendeleev ridges are the extension of the continent and the Arctic continental shelf of Russia is 1.2 million square kilometer more than it was though earlier.
2001 – Russia was the first of the countries – signatories of the 1982 Convention that submitted an application on setting the shelf borders to the UN Commission on the Limits of the Continental Shelf. This application

states that the Russia jurisdiction covers the Podvodnikov Depression, the Mendeleev and Lomonosov ridges. The application was returned for further improvement.

2004 – The international Arctic Expedition – The Arctic Coring was the first in the history to drill the Lomonosov Ridge. Rock samples were taken from the depth of 428 m and incurred US$12.5 million of costs. The bit failed to penetrate deeper than the sedimentary cover.

Denmark insists that the Lomonosov Ridge belongs to it. In 2004 Denmark assigned US$38 million to search of proofs that the Lomonosov Ridge is connected with the Greenland Island.

Canada lays claims to the Alpha Ridge and the Mendeleev Ridge.

The response of the Arctic states to the Russian Expedition "Arctic-2007" was as follows:

Denmark:

- In 2007 the Lomrog Expedition was sent to the North Pole.

USA:

- Senate Committee on Commerce, Science & Transportation approved a draft law on allotment of US$8.2 billion to the US coastal guard.
- Construction of two new icebreakers in addition to two already operating "Healy" and "Polar Sea" and updating of the third one "Polarstern".
- Increase of the coastal guard number to 45,000 people.
- In August 2008 USA send the icebreaker "Healy" to Arctic "for mapping the relief of the Arctic seabed".

Canada:

- Plans to allot $7 billion to construction of eight ships for Arctic patrolling.
- Plans to construct a deepwater port in the Arctic-Bay on the northern tip of the Buffin Island for military and merchant ships.
- A naval base is under construction in Nanisivik area near the eastern entrance into the strategically important Northwest Passage linking the Atlantic and Pacific Oceans.
- Plans to deploy an army training camp in Resolute Bay, Nunavut Province, on the Cornwallis Island 595 km from the North Pole for training of military men to operation in Arctic conditions.
- Plans to increase to 5,000 of Canadian Eskimo rifle men in patrol units.

Conclusions

In the coming years the Arctic region of Russia shall show itself as a scaly resource base that, thanks to production of mineral deposits, and first of all hydrocarbons, and their sale on the world markets will make a significant contribution into thriving of the Russian economics.

References

Dodin DA (2005) Sustainable Development of the Arctic. Problems and Perspectives, St Petersburg, Nauka

Kovalev AA (2003) Present International Sea Law and Practice of Its Usage, Moscow, Nauchnaja kniga

Russian Arctic: On the Edge of Catastrophe (1996) Moscow, The Centre of Ecological Politics of Russia

The Arctic: Russia's Interests and International Conditions of Its Realization (2002) Moscow.

Two US programs during IPY*

William J. Wiseman, Jr.[1], Martin O. Jeffries[1,2], Clarence Pautzke[3] and Francis Wiese[3]

[1] National Science Foundation, Office of Polar Programs, 4201 Wilson Blvd., Suite 755, Arlington, VA 22230, USA, wwiseman@nsf.gov
[2] Geophysical Institute, University of Alaska, Fairbanks, AK 99775, USA, mjeffrie@nsf.gov
[3] North Pacific Research Board, 1007 W. 3rd, Anchorage, AK 99501, USA, cpautzke@nprb.org, francis.wiese@nprb.org

Abstract

The focus on the poles during the IPY has resulted in the initiation of a number of major programs. Two such US programs are the Arctic Observing Network (AON) and the combined Bering Ecosystem Study (BEST)–Bering Sea Integrated Ecosystem Research Program (BSIERP). AON is conceived to be a system of atmospheric, land- and ocean-based environmental observing capabilities that will significantly advance the volume and quality of our observations of Arctic environmental conditions. Data from the AON will enable the Study of Environmental Arctic Change (SEARCH), a U.S. initiative associated with the International Study of Arctic Change (ISAC), to document the manifold significant and rapid changes occurring in the Arctic. BEST–BSIERP is a partnership between the US National Science Foundation (NSF) and the North Pacific Research Board (NPRB) to characterize the eastern Bering Sea shelf ecosystem and how it might change in response to a climate-induced loss of sea ice. It maintains international ties through the Ecosystem Studies of Sub-Arctic Seas (ESSAS) program. We describe the status and scope of these two programs, as well as plans for future development and opportunities for international collaboration.

Introduction

The National Science Foundation (NSF) was designated as the lead federal agency in the United States for IPY (International Polar Year). As part of its own contribution to supporting IPY science it held targeted competitions. Projects contributing to an Arctic Observing Network were specifically solicited during one of these competitions. Additional projects contributing to such a network were funded through other parts of the IPY solicitations and through the core programs within the

* The views expressed in this paper are solely those of the authors and do not necessarily reflect the opinions of their parent organizations.

J.C.J. Nihoul and A.G. Kostianoy (eds.), *Influence of Climate Change on the Changing Arctic and Sub-Arctic Conditions*,

Foundation. Many other projects were supported that contribute to IPY goals. One of these involves a unique coordination of programs between NSF and the North Pacific Research Board (NPRB).

The Arctic Observing Network

Background

The National Science Foundation policies allow awards of up to 5 years in duration, occasionally with specified options for an additional 5 years of support. Typical awards, though, are for 3 or 4 years' duration. These awards tend to focus on hypothesis testing or process description. The Foundation, though, recognizes that some questions require longer term experiments or observational periods than allowed for by the standard awards. This creates a tension within the Foundation when it comes to meeting the needs for long-term observing. Significant successes in addressing these issues have resulted from the establishment of the Long Term Ecosystem Research (LTER) program, including the arctic LTER site at Toolik Lake and the subarctic LTER site at Bonanza Creek. In other cases, principal investigators (PIs) have successfully achieved continuing support for long-term observations through the regular programs by writing proposals that reviewed well in communities that recognized the critical need for such time series. Examples include support for space weather observations, atmospheric CO_2 observations, polar ozone and ultra-violet radiation observations, and the Bermuda Atlantic Time Series observations.

The first competition for arctic long-term observatories was held in 1999 and the investments in such activities have increased steadily since that time. A later review of arctic research support and logistics (Schlosser et al. 2003) specifically addresses the need for such observations and the planning, implementation, and support for a pan-arctic observing network, while recognizing that such a network could not be established and maintained without international collaboration. Two studies by the National Academies (NRC 2004, 2006) added further support to the concept of establishment of an Arctic Observing Network during the International Polar Year.

Prior to and continuing through the planning of the International Polar Year, a U.S. interagency program, including NSF, known as the Study of Environmental Arctic Change (SEARCH), was organizing itself around three major goals – observing change, understanding change, and responding to change. Many of the issues germane to the SEARCH observing change goal are commensurate with those of an Arctic Observing Network. Consequently, a major thrust of the first IPY competition announced by the National Science Foundation involved a request for proposals to contribute to an Arctic Observing Network.

Recognizing the significant existing investments of other agencies in arctic observations and desiring to avoid duplication of effort, NSF invited other agencies to coordinate with this competition from the outset. This was deemed a realistic manner in which to maximize the value of NSF's investments in an Arctic Observing System and to alert the other agencies of what we intended to support, in the hopes that some of these investments in research observation systems might later transition to operational systems supported by the other agencies. The NSF decision to engage informally with other Federal agencies early in the development of AON has since been formalized under the auspices of the Inter-Agency Arctic Research Policy Committee (IARPC 2007).

The NSF Arctic Observing Network

Twenty-one proposals were funded during the first NSF IPY competition. Combined with 13 existing projects funded through the long-term observing competitions begun in 1999, this results in 34 projects contributing to the Arctic Observing Network. By far the greatest number (15) are ocean and sea-ice related. Seven are atmospheric, four focus on hydrology and the cryosphere, three on terrestrial ecosystems, two on human dimensions, and two on data management (Table 1).

Table 1. Titles and URLs for AON projects.

Sea ice and oceans
Collaborative Research: North Pole Station: A Distributed Long-Term Environmental Observatory
http://www.nsf.gov/awardsearch/showAward.do?AwardNumber=0352754
The Beaufort Gyre System: Flywheel of the Arctic Climate?
http://www.nsf.gov/awardsearch/showAward.do?AwardNumber=0424864
Design and Initialization of an Ice-Tethered Profiler Array Contributing to the Arctic Observing System
http://www.nsf.gov/awardsearch/showAward.do?AwardNumber=0519899
Coordination, Data Management and Enhancement of the IABP
http://www.nsf.gov/awardsearch/showAward.do?AwardNumber=0520287
Ocean-Ice Interaction Measurements using Autonomous Ocean Flux Buoys in the Arctic Observing System
http://www.nsf.gov/awardsearch/showAward.do?AwardNumber=0520328
Comparison of Water Properties and Flows in the U.S. and Russian Channels of the Bering Strait – 2005–2006
http://www.nsf.gov/awardsearch/showAward.do?AwardNumber=0528632
IPY: Collaborative Research on the State of the Arctic Sea Ice Cover: An Integrated Seasonal Ice Zone Observing Network (SIZONET)
http://www.nsf.gov/awardsearch/showAward.do?AwardNumber=0632398

Ice mass balance buoy network: Coordination with DAMOCLES

http://www.nsf.gov/awardsearch/showAward.do?AwardNumber=0612391

Collaborative Research: A Modular Approach to Building an Arctic Observing System for the IPY and Beyond in the Switchyard Region of the Arctic Ocean

http://www.nsf.gov/awardsearch/showAward.do?AwardNumber=0633878

IPY: An Innovative Observational Network for Critical Arctic Gateways – Understanding Exchanges through Davis and Fram Straits

http://www.nsf.gov/awardsearch/showAward.do?AwardNumber=0632231

IPY: COLLABORATIVE RESEARCH: The Pacific Gateway to the Arctic – Quantifying and Understanding Bering Strait Oceanic Fluxes

http://www.nsf.gov/awardsearch/showAward.do?AwardNumber=0632154

IPY: Observing the dynamics of the deepest waters in the Arctic Ocean

http://www.nsf.gov/awardsearch/showAward.do?AwardNumber=0632201

IPY: Towards an Arctic Observing Network: An array of Ice-Tethered Profilers to sample the upper ocean water properties during the International Polar Year

http://www.nsf.gov/awardsearch/showAward.do?AwardNumber=0631951

IPY: Toward developing an Arctic Observing Network: An array of surface buoys to sample turbulent ocean heat and salt fluxes during the IPY

http://www.nsf.gov/awardsearch/showAward.do?AwardNumber=0632041

IPY: Collaborative Research: Aerial Hydrographic Surveys for IPY and Beyond: Tracking Change and Understanding Seasonal Variability

http://www.nsf.gov/awardsearch/showAward.do?AwardNumber=0634226

Atmosphere

Core Measurements at Summit, Greenland Environmental Observatory

http://www.nsf.gov/awardsearch/showAward.do?AwardNumber=0336450

Collaborative Research: IPY: Cloud properties across the Arctic Basin from surface and satellite measurements – An existing Arctic Observing Network

http://www.nsf.gov/awardsearch/showAward.do?AwardNumber=0632177

IPY: Pan-Arctic Studies of the Coupled Tropospheric, Stratospheric and Mesospheric Circulation

http://www.nsf.gov/awardsearch/showAward.do?AwardNumber=0632387

Development of data products for the University of Wisconsin High Spectral Resolution Lidar

http://www.nsf.gov/awardsearch/showAward.do?AwardNumber=0612452

IPY: Collaborative Research: A Prototype Network for Measuring Arctic Winter Precipitation and Snow Cover (Snow-Net)

http://www.nsf.gov/awardsearch/showAward.do?AwardNumber=0632131

The Collaborative O-Buoy Project: Deployment of a Network of Arctic Ocean Chemical Sensors for the IPY and beyond

http://www.nsf.gov/awardsearch/showAward.do?AwardNumber=0612331

IPY: Halogen Chemistry and Ocean-Atmosphere-Sea Ice-Snowpack (OASIS) Chemical Exchange During IPY

http://www.nsf.gov/awardsearch/showAward.do?AwardNumber=0732556

UV Spectral Irradiance Monitoring at Barrow, Alaska, and Summit, Greenland

http://www.biospherical.com/NSF/

Hydrology and the cryosphere

Long-term Measurements and Observations for the International Arctic Research Community on the Kuparuk River Basin, Alaska

http://www.nsf.gov/awardsearch/showAward.do?AwardNumber=0335941

Thermal State of Permafrost (TSP): The US Contribution to the International Permafrost Observatory Network

http://www.nsf.gov/awardsearch/showAward.do?AwardNumber=0520578

IPY: Development of a Network of Permafrost Observatories in North America and Russia: The US Contribution to the International Polar Year

http://www.nsf.gov/awardsearch/showAward.do?AwardNumber=0632400

Collaborative Research: IPY: Dynamic Controls on Tidewater Glacier Retreat

http://www.nsf.gov/awardsearch/showAward.do?AwardNumber=0732726

Terrestrial ecosystems

Development and implementation of the terrestrial Circumarctic Environmental Observatories Network (CEON)

http://www.nsf.gov/awardsearch/showAward.do?AwardNumber=0622406

IPY: Collaborative Research on Carbon, Water, and Energy Balance of the Arctic Landscape at Flagship Observatories and in a PanArctic Network

http://www.nsf.gov/awardsearch/showAward.do?AwardNumber=0632139

IPY: Collaborative Research: Study of arctic ecosystem changes in the IPY using the International Tundra Experiment

http://www.nsf.gov/awardsearch/showAward.do?AwardNumber=0632277

Human dimensions

IPY Collaborative Research: Is the Arctic Human Environment Moving to a New State?

http://www.nsf.gov/awardsearch/showAward.do?AwardNumber=0638408

International Polar Year Collaborative Project: Bering Sea Sub-Network: International Community-Based Observation Alliance for Arctic Observing Network (BSSN)

http://www.nsf.gov/awardsearch/showAward.do?AwardNumber=0634079

Data management

IPY: Exchange for Local Observations and Knowledge of the Arctic (ELOKA)

http://www.nsf.gov/awardsearch/showAward.do?AwardNumber=0632345

Collaborative Research, IPY: A Cooperative Arctic Data and Information Service (CADIS)

http://www.nsf.gov/awardsearch/showAward.do?AwardNumber=0632313

The oceanographic and sea-ice observations include, among others, moorings, CTD casts from ships and aircraft, ice-tethered buoys, gliders, inverted echo sounders, and remote sensing. Combined with other IPY programs supported by the European Union (DAMOCLES), the Canadian government (C3O and OCAC), and programs partially supported by Japan and NOAA (NABOS and CABOS), the coverage of the Arctic Ocean during IPY is impressive. The challenge will be to find the will to continue the essential observations after IPY.

The investments in atmospheric studies are fewer in number, but still important. They involve both core (basic) measurements at permanent stations and process

studies at remote temporary sites. Development of new instrumentation for studies of atmospheric chemistry over ice has been included, as well as large scale lidar studies of the polar vortex. Many of these include investments by other agencies and countries, as well.

The terrestrial ecology and permafrost studies supported during IPY are also wide-spread and include collaborative studies in Scandinavia, Iceland, Greenland, Canada, and Russia. Two major glaciological field studies were supported specifically as IPY ice sheet projects, but certainly contribute to an observing network – one on McCall Glacier, continuing a record from the last IPY, and one to 'weigh' the Greenland ice sheet. Two projects dealing with human dimensions were supported. One involves local communities around the Bering Sea, in both the US and Russia, in a study of marine species of economic and subsistence importance and how their abundance varies spatially and temporally. There is an intention to determine which aspects of traditional knowledge and western scientific knowledge concerning these issues correlate well. The second aims "to understand how socio-economic systems respond to rapid environmental change, and how local response interacts with broad forces of development and government policies to affect the well-being of Arctic residents."

Finally, recognizing the importance of data to the legacy of IPY, in general, and to an effective Arctic Observing Network, in particular, two data management proposals were supported. The first, Cooperative Arctic Data and Information Service (CADIS), "will provide the discovery, access, and use of scientific data by providing near-real-time data delivery, a repository for data storage, a portal for the discovery, and tools to manipulate data." The second, Exchange for Local Observations and Knowledge in the Arctic (ELOKA), is a pilot project to establish a data repository and portal for local traditional knowledge, while maintaining local control of the data.

Planning for the Arctic Observing Network continues in anticipation of a network that will long survive the pulse of activity during IPY. Because of the short lead times associated with planning for IPY, a considered design of the network was not available prior to funding decisions. The significant gaps in observing systems throughout the Arctic ensure that the data being collected by the funded projects will be important in understanding change throughout the Arctic. Nevertheless, reanalyses of existing data and observing system simulation experiments (OSSEs) will enhance the future development of the system. Initial efforts along these lines have recently been supported.

International relationships

It is clear that no one country can afford the investment necessary to adequately observe all aspects of the changing arctic system. Cooperation and collaboration are necessary to acquire the data necessary to understand the system. A similar level of cooperation and collaboration is needed to effectively and efficiently interpret those data. In the oceanographic and sea-ice realms, that collaboration

has been initiated by the SEARCH and DAMOCLES participants through the program SEARCH for DAMOCLES (S4D). In the terrestrial ecosystem community, the Circum-Arctic Environmental Observatories Network (CEON) is a vehicle for such cooperation. SEARCH scientists, *sensu lato*, have established international collaborations through the International Study of Arctic Change (ISAC), which seeks answers to similar questions as those posed by the US SEARCH program. Fertile ground exists for contributions from AON to the nascent Sustained Arctic Observing Network (SAON).

BEST–BSIERP

Background

The second program we describe is a collaboration between two organizations. The National Science Foundation has invested in the Bering Sea Ecosystem Study (BEST). The North Pacific Research Board has funded the Bering Sea Integrated Ecosystem Research Program (BSIERP). Neither program is supported by funds specifically allocated for IPY activities. Rather, they are funded by investments from the core funds of both organizations. Nevertheless, the coordinated program maintains ties to the IPY through ESSAS (Ecosystems Studies of Sub-Arctic Seas). Establishing a coordinated program between two organizations with different cultures, one an agency of the federal government and the other not, was not a trivial task. It was accomplished only through the good will and support of upper management in both organizations.

The Bering Sea, particularly the eastern Bering Sea shelf, is a region of significant importance to the United States. The Bering Sea is the source of approximately 40% of the US commercial fisheries catch with a value exceeding $3 billion annually after processing (M. Sigler, personal communication 2008). It also provides, directly or indirectly, some 11 million Kg of subsistence harvest supporting 55,000 Alaskan natives. Three quarters of the subsistence harvest is taken directly from the ocean. Finally, the communities that have existed around the Bering Sea for centuries have an important cultural link to the system.

The preponderance of anecdotal evidence from recent research in the Bering Sea has suggested that the ecosystem varies on multiple time scales. Regime shifts are known to be important from the instrumental record. Trends are suspected to be ongoing. In particular, reductions in the extent and duration of sea ice are believed to be occurring. Because of the societal benefits that accrue from this ecosystem, it is important to understand how it functions and to attempt prediction of the potential response of the system to climate change. One such prediction, which provided impetus to both the BEST and BSIERP programs is the oscillating control hypothesis (Hunt et al. 2002), which suggest that variations in the timing

of ice retreat in the spring will determine whether the system is predominantly top-down or bottom-up controlled and whether the spring bloom drives a predominantly benthic or pelagic ecosystem.

For many years, both NSF (BEST 2004; BEST Science Steering Committee 2005), largely through conversation with the research community facilitated by George Hunt, and NPRB (NPRB 2005) had been considering a study of the Bering Sea as a large marine ecosystem. Each had envisaged a physics-to-humans study. It quickly became apparent to both organizations that such a study was beyond the resources of either alone. With support from the upper management of both organizations, a coordinated competition was held. The conceptual structure was that NSF would solicit proposals dealing with the physics, chemistry and lower trophic levels, while NPRB would solicit proposal that dealt with the upper trophic levels. Both organizations would be involved in the human dimensions studies of the program. Furthermore, to make the project manageable, the geographic domain of the study was restricted to the eastern Bering Sea shelf.

Programmatic structure

The BEST–BSIERP program (http://bsierp.nprb.org/) is designed to provide the understanding of the Bering shelf ecosystem necessary to anticipate its future trajectory under scenarios of climate variability, particularly one of a changing sea ice regime. Through an extensive field program, it will contribute to the development of a series of vertically integrated models, while supporting additional competing modeling projects that will inform the integrated model (Fig. 1).

The models are anchored in the physics of the system. The modelers will begin by identifying general circulation models (GCMs) that best reproduce 20th century conditions in the Bering Sea region. Ensemble runs from these models under IPCC AR4 scenarios will be used to initialize and force a ROMS (Regional Ocean Modeling System) model of the Bering Sea with 10 km resolution everywhere and 3 km resolution over the eastern Bering Sea shelf. The model includes a new sea ice model that combines an elastic-viscous-plastic rheology and a one-layer ice and snow thermodynamics model. Nutrient-phytoplankton-zooplankton-detritus (NPZ-D) models will be embedded within the ROMS modeling framework.

A parallel physical model is also being developed. This model, which does not include biology, results from coupling a POP (Parallel Ocean Program) ocean model to a complicated dynamic-thermodynamic ice model that utilizes 12 categories of undeformed ice, ridged ice, ice enthalpy, and snow. It explicitly simulates sea ice ridging based on ice deformation without causing excessive buildup of ice thickness, an important aspect for a region where ice is thin and easily diverges and converges. The curvilinear grid averages 7 km in resolution, but reaches a resolution of 2 km near the Alaskan coast. It extends south to 35^{o} N,

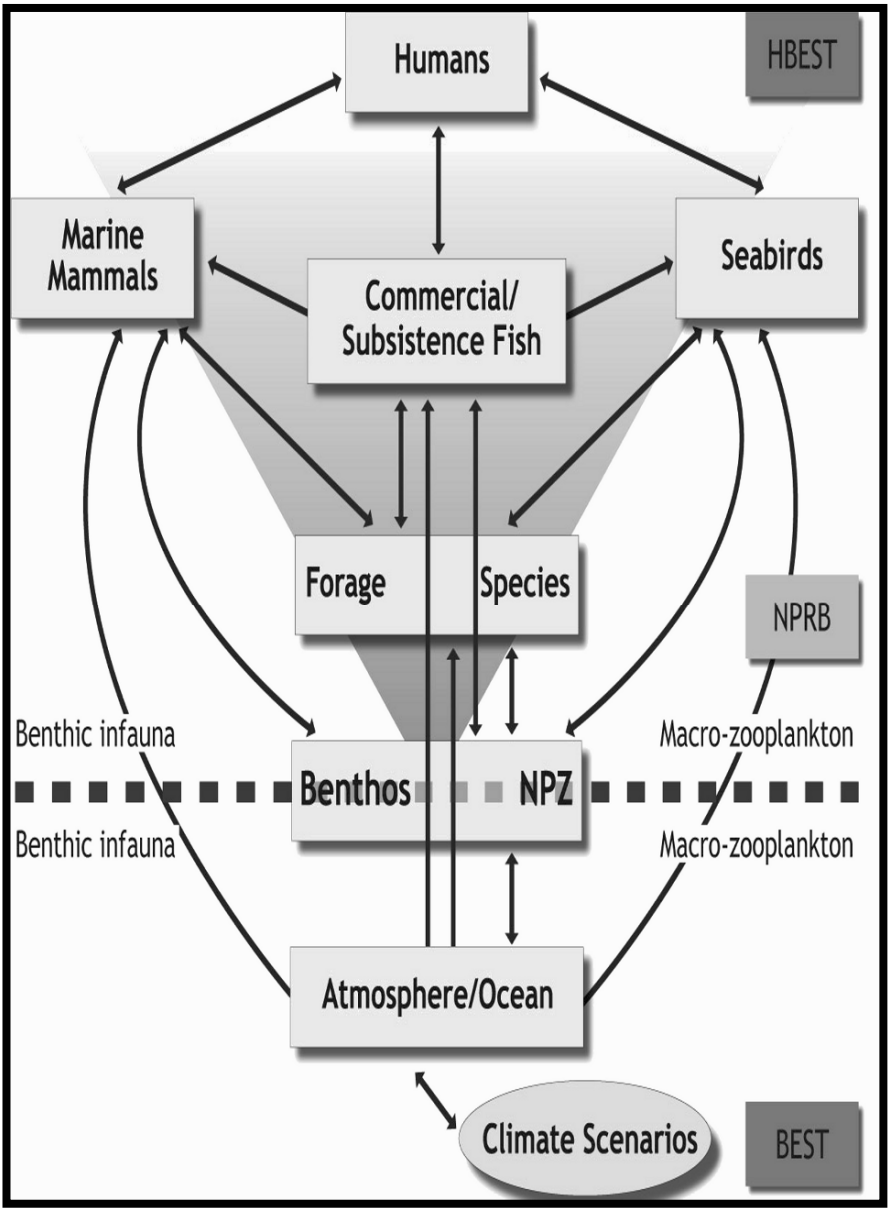

Fig. 1. Conceptual diagram of the ecosystem structure to be studied by BEST–BSIERP through integrated field and modeling efforts.

where it is nested within a 0.65° global model. It is forced by reanalysis products (NCAR/NCEP and ECMWF ERA40). As with the ROMS model, tides are included. The main goal of the project is accurate understanding of the dynamics responsible for the observed ocean and ice conditions during the coordinated field programs.

The nutrient-phytoplankton-zooplankton-detritus model, including benthic secondary production, within the ROMS model focuses on the lower trophic levels. This model is coupled to an energy flow model of forage fish and euphausiid abundance in space and time (FEAST). The model includes behavior rules calibrated against field observations. It allows for local depletion of primary and secondary production, thus accommodating both bottom-up and top-down control. Scenarios of changing predation from above will be included, as will loss to commercial fishing through economic models of the fishing industry.

In parallel with this integrated model, investigators are supported to develop a behavioral model of predation pressures on forage fish by piscivorous fish, birds, and marine mammals. Simultaneously other investigators will use historical data to develop a correlative multispecies biomass dynamics model including climate effects.

The field portion of the program is designed to provide a description of the Bering Sea ecosystem at different times of the year during consecutive years. While the field data will not provide an estimate of temporal trends of the structure of the ecosystem, comparison with historical data may allow such an estimate to be made. Furthermore, by providing data for model calibration and validation, it is anticipated that the models mentioned above, when forced with future climate scenarios may allow estimation of the trajectory of the ecosystem and its impact on the local human population.

The field program will be supported by a series of process study cruises, survey cruises, and some cruises which combine the two activities. The state of the water column will be sampled on all cruises to provide core physical and chemical data to the participants. Moorings will provide time series of the physical and biological parameters characterizing the water column. The import of iron in sea ice on the development of the spring bloom is also considered. Individual projects have been supported to calibrate and apply new chemical techniques for the estimation of primary production in the water column, as well as the role of ice algae in the food chain. Projects have also been supported to describe the plankton community structure and associated rates to be used in constraining models. Studies of the benthos include estimation of both community structure and rates of nutrient regeneration. One project is devoted to jellyfish population dynamics. A number of projects study aspects of the ecology of pollock, cod, and arrowtooth flounder. These include the time-varying distribution of the organisms as measured by multiple techniques, their diet, and seasonal energetics. Whales, walruses, and fur seals are the subject of another large suite of projects dealing with distribution, diet, reproductive success, and response to prey persistence. Seabirds are the topic area for another set of focused studies, particularly the thick

billed murre and black legged kittiwake. These studies involve both distribution and assessment of the stress level of the birds in response to variable food resources.

Finally, a series of human dimensions projects have been supported at six different communities around the Bering Sea. These communities were selected because of their unique relationships with the Bering Sea ecosystem.

Both BEST and BSIERP have supported data management projects. These are coordinating the data formats and mirroring each other's holdings so that data access is transparent to the PIs involved in the program. Data is expected to be available to all members of the program within 1 year of collection. Ultimately, data will be deposited in national data archives.

The first BEST cruise took place during the summer of 2007 with a restricted suite of funded projects. Multiple cruises are completed or planned for 2008, 2009, and 2010. The US Coast Guard icebreaker Healy is the planned research platform when the water is ice-covered in spring. Healy and a series of non-ice-strengthened ships are scheduled for sampling cruises during the summer and early fall. While berths are at a premium on the cruises, particularly the icebreaker cruises, unfunded collaborators are welcome on a 'not-to-interfere' basis when an unused berth is available. Oceanographers from Ocean University of China in Qingdao and University of Oldenburg accompanied a recent cruise. Berths are also a priority for outreach and educational activities. All cruises, thus far, have included one or more teachers who maintained blogs for their classes and the general public. The media have accompanied the ships. Stops have been made in native communities allowing tours of the ship and presentations concerning the studies. On occasion, a community member has accompanied the ship for a short survey leg.

Conclusions

The International Polar Year offers an opportunity, which is unique in recent decades, for coordinated international collaboration in the study of the important polar regions. The legacy of these collaborations will significantly impact the careers of the next generation of polar scientists. Possibly foremost amongst these impacts will be the data sets accumulated during IPY. The free exchange of data and ideas, both during and following IPY, must be a priority for all participants.

References

Bering Ecosystem Study (BEST) (2004) Science Plan. Fairbanks, AK: Arctic Research Consortium of the US, 82 pp

BEST Science Steering Committee (2005). Implementation Plan Bering Ecosystem Study Program. Unpublished report, 43 pp http://www.arcus.org/Bering/reports/downloads/BEST_Implementation_Plan.pdf

Hunt GL Jr, Stabeno P, Walters G, Sinclair E, Brodeur RD, Napp JM, Bond NA (2002) Climate change and control of the southeastern Bering Sea pelagic ecosystem. Deep-Sea Res. Part II 49:5821–5853

IARPC (Inter-Agency Arctic Research Policy Committee) (2007) Arctic Observing Network: Toward a US Contribution to Pan-Arctic Observing. Arctic Research of the United States, vol. 21, 94 pp.

NPRB (North Pacific Research Board) (2005) North Pacific Research Board Science Plan. North Anchorage, AK: Pacific Research Board, 198 pp

NRC (National Research Council) (2004) A U.S. Vision for the International Polar Year, 112 pp (http://books.nap.edu/catalog.php?record_id=11013#orgs)

NRC (National Research Council) (2006) Toward an Integrated Arctic Observing Network, 128 pp. (http://www.nap.edu/catalog.php?record_id=11607)

Schlosser P, Tucker W, Warnick W, York A (eds.) (2003) Arctic Research Support and Logistics: Strategies and Recommendations for System-Scale Studies in a Changing Environment. Fairbanks, AK: Arctic Research Consortium of the United States, 81 pp (http://www.arcus.org/Logistics/ArcticLogistics_10_03.pdf)